ESIMS Targeted Synthesis of Novel $\{Pt_2S_2\}$ Derivatives

A thesis

submitted in partial fulfilment

of the requirements for the degree

OF

Doctor of Philosophy in Chemistry

AT

The University of Waikato

BY

Ryland Gates Fortney-Zirker

THE UNIVERSITY OF
WAIKATO
Te Whare Wānanga o Waikato

2024

Abstract

Electrospray ionisation mass spectrometry (ESIMS) was used to investigate ring-opening reactions of several epoxides with the nucleophilic dinuclear Pt^{II} complexes $[Pt_2(\mu\text{-}E)_2(PPh_3)_4]$ (E = S, **1a**; Se, **1b**) and several activated cyclopropanes, *N*-tosylaziridine, and thiirane with **1a**. Epoxides cyclohexene oxide, styrene oxide, epibromohydrin, and 2,2-dimethyloxirane were found to undergo ring-opening when reacted with **1a** and derivatives $[Pt_2(\mu\text{-}S)(\mu\text{-}S{-}C_6H_{10}OH)(PPh_3)_4]BPh_4$ (**5**[BPh_4], $[Pt_2(\mu\text{-}S)(\mu\text{-}S{-}C_8H_8OH)(PPh_3)_4]$BETI (**6**[BETI]), $[Pt_2(\mu\text{-}S{-}CH_2CH(OH)CH_2{-}\mu\text{-}S)$-$(PPh_3)_4][PF_6]_2$ (**3**$[PF_6]_2$), and $[Pt_2(\mu\text{-}S)(\mu\text{-}S{-}CH_2C(Me)_2OH)(PPh_3)_4]BPh_4$ (**7** [BPh_4]) were respectively isolated and structurally characterised with $^{31}P\{^1H\}$ and ^{195}Pt nuclear magnetic resonance (NMR) spectroscopy, and for **5**, **3** and **7** single crystal X-ray diffraction (XRD) studies. **6** was found to be a mixture of isomers, and crystals suitable for a single crystal XRD experiment were not obtained. Both styrene oxide and epibromohydrin underwent ring-opening when reacted with **1b** and the respective derivatives $[Pt_2(\mu\text{-}Se)(\mu\text{-}Se{-}C_8H_8OH)(PPh_3)_4]^+$ and $[Pt_2(\mu\text{-}Se{-}CH_2CH(OH)$-$CH_2{-}\mu\text{-}Se)(PPh_3)_4]^{2+}$ were characterised by ESIMS. The fully substituted epoxide 2,3-dimethyl-2,3-epoxybutane did not undergo ring-opening when treated with **1a** in refluxing methanol for several hours. 5,6-Epoxy-5,6-dihydro-[1,10]-phenanthroline resulted in ring-opening when reacted with **1a** however the resulting derivative $[Pt_2(\mu\text{-}S)(\mu\text{-}S{-}C_{12}H_8N_2O)(PPh_3)_4]^+$ (**8**) was found to decompose readily in solution. Cyclopropanes cyclopropyl methyl ketone and *trans*-1,2-dibenzoylcyclopropane did not undergo ring-opening when reacted with **1a**. The more activated 2,2,3,3-tetracyanocyclopropane and diethylcyclopropane-1,2-dicarboxylate both re-

sulted in ring-opening when reacted with **1a** resulting in the isolation of derivatives $[Pt_2(\mu\text{-}S)(\mu\text{-}S{-}C(CN)_2)(PPh_3)_4]$ (**12**) and $[Pt_2(\mu\text{-}S)(\mu\text{-}S{-}C_2H_4CH(CO_2Et)_2)(PPh_3)_4]$BETI (**11**[BETI]) respectively which were structurally characterised by heteronuclear NMR spectroscopy (**12** $^{31}P\{^1H\}$, $^{195}Pt\{^1H\}$; **11** ^1H, $^{31}P\{^1H\}$) and single crystal XRD studies. **12** was found to have a carbanionic center and is proposed to result from an intramolecular rearrangement of the initially formed $[Pt_2(\mu\text{-}S)(\mu\text{-}S{-}C(CN)_2C(CN)_2CH_3)(PPh_3)_4]^+$ (**31**). Bromomethylcyclopropane did not result in ring-opening when reacted with **1a**, however alkylation resulted in $[Pt_2(\mu\text{-}S)(\mu\text{-}S{-}CH_2C_3H_5)(PPh_3)_4]^+$ (**10**) which was isolated as **10**$[BPh_4]$ and structurally characterised by $^{31}P\{^1H\}$-NMR spectroscopy and single crystal XRD. **10**$[BPh_4]$ did not undergo ring-opening when refluxed in methanol. *N*-tosylaziridine resulted in the ring-opened derivative $[Pt_2(\mu\text{-}S)(\mu\text{-}S{-}C_2H_4NHtosyl)(PPh_3)_4]^+$ (**13**) when reacted with **1a** and was isolated as **13**$[PF_6]$ and structurally characterised by $^{31}P\{^1H\}$-NMR spectroscopy and single crystal XRD. Thiirane appeared to rapidly undergo ring-opening when reacted with **1a** however only polymeric decomposition species were detected by ESIMS. The previously reported reaction of **1a** and 2-chloro-*N*-methylpyridinium iodide (**14**[I]) was reexamined. Salts of **14** sans iodide were synthesized using alkylating agents trimethyloxonium tetrafluoroborate or dimethyl sulfate giving **14**$[BF_4]$ or **14**$[CH_3SO_4]$ respectively. The reaction of **1a** and **14** was found to result in the dicationic complex $[Pt_2(\mu\text{-}S)(\mu\text{-}S{-}C_6H_7N)(PPh_3)_4]^{2+}$ (**2**) which was isolated as the bis-hexafluorophosphate salt **2**$[PF_6]_2$ and structurally characterised with $^{31}P\{^1H\}$-NMR spectroscopy, $^{195}Pt\{^1H\}$-NMR spectroscopy, and single crystal XRD. The 2-mercapto-*N*-methylpyridinium ligand in **2** was proposed to be an excellent leaving group and the reaction of **2** with excess bromide resulted in the isolation of the mixed-bridged complex $[Pt_2(\mu\text{-}S)(\mu\text{-}Br)(PPh_3)_4]BPh_4$ (**16**$[BPh_4]$) which was structurally characterised with $^{31}P\{^1H\}$-NMR spectroscopy and single crystal XRD. The thiols *N*-acetylcysteamine, 2-mercapto-1-methylimidazole, and 2-aminothiophenol were reacted with **2** to give $[Pt_2(\mu\text{-}S)(\mu\text{-}S{-}C_2H_4NHC(=O)CH_3)(PPh_3)_4]^+$ (**38**), $[Pt_2(\mu\text{-}S)(\mu_{NS}\text{-}S{-}C_3H_2N_2CH_3)(PPh_3)_4]^+$ (**17**), and $[Pt_2(\mu\text{-}S)(\mu\text{-}S{-}C_6H_4NH_2)$-

$(PPh_3)_4]^+$ (**39**) respectively which were isolated as **38**[BF_4], **17**[BETI], and **39**[BF_4]. **17**[BETI] was structurally characterised ($^{31}P\{^1H\}$-NMR spectroscopy, $^{195}Pt\{^1H\}$-NMR spectroscopy, single crystal XRD) and found to contain a novel 6-membered Pt-S-Pt-S-C-N heterocycle. **38** was characterised using NMR spectroscopy (^1H, ^{13}C, $^{31}P\{^1H\}$, and $^{195}Pt\{^1H\}$). **39** was characterised using $^{31}P\{^1H\}$-NMR spectroscopy. **2** was reacted with selenourea resulting in the detection by ESIMS of the mixed-bridged $[Pt_2(\mu\text{-}S)(\mu\text{-}Se)(PPh_3)_4]^+$ (**23**) which decomposed over the course of several days to **1a** and **1b**. When the diaryldichalcogenides Ph_2Se_2, Ph_2Te_2, di-4-ethoxy-phenyl-ditelluride were reduced with hydrazine to the corresponding chalcogenolate anion and reacted with **2**, substitution of the 2-mercapto-*N*-methylpyridinium zwitterion resulted and mixed-bridged derivatives $[Pt_2(\mu\text{-}S)(\mu\text{-}E{-}R)(PPh_3)_4]^+$ (E-R = Se-Ph, **18**; Te-Ph, **47**; Te-C6H4-OEt, **19**) detected by ESIMS. **18**[BF_4] and **19**[BF_4] were isolated and structurally characterised with heteronuclear NMR spectroscopy ($^{31}P\{^1H\}$-NMR, $^{195}Pt\{^1H\}$-NMR) and single crystal XRD. A bridging hydrazine species was observed when reacting **2** with hydrazine reduced diaryldichalcogenides, and the reaction between **2** and hydrazine was found to result in $[Pt_2(\mu\text{-}S)(\mu\text{-}NH{-}NH_2)(PPh_3)_4]^+$ (**21**) which was isolated as **21**[BPh_4] and structurally characterised with $^{31}P\{^1H\}$ and $^{195}Pt\{^1H\}$-NMR spectroscopy.

Acknowledgements

First and foremost, I would like to express my deepest gratitude to my chief supervisor, Emeritus Professor Bill Henderson, for his invaluable guidance, encouragement, and support throughout my PhD journey. His expertise and insightful advice have been instrumental in shaping this thesis.

I am also immensely grateful to my other supervisors, Associate Professor Graham Saunders and Professor Joseph Lane, for their continuous support, constructive feedback, and encouragement. Their collective wisdom and attention to detail have greatly enhanced the quality of my work.

A special thanks goes to Allen Oliver, Research Professor at Notre Dame University, who not only contributed significantly to my understanding of single crystal X-ray diffraction but also generously hosted me at Notre Dame. His guidance and hospitality during my time there were invaluable.

I would also like to acknowledge the generous support of the Claude McCarthy Foundation and the Bryan M. Craven scholarship, which enabled me to attend the American Crystallographic Association's summer camp at Northwestern University. This experience was crucial in deepening my understanding of crystallography and advancing my research.

I would also like to extend my heartfelt thanks to Emeritus Professor Brian Nicholson. Although he retired around the beginning of my PhD, his immense help in crystallography greatly shaped my understanding of the field. His willingness to share his knowledge left a lasting impact on my research.

My sincerest thanks also go to Jenny Stockdill and Annie Barker for their invalu-

able technical assistance and support in maintaining the lab and equipment. Their hard work behind the scenes ensured the smooth progress of my experiments.

I would also like to thank my colleagues Dr. Hayden Thomas and Matthew Risi. Hayden's immense help with NMR, particularly in setting up ^{195}Pt experiments, has been crucial to the success of my work. His technical skills and willingness to assist were invaluable. Matthew has been a great source of support in our discussions about research and in troubleshooting instrument failures. His calm approach and problem-solving mindset made dealing with setbacks much easier.

Furthermore, I would like to express my sincere gratitude to Northwestern University, the University of Notre Dame, and the University of Auckland for their assistance in collecting single crystal X-ray diffraction data sets. In particular, I would like to thank Tatiana Groutso at the University of Auckland for her gracious and generous help throughout this process.

I am also thankful to New Zealand eScience Infrastructure for the use of their high-performance computing facilities. Their resources and support were essential for conducting the computational aspects of my research.

Lastly, I would like to thank my parents, Dan Zirker and Carolyn Fortney, for their unwavering love and support. Their belief in me has been a constant source of motivation. I am also deeply grateful to my partner, Ashley Peters, for her encouragement, patience, and understanding throughout this journey.

Table of Contents

List of Figures

List of Tables

List of Schemes

List of Abbreviations

NMR	nuclear magnetic resonance
δ	chemical shift (in ppm)
ppm	parts-per-million
Hz	Hertz
MHz	Megahertz
J	coupling constant
T_1	spin-lattice relaxation time
SSCC	spin-spin coupling constant
DEPT-135	distortionless enhancement by polarisation transfer (at 135°)
NOE	nuclear Overhauser effect
FWHM	full width at half maximum
ESIMS	electrospray ionisation mass spectrometry
m/z	mass/charge ratio
r.i.	relative intensity
CSD	Cambridge Structural Database
PDB	Protein Data Bank
XRD	X-ray diffraction
Å	Ångström
MLCT	metal-to-ligand charge transfer
FTIR	Fourier-transform infrared spectroscopy
IR	infrared spectroscopy
TGA	thermogravimetric analysis
mp	melting point
DFT	Density Functional Theory
NCI	non-covalent interactions
QTAIM	quantum theory of atoms in molecules
BCP	bond critical point
RCP	ring critical point
ρ	electron density
kJ	kilojoule
Me	methyl
Et	ethyl

OMe	methoxy
OEt	ethoxy
TCCP	1,1,2,2-tetracyanocyclopropane
BETI	bis(pentafluoroethanesulfonyl)imide
DCM	dichloromethane
PFPE	perfluoropolyether
TEA	triethylamine
bipy	2,2-bipyridine
epoxyphen	5,6-epoxy-5,6-dihydro-[1,10]-phenanthroline
phen	1,10-phenanthroline
PPh_3	triphenylphosphine
PPr_3^n	tri-n-propylphosphine
TPPO	triphenylphosphine oxide
dppm	1,1-bis(diphenylphosphino)methane
dppe	1,2-bis(diphenylphosphino)ethane
dppp	1,3-bis(diphenylphosphino)propane
dppb	1,4-bis(diphenylphosphino)butane
dppf	1,1-bis(diphenylphosphino)ferrocene

Chapter 1

Introduction

1.1 Literature review

1.1.1 Early Sulfur Derivatives of Platinum

The proclivity of sulfur for heavy metals is evident in the natural world, with a substantial variety of mineral sulfides in great abundance. One such mineral of the platinum metals which exemplifies this affinity is Cooperite ($Pt_{0.6}Pd_{0.3}Ni_{0.1}S$). First classified in 1928 by R. Cooper, the mineral primarily consists of square planar $Pt^{II}S_4$ units with each sulfur tetrahedrally coordinated to platinum.[1] Metal sulfides are also prevalent in biological systems,[2] are found to be significant in catalysis,[3,4] display a wide range of structural diversity,[5,6] and have interesting applications in solid state chemistry.[7] Despite this attention, platinum sulfide chemistry has remained relatively unexplored.

In 1903, Hofmann and Höchtlen isolated the first platinum η^2-pentasulfido complex $[NH_4]_2[Pt(\eta^2\text{-}S_5)_3]$,[8] which was interestingly also the first purely inorganic chiral compound.[9] This tentatively marked the creation of a field which would not see much interest until the mid 20^{th} century, when Chatt and Hart synthesised the di-μ-thiolate Pt^{II} complexes $[Pt_2Cl_2(\mu\text{-}SR)_2(PPr^n{}_3)_2]$ (R = Et, Ph, *p*-$C_6H_4NO_2$, *p*-C_6H_4OMe)[10–12] and Pd^{II} complex $[Pd_2Cl_2(\mu\text{-}SEt)_2(PBu_3)_2]$.[13] This was followed in 1966 when Baird and Wilkinson isolated a novel Pt-S-Pt complex[14,15] which was ini-

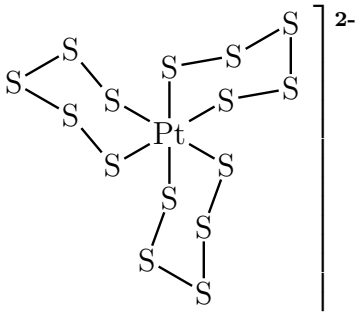

$[Pt(\eta^2\text{-}S_5)_3]^{2-}$

tially thought to be the dinuclear complex $[Pt_2(CO)_2(PPh_3)_2(S)]$ before structural characterisation by X-ray diffraction revealed the bridging sulfide complex $[Pt_2(\mu\text{-}S)(CO)(PPh_3)_3]$ with a triangular $\{Pt_2S\}$ core.[16]

1.1.2 The $\{Pt_2S_2\}$ core

Perhaps the most significant moment so far in platinum sulfide chemistry arrived a decade later with the isolation of the bridging Pt^{II} sulfido complex $[Pt_2(\mu\text{-}S)_2(PMe_2Ph)_4]$ by Chatt and Mingos,[17] and soon after the triphenylphosphine analogue $[Pt_2(\mu\text{-}S)_2(PPh_3)_4]$ (**1a**) by Ugo *et al.* who was examining chalcogenide poisoning of catalytic surfaces.[18]

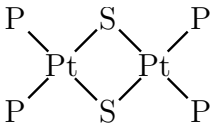

1a

Figure 1.1: Structure of $[Pt_2(\mu\text{-}S)_2(PPh_3)_4]$ (**1a**), P = PPh_3.

Preliminary studies on the reactivity of these new complexes found them to be prone to alkylation with methyl iodide and benzyl bromide.[17,18] The alkylated complex $[Pt_2(\mu\text{-}S)(\mu\text{-}SCH_2Ph)(PMe_2Ph)_4]Br$ was isolated and characterised with ^1H NMR spectroscopy and conductance measurements confirming it be a 1:1 electrolyte.[17] When reacting the mononuclear triphenylphosphine Pt^{II} complex *cis*-$[PtCl_2(PPh_3)_2]$ with sodium sulfide in ethanol, Chatt and Hart[17] isolated a species

suspected of being the mononuclear complex $[PtS_4(PPh_3)_2]$ with a PtS_4 ring, similar to the six-membered metal polysulfide rings reported by Hofmann and Höchtlen.[8] This assignment was later confirmed using crystallographic evidence by the work of Mingos *et al.*[19]

1.1.3 First example of metalloligand behaviour, categorised as aggregates

Also examined were the ligating properties of the sulfide centers in the $\{Pt_2S_2\}$ compounds, with coordination of a Pt^{II} fragment resulting in the white crystalline trinuclear complex $[Pt_3(\mu_3\text{-}S)_2(PMe_2Ph)_6]^{2+}$.[17] Similar behavior was also observed with the arsine complex *cis*-$[PtCl_2(AsMe_2Ph)_2]$ in the isolation of $[Pt_3(\mu_3\text{-}S)_2(PMe_2Ph)_4(AsMe_2Ph)_2]Cl_2$. The trimetallic system $[Pt_3(\mu_3\text{-}S)_2(PMe_2Ph)_6]^{2+}$ was later reexamined by Bushnell *et al.* resulting in a greatly increased yield and structural elucidation with an X-ray diffraction study.[20] The Pt-Pt contacts were all found to be slightly over 3Å and hence too long to be classified as formal bonding. $^{31}P\{^1H\}$-NMR and $^{195}Pt\{^1H\}$-NMR data were also consistent with the refined crystal structure of the trimetallic complex, and provided additional evidence for a lack of formal metal-metal bonding. The presence of a formal Pt-Pt bond has found to be independent of the Pt-Pt coupling constant,[21] and where such a metal-metal interaction exits, electronic communication throughout the complex is extended and is reflected in the increased magnitude of long range coupling constants. In the trinuclear complex $[Pt_3(\mu_3\text{-}S)_2(PMe_2Ph)_6]^{2+}$, the long range coupling constants $^4J(P{-}P)$ and $^3J(Pt{-}P)$ were found to be small, < 5 Hz and -25 Hz respectively,[20] which is significantly less than for trinuclear compounds of similar geometry which *do* contain formal metal-metal bonding.[22] When Mingos *et al.* examined Pd^{II} derivatives of $[Pt_2(\mu\text{-}S)_2(PPh_3)_4]$, crystallographic evidence of the pentanuclear complex $[\{Pt_2(\mu_3\text{-}S)_2(PPh_3)_4\}_2Pd]^{2+}$ revealed a similar separation between metal centers of approximately 3.15 Å, leading to a qualitative description of these derivatives as independent 16 electron square-planar metal centers, and referring to them as 'ag-

gregates' rather than clusters.[23]

1.1.4 A versatile metalloligand

The triplatinum complex $[Pt_3(\mu\text{-}S)_2(PMe_2Ph)_6]^{2+}$ was the first multinuclear aggregate of **1a** isolated,[17] however the utility of the $\{Pt_2S_2\}$ core as a synthon for building multimetallic aggregates was not fully realised until work done by Mingos *et al.* in the early 1980s. A variety of Lewis acidic Hg^{2+}, Ni^{2+}, Au^{+}, Ag^{+}, and Pd^{2+} fragments were ligated producing aggregates such as the hexanuclear $[\{Pt_2(\mu_3\text{-}S)_2(PPh_3)_4\}_2Ag_2]^{2+}$ with an Ag···Ag contact of 2.815 Å and the pentanuclear $[\{Pt_2(\mu_3\text{-}S)_2(PPh_3)_4\}_2Pd]^{2+}$ with square-planar geometry at the Pd^{II} center.[23,24]

Reported coordination geometries taken up at the ligated heterometals since have been linear,[25] angular,[26] T-shaped,[24] Y-shaped,[27] tetrahedral,[28] square planar,[20,23,29] and distorted trigonal-pyramidal.[30] This examination of Lewis acid-base reactions with $Pt_2(\mu\text{-}S)_2(PPh_3)_4$ and various transition metal fragments found facile routes to heterometallic complexes with a surprising variety of geometries and nuclearities.[23,31]

The non-bonding separation of bridging sulfide centers, moderately long Pt-S bond distances, and variable dihedral angle between the planes of the 16 electron square planar d^8 platinum centers define a dynamic and accommodating metalloligand, capable of coordinating a wide variety of transition metal and main group fragments in a mono- or bi-dentate configuration. A selection of metal centers coordinated by the $\{Pt_2S_2\}$ core which highlight this great diversity include Zn^{II},[32] Fe^{III},[33] Co^{III},[34] Os^{II},[35] Mo^{VI},[36,37] V^{V},[37] Au^{III},[38] Pb^{IV},[39] Bi^{III},[40] Tl^{III},[41] and U^{VI}.[37]

An interesting study examined heterometallic systems with d^6 metals coordinated by π-hydrocarbon donor ligands, with the Ru^{II} complex $[Pt_2(\mu_3\text{-}S)_2(PPh_3)_4Ru(\eta^6\text{-paracymene})]^{2+}$ isolated and characterised by X-ray diffraction.[35] This *pseudo*-five-coordinate complex was found to be stable towards addition of CO or pyridine, and exemplifies the balance of steric and electronic characteristics of the $\{Pt_2S_2\}$ core. Another interesting feature of these systems are the relatively close distances of the d^8 and d^6 metals (2.96 Å), making them candidates for the exploration of

bimetallic catalysis and electrochemical communication.[35]

1.1.5 Alternate ancillary ligands

There are several reviews on the $\{Pt_2S_2\}$ core.[42] A majority of these focus on the triphenylphosphine analogue **1a** largely due to the ease of handling PPh_3, and a strong tendency for crystallinity in derivatives.[42b] The tertiary phosphines of the initially chosen PPh_3 and PMe_2Ph ancillary ligands have favorable electron donating properties and their bulky substituents provide a steric barrier to the unsaturated metal centers. The kinetically stable and bulky triphenylphosphine ligand predominates in a majority of the research done on the $\{Pt_2S_2\}$ core. The ligand exchange properties of the $\{Pt_2S_2\}$ core have been examined. Chelating diphosphines such as dppp (1,2-bis(diphenylphosphino)propane) and dppe (1,2-bis(diphenylphosphino)-ethane) have been explored,[43] studies have also been carried out on electronically active dppf (1,1′-bis(diphenylphosphino)ferrocene),[44,45] and the pyridine-containing dppy (2-diphenylphosphinopyridine).[31] Using the dppy analogue $[Pt_2(\mu\text{-}S)_2(dppy)_4]$, Yam and co-workers were able to synthesize a heptanuclear heterometallic cluster with Ag^I which contains an unusual Ag_3 unit bridging two $[Pt_2(\mu_3\text{-}S)_2(dppy)_4]$ moieties.[31]

Arsine derivatives $AsPh_3$ and $AsPh_2(CH_2)_2AsPh_2$ were found to be much poorer electron donors, resulting in an increase of the Pt-S distance and reduction of the nucleophilic character expressed by the $\{Pt_2S_2\}$ core.[46,47]

1.1.6 Dihedral angle of the $\{Pt_2S_2\}$ core

Arguably the most remarkable feature of complexes with the $\{Pt_2S_2\}$ core is the variable hinge or dihedral angle θ (Pt1-S1-S2-Pt2), which has led to their description as butterflies.[42b] A computational study by Capdevila *et al.*[48] using optimised geometries of approximated $\{Pt_2S_2\}$ complexes compared the energy cost associated with changing θ (planar vs. hinged) at the MP2[49] level of calculation. The primary factors were determined to be electronic in nature and independent of the deriva-

tised thiol (alkyl or aryl) with the minimisation of through-ring thiol antibonding orbital interaction dominating. This energy cost was also found to be sufficiently low, such that these complexes can be thought of as fluxional in solution.[50]

There exists a large variation of reported dihedral angles in crystal structures of complexes with underivatised sulfide ligands such as $[Pt_2(\mu\text{-}S)_2(PMe_2Ph)_4]$ $\theta = 121^\circ$,[51] $[Pt_2(\mu\text{-}S)_2(dppy)_4]$ $\theta = 180^\circ$,[31] and $[Pt_2(\mu\text{-}S)_2(dppe)_4]$ $\theta = 140.2^\circ$.[52] Complexes where one or both sulfide center is derivatised tend to be hinged, however examples to the contrary can be found in the Ag^I complex $[Pt_2(\mu_3\text{-}SAgCl)(PPh_3)_4]$[53] and Au^I complex $[Pt_2(\mu_3\text{-}SAuCl)_2(PPh_3)_4]$[25] which are isostructural and have planar $\{Pt_2S_2\}$ cores with coordinated metal fragments extending above and below the plane of the core.

1.1.7 Protonation and hydrogen bonding

Protonation of the strongly basic $\{Pt_2S_2\}$ core results when in protic solvents, and the monoprotonated complexes $[Pt_2(\mu\text{-}S)(\mu\text{-}SH)L_4]^+$ for L = PPh_3[54] and L = dppe, dppp[55] have been isolated and characterised. Interestingly, the phosphorus environments of the dppe and dppp complexes were determined to be equivalent by $^{31}P\{^1H\}$-NMR, suggesting fluxional behavior of the proton between sulfide centers,[55] while two distinct phosphorus environments were observed for the PPh_3 complex.[54]

The ability of the electron rich $\{Pt_2S_2\}$ core to engage in hydrogen bonding has been demonstrated conclusively, with the solvates of ethanol and hexafluoropropan-2-ol structurally characterised.[56] In the ethanol solvate, $[Pt_2(\mu\text{-}S)_2(PPh_3)_4]\cdot 2\,EtOH$, only one sulfido ligand is involved in a hydrogen bond, with the second ethanol engaged in a hydrogen bond with the first ethanol. The dihedral angle $\theta = 133.3^\circ$ compares nicely with the protonated complex $[Pt_2(\mu\text{-}S)(\mu\text{-}SH)(PPh_3)_4]^+$ of $\theta = 135^\circ$.[54]

1.1.8 Reactions with organic electrophiles

The $\{Pt_2S_2\}$ core was initially found to readily undergo alkylation reactions with organic electrophiles such as MeI and $PhCH_2X$ (X = Cl, Br),[17,18] and is in fact such

an exceptional nucleophile that alkylation reactions were observed with the weak electrophiles dichloromethane and chloroform.[57,58] It was found that the resulting monoalkylated cationic complexes are also susceptible to further alkylation and eventually complex degradation to form mononuclear species.[45] These species have been isolated and structurally characterised as $[(dppy)_2PtS_2CH_2]$[59] and $[(PMe_2Ph)_2PtS_2CH_2]$.[60] The reactivity with dichloromethane was examined further with chelating diphosphines dppp and dppe, and a positive correlation was found between the electron donating nature of the diphosphine and the nucleophilicity of the core.[61] Furthermore, the flexibility of the terminal phosphine was also implicated in the reaction kinetics, with the more rigid dppe undergoing faster degradation to mononuclear products.

A wide variety of alkylating[42f,62] and arylating[63] agents have been examined, and using the rich electron donating properties of the sulfide lone pairs, this has proven to be an efficient platform for generating otherwise complicated thiolates. Through choice of alkylating agent or arylating agent, it is possible to selectively functionalise the $\{Pt_2S_2\}$ core producing monocations $[Pt_2(\mu\text{-}S)(\mu\text{-}SR)(PPh_3)_4]^+$ or dications $[Pt_2(\mu\text{-}SR)_2(PPh_3)_4]^{2+}$. When reacted with an α,ω-dialkylating agent, an overhead-bridging dication such as $[Pt_2(\mu\text{-}SR\mu\text{-}S)(PPh_3)_4]^{2+}$[42d] results. While the first alkylation of the $\{Pt_2S_2\}$ core can be achieved with mild alkylating agents, the second alkylation must be achieved with a stronger agent, such as Me_2SO_4, or with more forcing conditions[64] as the underivatised sulfide center has a reduced nucleophilicity. A range of dialkylated derivatives of the form $[Pt_2(\mu\text{-}SCH_3)(\mu\text{-}SR)(PPh_3)_4]^{2+}$ have been prepared using Me_2SO_4 in this manner.[65] Reacting the $\{Pt_2S_2\}$ core with a chelating diphosphine such as dppp was found to increase the basicity of the sulfide centers, evidenced by facile dialkylation of the complex.[66] The nucleophilicity of the underivatised sulfide center is however sufficient to exhibit an S$\cdots\pi$-fluoroaryl interaction in the crystal structure of alkylated complex $[Pt_2(\mu\text{-}S)(\mu\text{-}SCH_2C_6F_5)(PPh_3)_4]^+$.[67] The analogous benzylated complex $[Pt_2(\mu\text{-}S)(\mu\text{-}SCH_2Ph)(PPh_3)_4]^+$ does not mirror this behaviour, with the phenyl ring pro-

jected away from the $\{Pt_2S_2\}$ core.[66] Interestingly, alkylated $\{Pt_2S_2\}$ complexes can behave as metalloligands through the underivatised sulfide center. This has been investigated with Hg^{II} and Au^{I} fragments giving complexes of the type $[Pt_2(\mu\text{-S-R})(\mu\text{-SML})(PPh_3)_4]^{2+}$ (ML = HgPh, $AuPPh_3$),[68] and has also been found in the fluoroaryl complex with the addition of Ph_3PAuCl.[67]

A rare example of a quadruply bridging sulfide μ_4-S has also been isolated. Starting with a dicationic monofunctionalised complex $[Pt_2(\mu\text{-S})(\mu\text{-SR})(PPh_3)_4]^{+}$ (R = 1-methylimidazolium), addition of AgOTf ($OTf^{-} = O_3SCF_3^{-}$) resulted in the aggregate $[Pt_2\{\mu_4\text{-S}(AgOH_2)(AgOTf)\}(\mu\text{-SR})(PPh_3)_4]^{3+}$.[69]

1.1.9 Desulfurisation of the $\{Pt_2S_2\}$ core

The facile synthesis of functionalised thiols and sequential building of heterometallic polynuclear aggregates demonstrates the great utility of the $\{Pt_2S_2\}$ core in reaching these complicated systems.[42b] Accordingly, the desulfurisation of the $\{Pt_2S_2\}$ core has also been examined in hopes of releasing the designed thiolates or progressing from aggregates → clusters. Reduction by CO has been successfully used to excise a bridging sulfide and generate a heterometallic Pt_2SM cluster (M = Ag,Cu).[70] The stabilisation of such clusters was found to depend on a chloride being bound to the heterometal. Integral in this process is the delicate balancing act performed by carbonyl, which has a high affinity for sulfur, mild reducing properties, and is an excellent π-acceptor.

1.1.10 Heteroatom bridged systems $[Pt_2(\mu\text{-S})(\mu\text{-X})(PPh_3)_4]^{+}$

The replacement of a μ-sulfido ligand in $[Pt_2(\mu\text{-S})_2(PPh_3)_4]$ was found to occur when exposed to both oxidising and non-oxidising sources of iodine.[71] The novel complex $[Pt_2(\mu\text{-I})(\mu\text{-S})(PPh_3)_4]^{+}$ was isolated and structurally characterised by $^{31}P\{^{1}H\}$-NMR and X-ray crystallography, revealing a planar $\{Pt_2SI\}$ core. Interestingly, the novel amido complex $[Pt_2(\mu\text{-S})(\mu\text{-NH}_2)(PPh_3)_4]^{+}$ has also been isolated, and is synthesised via reaction of $[Pt_2(\mu\text{-S})_2(PPh_3)_4]$ with 2-chloro-1-methylpyridinium

tetraphenylborate.[72] The iodide salt of the pyridinium complex was serendipitously found to react with $[Pt_2(\mu\text{-}S)_2(PPh_3)_4]$ to give the bridging iodo $[Pt_2(\mu\text{-}S)(\mu\text{-}I)\text{-}(PPh_3)_4]^+$.[71] Currently we are working on expanding this method for the synthesis of other heteroatom bridged species.

1.1.11 $\{Pt_2E_2\}$ complexes: the selenide and telluride analogues

While a significant amount of work has been done on complexes containing the $\{Pt_2S_2\}$ core, less is known about the selenide[73] and telluride[74] analogues. The selenide complex $[Pt_2(\mu\text{-}Se)_2(PPh_3)_4]$ (**1b**) has similar or greater nucleophilic character than the sulfide analogue **1a** and can be mono- or di-alkylated to form a variety of selenolates.[73d] It has also been found to decompose in chlorinated solvents.[75] The di-protonated $[Pt_2(\mu\text{-}SeH)_2(PPh_3)_4]^{2+}$, formed under acidic conditions, has been isolated and characterised.[124c] The sulfide analogue $[Pt_2(\mu\text{-}SH)_2(PPh_3)_4]^{2+}$ has been observed, but is yet to be isolated. This diprotonated $\{Pt_2Se_2\}$ core revealed a dihedral angle $\theta = 71.9^\circ$ which can be considered unusually acute cf. the underivatised parent complex $\theta = 180^\circ$[76] and $\theta = 128^\circ$ for Sn^{IV} aggregate $[Pt_2\text{-}(\mu_3\text{-}Se)_2(PPh_3)_4(SnBuCl_2)]^+$.[73e] The behaviour of $\{Pt_2Se_2\}$ as a metalloligand mirrors the sulfide analogue in ligating metal fragments through one or both selenide centers.[184c,124c,73e,184c,124c,184c] However, the selenide system has been shown to undergo metal scrambling reactions,[124a] something that has rarely been observed with $\{Pt_2S_2\}$.[77] Our recent contributions to this field have shown the selenide system can be arylated[124f] in analogous fashion to **1a**,[63] and can undergo ligand exchange reactions with diaryl dichalcogenides resulting in the isolation of trimetallic aggregate $[\{Pt(PPh_3)\}_3(\mu_3\text{-}Se)(\mu\text{-}TePh)_3]PF_6$, which was structurally characterised by X-ray diffraction.[78]

1.2 Electrospray ionisation mass spectrometry

Electrospray ionisation mass spectrometry (ESIMS) was developed as a soft ionisation technique for analysis of large biomolecules by Fenn *et al.*[79] for which he was jointly awarded the 2002 Nobel Prize in chemistry.[79d] ESIMS has successfully been applied to coordination chemistry where the ionisation of thermally sensitive or labile molecules is required.[80] The rapid process allows the progress of reactions to be followed and consumes a very small amount of sample ($\approx$ 1 μg). In particular, $\{Pt_2E_2\}$ (E = S, Se) chemistry has utilised this technique in a combinatorial-like process of 'synthetic prospecting', whereby micro-scale reactions are screened by ESIMS and favorable reactions are reproduced macroscopically for characterisation by traditional techniques.[42d,124a,c,a,c] The functionalised derivatives or multimetallic aggregates of these systems are often cationic, enhancing the detection of these species in solution.[38,54] As reaction solutions contain species with differing ionisation efficiencies, the feasibility of ESIMS to detect species in solution has been demonstrated.[42d] An alkylated derivative $[Pt_2(\mu\text{-}S)(\mu\text{-}SCH_2Ph)(PPh_3)_4]^+$, known to have a high ionisation efficiency[81] was analysed by ESIMS in an equimolar methanolic solution of the parent complex $[Pt_2(\mu\text{-}S)_2(PPh_3)_4]$ **1a**. Despite the neutral parent complex **1a** being sparingly soluble, its protonated cation $[Pt_2(\mu\text{-}S)(\mu\text{-}SH)(PPh_3)_4]^+$ was detected in approximately equal intensity with the monobenzylated derivative.[42d] Modulating the capillary exit voltage can provide additional information on the reaction solution, for example an increase can enhance the fragmentation of analyte ions[82] or a decrease can reveal the presence of thermally sensitive ions.[83] The analysis process is also rapid, enabling the screening of multiple reaction solutions and the ability to closely follow a reactions progress.[42c] ESIMS is also particularly effective for the identification of cationic species containing polyisotopic elements, due to their unique molecular isotope patterns. For example, the protonated $[Pt_2(\mu\text{-}S)(\mu\text{-}SH)(PPh_3)_4]^+$ and radical cation $[Pt_2(\mu\text{-}S)_2(PPh_3)_4]^+$ have identical isotope patterns at *m/z* 1503.25 and 1502.24 respectively. A combination of these cationic species produces a unique isotope pattern located at *m/z* 1503.25, sufficiently different to

distinguish from the constituent patterns.[42c]

1.3 Computational chemistry

Over the past few decades, the concomitant rise of computing power and increasing ease of access to such facilities[84] has seen quantum chemical calculations, and in particular the use of approximate Density Functional Theory (DFT),[85] commonly employed alongside traditional spectroscopic and electrochemical analyses.[86] The recent prominence experienced by DFT over traditional *ab initio* wave function theory (WFT) processes such as Hartree-Fock,[87] Møller-Plesset,[49] and coupled cluster[88] is largely due to the excellent balance of chemical accuracy with computational efficiency achieved by DFT,[89] allowing calculations on large ($N_{atoms} > 10$) systems such as transition metal complexes.[90] The foundations of DFT can be traced to the work of Hohenberg and Kohn,[91] who proved the ground state energy of an inhomogeneous electron gas could be determined by the use of a density functional, assuming the ground state electron density was known. Shortly after, Kohn and Sham[92] reduced the quantum many-body problem to a set of non-interacting electrons in an effective potential with self-consistent Kohn-Sham (KS) equations, which account for the nonrelativistic kinetic energy of the system, the classical coulomb interactions, and importantly, the exchange-correlation (XC) energy. This energy, which is known exactly only for a uniform interacting electron gas, is approximated for more complex systems by XC functionals of which the most rudimentary is the local spin-density approximation (LDSA).[93] XC approximations have been developed with increasing levels of sophistication[94] to address the accurate adjustment of this contribution to the ground state energy.[95,96] Modern DFT calculations in transition metal chemistry employ a wide range of functionals, including those that account for long range dispersion such as the hybrid meta-generalised gradient approximation (meta-GGA) functional ωB97X-D.[97] When dealing with heavy atoms, scalar relativistic effects become nontrivial and are modeled with the use of effective core potentials (ECP).[89] Time-dependent DFT (TD-DFT), developed by Runge and Gross[98] is a modification

of DFT initially employed to describe scattering experiments, is a reliable means of calculating excited states and has been applied to modelling the interaction of electromagnetic fields with matter.[99] These developments to DFT have made quantum chemical calculations more accessible for large systems, such as coordination complexes,[89] with a fraction of the computational cost required for WFT processes and ever increasing chemical accuracy.[96,100]

Quantum chemical calculations have been used several times in the examination of the $\{Pt_2S_2\}$ core, with initial studies making use of *ab initio* processes, such as the examination of coordinatively unsaturated aggregates with Hartree-Fock calculations.[101] Another study examined various d^8 metals Rh^{I}, Ir^{I}, Ni^{II}, Pd^{II}, Pt^{II}, and Au^{III} in binuclear complexes with bridging chalcogenides of the formula $[M_2(\mu\text{-}ER)_2L_4]$ (E = O, S, Se, Te;R = alkyl) using the MP2 approach.[102] More recently, González-Duarte *et al.* utilised DFT to examine various aspects of the $\{Pt_2S_2\}$ core, such as the observed degradation in chlorinated solvents,[61] redox properties,[46,103] aliphatic C−X (X = halogen)[104] and aromatic C−F[105] bond activations, and behaviour in protic acids.[43] DFT has also been employed to examine coordination geometries and ligand dissociation energies in Cd^{II} and Zn^{II} aggregates of $[Pt_2(\mu\text{-}S)_2(PPh_3)_4]$.[32] DFT has been used to rationalise the behavior of the monothiocarbamato complex $[Pt_2(\mu\text{-}S)(\mu\text{-}SC(O)NMe_2)(PPh_3)_4]^+$ towards Hg^{II} fragments and suspected Hg···O interactions in the resulting dicationic aggregate.[106] Interesting supramolecular Pd^{II} and Pt^{II} macrocycles of self-assembled $\{M_2S_2\}$ units were probed with DFT revealing significant electronic communication throughout the bridging dithiolate ligands.[107] This is perhaps the quintessential example of a chemical system, coincidentally involving the $\{Pt_2S_2\}$ core, that has only recently been accessible for quantum chemical calculations thanks to the development of DFT and readily available computational infrastructure.

1.4 Project goals

The work reported herein will aim to further develop the rich chemistry of both **1a** and **1b**, primarily employing ESIMS as a synthetic targeting tool. Reactions will be first examined in the micro-scale by ESIMS, and depending on the resulting spectra, carried out on a larger scale for further analysis by ESIMS and traditional techniques such as NMR spectroscopy and single-crystal XRD.

1.5 General experimental

$[Pt_2(\mu\text{-}S)_2(PPh_3)_4]$ **1a** was synthesised from $cis-[PtCl_2(PPh_3)_2]$ and powdered sodium sulfide nonahydrade (Sigma) in a benzene suspension following a procedure in the literature.[68] $[Pt_2(\mu\text{-}Se)_2(PPh_3)_4]$ **1b** was synthesised by a modification of the literature method.[73e,76] Sodium tetraphenylborate, ammonium hexafluorophosphate, and sodium tetrafluoroborate were obtained from Sigma. Lithium bis(pentafluoroethanesulfonyl)imide was obtained from 3M. Reagent or laboratory grade solvents were used without regard for the exclusion of light, air, or water. High resolution mass spectra were recorded on a Bruker MicrOTOF instrument which was calibrated periodically using a solution of sodium formate in methanol. Although care was taken to calibrate prior to data collection, due to the age of the instrument occasionally mass drift occurred during use and some spectra reported herein display a larger mass difference than typically accepted for a high resolution instrument. Elemental analyses were obtained by either the Chemical Analysis Facility of Macquarie University of Sydney, Australia or the Campbell Microanalytical Laboratory of the University of Otago, Dunedin, New Zealand. Calculated isotope patterns and synthetic combinatorial patterns were generated using an in-house FORTRAN program[108] implementing the multidimensional Fourier transform algorithm of Ipsen.[109] ^{1}H (600.17 MHz), $^{13}C\{^{1}H\}$ (150.91 MHz), $^{31}P\{^{1}H\}$ (242.95 MHz), and $^{195}Pt\{^{1}H\}$ (129.02 MHz) NMR spectra were recorded on a JEOL JNM-ECZ600R/S1 spectrometer. $^{31}P\{^{1}H\}$ (121.49 MHz) NMR spectra were recorded on a Bruker DMX

spectrometer. The molecular graphics program Pymol[110] was used to prepare crystallographic images which were annotated for inclusion in LaTeXwith vector graphics editor Inkscape.[111]

Simulated spin systems

Platinum has only one stable NMR active isotope (^{195}Pt, $I = \frac{1}{2}$) which is also the most abundant at 33.8%. Hence, complexes containing two Pt centers, such as those reported in this thesis, will be NMR inactive $(1 - .338)^2 = 43.8\%$, active in only one Pt nucleus $(.338)^1 * (1 - .338)^1 * 2_n = 44.8\%$, and active in both Pt nuclei $(.338)^2 = 11.4\%$. These relative ratios were represented in the simulation by constructing multiple spin systems and weighting them accordingly in the program Mnova.[112] Spin-spin coupling constants (SSCC) were estimated from recorded spectra where possible. Resolution (sweep/points), instrument operating frequency, and line widths ($\Delta\nu$) were adjusted to conform with experimentally acquired spectra.

Chapter 2

Nucleophilic ring-opening reactions of various epoxides with $[Pt_2(\mu\text{-}S)_2(PPh_3)_4]$

2.1 Introduction

Ring-opening reactions of epoxides, also referred to as oxiranes, by thiol nucleophiles have been very well studied,[113] and are often so rapid and predictable they can be considered as thiol-click chemistry.[114] In particular, nucleophilic ring-opening reactions of epoxides by thiols and selenols (Scheme 2.1) provide accessible routes to β-hydroxy sulfides and selenides, which are have a wide range of applications including as synthons for pharmaceuticals[115] and natural products.[116] The importance of these reactions is further evidenced by the large amount of work in the literature, where there is an increasing drive to find novel routes to these synthons that avoid organic solvents and toxic catalysts. Recent additions have explored these reactions

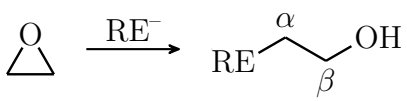

Scheme 2.1: A general scheme for epoxide ring-opening by a chalcogenide anion (E = S, Se) resulting a β-hydroxy compound.

in water,[117–119] solvent-free conditions,[120,121] or recyclable ionic-liquid systems.[122]

The nucleophilic propensity of the μ-sulfide centers in $[Pt_2(\mu\text{-}S)_2(PPh_3)_4]$ **1a** has been extensively explored,[42b] and in particular they have been shown to readily engage in alkylation reactions,[17] even with mild alkylating agents such as chlorinated organic solvents.[123] The μ-selenide analogue $[Pt_2(\mu\text{-}Se)_2(PPh_3)_4]$ **1b** similarly exhibits strong nucleophilic character,[124] although as of yet has received only a fraction of the interest enjoyed by the sulfide analogue **1a**. However, despite the preponderance of literature on the alkylation and arylation chemistry of these systems, nucleophilic ring-opening reactions of three-membered homo- and hetero-cycles has yet to be examined. The potent nucleophilicity of the bridging sulfide and selenide ligands in **1a** and **1b** should provide a facile route to novel derivatives of these complexes containing β-hydroxy sulfide and selenide ligands.

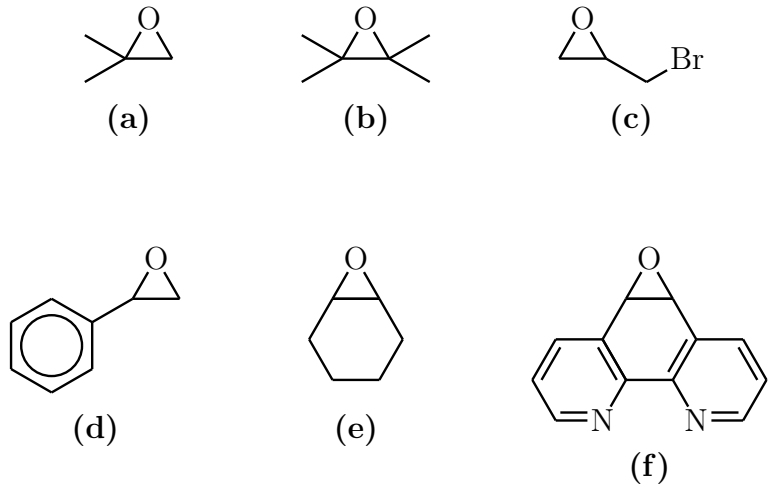

Figure 2.1: Epoxides to be examined: **(a)** 2,2-dimethyloxirane, **(b)** 2,3-dimethyl-2,3-epoxybutane, **(c)** epibromohydrin, **(d)** styrene oxide, **(e)** cyclohexene oxide, **(f)** 5,6-epoxy-5,6-dihydro-[1,10]-phenanthroline

To rapidly examine potential ring-opening reactions on a micro-gram scale, Electrospray ionisation mass spectrometry (ESIMS) will be employed as a solution-based screening tool for directing synthesis of targeted derivatives. ESIMS was initially developed to facilitate gentle ionisation of large bio-molecules and proteins,[79] and has found increasing use analyzing delicate inorganic species in solution.[125] Although

ESIMS is destructive, the highly-sensitive mass spectrometer requires only µg quantities of material, ideal when dealing with costly platinum group metals. Additionally, the technique is rapid and solution based, allowing for reactions to be followed in near real time. As the complexes **1a** and **1b** and their derivatives ionize readily and contain several polyisotopic elements, ESIMS is particularly suited for directed synthetic studies of novel derivatives of **1a** and **1b**,[80] so much so that the combinatorial technique has previously been referred to as "synthetic prospecting".[126] Starting with the alkylating agent epibromohydrin, the examination of several common epoxides (Figure 2.1) with **1a** and **1b** is reported. If successful, the ring-opening reactions will be repeated macroscopically and the resulting derivatives characterised with traditional techniques, complementing the initial ESIMS examinations.

2.2 Epibromohydrin: building a bridge via ring-opening and alkylation

In a study examining nucleophilic attack on epibromohydrin by the catecholate anion, ring-opening was found to dominate alkylation but was temperature dependant and the reaction rates were comparable at around 146 °C.[127] Both routes resulted in intramolecular ring-opening of the β-ether oxirane at the less substituted carbon to give a new six-membered ring. Epibromohydrin has been used previously as an alkylating agent prior to intramolecular nucleophilic ring opening to effect cylopropane formation in epoxy bis-sulfones[128] and epoxy-α-cyanosulfones[129] and in the synthesis of cyclic guanidines.[130] Attack by the hard nucleophile hydroxide on epihalohydrins (X = Cl, Br) has been examined computationally in both acidic and basic conditions.[131] For epibromohydrin, the alkylation reaction was preferential in basic conditions as the Br^- was a superior leaving group, while nucleophilic ring-opening at the methylene C3 carbon was favored in acidic conditions. A general trend observed across all epihalohydrins was an avoidance of nucleophilic ring-opening at the

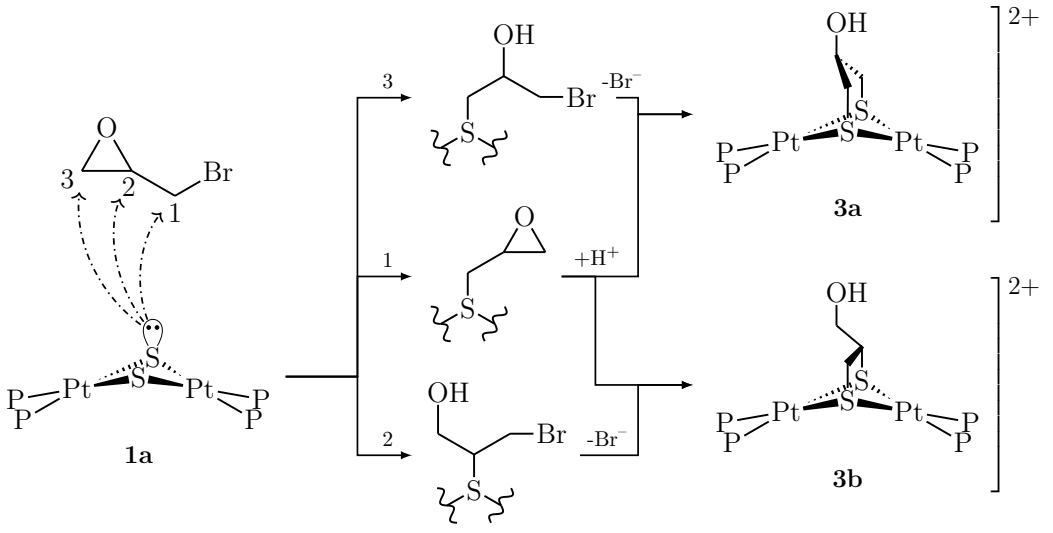

Scheme 2.2: Proposed reaction scheme showing sites of nucleophilic attack on epibromohydrin by **1a**. The resulting cationic intermediates undergo further alkylation or ring-opening intramolecularly via the underivatised sulfide resulting in two possible isomers **3a** or **3b**.

sterically crowded methine C2 position.

Platinum(II) phosphine dimers with a $\{Pt_2S_2\}$ core are known to readily undergo alkylation,[17,18] even with mild alkylating agents, due to the high nucleophilicity of the sulfide centers. However, dialkylations of these dimers are more difficult to achieve, and typically involve very strong alkylating agents[126,132] or forcing conditions.[66] Dialkylated species of $[Pt_2(\mu\text{-}S)_2(PPh_3)_4]$ **1a** with an overhead bridge are more accessible, and have been synthesised with dialkylating agents such as *cis*-1,4-dichlorobut-2-ene.[124e,133] Hence, the reaction between **1a** and epibromohydrin was carried out to see if a mild alkylating agent with a reactive epoxide could provide a convenient route to a diaklyated derivative of **1a** (Scheme 2.2).

The reaction between **1a** and epibromohydrin in methanol resulted in a gradual

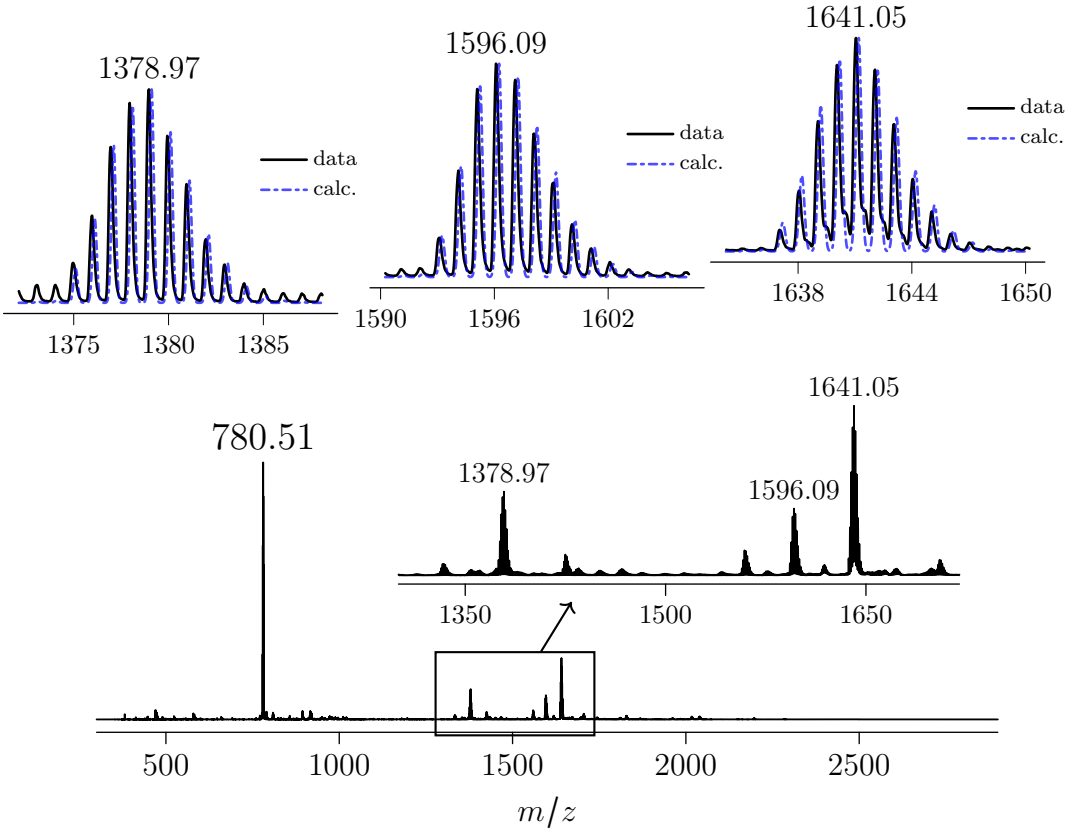

Figure 2.2: ESI mass spectrum of **1a** and epibromohydrin. The main inset is an expanded view of the mass range *m/z* 1320 - 1700. The top insets are observed peaks at *m/z* 1378.97, 1596.09, and 1641.05 compared to calculated isotope patterns for $[Pt_2(\mu\text{-}S{-}CH_2CH(OH)CH_2{-}\mu\text{-}S)(PPh_3)_3Br]^+$, and ion pairs $[\mathbf{3}][Cl]^+$, and $[\mathbf{3}][Br]^+$ respectively.

change from a cloudy orange solution to clear and colorless, typically observed for **1a** when both sulfide centers are functionalised.[124e] The reaction solution was quickly examined by ESIMS and the recorded mass spectrum is displayed in Figure 2.2. The base peak of the spectrum is a dication at *m/z* 780.51 and is assigned as the dialkylated tricyclic ring-opened species $[Pt_2(\mu\text{-}S{-}C_3H_5OH{-}\mu\text{-}S)(PPh_3)_4]^{2+}$ (**3**) and has a calculated isotope pattern in close agreement with the observed peak (calc. *m/z* 780.64). The spectrum has various lower intensity ions ca. *m/z* 1300 to 1700 as seen in the inset of Figure 2.2. At *m/z* 1559.12 is a cation assigned as the deprotonated parent dication $[M - H]^+$ (calc. *m/z* 1559.27), consistent with a moderately acidic hydroxyl group. The moderately intense peak at *m/z* 1378.95 appears to be a result of triphenylphosphine ligand substitution in **3** by Br^-, and is assigned as $[Pt_2(\mu\text{-}S{-}C_3H_5OH{-}\mu\text{-}S)(PPh_3)_3Br]^+$ (calc. *m/z* 1379.11). Such bromide displacement of triphenylphosphine in dicationic species has been observed previously[132] and was mitigated by the addition of a molar equivalent of the phosphine ligand.

The analogous Cl^- and I^- cations are observed at *m/z* 1334.00 (calc. *m/z* 1334.16) and *m/z* 1424.94 (calc. *m/z* 1425.09) respectively, with the halide source possibly the commercially acquired epibromohydrin or lingering anions within the

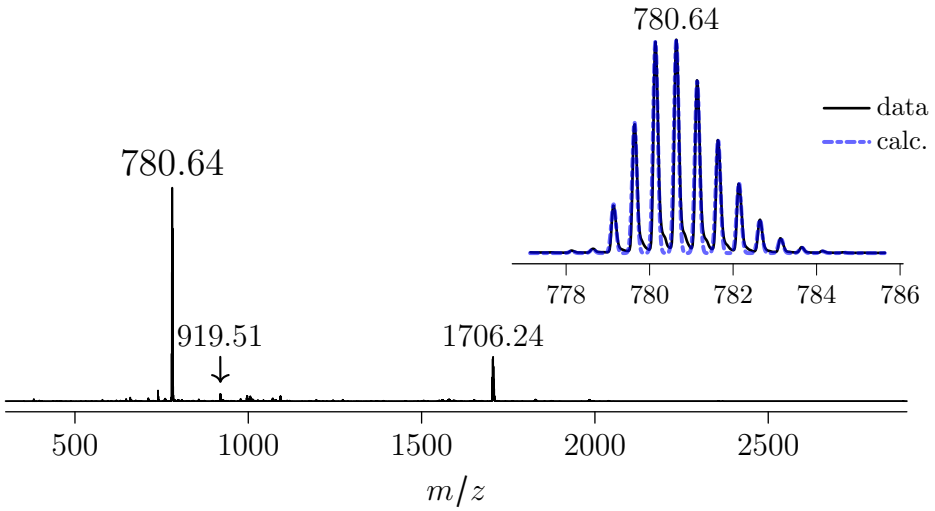

Figure 2.3: ESI mass spectrum of [**3**]PF_6 in methanol/CH_2Cl_2. The inset is an isotope pattern comparison of the peak at *m/z* 780.64 and a calculated pattern for the proposed dication $[Pt_2(\mu\text{-}S{-}CH_2CH(OH){-}CH_2{-}\mu\text{-}S)(PPh_3)_4]^{2+}$ (calc. *m/z* 780.64), capillary exit voltage 60 V.

spectrometer. Monocationic ion pairs $[M][X]^+$ formed by the dicationic **3** and the anions Cl^-, Br^-, and PF_6^- are also observed in the mass spectrum at *m/z* 1596.10 (calc. *m/z* 1596.25), *m/z* 1641.05 (calc. *m/z* 1641.20), and *m/z* 1706.09 (calc. *m/z* 1706.24) respectively. As ammonium hexafluorophosphate had not been added to the reaction solution, the source of this non-coordinating anion is most likely contamination within the spectrometer.

An identical preparation was carried out with a molar equivalent of PPh_3 added to the reaction solution to counter halide ligand substitution. An off-white solid was isolated from the reaction solution by the metathetic reaction with NH_4PF_6. The acquired ESIMS spectrum in Figure 2.3 shows a successful suppression of any triphenylphosphine substitution, and appears much cleaner than the reaction solution of the initial experiment. The peak at *m/z* 1706.24 is assigned as the monocationic ion pair $[\mathbf{3}][PF_6]^+$. A dicationic peak of low relative intensity at *m/z* 919.51 is tentatively identified as the triphenylphosphine oxide (TPPO) adduct ion $[\mathbf{3}][O{=}PPh_3]^{2+}$

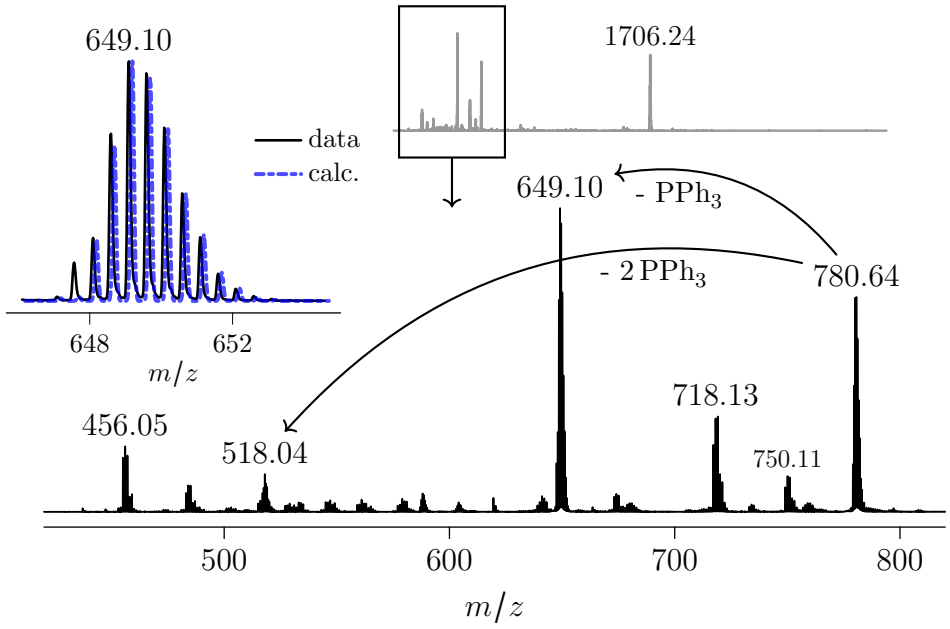

Figure 2.4: ESI mass spectrum of $[\mathbf{3}][PF_6]_2$ in CH_2Cl_2/methanol at an elevated capillary exit voltage of 180 V to induce fragmentation. An expanded view of the mass range *m/z* 400 - 800 is below the full spectrum in the top inset. The left inset is an isotope pattern comparison of the dication observed at *m/z* 649.10 and a calculated pattern for $[M - PPh_3]^{2+}$ (calc. *m/z* 465.04).

(calc. *m/z* 919.68). The source of TPPO is most likely excess or displaced triphenylphosphine in the reaction solution that has been oxidised, either aerially or within the mass spectrometer. TPPO is known to engage readily in hydrogen bonding through the phosphoryl oxygen.[134–136] To probe the proposed ring-opened derivative **3** further, a capillary exit voltage of 180 V was employed to induce fragmentation and another ESI mass spectrum was recorded (Figure 2.4).

Typical fragmentation ions for derivatives of **1a** when exposed to increased capillary exit voltages are related to triphenylphosphine loss.[29a] The loss of one and two triphenylphosphine ligands from **3** are observed at *m/z* 649.10 and *m/z* 518.05 respectively, with the latter detected at a very low relative intensity, consistent with a highly unstable exposed Pt^{II} center and large molecular charge (Figure 2.5 *(b)*). The known cyclometallated Pt fragmentation ion $[(Ph_3P)P\overline{t(PPh_2C_6H_4)}]^+$ [137] is observed at *m/z* 718.14 with related ions assigned as $[P\overline{t(PPh_2C_6H_4)}]^+$ (calc. *m/z* 465.05) and $[(Ph_3P)P\overline{t(PPh_2C_6H_4)}S]^+$ (calc. *m/z* 750.11) observed at *m/z* 456.04 and *m/z* 750.11 respectively. A comparison of the observed peaks at *m/z* 456.05 and 718.13 and calculated isotope patterns for the proposed cations are displayed in Figure 2.5. The intensity of the ion pair $[\mathbf{3}][PF_6]^+$ observed in the spectrum at *m/z* 1706.25 is at a higher relative intensity, consistent with charge reduction pathways of dicationic species exposed to a high voltage.

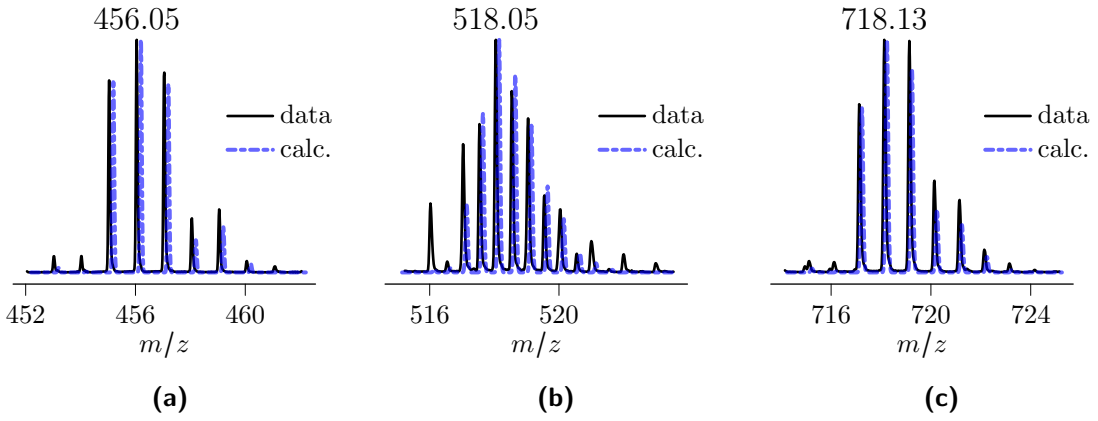

Figure 2.5: Isotope pattern comparisons from Figure 2.4. Observed peaks are compared with calculated patterns for **(a)** $[P\overline{t(PPh_2C_6H_4)}]^+$; **(b)** $[\mathbf{3}$ - 2 $PPh_3]^{2+}$; **(c)** $[(Ph_3P)P\overline{t(PPh_2C_6H_4)}]^+$.

To further investigate the isolated hexafluorophosphate salt [**3**][PF_6]$_2$, a $^{31}P\{^1H\}$-NMR experiment was carried out on a chloroform-*d* solution of the complex. The resulting spectrum (Figure 2.6) is representative of a symmetric dialkylated derivative of **1a**,[54,64] the single resonance appearing as a sharp singlet at δ 19.2 ppm with a $^1J_{(PtP)}$ coupling of 3040 Hz. Upon closer inspection of the high field satellite, it appears to be two nearly coincident satellites, while the low field satellite at δ 31.6 ppm is coincident. The difference between the $^1J_{(PtP)}$ couplings is around 40 Hz, indicative of a slight magnetic asymmetry in **3**. The relatively close magnitudes of these couplings strongly suggest the structural configuration of **3** is indeed the symmetric overhead-bridged $[Pt_2(\mu\text{-}S{-}CH_2CH(OH)CH_2{-}\mu\text{-}S)(PPh_3)_4]^{2+}$ (**3a**, Scheme 2.2).

A sharp resonance of moderate relative intensity at δ 29.8 ppm and is assigned as TPPO, although the reported chemical shift of TPPO in $CDCl_3$ from the literature is slightly upfield at δ 29.3 ppm.[138] The presence of TPPO is consistent with the observation of hydrogen bonding adducts of the phosphine oxide in ESI mass spectra. Aerial oxidation of triphenylphosphine (which was added to the reaction solution to suppress charge induced ligand substitution by halide ions) seems the most likely source. Interestingly, another sharp peak of lower relative intensity (Figure 2.6 †)

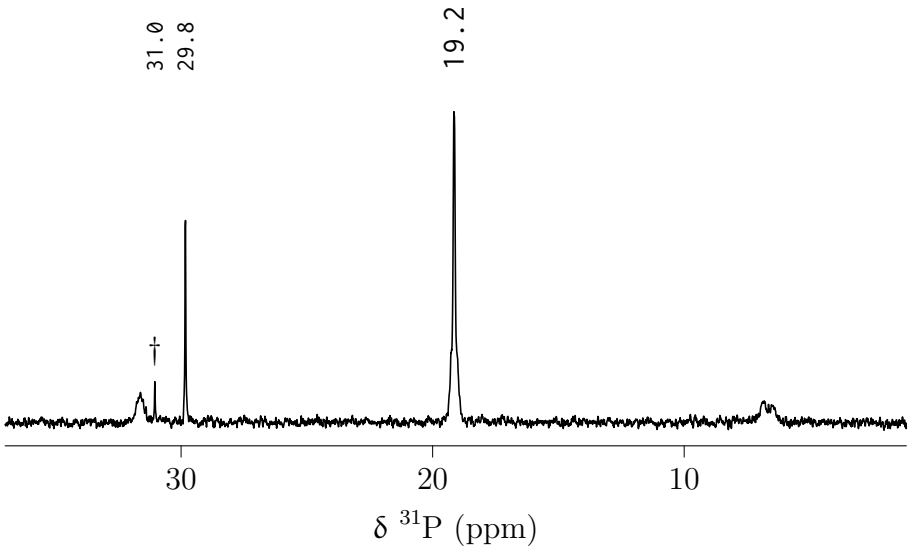

Figure 2.6: $^{31}P\{^1H\}$-NMR (121.49 MHz, $CDCl_3$) of **3**[PF_6]$_2$. The resonance at δ 31.0 ppm is marked †.

appears at δ 31.0 ppm. Previous ^{31}P NMR experiments have established downfield chemical shifts occur when TPPO is exposed to hydrogen bond donors,[139] and that $\Delta\nu$ correlates with the strength of the donor. A study involving the effect of hydrogen bond donors on the ^{31}P NMR δ of triethylphosphine oxide (TEPO) determined a high correlation between donor strength and downfield shift, with alkyl alcohols in the range of 1-7 ppm.[140] The resonance at δ 31.0 ppm is perhaps the result of a hydrogen bonding TPPO adduct with **3** in solution, wich would be consistent with a slight downfield shift for TPPO. Triphenylphosphine sulfide, which has been observed previously in ^{31}P{^{1}H}-NMR experiments carried out on derivatives of **1a**,

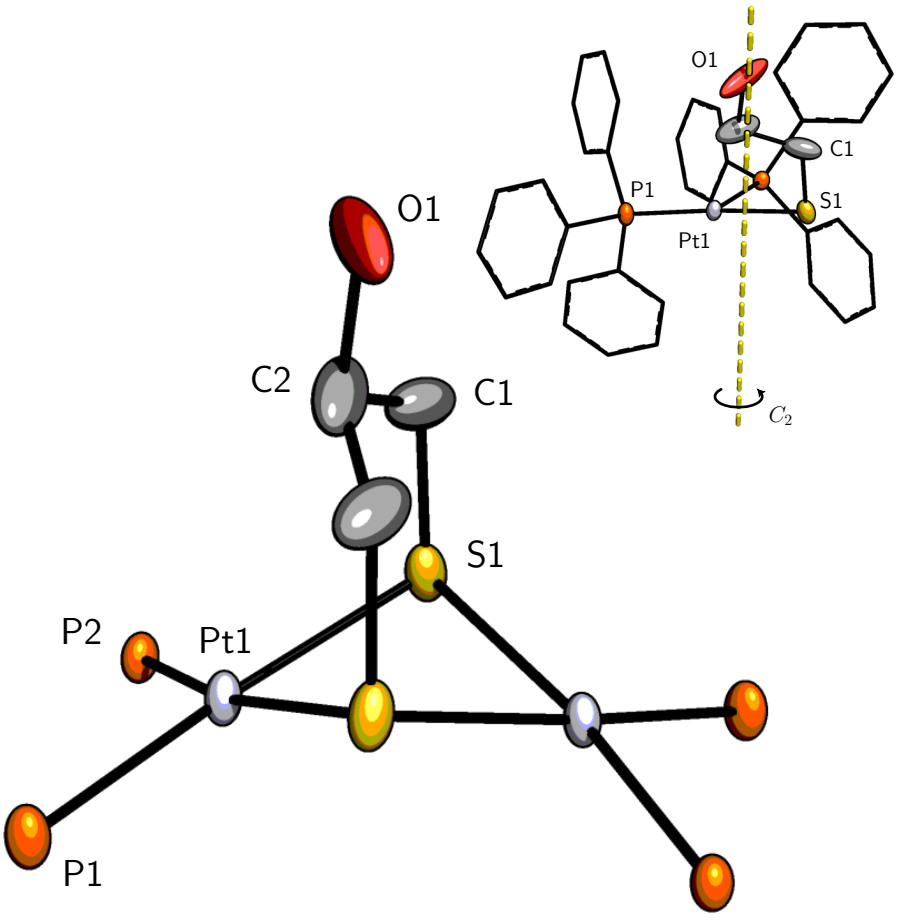

Figure 2.7: The crystal structure of **3**$[PF_6]_2 \cdot CH_2Cl_2$, omitted for clarity are PF_6^- anions, solvent, and phenyl rings of PPh_3 ligands. Thermal ellipsiods are displayed at 50% probability. The inset shows the asymmetric unit and two-fold rotation axis passing through the $\{Pt_2(\mu\text{-}SR)_2\}$ core, phenyl rings of PPh_3 shown in a stick representation for clarity.

resonates further downfield (δ 43.2 ppm in $CDCl_3$) and is ruled out.[138]

Clear colorless hexagonal crystals of [**3**]$(PF_6)_2$ were obtained by vapor diffusion of diethyl ether into a CH_2Cl_2 solution of the complex. Rapid solvent loss was observed when examining the crystals under a microscope, and perfluoropolyether (PFPE) oil was used to seal and fix them to the microloop for analysis. The complex crystallises as the dichloromethane solvate in *C2/c* (Figure 2.7), and has two independent hexafluorophosphate anions, one of which has a slight positional disorder and is very close to an inversion center. The other anion is positioned axially on a two-fold rotation axis and refines without issue. Running through the center of the dication is the same two-fold rotation axis, and as such the anisotropic displacement parameters of O1 and C2 were heavily skewed and required restraints to model properly as these atoms lie very close to, but not on the rotation axis. Derivatives of **1a** with this central two-fold rotational symmetry element are not uncommon, and are found in the similar overhead-bridged dicationic $[Pt_2(\mu\text{-}S{-}CH_2CH{=}CHCH_2{-}\mu\text{-}S)(PPh_3)_4][BPh_4]_2$[124e] and the β-diketonate Cu^{II} cation $[Pt_2(\mu_3\text{-}S)_2(PPh_3)_4Cu(CH_3COCHCOCH_3)][PF_6]$.[29a] The symmetry of the complex is evident in the similarity of the Pt−S and Pt−P bond lengths, consistent with the observed $^{31}P\{^1H\}$-NMR spectrum. The dihedral angle Pt1-S1-S1a-Pt1a is significantly hinged at 134.38°, similar to other thiolato overhead-bridged dications.[62c,124e] The Pt^{II} centers are very close to

Table 2.1: Selected bond lengths (Å), angles (°), and torsions (°) for **3**$[PF_6]_2 \cdot CH_2Cl_2$. Atoms marked (′) are generated with symmetry code $[2-x, y, \frac{3}{2}-z]$.

Pt1-P1	2.2890(18)	P2-Pt1-S1′	167.51(6)
Pt1-P2	2.2964(16)	P2-Pt1-S1	87.29(6)
Pt1-S1′	2.3580(16)	S1-Pt1-S1′	80.22(7)
Pt1-S1	2.3694(17)	C1′-S1′-Pt1	103.2(3)
C1′-C2	1.524(14)	C1-S1-Pt1	102.8(4)
C1-C2	1.509(14)	C2-C1-S1	116.7(9)
S1-C1	1.801(9)	O1-C2-C1	107.0(10)
O1-C2	1.43(2)	Pt1-S1-C1-C2	24.7(9)
P1-Pt1-P2	99.36(6)	Pt1-S1-S1′-Pt1′	134.38(8)
P1-Pt1-S1′	93.13(6)	S1-C1-C2-O1	174.3(9)
P1-Pt1-S1	173.27(6)	S1-C1-C2-C1′	49(1)

an ideal square-planar geometry, quantified by a τ_4' parameter of 0.12.[141] After application of thermal and positional restraints, chemically reasonable bond distances for the overhead bridge were obtained, comparable to the similar overhead-bridged derivative $[Pt_2(\mu\text{-}S{-}CH_2C(=O)CH_2{-}\mu\text{-}S)(PPh_3)_4][BPh_4]_2$.[62c]

A polymorph of **3**$[PF_6]_2$ was identified by a subsequent single-crystal XRD experiment (Figure 2.8). Although the recorded data are of insufficient quality for publication, with the help of significant positional and thermal constraints on the phenyl rings of the PPh_3 ligands, the core of the structure was refined anisotropically revealing the structure as the C2 isomer of the DCM solvate. Two PF_6 counterions were located and included in the refinement. Interestingly, the OH group lies over a Pt center with a Pt-O distance of 2.90 Å. While this is substantially longer than a formal bonding distance (≈ 2 Å), it is closer than the similar dication $[Pt_2(\mu\text{-}S{-}CH_2C(=O)CH_2{-}\mu\text{-}S)(PPh_3)_4]^{2+}$ in which the ketone had a Pt-O separation of 3.79 Å.[62c] The Pt-P bonds for Pt2 appear to be longer (Pt2-P4, 2.307(8); Pt2-P3, 2.308(8) Å) than for Pt1 (Pt1-P1, 2.282(6); Pt1-P2, 2.286(6) Å), possibly due to the close proximity of O1 and Pt2. Unfortunately, the poor data quality and resulting

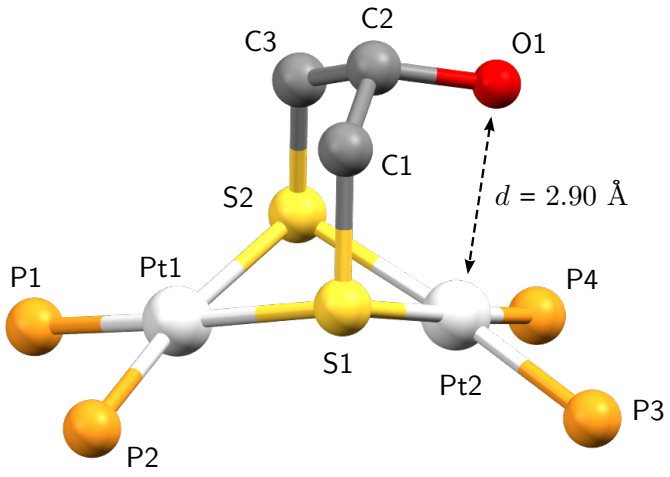

Figure 2.8: Crystal structure of the C2 isomer of **3**$[PF_6]_2$, crystallising in $P2_1/c$. Phenyl rings of PPh_3 ligands, PF_6^- counterions, and protons of C1, C2, C3, and O1 are omitted for clarity.

high esd's in the isomer preclude any rigorous comparison of bond distances. Aside from the apparent slightly asymmetry of the Pt-P coordination environments and orientation of the alcoholic OH, bond distances and angles in the isomer appear to agree with the dichloromethane solvate. The Pt^{II} centers in the isomer also adhere to the expected square-planar geometry despite the moderately acute hinge torsion of 132° positioning the bulky triphenylphospine ligands in close proximity.

2.3 Epibromohydrin and $[Pt_2(\mu\text{-}Se)_2(PPh_3)_4]$

The epoxide epibromohydrin was next reacted with the μ-selenide complex $[Pt_2(\mu\text{-}Se)_2(PPh_3)_4]$ **1b** in methanol, with the initially cloudy brown reaction solution transforming to a clear red-brown solution after 48 hours of stirring at room temperature. The ESI mass spectrum of the reaction solution is shown in Figure 2.9. The proposed derivative resulting from alkylation and ring-opening $[Pt_2(\mu\text{-}Se{-}CH_2CH(OH)CH_2{-}\mu\text{-}Se)(PPh_3)_4]^{2+}$ **4** (calc. *m/z* 828.09) is observed at *m/z* 827.95, and is the base peak of the spectrum.

Similar to the reaction of epibromohydrin with the sulfide analogue **1a**, halide ligand substitution with triphenylphosphine appears to be occurring as the proposed $[\mathbf{4} - PPh_3][X]^+$ (X = Cl, Br, I) cations are observed at *m/z* 1428.92, 1472.88, and 1520.87 respectively. A low-intensity cation at *m/z* 1655.06 is tentatively assigned as

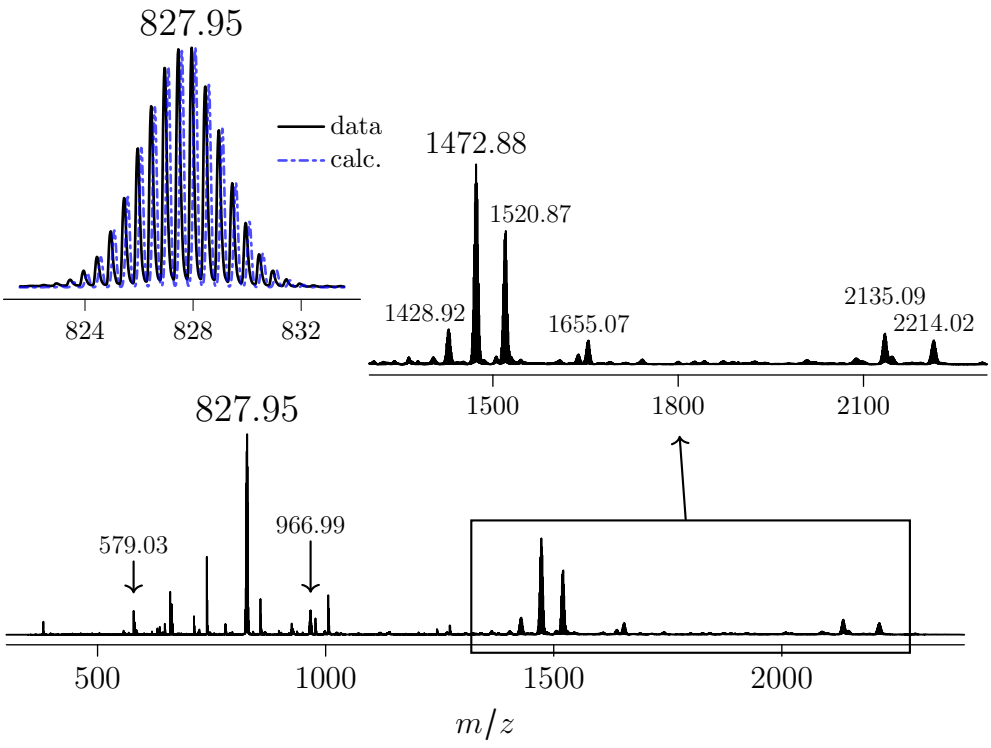

Figure 2.9: ESI mass spectrum of **1b** and epibromohydrin in methanol after 48 hours. The left inset is an isotope pattern comparison of the peak observed at *m/z* 827.95 and a calculated pattern for the proposed dicationic species $[Pt_2(\mu\text{-}Se{-}CH_2CH(OH)CH_2{-}\mu\text{-}Se)(PPh_3)_4]^{2+}$ **4** (calc. *m/z* 828.08). The right inset is an expanded view of the mass range *m/z* 1300 - 2300. Capillary exit voltage 60 V.

$[\mathbf{4} - \mathrm{H}]^+$. Two cations at *m/z* 2135.09 and 2214.02 are assigned as trimetallic species $[Pt_2(\mu_3\text{-}Se)_2(PPh_3)_4PtX]^+$ (X = SeH, calc. *m/z* 2135.11; Se_2H, calc. *m/z* 2214.03). Although both these ions have a low relative intensity, calculated isotope patterns for these proposed species closely match the observed data. Analogous ions were not observed in the previous reaction of epibromohydrin with the sulfide analogue **1a**. Interestingly, a dication observed in the spectrum at *m/z* 966.99 is assigned as a triphenylphosphine oxide (TPPO) adduct with the parent dication, $\mathbf{4}[OPPh_3]^{2+}$ (calc. *m/z* 967.13), presumably due to a non-covalent interaction between the basic oxygen of the λ^5-phosphanone and the alcoholic proton of the dication. The analogous ion was also identified by ESIMS in solutions of complex **3**. Additional ESIMS evidence for TPPO in the reaction solution is a peak at *m/z* 579.03, proposed to be the sodium aggregate ion $[Na][OPPh_3]_2^+$.

The reaction was repeated with a molar equivalent of PPh_3 used to suppress halide ligand substitution, and was examined immediately by ESIMS (Figure 2.10). As was the case for the sulfide analogue **3**, the mass spectrum is now devoid of any

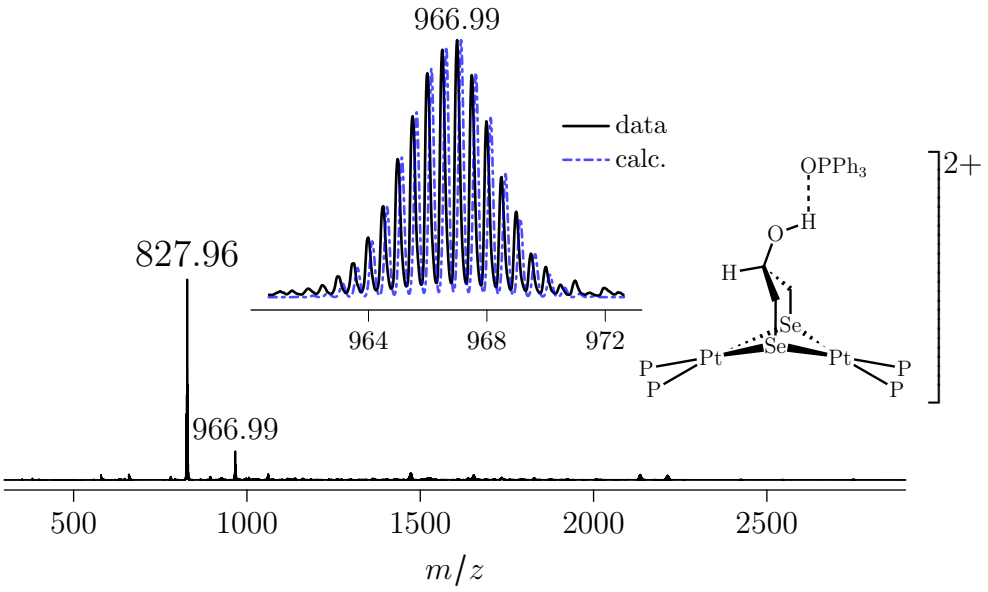

Figure 2.10: ESI mass spectrum of **1b** and epibromohydrin with a molar equivalent of PPh_3 added to suppress halide ligand substitution. The inset is an isotope pattern comparison of the peak observed at *m/z* 966.99 and a calculated isotope pattern for $[\mathbf{4}][OPPh_3]^{2+}$ (calc. *m/z* 967.13, right inset). Capillary exit voltage 60 V.

halide substitution ions of the type [**4** - PPh_3 + X]$^+$ (X = Cl, Br, I). The previously assigned TPPO hydrogen bonding adduct ion is still present at *m/z* 966.99. There is a strong agreement between the observed peak and a calculated isotope pattern for this proposed aggregate ion **4**[$OPPh_3$]$^{2+}$, as can be seen in Figure 2.10.

The dication was isolated with sodium hexafluorophoshpate to give **4**·[PF_6]$_2$. The ESI mass spectrum of the collected solid dissolved in DCM/methanol is very similar to the mass spectrum in Figure 2.10. An additional peak observed at *m/z* 1800.87 is tentatively assigned as the expected aggregate ion of the parent dication and hexafluorophosphate [**4**][PF_6]$^+$ (calc. *m/z* 1801.14). There is also a peak *m/z* 1061.01 at a low relative intensity, tentatively assigned as [Pt(PPh_3)$_3$Br]$^+$ (calc. *m/z* 1061.16). This peak was not observed in the previous reaction of **1a** and epibromohydrin, and is presumably related to the increased concentration of triphenylphosphine and the weaker Pt-Se bond.[184c]

Fragmentation of [**4**](PF_6)$_2$ was investigated by ESIMS by increasing the capillary

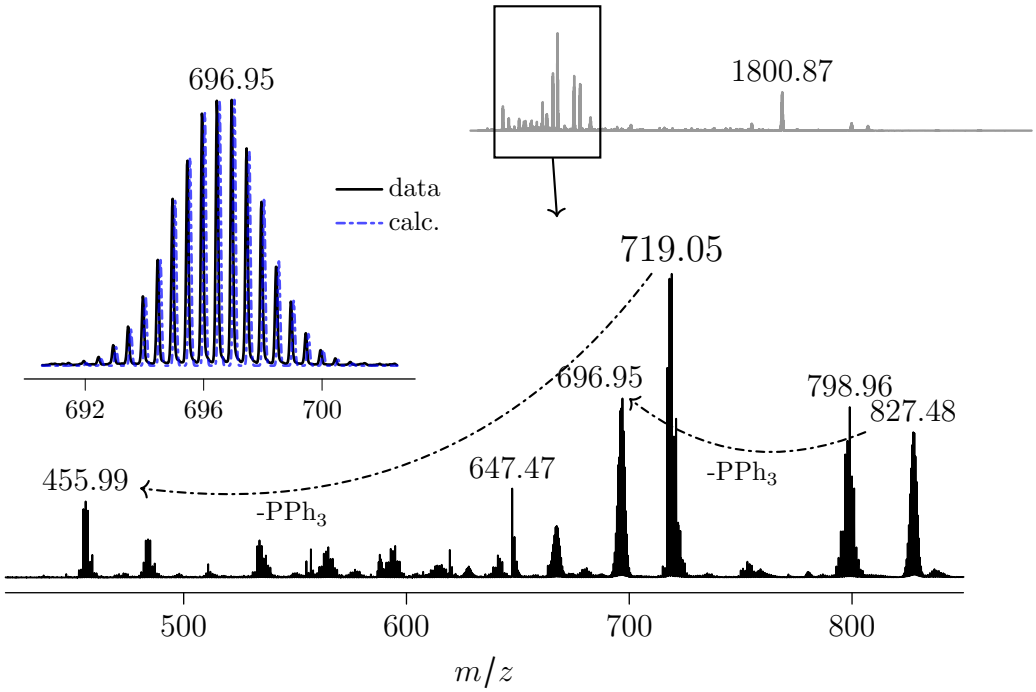

Figure 2.11: An expanded view of the ESI mass spectrum of **4**[PF_6]$_2$ in DCM/methanol. The left inset is an isotope pattern comparison of the peak observed at *m/z* 696.95 and a calculated pattern for [**4** − PPh_3]$^+$ (calc. *m/z* 697.04). The top inset is the complete mass spectrum. Capillary exit voltage 180 V.

exit voltage to 180 V (Figure 2.11). Some immediate parallels can be drawn with the fragmentation spectrum for the sulfide analogue and epibromohydrin, such as the increase in relative intensity of the $[\mathbf{4}][PF_6]^+$ cation at *m/z* 1800.87, the triphenylphosphine loss dication $[\mathbf{4} - PPh_3]^{2+}$ at *m/z* 696.95 (calc. *m/z* 697.04), and various mononuclear cyclometallated platinum species. At *m/z* 455.98 is a peak assigned as $[\overline{Pt(PPh_2C_6H_4)}]^+$ (calc. *m/z* 456.05). Two other peaks with isotope patterns consistent with mononuclear platinum species are at *m/z* 719.05 and *m/z* 798.95. The peak at *m/z* 719.05 is tentatively assigned as an overlapping combination of two mononuclear Pt^{II} species, the known cyclometallated $[(Ph_3P)\overline{Pt(PPh_2C_6H_4)}]^+$ (calc. *m/z* 718.14)[137] and hydride $[Pt(PPh_3)_2H]^+$ (calc. *m/z* 720.15).[82] The peak at *m/z* 798.95 displays an isotope pattern that is more complicated and is tentatively assigned as a combination of three different mononuclear platinum species: the oxidised selenide species $[Pt(PPh_3)_2Se]^{\bullet+}$, the selenol $[Pt(PPh_3)_2SeH]^+$, and the cyclometallated selenol $[(Ph_3P)\overline{PtPPh_2C_6H_4-Se}]^+$. High-mass cations observed in the spectrum at *m/z* 2134.77 and 2213.68 are tentatively assigned as $[Pt_2(\mu_3\text{-}Se)_2(PPh_3)_4PtSeH]^+$ and $[Pt_2(\mu_3\text{-}Se)_2(PPh_3)_4Se_2H^+]$ respectively.

In comparison with the reaction of epibromohydrin and **1a**, a similar reactivity in the **1b** system is observed, with the formation of an overhead-bridged species via alkylation/ring-opening followed by an intramolecular ring-opening/alkylation. Phosphine ligand substitution on the dication **4** by free halide anions is also observed and successfully mitigated with the addition of PPh_3. The increase in observed fragmentation species, some of which are assigned as mononuclear Pt^{II} species, and the tentative identification of the trimetallic aggregates are all consistent with a weaker Pt-Se bond and the associated propensity for the selenide system to undergo metal scrambling reactions. Unfortunately, the isolated derivative $[\mathbf{4}](PF_6)_2$ was left for an extended period before characterisation by which time it has suffered decomposition as evidenced by ESIMS and $^{31}P\{^1H\}$-NMR spectroscopy. As the reaction was initially successful, it is highly recommended that the synthesis be repeated and the resulting derivative fully characterised.

2.4 Ring-opening of cyclohexene oxide by 1a

Cyclohexene oxide has been extensively examined in nucleophilic ring-opening reactions with sulfur nucleophiles[142] as the introduction of contiguous stereogenic centers in the resulting β-hydroxy-mercaptans/-sulfides is synthetically desirable.[143,144] For derivatised cyclohexene oxides, the reaction is well understood and highly regioselective, obeying the Fürst-Plattner rule[145] which favors a trans-diaxial configuration of the resulting 1,2-bifunctionalised product. Ring inversion to a more energetically favoured *trans* equatorial chair conformation is also typically observed for these derivatives. Various catalysts have been successfully employed to control stereoselectivity and enhance the sluggish ring-opening of the *meso*-epoxide such as ionic liquids,[122b] Schiff bases,[146] and dithiophosphorous acids.[147] Lewis acid catalysts have also received considerable attention,[148,149] of which the generally accepted catalytic effect involves a lowering of the epoxide's LUMO such that the energy difference with respect to the HOMO of the incoming nucleophile is significantly narrowed. A recent mechanistic DFT examination of Lewis acid catalysed nucleophilic ring-opening of cyclohexene oxide attributed the catalytic effect to a reduction in Pauli repulsion experienced by the incoming nucleophile.[150] Rather than manipulating the frontier orbitals of the epoxide, the Lewis acid is proposed to induce a strong polarizing interaction in the filled oxirane orbital which significantly reduces the steric repulsion experienced by the incoming nucleophile. The chair transition state was found to be significantly lower in energy than the alternative twisted boat-like conformation for all the systems examined.[150]

The stereogenic ring-opening of cyclohexene oxide by **1a** would result in a racemic derivative that, to the best of our knowledge, would represent the first example of a 1,2-β-mercaptocyclohexanol ligand exclusively S- coordinated to a metal center. Of the very few examples of mercaptocyclohexanol coordinating in the literature (Figure 2.12), the most relevant are chelates complexing as bidentate S,O- for the Re^{V} oxo complex[144] and terdentate O,S,O- for the thioether bis(2-hydroxycyclohexyl) sulfide uranium(VI) complex.[151] The remaining examples are all thioetherphosphinite

species of the type R−S−$C_6H_{10}O$−PPh_2 which are bidentate S,P- coordinated to iridium(I) and rhodium(I) centers.[143,152] The *trans*-equatorial chair configuration is exclusive for every reference structure mentioned.

A micro-scale reaction of $[Pt_2(\mu\text{-}S)_2(PPh_3)_4]$ **1a** and cyclohexene oxide produced positive results for ring-opened cations when examined by ESIMS only after several days sitting at room temperature. The sluggish reaction was attributed to steric hindrance at the oxirane carbons of the *meso* epoxide, and a subsequent reaction at mild refluxing conditions in methanol provided a similar mass spectrum (Figure 2.13) after 30 minutes. The observed isotope pattern of the peak at *m/z* 1602 is in excellent agreement with a calculated pattern for the proposed ring-opened derivative $[Pt_2(\mu\text{-}S)(\mu\text{-}S{-}C_6H_{10}OH)(PPh_3)_4]^+$ (**5**). The fragmentation behaviour of the proposed complex was probed by increasing the capillary exit voltage to 210 V. A clean mass spectrum consisting of three monocations resulted, the parent cation and two triphenylphosphine loss cations $[\mathbf{5} - PPh_3]^+$ at *m/z* 1339.12 (calc. *m/z* 1339.23), and $[\mathbf{5} - 2\,PPh_3]^+$ at *m/z* 1077.03 (calc. *m/z* 1077.13). Sodium tetraphenylborate was added to the clear yellow reaction solution and a yellow solid assigned as $[Pt_2(\mu\text{-}S)(\mu\text{-}S{-}C_6H_{10}OH)(PPh_3)_4][BPh_4]$ $\mathbf{5}\cdot BPh_4$ was collected.

To further investigate the proposed ring-opened derivative **5**, $^{31}P\{^1H\}$ and $^{195}Pt\{^1H\}$-NMR spectroscopy experiments were carried out on a chloroform-*d* solution of the complex. The ^{31}P spectrum (Figure 2.14) has two broad multiplets at δ 26.8 and

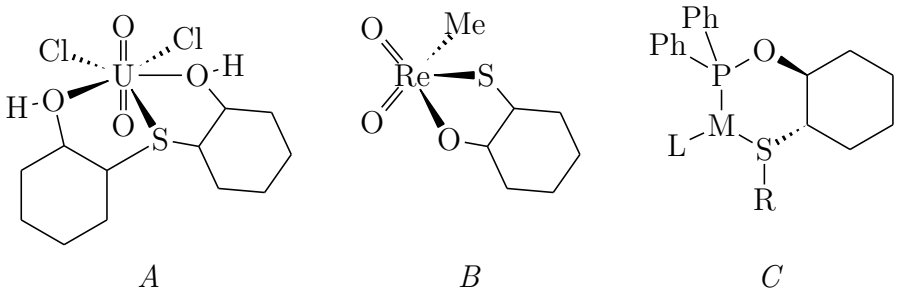

A *B* *C*

Figure 2.12: Referenced structures from the literature: (*A*) $[UCl_2O_2\text{-}S(C_6H_8OH)_2]$,[151] (*B*) $[O_2Re(SC_6H_8O)CH_3]$,[144] (*C*) thioetherphoshpinite S,P- chelate (M = Rh^I, Ir^I; L = cyclooctadiene, substituted acetamidoacrylate)[143,152]

22.4 ppm, each a pair of coincident resonances with ^{195}Pt satellites. Each peak (Figure 2.14 *insets*) appears as a complex multiplet, particularly the resonances at δ 26.8 ppm which display significant second-order features and direct estimation of $^{n}J_{(PP)}$ coupling information was not attempted. Precise chemical shifts for all resonances were determined by evaluation of the associated $^{1}J_{(PtP)}$ couplings. The low field resonances at δ 26.9 and 26.7 ppm have $^{1}J_{(PtP)}$ couplings 3225 (*trans* RS^{-}) and 2686 Hz (*trans* S^{2-}) that are greater (74 and 63 Hz respectively) than their respective counterparts at δ 22.4 and 22.5 ppm of 3151 and 2623 Hz. These couplings are assigned with respect to the greater *trans* influence of the underivatised sulfide and are consistent in magnitude with previously reported $^{1}J_{(PtP)}$ for alkylated derivative of **1a**.[58,153]

Due to the coincident resonances in the ^{31}P spectrum obfuscating P-P couplings, unambiguous determination of geminal phosphine pairs was accomplished with a ^{195}Pt{^{1}H}-NMR spectroscopy experiment (Figure 2.15). Evident in the spectrum are two ^{195}Pt resonances at δ -4262 and -4311 ppm, the latter appearing broader,

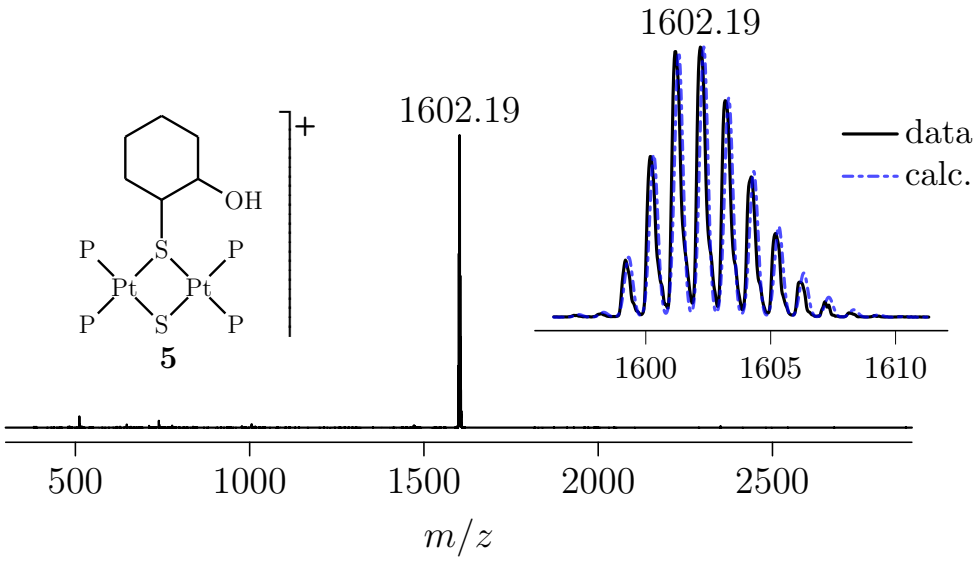

Figure 2.13: ESI mass spectrum of **1a** and cyclohexene oxide in methanol after mild refluxing for 40 minutes. The left inset is the proposed structure of **5**. The right inset is an isotope pattern comparison of the peak at *m/z* 1602.19 and a calculated pattern for $[Pt_2(\mu\text{-}S)(\mu\text{-}S{-}C_6H_{10}OH)(PPh_3)_4]^+$ **5**, calc. *m/z* 1602.33. Capillary exit voltage 60 V.

separated by 6200 Hz (48 ppm). Both resonances appear as doublets of doublets, an expected multiplicity for mixed-bridged derivatives of **1a**. Significant $^{2}J_{(\mathrm{PtPt})}$ coupling results in satellites observed at a reduced intensity reflecting the isotopomer composed of two ^{195}Pt nuclei, which constitutes approximately 11.4% of the sample. Any $^{3}J_{(\mathrm{PtP})}$ couplings present were small with respect to peak FWHM of 170 and 265 Hz (δ -4262 and -4310 ppm respectively) and were not estimated. The resonance at δ -4262 ppm has $^{1}J_{(\mathrm{PtP})}$ couplings of 3227 and 2631 Hz while δ -4311 has $^{1}J_{(\mathrm{PtP})}$ couplings of 3144 and 2691 Hz. These couplings reveal an interesting structural configuration in **5** with respect to the ^{31}P chemical shift in which both a high and low field resonating ^{31}P nucleus is bound to a particular platinum center. Additionally, the larger $^{1}J_{(\mathrm{PtP})}$ couplings (*trans* RS^{-} and *trans* S^{2-}) belong to Pt-P bonds *trans* across the dimer.

The large $^{2}J_{(\mathrm{PtPt})}$ coupling was estimated to be 977 Hz. This coupling is on the very upper end of recorded $^{2}J_{(\mathrm{PtPt})}$ (non-bonded) couplings in the literature,[154] and

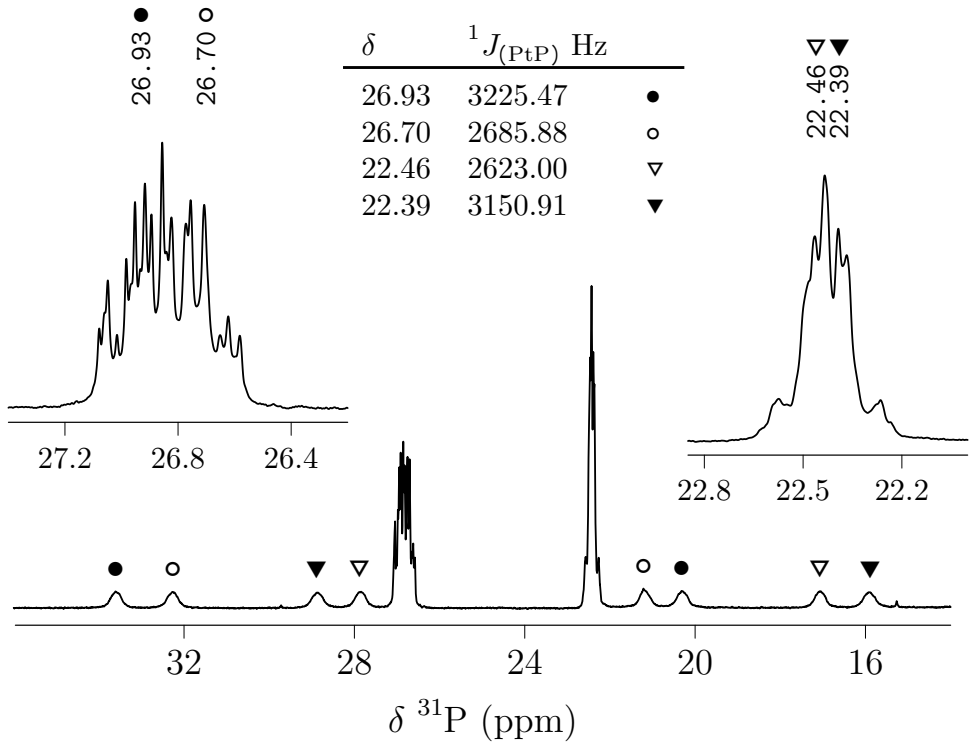

Figure 2.14: $^{31}P\{^{1}H\}$-NMR (242.95 MHz, $CDCl_3$) of **5**. The insets are enhanced views of the multiplets at δ 26.8 (*left*) and 22.4 (*right*) ppm.

is comparable to methylated **1a** ($^2J_{(\mathrm{PtPt})}$ 970 Hz) isolated by Mingos *et. al.*[58] The lowest field multiplet peak of the resonance at δ -4262 ppm was primarily used to estimate this coupling, as the overlapping peaks in the center of the multiplet preclude accurate estimation. The $^2J_{(\mathrm{PtPt})}$ satellites of high field multiplet peak at δ -4333 ppm were fitted with a Lorentzian function and provided a similar coupling of 975 Hz.

To unambiguously characterise the structure of **5**, a single-crystal XRD experiment was carried out on crystals of $\mathbf{5}\cdot\mathrm{BPh_4}$ grown from a chloroform solution (Figure 2.16). The structure crystallizes in the space group $P2_1/c$, is complete with a $\mathrm{BPh_4^-}$ counterion, and has a hinged conformation in the dihedral angle (Pt1-S1-S2-Pt2 torsion) of 139.53°, typical for alkylated derivatives of **1a**. The Pt-Pt separation is 3.338(1) Å, and each $\mathrm{Pt^{II}}$ center is obeying a coordination geometry index (τ_4)[141] very close to ideal square-planar (Pt1 = 0.15, Pt2 = 0.12). The mercapto-cyclohexanol ligand is asymmetrically positioned such that the alcohol oxygen O1 is oriented in the area of Pt1 (3.205(4) Å). Although the hydroxyl proton was located in the difference map, it was included with a riding model and is oriented in close proximity

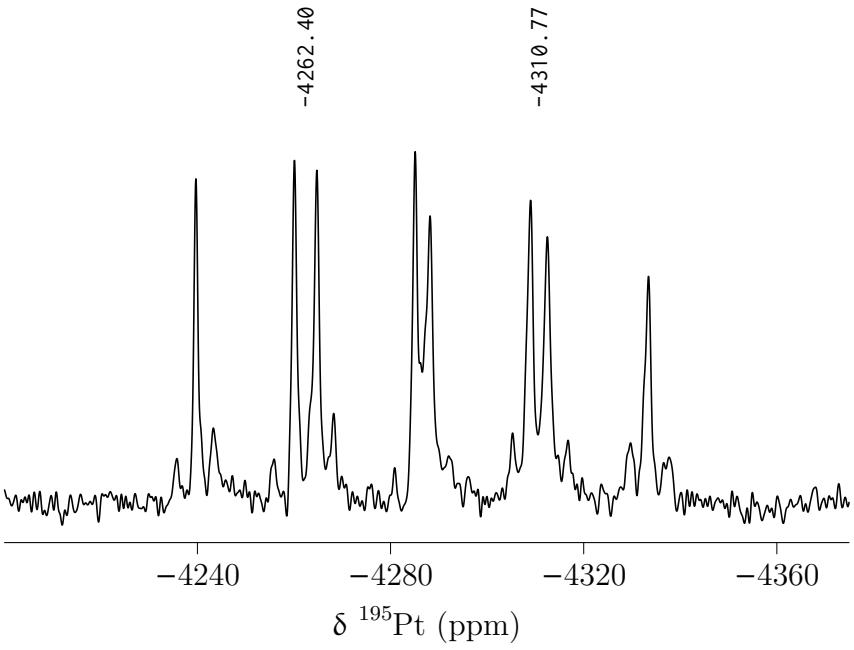

Figure 2.15: $^{195}\mathrm{Pt}\{^1\mathrm{H}\}$-NMR (129.02 MHz, $\mathrm{CDCl_3}$) of **5**.

to both Pt1 and S2 (O1-S2 3.292(4) Å, O1-H1-S2 152(4)°) raising the possibility of a bifurcated hydrogen-bonding interaction. Pt-H-X interactions, treated formally as 3c-4e bonds, are known[155] and $J_{(PtH)}$ couplings for this interaction have been observed by ^{1}H-NMR spectroscopy for Pt-H distances of around 2 Å.[156] There was however no evidence in the ^{1}H-NMR spectrum of **5** of any significant $^{1}J_{(PtH)}$ coupling, the hydroxyl proton appearing as a doublet at δ 5.9 ppm absent of any ^{195}Pt satellites. The sulfide centers in **1a** have been shown to participate in hydrogen bonding with the solvates of ethanol and hexafluoroisopropanol isolated and characterised crystallographically (S-O, 3.42 and 3.14 Å respectively).[56] Interestingly, a bifurcated hydrogen bonding arrangement was noticed in the ethanol solvate with both sulfide centers participating.

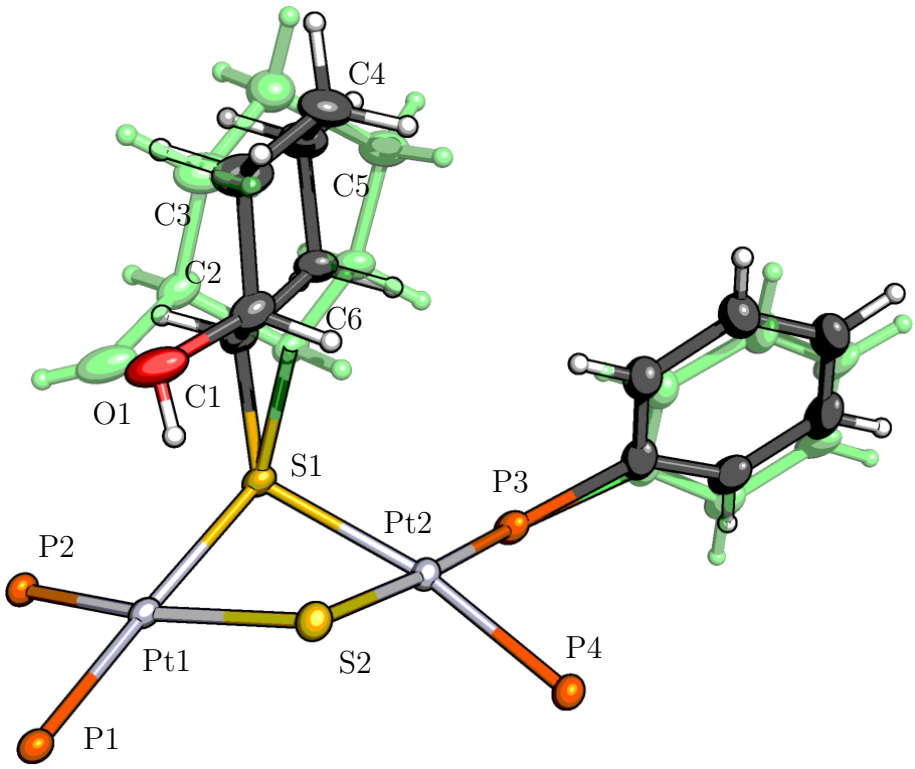

Figure 2.16: The structure of **5**[BPh_4], thermal ellipsoids at 50% probability. The tetraphenylborate anion and all but one phenyl ring of the PPh_3 ligands have been omitted for clarity. The positional disorders in the mercapto-cyclohexanol ligand and phenyl ring of P3 triphenylphosphine ligand are shown.

The Pt-P, Pt-S, and Pt-SR bond lengths (Table 2.2) help to rationalize the observed $^{1}J_{(\mathrm{PtP})}$ couplings and are consistent with the proposed structural configuration revealed by $^{31}\mathrm{P}\{^{1}\mathrm{H}\}$ and ^{195}Pt-NMR spectroscopy data. The phosphines coordinated to Pt1 have both shorter (P1-Pt1 2.282(1) Å) and longer (P2-Pt1 2.297(1) Å) Pt-P bonds than those of Pt2 (P3-Pt2 2.290(1), P4-Pt2 2.291(1) Å). The Pt-S and Pt-SR bonds follow a similar pattern, with Pt1 having shorter Pt-S (Pt1-S2 2.332(1) Å) and longer Pt-SR (Pt1-S1 2.361(1) Å) bonds compared to Pt2 (Pt2-S2 2.344(1), Pt2-S1 2.352(1) Å). These distances are consistent with the underivatised sulfide S2 exerting a larger *trans* influence on P2 than P3, and P1 experiencing a weaker thiolato *trans* influence than P4. Hence, the related pairs of $^{1}J_{(\mathrm{PtP})}$ coupling constants, as revealed by $^{195}\mathrm{Pt}\{^{1}\mathrm{H}\}$-NMR spectroscopy, can be assigned. The $^{1}J_{(\mathrm{PtP})}$ coupling constants of 3227 and 2631 Hz are assigned to P2 and P1 (Pt1) respectively while 3144 and 2691 Hz are assigned to P4 and P3 respectively (Pt2). A positional disorder was identified as the C1 enantiomer of the mercapto-cyclohexanol ligand (also in a *trans*-equatorial chair configuration) and refined to an occupation of ≈ 20%. Fortuitously, both disorders in the ligand occupy a similar volume in the unit cell. In contrast to the main enantiomer, the alcohol oxygen O1 is oriented closer

Table 2.2: Selected bond lengths (Å), angles (°), and torsions (°) for **5**[BPh_4].

Pt1-P2	2.2965(7)	P2-Pt1-S2	166.48(2)
Pt1-S2	2.3319(6)	P2-Pt1-S1	85.95(2)
Pt1-P1	2.2816(7)	S2-Pt1-S1	81.49(2)
Pt1-S1	2.3611(7)	P1-Pt1-P2	100.89(2)
Pt2-S2	2.3439(6)	P1-Pt1-S2	91.94(2)
Pt2-P4	2.2909(6)	P1-Pt1-S1	172.51(2)
Pt2-P3	2.2900(7)	S2-Pt2-S1	81.42(2)
Pt2-S1	2.3523(6)	P4-Pt2-S2	85.95(2)
O1-C2	1.421(5)	P4-Pt2-S1	166.74(2)
C3-C4	1.523(10)	P3-Pt2-S2	176.29(2)
C3-C2	1.539(10)	P3-Pt2-P4	97.76(2)
C1-C2	1.524(5)	P3-Pt2-S1	94.87(2)
C1-C6	1.529(5)	O1-C2-C3	105.9(4)
C1-S1	1.837(3)	O1-C2-C1	111.4(3)
C4-C5	1.520(7)	C2-O1-H1	109(3)
C5-C6	1.537(5)	S1-C1-C2-O1	-67.3(4)
O1B-C2B	1.45(2)	S1-C1B-C2B-O1B	66(1)

to and almost directly above the square-planar plane of Pt1 (3.13(2) Å). In both enantiomers, the mercapto-cyclohexanol is in a *trans*-equatorial arrangement (S1-C1-C2-O1 −67.3(4)°, S1-C1B-C2B-O1B 66(1)°) and the cyclohexane ring in a chair conformation, consistent with previously reported structures.[143,151,152] A second positional disorder in a phenyl ring of triphenylphosphine ligand P3 was also modelled (Figure 2.16), presumably related to the slightly modified steric displacement occupied by the enantiomeric disorder of the mercapto-cyclohexanol ligand.

To further probe the possible O1-H1···S2 intramolecular interaction in **5**, Non Covalent Interactions (NCI) theory[157] and Bader's quantum theory of atoms in molecules (QTAIM)[158,159] were employed to examine the local topology and provide a qualitative assessment of any hydrogen bonding present on a DFT optimised structure. As can be seen in a plot of the reduced density gradient (s) and sign(λ_2)ρ (Figure 2.17), NCI analysis predicts reasonably strong attractive (blue) and repulsive interactions (red) of -0.034 and 0.033 au respectively. Upon inspection of NCI isosurfaces in real space (Figure 2.18), the attractive interaction can be assigned to the OH···S hydrogen bond, and the center of the {Pt_2S_2} ring identified as the location of the repulsive interaction. QTAIM analysis indicates the presence of a

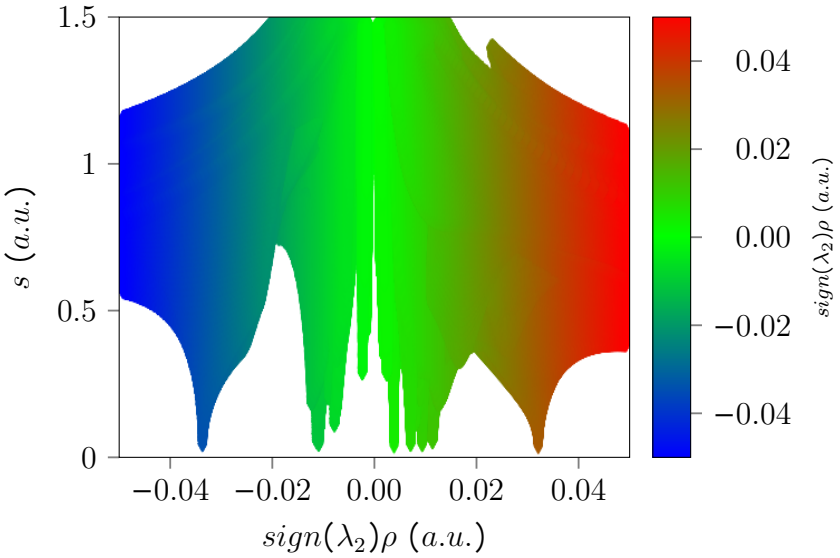

Figure 2.17: The reduced density gradient s $(a.u.)$ plotted against $sign(\lambda_2)\rho$ $(a.u.)$ for the DFT optimised structre of [Pt_2(μ-S)(μ-S−C_8H_8OH)(PPh_3)$_4$]$^+$ (**5**).

(3,-1) bond critical point (BCP) bisecting the H1···S2 vector, corroborating the prediction of a moderately strong hydrogen bond. These interactions do not necessarily require a vanishing density gradient, as has been shown for the intramolecular hydrogen bonding interaction in 1,2-propanediol.[160]

However, it is known that such a critical point lying between a donor and acceptor atom are generally a good indication of a significant interaction.[161] A (3,+1) ring critical point (RCP) is found at the center of the $\{Pt_2S_2\}$ ring, consistent with NCI analysis. Additionally, another RCP is found centrally between the $\{Pt_2S_2\}$ ring and the mercapto-cyclohexanol ligand complimenting the NCI isosurface prediction of a

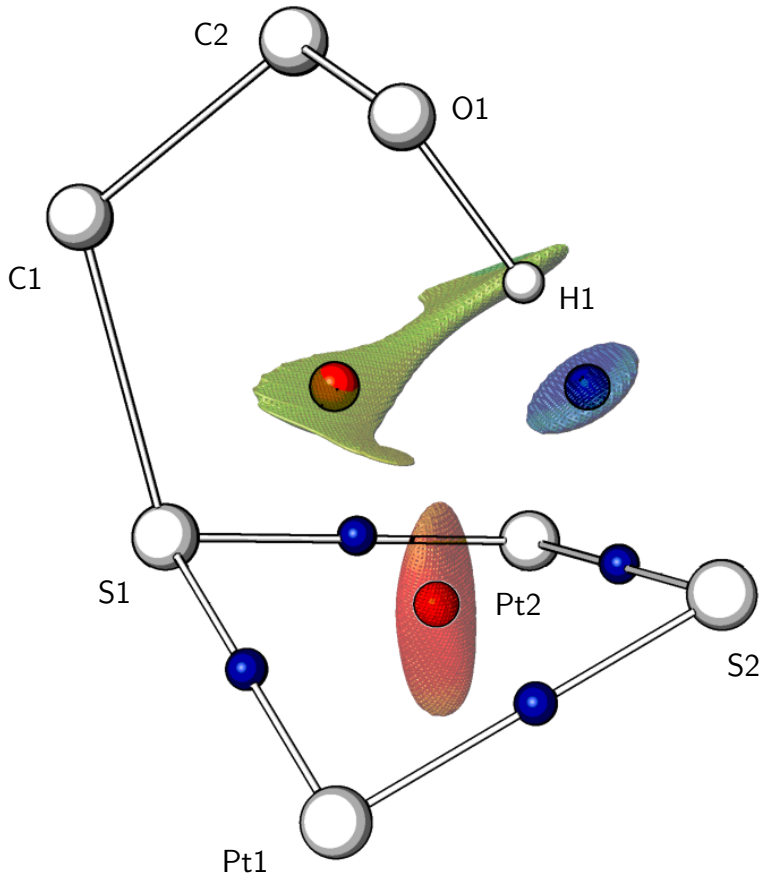

Figure 2.18: A simplified representation of the DFT-optimised structure of **5**, showing the reduced density gradient s (0.3 a.u.) isosurface mapped with sign$\lambda_2\rho$ (-0.04, 0.04 a.u.) in a *blue-green-red* color gradient. The blue and red spheres are (3,-1) BCP and (3,+1) RCP respectively.

weakly repulsive area. No attractive interaction was predicted by either analytical method for a H1···Pt2 hydrogen bond, consistent with an absence of any $^{1}J_{(\mathrm{PtH})}$ coupling in the ^{1}H-NMR spectrum. The electron density ($\rho(\mathbf{r})$) at the BCP of a hydrogen bond correlates with the binding energy (BE), and a recent comprehensive examination using regression analysis proposed a more accurate prediction for both neutral and charged hydrogen bonds based on $\rho(\mathbf{r})$ at the BCP.[162]

In the ring-opened derivative **5**, if the hydrogen bond S2···H1 is considered a charged interaction (treating the underivatised sulfide as a S^{2-} moiety), Equation 2.1b with $\rho_{(\mathrm{BCP})} = 0.3419{\times}10^{-1}$ au, as determined from the BCP between S2 and H1, gives a BE of -12.43 kcal·mol^{-1}. Conversely, if the intramolecular interaction is treated as neutral a BE of -6.89 kcal $\cdot$ mol^{-1} results. While these appear substantially different, qualitatively they both fall in the range of weak to medium strength interactions dominated by electrostatics as classification is type dependent.[162]

$$\mathrm{BE} = -223.08 \times \rho_{BCP} + 0.7423 \qquad \text{neutral} \tag{2.1a}$$

$$= -332.34 \times \rho_{BCP} - 1.0661 \qquad \text{charged} \tag{2.1b}$$

2.5 Ring-opening reactions of styrene oxide with 1a

Examinations of nucleophilic ring-opening of substituted epoxides in the literature found that styrene oxide behaves quite differently to the other asymmetrical substituted oxiranes examined,[163] as nucleophilic attack can occur at the more sterically hindered carbon depending on the catalyst and solvent system employed. For example, in solvent free conditions using LiOH as catalyst, nucleophilic attack by PhSH at the less-substituted ring carbon of styrene oxide is predominant (90:10).[120] Using the same nucleophile in methanol with triethylamine (TEA) as catalyst gives a roughly equal mixture of regioisomers,[164] whereas solvent free conditions and $InCl_3$ as catalyst overwhelmingly results in attack at the phenyl substituted ring carbon in a 95:5 ratio.[119]

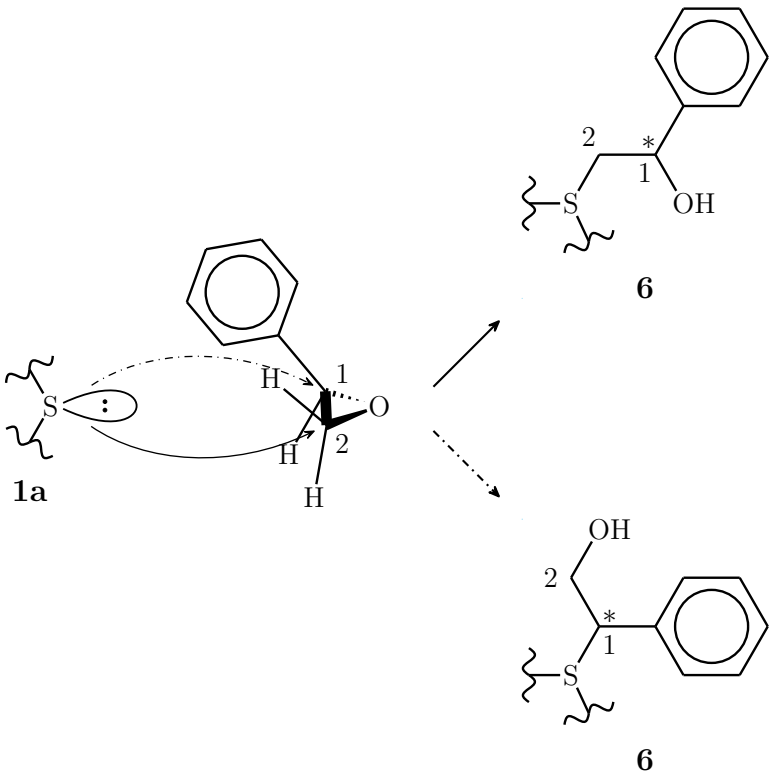

Scheme 2.3: Proposed nucleophilic ring-opening of racemic styrene oxide by a sulfide center in **1a**, showing both possible sites of attack and the resulting structural isomers with introduced stereocenters (*).

1a is widely recognised as a potent nucleophile, thanks to its well-established ability to participate in a broad range of binding arrangements through one or both of the bridging sulfide centers.[42b] Facilitating the strong nucleophilicity and diverse coordination potential is the high variability in the dihedral 'hinge' angle ($120° < \theta < 180°$) between the square-planar Pt^{II} centers. This reactivity is somewhat moderated by the steric bulk of triphenylphosphine ligands, which impose geometric constraints on θ and potential electrophiles that **1a** can successfully attack.

The micro-scale reaction between **1a** and styrene oxide in methanol was examined by ESIMS after stirring for 24 hours at room temperature (Figure 2.19). The mass spectrum contained only one peak at *m/z* 1624.15, assigned as the ring-opened derivative $[Pt_2(\mu\text{-}S)(\mu\text{-}SC_8H_8OH)(PPh_3)_4]^+$ **6**. A calculated pattern for the proposed species (calc. *m/z* 1624.31) is in close agreement with the observed peak at *m/z* 1624. To examine the fragmentation of the base cation, the capillary exit voltage was raised to 210 V and the ESIMS spectrum recorded (Figure 2.19 *right inset*). As is typical for derivatives of **1a**, the loss of triphenylphosphine was observed as

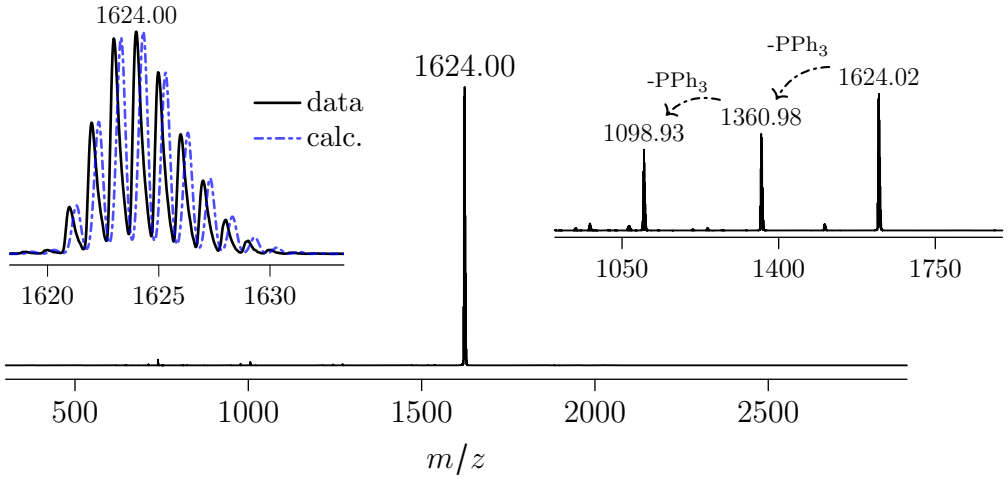

Figure 2.19: ESI mass spectrum of the micro-scale reaction of **1a** and styrene oxide in $CHCl_3$/methanol, capillary exit voltage 60V. The left inset is an isotope pattern comparison of the observed peak at *m/z* 1624 and a calculated pattern for the proposed composition of the styrene oxide ring-opened derivative **6**, $C_{80}H_{69}OP_4Pt_2S_2$ (calc. *m/z* 1624.31). The right inset is the same reaction solution at an increased fragmentation capillary exit voltage of 240V, showing the loss of PPh_3 from the parent cation.

evidenced by cations $[\mathbf{6} - \mathrm{PPh_3}]^+$ at *m/z* 1361.20 (calc. *m/z* 1361.21) and $[\mathbf{6} - 2\,\mathrm{PPh_3}]^+$ at *m/z* 1098.88 (calc. *m/z* 1099.12). The cyclometallated mononuclear cation $[(\mathrm{Ph_3P})\mathrm{Pt}(\mathrm{PPh_2C_6H_4})]^+$ was also observed at *m/z* 718.11 (calc. *m/z* 718.14) at a low relative intensity, indicative of significant fragmentation occurring in parent ion **6**. Due to the observation of a single cation in the mass spectrum collected under gentle fragmentation conditions, the synthesis was repeated on a macroscopic scale and the resulting product isolated as the bis(pentafluoroethylsulfonyl)imide (BETI) salt [**6**]BETI.

To further characterise the proposed ring-opened derivative, a $^{31}\mathrm{P}\{^1\mathrm{H}\}$-NMR spcectroscopy experiment in $\mathrm{CDCl_3}$ was carried out providing a somewhat complicated spectrum (Figure 2.20) with several noteworthy features that warrant further discussion. Two distinct sets of four resonances are immediately identifiable, each resonance accompanied by a set of ^{195}Pt satellites which have been assigned and

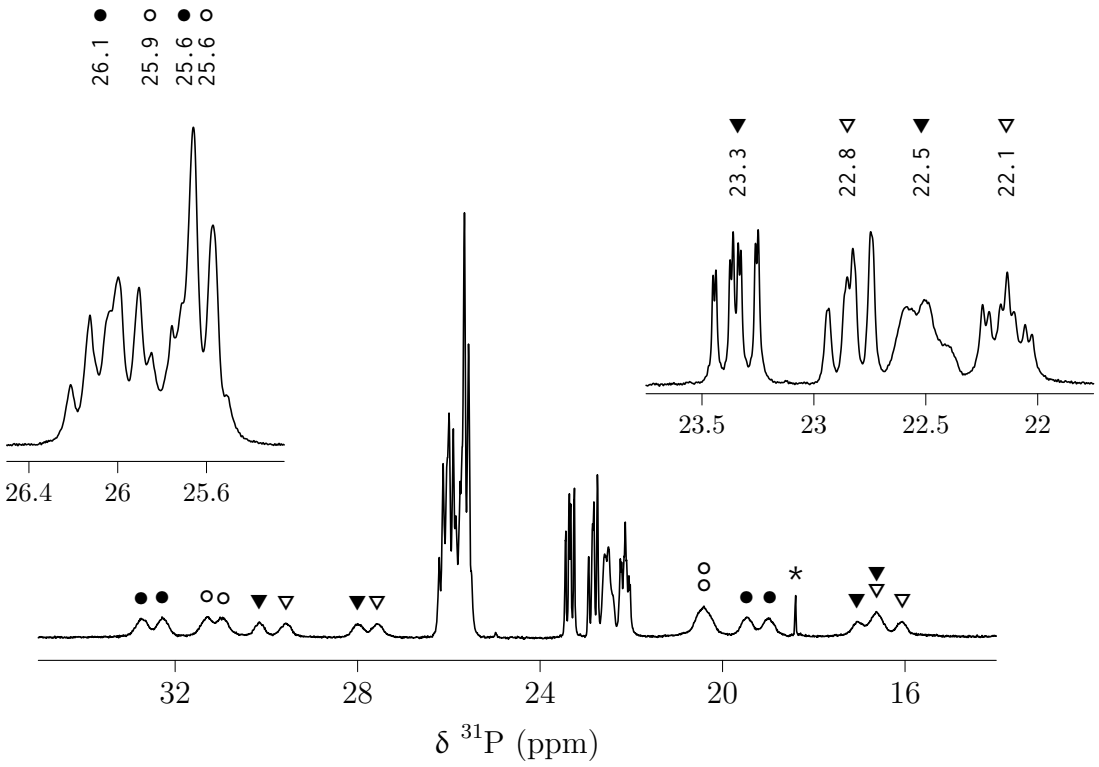

Figure 2.20: $^{31}\mathrm{P}\{^1\mathrm{H}\}$-NMR (242.95 MHz, $\mathrm{CDCl_3}$) of the complex [**6**]BETI. The peak marked * is an impurity.

marked in Figure 2.20 with the assistance of a ^{195}Pt{^{1}H}-NMR spectroscopy experiment, which will be discussed shortly (*vide infra*). Each phosphorus resonance and accompanying $^{1}J_{(\mathrm{PtP})}$ satellites have been delineated with a unique marker corresponding to the platinum resonance to which they are coupled.

Upon a cursory visual inspection of the resonance groups and their respective ^{195}Pt satellites, a marked difference in peak area is apparent and is calculated to be approximately a 60:40 ratio of resonance groups for δ 26 (Figure 2.20 *left inset* ∘, •) and 22 (*right inset* ▼, ▽) ppm respectively. Integration of peak areas for quantitative analyses of ^{31}P{^{1}H}-NMR spectra is often complicated by an uneven heteronuclear NOE and sometimes a significant T_1 variation between phosphorous species.[165] In the case of **6**, a rough quantitation of the two resonance groups is considered suitable as $^{1}J_{(\mathrm{PH})}$ or $^{2}J_{(\mathrm{PH})}$ couplings are proposed not be present in either isomer, and significant T_1 variation in the chemically similar phosphines should be minimal. These features are unusual for an alkylated derivative of **1a**, and, considering the clean mass spectrum, suggest ring-opening has occurred at both carbon positions of the oxirane and the isolated derivative **6** is a mixture of structural isomers. For both sets of resonances, the smaller $^{1}J_{(\mathrm{PtP})}$ couplings in the 2500-2700 Hz range are assigned to phosphines *trans* to the bridging underivatised sulfide (which has a larger *trans* influence[166]), while the larger couplings of 3200-3400 Hz are assigned to phosphines *trans* to the bridging thiolato ligand. These assignments are consistent with other mono-alkylated derivatives of the type $[Pt_2(\mu\text{-}S)(\mu\text{-}S{-}R)(PPh_3)_4]^+$ in the

Table 2.3: ^{31}P{^{1}H}-NMR and ^{195}Pt{^{1}H}-NMR chemical shifts and $^{1}J_{(\mathrm{PtP})}$ couplings for complex [**6**]BETI.

	δ(^{31}P, ppm)	$^{1}J_{(\mathrm{PtP})}$ (Hz)		δ (^{195}Pt, ppm)	$^{1}J_{(\mathrm{PtP})}$ (Hz)
•	26.1	3216	∘	-4278	3233, 2631
∘	25.9	2640	•	-4306	3230, 2593
•	25.6	2595	▽	-4336	3287, 2643
∘	25.6	3229	▼	-4368	3299, 2661
▼	23.3	3308			
▽	22.8	3298			
▼	22.5	2655			
▽	22.1	2646			

literature.[36,123]

The more low field (high frequency) cluster around δ 26 ppm (•, ∘) is composed of four tightly grouped resonances, several of which are nearly coincident. These overlapping resonances are complicated further by significant second-order features which preclude precise elucidation of multiplicity or ${}^{n}J_{(\mathrm{PP})}$ coupling constants. Individual resonance frequencies were located by careful evaluation of ^{195}Pt satellites, both δ and ${}^{1}J_{(\mathrm{PtP})}$ couplings are tabulated in Table 2.3. The four resonances spanning δ 22 to 23.5 ppm (▽, ▼) are however separated sufficiently to observe peak multiplicity and, sans the resonance at δ 22.6 ppm, extract ${}^{n}J_{(\mathrm{PP})}$ coupling constants. All resonances in this grouping appear as doublets of doublets of doublets due to ${}^{2}J_{(\mathrm{PP})}$ *cis* and ${}^{4}J_{(\mathrm{PP})}$ *cis* and *trans* couplings (Scheme 2.4). Longer distance ${}^{3}J_{(\mathrm{PtP})}$ couplings are no doubt present in both isomers, however the magnitude of these couplings are insufficient for resolution. Notable in these four resonances are pronounced second order features manifest in a sloped-roof peak shape, typically observable when the difference between resonance frequencies are close in energy to the coupling between them ($\frac{\Delta\nu}{J}$ < 5 Hz). For the inner two resonances (δ 22.8 ▽ and 22.5 ▼) this effect is more profound ($\frac{\Delta\nu}{{}^{4}J_{(\mathrm{PP}_{trans})}}$ = 3 Hz) and significant peak broadening is also observed.

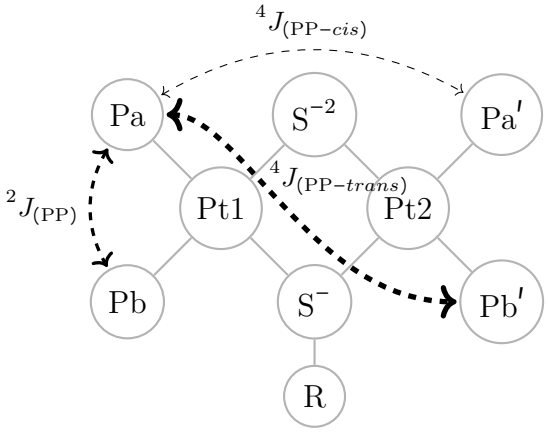

Scheme 2.4: A simplified representation of ${}^{n}J_{(\mathrm{PP})}$ couplings for alkylated derivatives of **1a** from the perspective of a phosphorus enviornment *trans* to a thiolato RS^{-} ligand (Pa). The thickness of the dashed coupling lines correspond to their relative observed magnitude in the high field isomer of **6** (▽, ▼).

The two low field resonances at δ 23.3 and 22.8 ppm are both *trans* to a bridging thiolato ligand ($^{1}J_{(\mathrm{PtP})}$ couplings of 3308 and 3298 Hz respectively) and have a significantly different peak shape due to a much smaller $^{4}J_{(\mathrm{PP})}$ *cis* coupling of 3 Hz. The former resonance, δ 23.3 ppm, has a very sharp peak shape and consequently provides $^{2}J_{(\mathrm{PP})}$ *cis* and $^{4}J_{(\mathrm{PP})}$ *trans* couplings of 18.7 and 27 Hz with a higher confidence. Although the resonance at δ 22.9 ppm suffers from line broadening prohibiting estimation of the $^{4}J_{(\mathrm{PP})}$ *cis* coupling, $^{2}J_{(\mathrm{PP})}$ *cis* and $^{4}J_{(\mathrm{PP})}$ *trans* couplings of 19.5 and 28 Hz respectively were recorded. Conversely, the two high field resonances at δ 22.5 and 22.1 ppm are both *trans* to a bridging disulfide ligand ($^{1}J_{(\mathrm{PtP})}$ couplings of 2655 and 2646 respectively) and a $^{4}J_{(\mathrm{PP})}$ *cis* coupling of 7 Hz can be estimated for the latter. The resonance at δ 22.5 ppm is severely broadened prohibiting any definitive recording of coupling information. The $^{2}J_{(\mathrm{PP})}$ *cis* and $^{4}J_{(\mathrm{PP})}$ *trans* couplings of 19.5 and 27 Hz respectively for δ 22.1 ppm place this phosphine geminal *cis* to δ 22.8 ppm sharing the same $\mathrm{Pt^{II}}$ center, and *trans* across the dimer to δ 23.3 ppm.

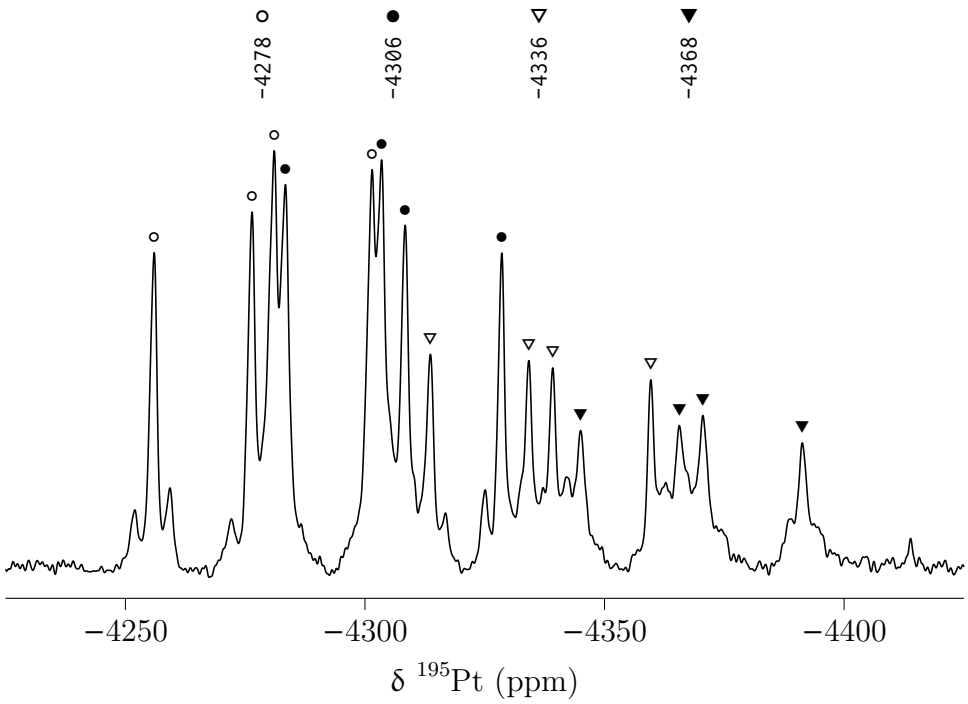

Figure 2.21: $^{195}\mathrm{Pt}\{^{1}\mathrm{H}\}$-NMR (129.02 MHz, $\mathrm{CDCl_3}$) of the complex [**6**]BETI, showing four overlapping resonances wiht *dd* multiplicity.

To help provide additional coupling information, a $^{195}Pt\{^{1}H\}$-NMR spectroscopy experiment was carried out on **6** (Figure 2.21). The acquired spectrum consists of four resonances, each with a doublet of doublet multiplicity. The two high field resonances at δ -4367 and -4336 ppm have a noticeably smaller peak area, and crude integration finds a similar ratio of 60:40 (low field vs. high field) as observed in the $^{31}P\{^{1}H\}$ spectrum, and the lowest frequency resonance δ -4368 (▼) is noticeably broader with a FWHM of 250 Hz cf. 204 Hz for δ -4336 ppm (▽). The low field resonances have a similar FWHM of 196 and 174 for ∘ and • respectively. The $^{1}J_{(PtP)}$ coupling constants are tabulated in Table 2.3. The ^{195}Pt chemical shift is quite sensitive with respect to the coordination environment,[167] which is manifest in significantly different resonance frequencies for the ^{195}Pt centers in each proposed isomer of **6** (Figure 2.22, 27 and 31 ppm for δ -4278, -4306 ppm and δ -4336, -4368 ppm respectively). A significant difference in resonance frequency of Pt^{II} centers is also observed in the $^{195}Pt\{^{1}H\}$-NMR spectrum of the ring-opened cyclohexene oxide derivative **5** (≈ 50 ppm for δ -4262 and -4310 ppm).

Additionally, it appears that a significant $^{2}J_{(PtPt)}$ coupling is present for resonances of both isomers (Figure 2.22), however the crowded spectrum confines estimation of this coupling to outer multiplet peaks of resonances δ -4278 (∘) and -4367 (▼) which have estimated $^{2}J_{(PtPt)}$ couplings of 930 and 860 Hz respectively. These

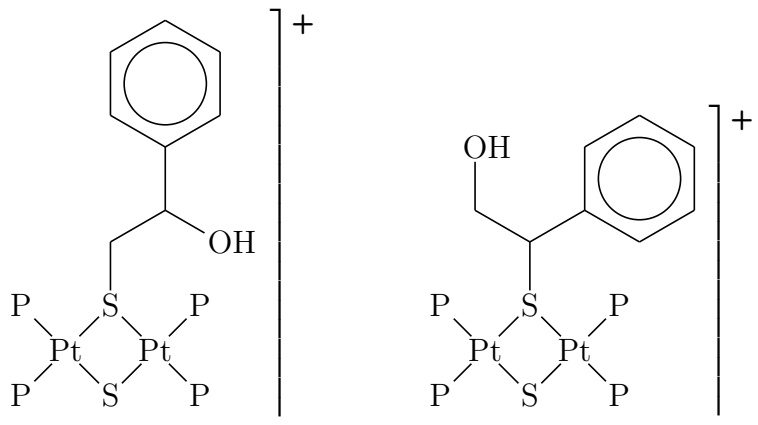

Figure 2.22: The two possible structural isomers of $[Pt_2(\mu\text{-}S)(\mu\text{-}SC_8H_8OH)(PPh_3)_4]^+$ **6**, each a pair of diastereoisomers (*see* Scheme 2.3). Triphenylphosphine ligands abbreviated as P for clarity.

are relatively large couplings for $^{2}J_{(\mathrm{PtPt})}$, which have been reported to be between 200-969 for bridging disulfide or thiolato ligands.[154,168] Previously reported values in the literature for $\{Pt_2S_2\}$ type derivatives range from 150 Hz in the Rh^{III} aggregate $[Pt_2(\mu_3\text{-}S)_2Rh(_{2,6}{-}Me_2C_6H_3NC)_2(PPh_3)_4]PF_6$[29b] to 380 Hz† in thallium-capped dppf complex $[Pt_2(\mu_3\text{-}S)_2Tl(dppf)_4]PF_6$[26a] to 970 Hz in the methylated derivative of **1a** $[Pt_2(\mu\text{-}S)(\mu\text{-}S{-}CH_3)(PPh_3)_4]^+$.[58] The observation of large $^{2}J_{(\mathrm{PtPt})}$ couplings, despite significant Pt-Pt separation (> 3Å) and no formal Pt-Pt bonding), has been attributed to efficiency in spin density transfer by the bridging sulfide and thiolato ligands.[58] In this work, large $^{2}J_{(\mathrm{PtPt})}$ couplings of 980 Hz for the neutral species with a bridging thiolato-carbanion ligand $[Pt_2(\mu\text{-}S)(\mu\text{-}S{-}C(CN)_2)(PPh_3)_4]$ **12** and 977 Hz for the ring-opened cyclohexene oxide derivative $[Pt_2(\mu\text{-}S)(\mu\text{-}S{-}\text{cyclohexanol})\text{-}(PPh_3)_4]^+$ **5** have been recorded.

Large magnets, such as the 14.1 Tesla field employed in the $^{31}P\{^{1}H\}$-NMR and $^{195}Pt\{^{1}H\}$-NMR spectroscopy experiments on **6**, are typically avoided when exam-

†Estimated from published $^{195}Pt\{^{1}H\}$-NMR (64.518 MHz, $CDCl_3$) spectrum[26a]

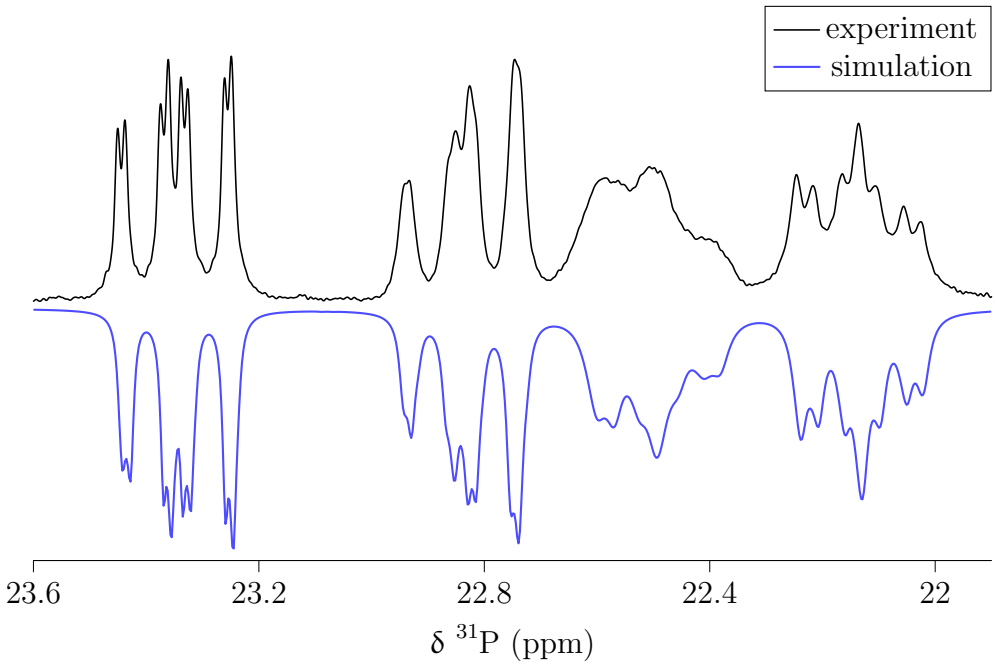

Figure 2.23: A comparison of the observed $^{31}P\{^{1}H\}$-NMR (242.95 MHz, $CDCl_3$) spectrum of **6** and a simulated spin system of estimated $^{n}J_{(\mathrm{PP})}$ and $^{3}J_{(\mathrm{PtP})}$ couplings for the high field isomer (▽, ▼).

ining large transition metal dimers due to the unfavorable effects of chemical shift anisotropy. In this particular case the strong field has aided in resolving individual phosphorus environments of the high field isomer, enabling a more comprehensive analysis of the complicated $^{n}J_{(\mathrm{PP})}$ couplings in a mono-alkylated derivative of **1a**. For comparison, the resonances around δ 23 ppm (Figure 2.20: ▽, ▼) in **6** appear as a complicated second-order multiplet when recorded on a 9.4 Tesla instrument.

To investigate the estimated $^{n}J_{(\mathrm{PP})}$ couplings and proposed structural assignments for the high field isomer, (▽, ▼), a simulated spin system was constructed for the $^{31}\mathrm{P}\{^{1}\mathrm{H}\}$-NMR spectrum which is shown in Figure 2.23 compared to the experimentally observed spectrum. Overall the simulated spin system reproduces the observed multiplicities and secon-order effects of the highly coupled system, providing more confidence to the estimated couplings and the structural relationships inferred from the $^{31}\mathrm{P}$ and $^{195}\mathrm{Pt}$ NMR spectroscopy data. The line widths of all resonances were individually altered to approximate the observed broadening. Referencing $^{n}J_{(\mathrm{PP})}$ couplings for derivatives of **1a** proved difficult as reported values in the literature are scant for these dimers. The only reported $^{4}J_{(\mathrm{PP})}$ *cis* and *trans* couplings for an alkylated derivative of **1a** in the literature have magnitudes of 20 and 2 Hz respectively.[58] In this early work on alkylation of **1a** by Mingos *et. al* $^{31}\mathrm{P}$ couplings were assigned by fitting acquired spectral data with a simulated spin system, which also estimated 24 Hz for $^{2}J_{(\mathrm{PP})}$ in the nearly coincident phosphorus resonances. A somewhat larger $^{4}J_{(\mathrm{PP})}$ *trans* coupling of 10.5 Hz was reported for a $\mathrm{Rh^{I}}$ capped complex of **1a** by the same research group.[29c] A $^{4}J_{(\mathrm{PP})}$ *trans* coupling of 7.9 Hz was recorded for the complex $[(\mathrm{ClPtPPh_3})_2(\mu\text{-}\mathrm{Cl})_2]$,[169] although the harder bridging chloride ligands are most likely poorer than bridging thiolato or sulfides at facilitating *trans*-dimer couplings.[170] It is known that for transition metal phosphines with of the type $\mathrm{ML_2}$ (L = phosphine), $^{2}J_{(\mathrm{PP})}$ *cis* couplings are generally smaller and negative in sign while *trans* couplings are positive and usually much larger, especially for the later transition metals.[171–173] Indeed the simulated spin system has a closer agreement with the observed spectrum if $^{2}J_{(\mathrm{PP})}$ and $^{4}J_{(\mathrm{PP})}$

cis couplings are treated as negative in sign. Examples of $^{4}J_{(\mathrm{PP})}$ *cis* couplings in the literature for more general Pt^{II} dimers with bridging thiolate ligands are also sparse, and are typically small (< 10 Hz).[20,170] Some $^{2}J_{(\mathrm{PP})}$ *cis* couplings for similar triphenylphosphine Pt^{II} mononuclear thiourea complexes have recorded magnitudes around 20 Hz.[174]

It is unusual for sterically unencumbered mono-alkylated derivatives of **1a** to exhibit two significantly separated ^{31}P resonances (*trans* to S^{2-} or RS^{-}). There are however plenty examples in the literature[58,175] and in this work, for example the ring-opened dimethyl oxirane derivative **24**, where these resonances are coincident ($\Delta\nu$ < 0.5 ppm). Resolution into magnetically inequivalent phosphorus environments has been observed in di-alkylated dicationic derivatives of **1a** with an overhead bridge (for example μ-S−$(CH_2)_n$−μ-S), and was rationalised by the introduction of rigidity in the $\{Pt_2S_2\}$ core imparted by the bridge.[133,176,177] Considering the gamut of nucleophilic ring-opening reactions of styrene oxide in the literature, the large variation in the site of attack on the oxirane is noteworthy, especially when compared with other asymmetric sterically crowded oxiranes such as 1,2-epoxyhexane and phenyl glycidyl ether for which ring-opening occurred exclusively at the less hindered carbon across several catalysts.[119] It seems reasonable to conclude based on ^{31}P and ^{195}Pt NMR spectroscopy evidence that a ring-opening reaction of styrene oxide by **1a** results in nucleophilic attack at both carbons. Furthermore, it is likely nucleophilic attack by **1a** at the more hindered carbon of styrene oxide would lead to a derivative with significantly more internal steric strain, possibly slowing ligand rotation and conformational equilibration sufficiently such that individual phosphorus environments are resolvable for this isomer. Not surprisingly many attempts at growing crystals of the hexafluorophosphate salt were unsuccessful. Several syntheses of **6** were carried out employing a variety of counterions, the resulting salts of which also failed in producing crystalline material suitable for a single-crystal XRD experiment.

2.6 Ring opening of styrene oxide by 1b

In previous work by Santi *et al.*,[178] *in situ* generated selenol was found to attack the more hindered carbon of styrene oxide, affording the corresponding β-hydroxyselenide in a ratio of 19:1 over the other regioisomer. This result was however not observed with other asymmetric epoxides examined, where nucleophilic attack at the less hindered carbon was observed almost exclusively.

The selenide Pt^{II} dimer $[Pt_2(\mu\text{-Se})_2(PPh_3)_4]$ **1b** was reacted in analogous fashion with styrene oxide in the micro-scale. The reaction solution was examined by ESIMS (Figure 2.24), revealing the presence of the proposed styrene oxide ring-opened product $[Pt_2(\mu\text{-Se})(\mu\text{-SeC}_8H_8OH)(PPh_3)_4]^+$ **25** at *m/z* 1719.05, along with two other cations at *m/z* 1040.03 and *m/z* 2042.95. The isotope pattern observed at *m/z* 1719.05 does have a strong correlation to a calculated pattern for the proposed species **25**, however there is a slight and consistent discrepancy in the intensities of the patterns along the left hand curve of *m/z* values, *m/z* 1717 → 1710. These discrepancies are less pronounced down the right-hand curve, hence it appears the

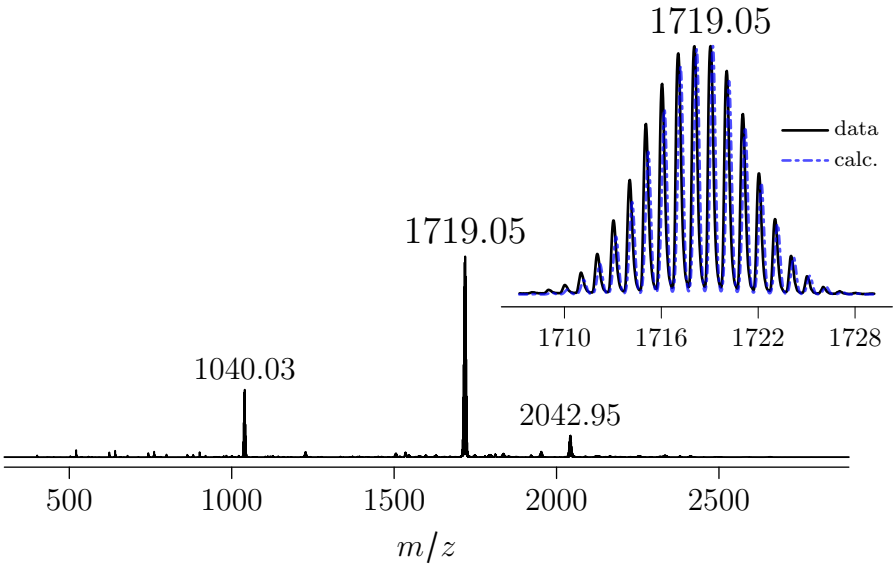

Figure 2.24: ESI mass spectrum of **1b** and styrene oxide in methanol. The inset is an isotope pattern comparison of the cation observed at *m/z* 1719.05 and $[Pt_2(\mu\text{-Se})(\mu\text{-Se}{-}C_8H_8OH)(PPh_3)_4]^+$ **25** (calc. *m/z* 1719.20). Capillary exit voltage 60 V.

observed isotope pattern is actually a composite of two cations, one of which is one mass unit less than the proposed **25** at *m/z* 1719.05. One possibility is concomitant alcohol deprotonation and oxidation of the underivatised selenide ligand, $[\mathbf{25} - H^+]^{\bullet+}$. The cationic derivatives of the selenide complex **1b** have been shown to exhibit strong Lewis basicity through the underivatised selenide ligand,[124c] and even more prone to oxidation than the derivative of the sulfide analogue **1a**.[78]

The peak at *m/z* 1040.03 of significant relative intensity is tentatively assigned as $[(Ph_3P)_2\overline{PtSe(C_8H_8O)}(C_8H_8OH)]^+$, with a close agreement between observed and calculated isotope patterns for this proposed species (Figure 2.25). This appears to be the result of decomposition from the initial ring-opened derivative **25**. A similar ethylenediamine Pt^{II} complex is known containing a selenoether coordiated in a bidentate fashion through a carboxylate oxygen $[(en)\overline{PtSe(CH_2CO}O)CH_2COOH]$.[179] More common are the mononuclear complexes with the corresponding bidentate S,O-lingads of the type $[(PPh_3)_2\overline{PtS(R^1R^2C}O)R^3]^+$. These commonly involve either a carboxylate moiety as a member of the chelate,[180–182] or other electron-withdrawing substituents geminal to the alkoxide.[183] Due to the sterically crowded geometry and reduced nucleophilicity of the selenolate ligand in cationic **25**, it seems unlikely a second ring-opening reaction would occur before decomposition into a mononuclear

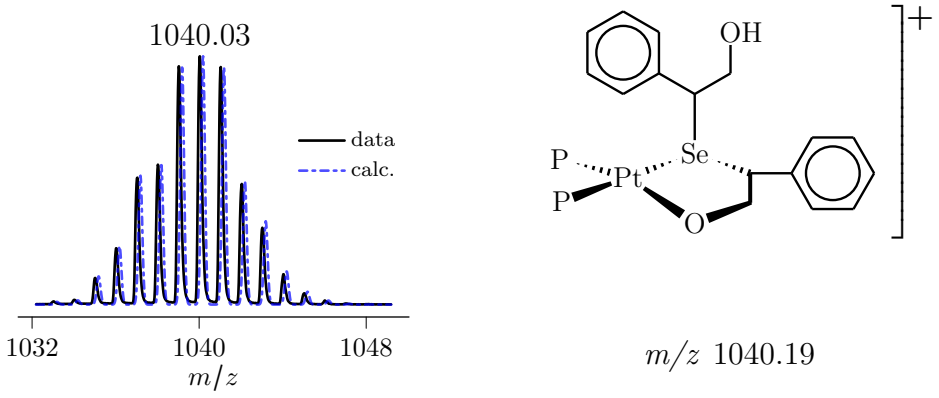

Figure 2.25: An isotope pattern comparison (left inset) from the ESI mass spectrum of **1b** and styrene oxide (Figure 2.24), of the peak observed at *m/z* 1040.03 and a calculated pattern for the proposed cation (right inset) $[\overline{PtSe(C_8H_8O)}(C_8H_8OH)(PPh_3)_2]^+$ (calc. *m/z* 1040.19).

species. Rather, the second ring-opening reaction would take place after decomposition, possibly facilitated by the mononuclear Pt^{II} fragment having a neutral charge due to a bidentate selenolate-alkoxide ligand $[Pt(Se{-}C_8H_8O)(PPh_3)_2]$. If the site of nucleophilic attack in the oxirane is the more sterically hindered geminal carbon, as was observed previously for various selenols, significant steric strain would be introduced to the core of **25**. Alternatively, the underivatised selenide center in **25** could possess sufficient nucleophilicity to engage in a subsequent ring-opening reaction, resulting in a dicationic complex with two bulky selenolate ligands, primed for molecular fragmentation to reduce steric strain and charge. This seems a likely prospect, as the basicity of the selenide centers in **1b** is such that the doubly protonated dication $[Pt_2(\mu\text{-SeH})_2(PPh_3)_4]^{2+}$ was isolated,[124c] something that has proved elusive for the sulfide analogue **1a**.

Aiding fragmentation in a sterically crowded **25** is the weaker Pt-Se bond,[184] manifest specifically for systems of **1b** in metal scrambling reactions,[73d] a phe-

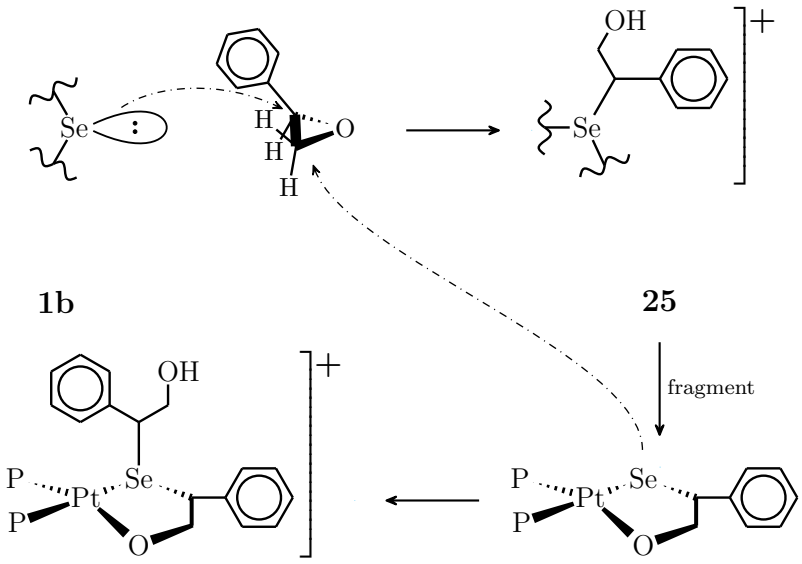

m/z 1040

Scheme 2.5: A proposed scheme for successive nucleophilic ring-opening reactions of styrene oxide by a selenide center in **1b**, showing a decomposition and rearrangement before the second ring-opening at the derivatised RSe^- ligand.

nomenon that involves the intermolecular rearrangement of metal sites and their corresponding ligands, and is rarely observed with derivatives of the sulfide analogue **1a**. A proposed scheme for the generation of the observed cation at m/z 1040 is presented in Scheme 2.5. At m/z 2042.95 is a cation of lower relative intensity that has yet to be assigned, however the isotope pattern is indicative of multiple polyisotopic elements such as selenium and platinum.

Although a micro-scale ESIMS examination of styrene oxide and **1b** provided sufficient evidence of ring-opening, no attempt was made to isolate the proposed derivative **25** on a macro scale for a full characterisation. As such, further examination of this system is highly recommended.

2.7 Ring-opening reactions of 2,2-dimethyloxirane and 2,3-dimethyl-2,3-epoxybutane with [Pt_2-(μ-S)$_2$(PPh_3)$_4$]

Previous epoxides reacted with [$Pt_2(\mu\text{-}S)_2(PPh_3)_4$] **1a** have undergone ring-opening reactions, even with sterically encumbered oxiranes such as cyclohexene oxide and styrene oxide. The fully protected 2,3-dimethyl-2,3-epoxybutane was found not to undergo any ring-opening reaction when reacted with **1a** as evidenced by ESIMS, even when the reaction solution was subjected to refluxing methanol for 48 hours. Hence, the importance of a sterically accessible α-carbon appears integral in the formation of a ring-opened derivative. The deprotected relative 2,2-dimethyloxirane was examined next (Scheme 2.6), and proceeds with the aid of forcing conditions.

After stirring for 17 hours at room temperature a micro-scale reaction of **1a** and 2,2-dimethyloxirane was deemed successful after examination by ESIMS. The base cation at *m/z* 1576, tentatively assigned as the epoxide ring-opened derivative [Pt_2-(μ-S)(μ-S$-CH_2C(CH_3)_2OH$)(PPh_3)$_4$]$^+$ **7**, had a calculated isotope pattern closely matching the observed peak (calc. *m/z* 1576.31). However, as evidenced by a small peak at *m/z* 1503 (assigned as protonated starting material **1a** + H^+) the reaction had not gone to completion.

The reaction was repeated on a macro-scale and carried out in gently refluxing

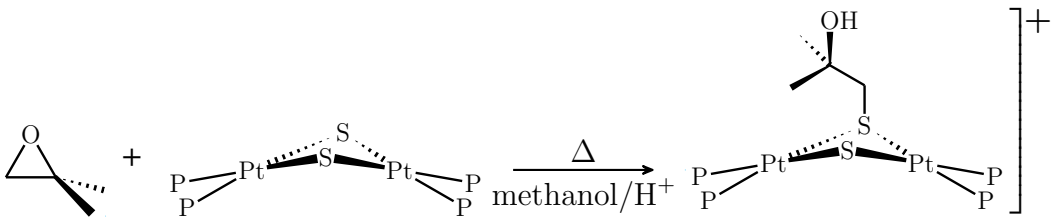

7

Scheme 2.6: Proposed reaction scheme for the ring-opening of dimethyloxirane by **1a** in methanol.

methanol, providing a clear yellow-orange solution after 40 minutes. ESIMS examination of the clear reaction solution confirms a successful synthesis of **7**, as the spectrum contains one cation at *m/z* 1576.12, assigned as **7**. Oxidised or protonated starting material ($[\mathbf{1a}]^+$ / $[\mathbf{1a}] + [H]^+$) were not present indicating completion. To examine fragmentation from this ion, an additional spectrum was acquired after increasing the capillary exit voltage to 210 V (Figure 2.26). Fragmentation monocations due to one and two triphenylphosphine loss from the parent cation **7** are observed at *m/z* 1313.13 and *m/z* 1051.02 respectively. The cationic derivative was isolated with sodium tetraphenylborate and further characterised by ^{1}H, ^{13}C{^{1}H}, and ^{31}P{^{1}H}-NMR spectroscopy in a chloroform-*d* solution.

Both ^{1}H and ^{13}C{^{1}H}-NMR spectroscopy confirmed a clean preparation of the proposed derivative **7**, the methylene protons appearing as a broad triplet at δ 2.31 ppm and six methyl protons as a sharp singlet at δ 0.68 ppm. Comparatively, the

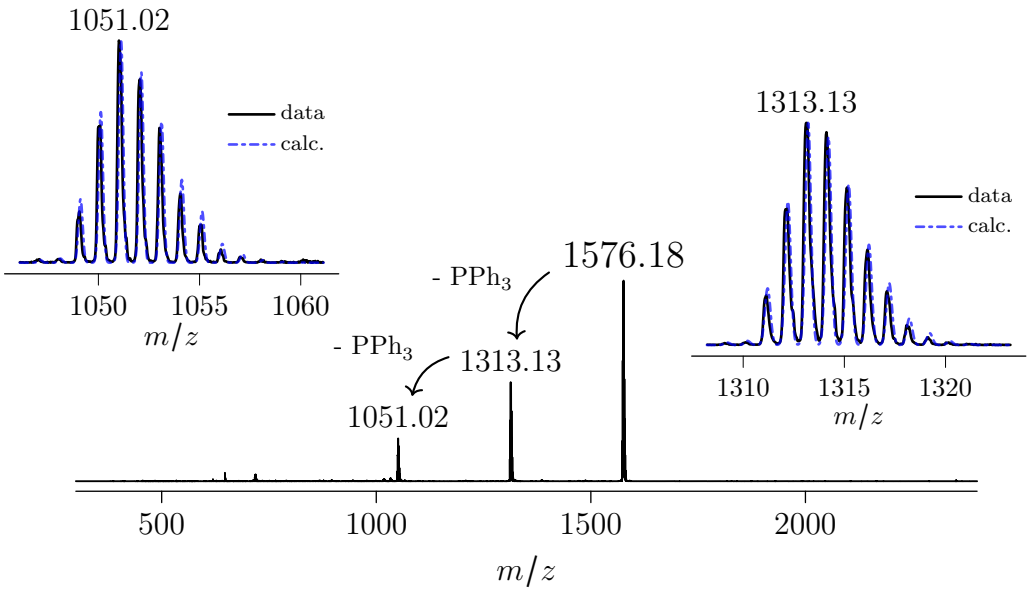

Figure 2.26: ESI mass spectrum of **1a** and 2,3-dimethyloxirane in methanol, at an increased capillary exit voltage of 210 V to examine fragmentation of the parent cation, the proposed $[Pt_2(\mu\text{-}S)(\mu\text{-}S{-}CH_2C(Me)_2OH)(PPh_3)_4]^+$ **7** (calc. *m/z* 1576.31). The insets are isotope pattern comparisons of (left inset) $[\mathbf{7} - 2\,PPh_3]^+$ (calc. *m/z* 1051.12) and the peak observed at *m/z* 1051.02 and (right inset) $[\mathbf{7} - PPh_3]^+$ (calc. *m/z* 1313.21) and the peak observed at *m/z* 1313.13.

shifts of the neat oxirane are δ 2.59 and 1.31 ppm respectively[†]. The observed upfield shifts in **7** are consistent with increased shielding upon coordination to the electron rich core of **1a**. The multiplicity in the methylene protons is assigned as a $^{4}J_{(PH)}$ coupling with an estimated magnitude of 5.3 Hz (Figure 2.27 *right inset*). A similar coupling estimated to be 4.2 Hz was identified in a mono-alkylated derivative of **1a**.[175] The hydroxyl proton appears as a very broad singlet resonating at δ 2.29 ppm, almost coincident with the methylene protons. The $^{13}C\{^{1}H\}$-NMR spectrum has three resonances at δ 70.1, 53.4, and 29.1 ppm and is consistent with the neat oxirane (δ 54.5, 53.9, and 23.1 ppm[185]) with the exception of the large downfield shift to δ 70.1 ppm, which is assigned to the thiolato-carbon.

$^{31}P\{^{1}H\}$-NMR corroborated the proposed ring-opening reaction, providing a very clean spectrum in Figure 2.27. The two main resonances at δ 24.5 and 23.6 ppm

[†] ^{1}H-NMR (90 MHz, $CDCl_3$) National Institute of Advanced Industrial Science and Technology (Japan)

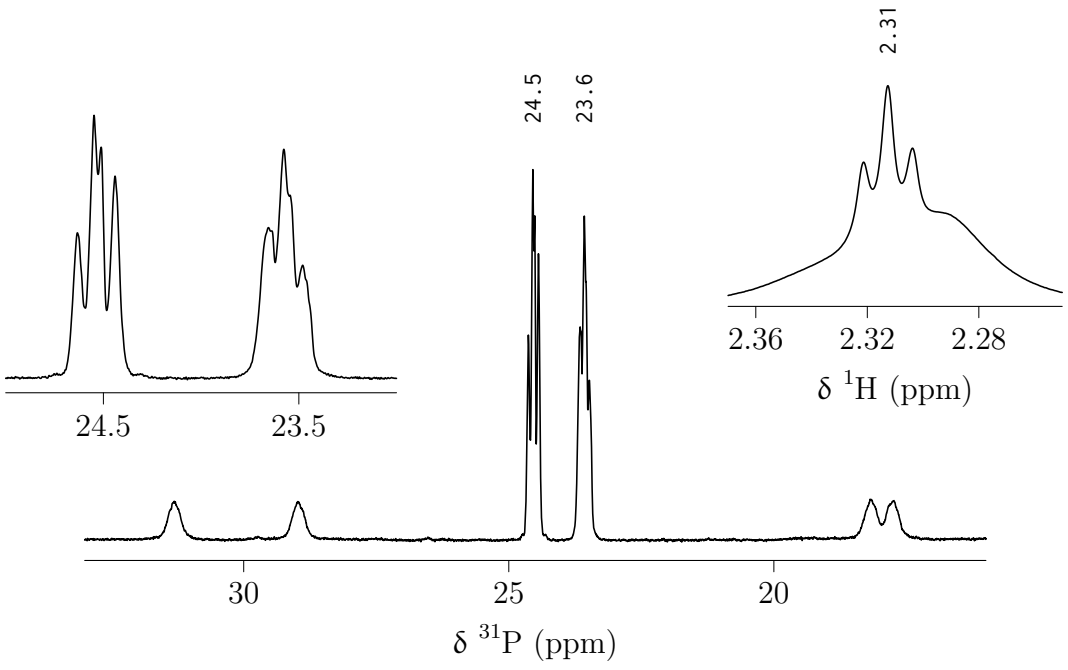

Figure 2.27: $^{31}P\{^{1}H\}$-NMR (242.95 MHz, $CDCl_3$) of ring-opened derivative **7**. The left inset is an enhanced view of the resonances at δ 24.5 and 23.6 ppm. The right inset is the ^{1}H-NMR (600 MHz, $CDCl_3$) spectrum, cropped to show the coincident resonances of the methylene protons (δ 2.31 ppm) and the hydroxyl proton (δ 2.29 ppm).

each of which have characteristic ^{195}Pt satellites. The estimated $^{1}J_{(\mathrm{PtP})}$ couplings are 3290 (*trans* RS^-) and 2630 Hz (*trans* S^{2-}) respectively. Unlike the ring-opened derivatives of styrene oxide and cyclohexene oxide (**6**, **5**), the phosphines *trans* to RS^- and S^{2-} are in a sufficiently similar magnetic environment manifest in nearly coincident resonances. The broadness of these resonances (FWHM ≈ 12 and 15 Hz for δ 24.5 and 23.6 ppm respectively) prevents reliable estimation of $^{n}J_{(\mathrm{PP})}$ couplings, however the overall shape of the multiplicities is consistent with observed multiplicities in the more sterically encumbered isomer of **6**. That is to say, the *ddd* peak morphology for these alkylated derivatives is dependent on the magnitude of the *cis* $^{4}J_{(\mathrm{PP})}$ coupling. If the phosphine is *trans* to RS^- (such as δ 24.5 ppm), $^{4}J_{(\mathrm{PP})}$ *cis* is smaller and eight sharper or four broader distinct peaks are observed. For a phosphine *trans* to S^{2-} (such as δ 23.6 ppm), $^{4}J_{(\mathrm{PP})}$ *cis* is larger (> 8 Hz), and the multiplet appears as a pseudo-triplet flanked by a pair of doublets or three broad peaks in a rough triplet-like arrangement (Figure 2.27 *left inset*).

Table 2.4: Selected bond lengths (Å) and angles (°) for **7**[BPh_4]·$(CH_2Cl_2)_2$.

Pt1-P4	2.2831(12)	P4-Pt1-P1	99.16(4)
Pt1-P1	2.2903(12)	P4-Pt1-S2	92.43(7)
Pt1-S2	2.320(2)	P4-Pt1-S1_2	97.5(2)
Pt1-S1_2	2.375(9)	P4-Pt1-S1_1	174.10(4)
Pt1-S1_1	2.3716(12)	P1-Pt1-S2	166.97(6)
Pt2-P2	2.2944(12)	P1-Pt1-S1_2	163.1(2)
Pt2-S2	2.337(2)	P1-Pt1-S1_1	86.73(4)
Pt2-P3	2.2970(12)	S2-Pt1-S1_1	81.74(7)
Pt2-S1_2	2.370(9)	P2-Pt2-S2	174.65(7)
Pt2-S1_1	2.3477(12)	P2-Pt2-P3	99.45(4)
S1_1-C1_1	1.877(7)	P2-Pt2-S1_2	169.78(19)
O1_1-C2_1	1.423(9)	P2-Pt2-S1_1	94.15(4)
C1_1-C2_1	1.535(10)	S2-Pt2-S1_1	81.90(7)
C2_1-C3_1	1.528(11)	P3-Pt2-S2	84.49(7)
C2_1-C4_1	1.494(10)	P3-Pt2-S1_2	89.4(2)
S1_2-C1_2	1.872(8)	P3-Pt2-S1_1	166.39(4)
O1_2-C2_2	1.424(10)	O1_1-C2_1-C1_1	109.6(6)
C1_2-C2_2	1.534(11)	O1_1-C2_1-C3_1	108.8(7)
C2_2-C3_2	1.527(12)	O1_1-C2_1-C4_1	107.4(7)
C2_2-C4_2	1.494(11)	C3_1-C2_1-C1_1	112.5(7)
C4_1-C2_1-C1_1	108.7(6)	O1_2-C2_2-C4_2	104.8(15)
C4_1-C2_1-C3_1	109.7(7)	C3_2-C2_2-C1_2	112.9(14)
O1_2-C2_2-C1_2	113.1(13)	C4_2-C2_2-C1_2	107.6(14)
O1_2-C2_2-C3_2	108.1(14)	C4_2-C2_2-C3_2	110.0(16)

To unambiguously characterise the proposed ring-opened derivative, a single-crystal XRD experiment was carried out of a sample of **7**[BPh_4] (Figure 2.28). The complex crystallises as the *bis*-dichloromethane solvate in the monoclinic space group $P2_1/n$ with $Z' = 1$. Selected bonds and angles are presented in Table 2.4. The

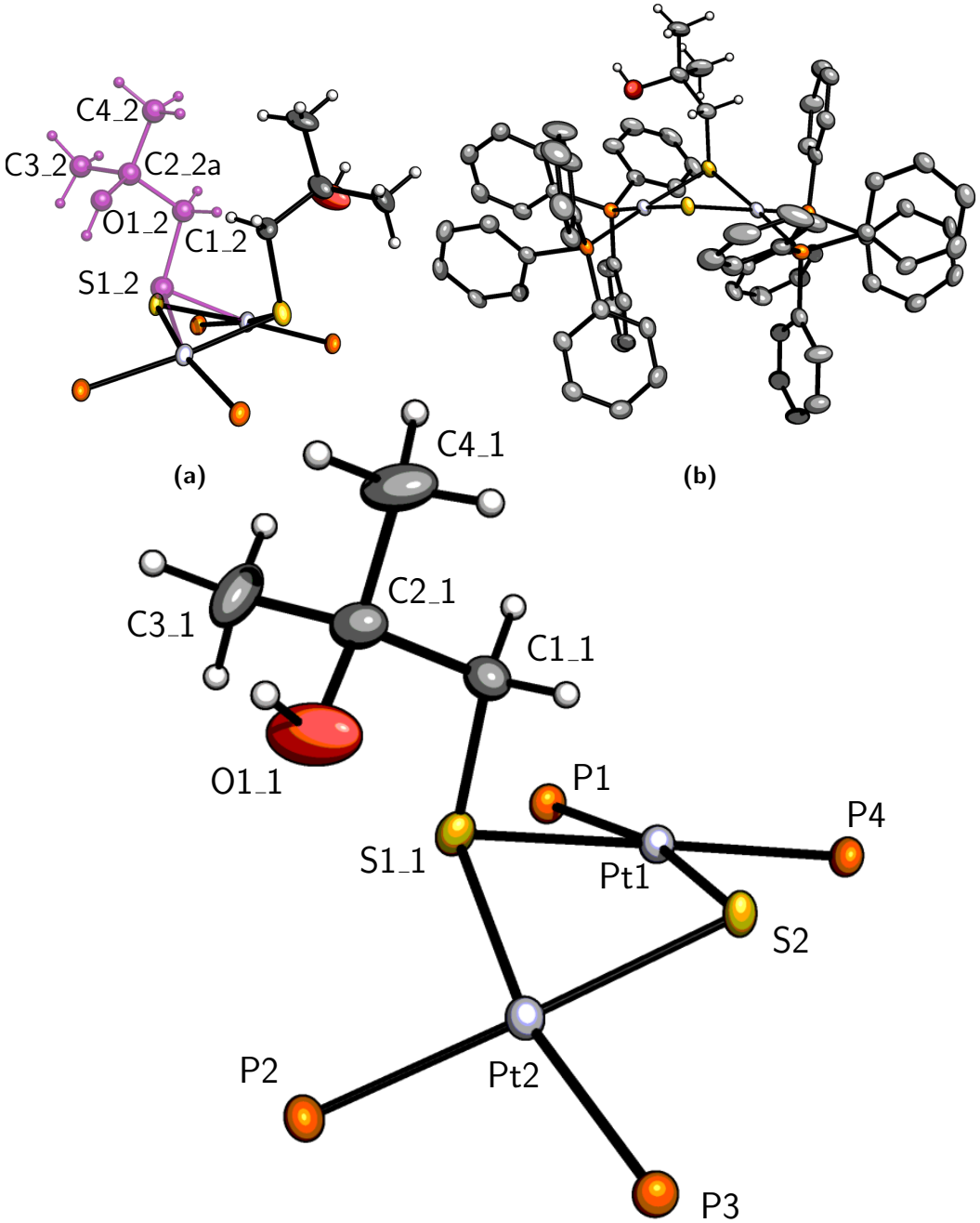

Figure 2.28: The crystal structure of **7**[BPh_4]$\cdot(CH_2Cl_2)_2$. The phenyl rings of the PPh_3 ligands, CH_2Cl_2 solvent, and BPh_4^- anion have been omitted for clarity. Thermal ellipsoids are displayed at 50% probability. Insets **(a)** and **(b)** show the minor component of the disordered mercapto-*iso*-butanol ligand and expanded view of the complex with triphenylphosphine ligands respectively.

presence of a single BPh_4^- anion in the salt confirms the monocationic nature of the complex. A positional disorder in the mercapto-*iso*-butanol ligand is present, and the major disorder has an occupation of approximately 70% after refinement. The dihedral angle across the dimer (Pt1-S1_1-S2-Pt2) is significantly hinged at 137.4(1)°, typical for monoalkylated derivatives of **1a**, and the non-bonded Pt-Pt contact is 3.291(1) Å consistent with the hinged conformation. Both Pt^{II} centers observed strict square-planar coordination geometry reflected in identical τ_4' parameters[141] of 0.13. The S-Pt distances for the underivatised sulfide S2 are consistently shorter than the corresponding distances for the thiolate S1_1, although this difference is considerably narrower for Pt2. The torsion along Pt1-S1_1-C1_1-C2_1 is very close to 180° and accordingly the methylene protons of C1_1 are bisecting the Pt1-S1_1 vector such that H1A_1 is positioned directly over the {Pt_2(μ-S)(μ-SR)} core.

2.8 Attempted ring-opening of 5,6-epoxy-5,6-dihydro-[1,10]-phenanthroline by 1a

1,10-Phenanthroline (phen) is a weakly basic electron-poor chelating bidentate ligand with a rigid frame, capable of complexing and stabilising metal ions in lower oxidation states due to an excellent π-acceptor character.[186] Additionally, accessible low-lying π^* states in phen allow significant metal-to-ligand charge-transfer[187,188] (MLCT) and accordingly these photophysical properties have been employed to create novel luminescent materials, molecular sensors, and photoswitchable complexes.[189–191]

Epoxidation of the phen ligand to 5,6-epoxy-5,6-dihydro-[1,10]-phenanthroline (epoxyphen) allows further customisation at the 5,6 positions of phen via nucleophilic ring-opening reactions and subsequent dehydration. For example, 1-aza-18-crown-6 functionalised phen has been N-coordinated in a bidentate fashion to a rhenium complex and successfully used as chemosensor for Pb^{2+} ions in solution.[192] Thiol nucleophiles have been exploited in a similar manner, with octahedral complexes (M = Re^{I}, Ru^{II}, Os^{II}, and Ir^{III}) bearing an epoxyphen ligand used as cysteine labeling reagents.[193] Conversely, glutathione has been used to ring-open epoxyphen prior to *N*-bidentate coordination to a luminescent Eu^{III} diketonate complex $Eu(ttfa)_3$ (ttfa = 2-thenyl-4,4,4-trifluorbutane-1,3-dionato).[194] Ring-opening of epoxyphen by thiol nucleophiles such as mercaptobenzimidazole and 1-thio-β-D-glucose have also been used to introduce functionality at the 5 position of phen.[195]

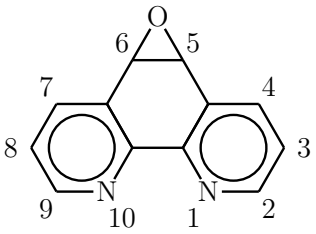

Figure 2.29: Epoxyphen numbered.

ESIMS was used to examine the micro-scale reaction of $[Pt_2(\mu\text{-}S)_2(PPh_3)_4]$ **1a** and epoxyphenanthroline after 5 minutes (Figure 2.30). A cation at *m/z* 1699.98 is tentatively assigned as the ring-opened epoxide derivative $[Pt_2(\mu\text{-}S)(\mu\text{-}SC_{12}H_9N_2O)(PPh_3)_4]^+$ **8** (calc. *m/z* 1700.32) and a calculated pattern for this proposed species

closely matches the observed peak, albeit this ion appears at a very low relative intensity of around 5%. The base peak at m/z 611.16 is assigned to the tris-epoxyphen sodium aggregate cation $Na(C_{12}H_8N_2O)_3^+$, and the di-aggregate $Na(C_{12}H_8N_2O)_2^+$ is assigned to a peak at m/z 415. Sodium adduct cations are not unusual to observe in ESI mass spectra, as sodium formate was routinely used to calibrate the spectrometer. These proposed species contain epoxyphen that has not undergone ring-opening and rather is proposed to be coordinated through the harder Lewis basic oxirane oxygen.

A large dicationic peak at m/z 881.53 is tentatively assigned to a Cu^{II} epoxyphenanthroline species that has not undergone nucleophilic ring-opening, $[Pt_2(\mu_3\text{-}S)_2(PPh_3)_4Cu(C_{12}H_8N_2O)]^{2+}$ **9**, and has rather been complexed by the nitrogen centers of epoxyphen and then undergone further bidentate complexion by the nucleophilic sulfides of **1a**. The observed isotope pattern at m/z 881.53 is in close agreement with a calculated pattern for the proposed dication **9**. The serendipitous identification of this species is somewhat surprising considering the mysterious

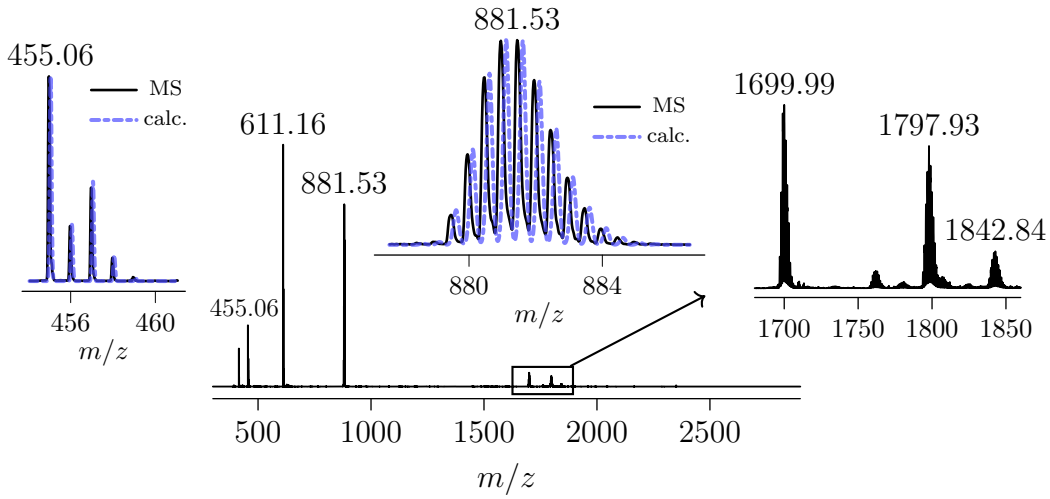

Figure 2.30: ESI mass spectrum of **1a** and 5,6-epoxy-5,6-dihydro-[1,10]-phenanthroline in methanol after 5 minutes. The right inset is an expanded view of the m/z range 1680 - 1860. The center and left insets are isotope pattern comparisons of the peaks observed at m/z 455.06 and 881.53 and calculated patterns for $[Cu(C_{12}H_8N_2O)_2]^+$ (calc. m/z 455.06) and $[Pt_2(\mu_3\text{-}S)_2(PPh_3)_4CuC_{12}H_8N_2O]^{2+}$ (**9**, calc. m/z 881.11). Capillary exit voltage 60 V.

source of copper ions, however the ESIMS instrument receives frequent use, and it is not uncommon for certain species to linger within the spectrometer, such as $[AuPPh_3]^+$. Additionally, the ESI apparatus can itself be considered an electrochemical cell, as a high voltage potential is facilitating droplet formation by converting ions to electrons.[196] In positive ion mode, electrochemical oxidation must necessarily be occurring at the liquid/metal interface of the capillary exit to maintain charge balance in the system, and this can include oxidation of capillary metal or residual sample at the interface, perhaps in this specific case, deposited in negative ion mode.[197] Furthermore, as the mass spectrum in Figure 2.30 was recorded after 5 minutes, a significant amount of unreacted **1a** was most likely present in solution and the bridging sulfide dimer is known to have accommodating properties as a bidentate metalloligand towards the Cu^{II} phenanthroline moiety *viz.* $[Pt_2(\mu_3\text{-}S)_2(PPh_3)_4Cu(phen)]^{2+}$.[29a]

Further evidence for the assignment of the Cu^{II} epoxyphenanthroline species **9** are the two cations observed at *m/z* 1797.93 and 1842.84, assigned as Cl^- and Br^- aggregate ion pars of the dication respectively ($[\mathbf{9}][X]^+$). The observed isotope patterns of these ions have a favorable but not high correlation with their respected calculated patterns, although this is not surprising considering the very low relative intensity with which they appear in the spectrum. Another interesting

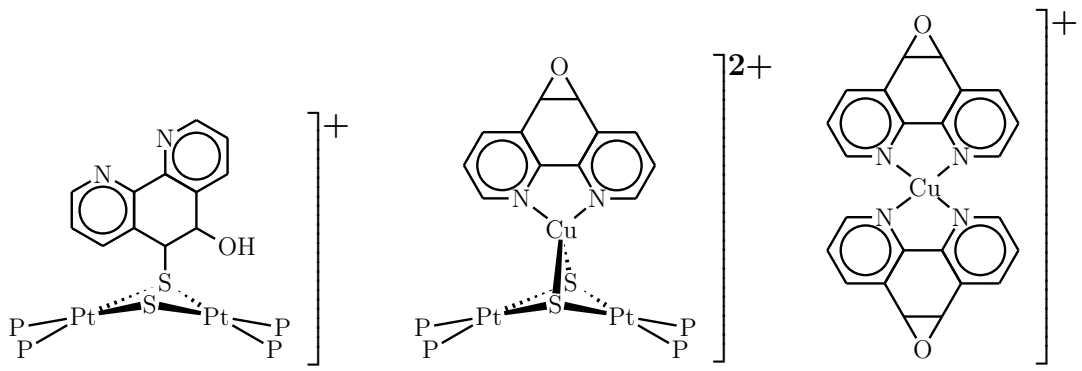

8, *m/z* 1700.32 **9**, *m/z* 881.45 **9a**, *m/z* 455.06

Figure 2.31: Proposed species $[Pt_2(\mu\text{-}S)(\mu\text{-}S{-}C_{12}H_8N_2OH)(PPh_3)_4]^+$ **8**, $[Pt_2(\mu_3\text{-}S)_2(PPh_3)_4CuC_{12}H_8N_2O]^{2+}$ **9**, $[Cu(C_{12}H_8N_2O)_2]^+$ **9a**.

peak at m/z 455.06 is assigned as the Cu^{I} tetrahedral di-phenanthroline complex $[Cu(C_{12}H_8N_2O)_2]^+$ **9a**, with a calculated isotope pattern in close agreement with the observed data. **9a** is presumably the result of reduction and ligand dissociation of the octahedral Cu^{II} complex $[Cu(epoxyphen)_2]^{2+}$,[198] which was not detected in the mass spectrum. Reduction is known to occur for Cu^{II} complexes within the mass spectrometer.

When the capillary exit voltage is increased to 210 V another dication at m/z 749.95, assigned as the PPh_3 loss ion of **9**, provides additional evidence for the assignment of **9**.

The reaction was repeated several days later after flushing the ESIMS instrument with methanol to help remove lingering Cu ions. Examination of the micro-scale reaction by ESIMS after one hour gave a similar spectrum as can be seen in Figure 2.32. Sodium adducts of excess phenanthroline are again assigned to peaks at m/z 415 and 611 and there is an absence of previously observed Cu species at m/z 455 and 881. The proposed ring-opened oxirane species **8** is assigned to the peak at m/z 1700.15, and the peak at m/z 1503.12 is assigned as protonated starting

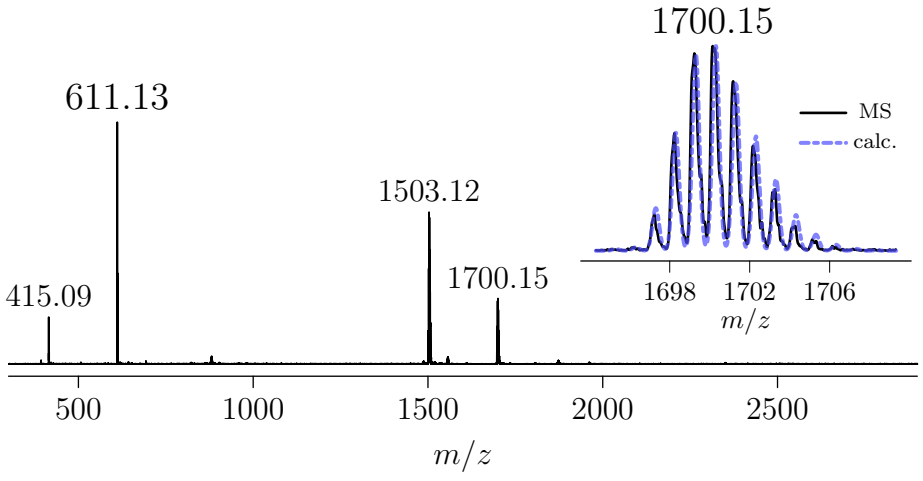

Figure 2.32: ESI mass spectrum of **1a** and 5,6-epoxy-5,6-dihydro--[1,10]-phenanthroline in methanol after 1 hour. The inset is an isotope pattern comparison of the observed peak at m/z 1700.15 and a calculated pattern for the proposed ring-opened oxirane species $[Pt_2(\mu\text{-}S)(\mu\text{-}S{-}C_{12}H_8N_2OH)(PPh_3)_4]^+$ **8** (calc. m/z 1700.32). Capillary exit voltage 60 V.

material **1a**$[H]^+$.

The reaction was again examined by ESIMS after 3 hours with little change and was left to stir at room temperature. After 30 hours, the reaction solution, which was noticeably more red in color, was examined once more by ESIMS (Figure 2.33). Curiously, the proposed oxirane ring-opened species **8** previously observed at *m/z* 1700.15 had shifted two mass units down to *m/z* 1698.27. This change is mass is interesting, and could be due to oxidation of the mercapto-phenanthranol ligand in **8** (proposed isomers **8a** and **8b** are presented in Scheme 2.7). A previous attempt at isolating ring-opened thiol-functionalised phenanthronols, very similar to the proposed derivative **8**, were hampered by dehydration which appeared to occur readily at mild conditions for a broad range of thiol nucleophiles (Scheme 2.8).[195] Aromatisation of the phenantholine was suggested as the driving force behind the dehydration, which is known to require significantly harsher conditions to proceed in 5-methoxy- or 5-dialkylamino-phenanthronol analogues.[192a] However, in the case of **8**, dehydration was ruled out as evidenced by an absence in any ESI mass spectra of the dehydration product [**8** - H_2O]$^+$. An additional change observed in the mass

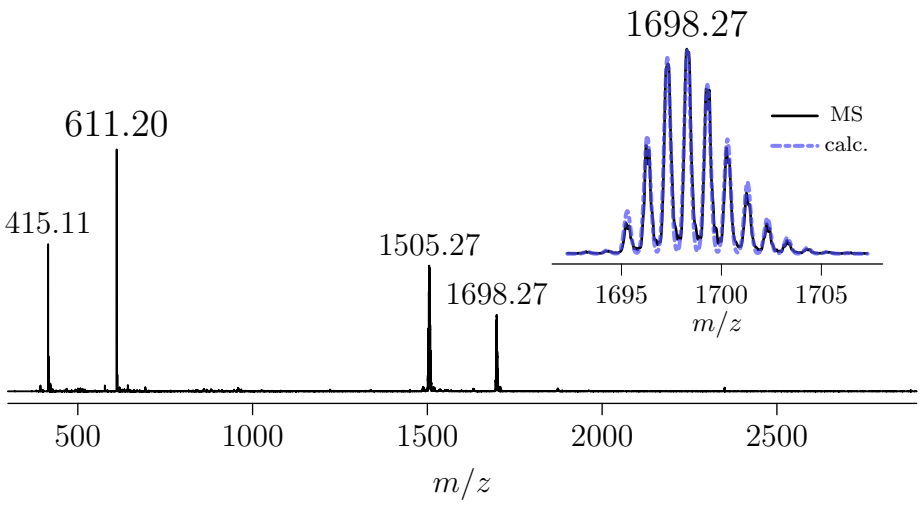

Figure 2.33: ESI mass spectrum of **1a** and 5,6-epoxy-5,6-dihydro-[1,10]-phenanthroline in methanol after 30 hours. The inset is an isotope pattern comparison of the peak observed at *m/z* 1698.27 and a calculated pattern for $[Pt_2(\mu\text{-}S)(\mu\text{-}S{-}C_{12}H_6N_2OH)(PPh_3)_4]^+$ **26** (calc. *m/z* 1698.30). Capillary exit voltage 60 V.

spectrum after 30 hours was a shift in the protonated starting material from *m/z* 1503 to *m/z* 1505 concomitant with a broader peak signal, possibly indicating an overlapping patter of two or more mono-cations. The μ-chloro species $[Pt_2(\mu\text{-}S)(\mu\text{-}Cl)(PPh_3)_4]^+$ (calc. *m/z* 1506.24) is known and appears in this region, and has previously been observed in oxidising conditions. As observed in the previous spectrum, the sodium adducts of epoxyphenanthroline are present at *m/z* 415 and 611.

The reaction solution was left on the bench for an extended period, and monitored by ESIMS after three weeks, and two months. Over this time, the reaction solution developed an increasingly dark red appearance, and after one month was almost opaque. In a simultaneous experiment over the same duration, a methanol solution of only the epoxyphenanthroline was prepared, and a similar change in color was not observed for the clear colorless solution after sitting in ambient conditions for two weeks. ESIMS of the reaction solution after three weeks was indicative of oxidative decomposition in **8**. The base peak at *m/z* 1487.9 was assigned as $[Pt_2(\mu\text{-}S)(\mu\text{-}OH)(PPh_3)_4]^+$, and a peak at *m/z* 1471.9 was assigned as $[Pt_2(\mu\text{-}O)(\mu\text{-}OH)(PPh_3)_4]^+$. Both calculated isotope patterns are in moderate agreement with the data. A very curious peak at *m/z* 1500.94 exhibited a typical isotope pattern for a dinuclear platinum species, although at one *m/z* lower than oxidised **1a** $[Pt_2(\mu\text{-}S)_2(PPh_3)_4]^{\bullet+}$ (calc. *m/z* 1502.23). This peak was tentatively assigned as the

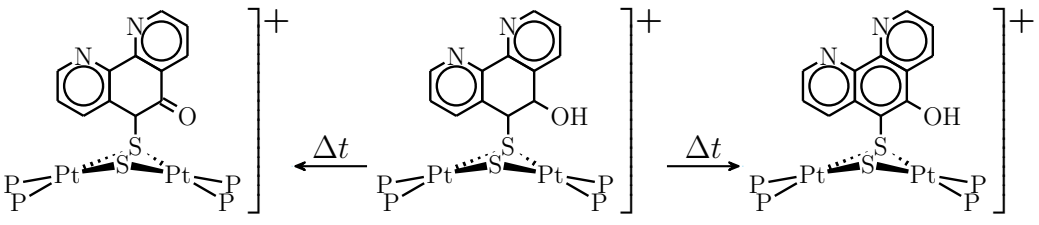

8a *m/z* 1698 | **8** *m/z* 1700 | **8b** *m/z* 1698

Scheme 2.7: Proposed species **8a** and **8b** resulting from a decrease of *m/z* 2 from $[Pt_2(\mu\text{-}S)(\mu\text{-}S{-}C_{12}H_8N_2OH)(PPh_3)_4]^+$ **8**, observed after 30 hours.

μ-alkoxide species $[Pt_2(\mu\text{-}S)(\mu\text{-}OCH_3)(PPh_3)_4]^+$ (calc. m/z 1501.28).

It appears that while the nucleophilic ring-opening of epoxyphenanthroline by **1a** occurs, isolation of the derivative **8** on a macro scale is complicated by a sluggish reaction and possible oxidation in solution. Considering the scant references for thiol-functionalised phenanthronols in the literature, it is noteworthy the proposed species **8** was observed by ESIMS.

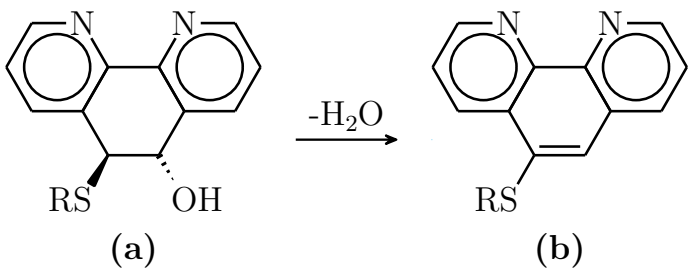

Scheme 2.8: The dehydration of a 5,6-bifunctionalised phen **(a)** resulting in aromatisation of the thioether phen **(b)**.

2.9 Experimental

2.9.1 General

Epoxides 2,2-dimethyloxirane, 2,3-dimethyl-2,3-epxoybutane, epibromohydrin, styrene oxide, cyclohexene oxide, and 5,6-epoxy-5,6-dihydro-[1,10]-phenanthroline were commercially obtained (Sigma). All reactions were carried out in ambient conditions. Reagent or laboratory grade solvents were used without purification.

2.9.2 Computational

Geometry optimisation and single point energy DFT calculations were carried out using the molecular geometry obtained from the crystal structure of **5**[BPh_4] using the ORCA[199] quantum chemisty program. The PBE0 hybrid functional[200] with DFT-D3 long-range dispersion correction by Grimme *et al.*[201,202] was employed with the def2-TZVP[203] basis set. The platinum atoms were treated with the def2-ECP[204] effective core potential. An analytical frequency calculation was performed on the optimised structure to check for negative frequencies. The reduced density gradient (RDG) and sign$\lambda_2(\rho)$ cube files were generated using the Multiwfn toolkit,[205] which was constrained with a modified grid that encompassed the specific area of chemical interest. PyMOL was used to integrate the molecular geometry with the RDG isosurface, colormapped with sign$\lambda_2(\rho)$ to identify areas of interest. A python script, using the matplotlib module,[206] was created to output the NCI plot of RDG vs. sign$\lambda_2(\rho)$.

2.9.3 Single crystal XRD experiments

X-ray diffraction data were collected on a Rigaku Oxford Diffraction XtaLAB-Synergy-S single crystal diffractometer with a PILATUS 200 K hybrid pixel array detector using Cu Kα radiation (λ = 1.54184 Å) at 99.9(5) K (**27**[BPh_4] and **7**[BPh_4]$\cdot(CH_2Cl_2)_3$). The intensity data were processed with the CrysAlis PRO[207] software suite and multi-scan empirical absorption corrections were applied using

spherical harmonics, implemented in the SCALE3 ABSPACK scaling algorithm. The structures were solved (**27**[BPh_4] and **7**[BPh_4]$\cdot(CH_2Cl_2)_3$ SHELXT-2018/2[208] using intrinsic phasing) and refined using SHELXL-2018/3[209] with full-matrix least-squares on F^2, all carried out in Olex2.[210] Unless otherwise stated, all non-hydrogen atoms were refined anisotropically and hydrogen atoms added with a riding model. Crystallographic data are tabulated in Table 2.5.

3$[PF_6]_2\cdot CHCl_3$

Small clear hexagonal plates of **3**$[PF_6]_2$ were grown from slow diffusion of diethyl-ether into a dichloromethane solution. A suitable sample was selected and immersed in perfluoropolyether (PFPE) oil prior to mounting. X-ray diffraction data were collected at 120 K on a Bruker APEX-II CCD diffractometer[211] using Mo Kα radiation (λ = 0.71073 Å) using a combination of ω- and φ-scans of 0.5°. Multi-scan empirical absorption corrections were applied using SADABS[212] (Bruker 2016). The structure was solved with the SHELXS-2008[213] structure solution program using Patterson Methods and expanded conventionally during structure refinement with full-matrix least-squares on F^2, which was carried out using the SHELXL-2018/3.[209] The complex crystallises in the monoclinic space group $C2/c$ ($Z' = \frac{1}{2}$) and has two PF_6^- anions per formula unit, confirming the dicationic charge. In the asymmetric unit, one-half PF_6^- anion lies on a $C2$ axis and another lies in very close proximity to an inversion center, and it's occupancy was fixed to 0.5. Bond distance restraints were placed on both counterions using the SADI instruction. A molecule of dichloromethane solvent was nearly coincident with the latter PF_6^- anion, and was fixed at 0.5 occupancy. As the refinement progressed, it was evident there was a substantial amount of dichloromethane solvent present, consistent with the observation of rapid solvent loss from the crystal. Several of these solvent molecules were positionally disordered about inversion centers or two-fold axes, and after several unsatisfactory attempts to reasonably model the disorder, the SQUEEZE[214] routine from PLATON[215] was employed removing approximately 160 e^- from a volume of

450 $Å^3$ per formula unit, representing aproximately 4 CH_2Cl_2 molecules. Due to the two-fold rotation axis passing through the center of the $\{Pt_2(\mu\text{-}SR)_2\}$ core, the thermal parameters of C1, C2, and O1 were severely distorted and gave chemically unreasonable distances (C1-C2 1.4 Å, C2-O1 1.6 Å, S1-C1 1.7 Å, C2-C1$'$[†] 1.68 Å) which resulted in a very assymetric overhead-bridge. To remedy this, pairs of 1,2 distances C2-C1, C2-C1$'$ and 1,3 distances O1-C1, O1-C1$'$ were restrained to be equal using the SADI instruction. Additionally, thermal restraints DELU, RIGU, and ISOR were applied to C1, C2, and O1. The application of these restraints resulted in much more chemically sensible bond distances, a nearly symmetric overhead bridge, and more reasonable thermal parameters, however this was not the case for O1. All non-hydrogen atoms were refined anisotropically and hydrogen atoms were added with a riding model and refined freely with the exception of C1, C2, and O1, for which no hydrogen atoms were added. The largest density peak of 2.57 $e \cdot Å^{-3}$ was located 0.86 Åfrom Pt1, consistent with spurious electron density. Structure solution and refinement was carried out in Olex2.[210]

5[BPh_4]

The complex crystallises in the monoclinic space group $P2_1/c$, $Z' = 1$, as a mixture of enantiomers at the C1 position of the mercapto-cyclohexanol ligand. Accordingly, the mercapto-cyclohexanol ligand in the complex was positionally disordered with a refined major:minor component ratio of approximately 80:20, each component connected to S1 and occupying a similar volume in the asymmetric unit. Due to the chemical equivalence of the components, the SAME instruction was applied to the second component along with rigid thermal restraints DELU and RIGU on both components. Additionally, the overlapping orientation of the components resulted in nearly coincident thermal ellipsoids and the SIMU restraint was applied to mitigate unreasonable thermal parameters with a cutoff of 0.7 Å. The EADP constraint was finally applied to prevent O1_2 and C3_2 from going NPD, taking

[†]symmetry code $[2 - x, +y, \frac{3}{2} - z]$

on the thermal displacement parameters of their respective counterpart atoms in the primary component O1_1 and C3_1. A positive displacement in the difference map was identified around O1_1 of the major component (0.95 e $\cdot$ Å^{-3}), and accordingly the hydroxyl hydrogen was added with the AFIX 147 instruction. The corresponding hydroxyl hydrogen for the minor component was added with AFIX 83. A positional disorder in a phenyl ring of a triphenylphosphine ligand P3 was also modelled. Although appearing to be positionally related to the disorder in the mercapto-cyclohexanol ligand, the third free variable was instead used to refine a roughly 60:40 composition. The FLAT and SIMU restraints were applied to the disordered components, which were left isotropic. Hydrogen atoms were included using a riding model and refined freely. In the final stages of refinement, attempts were made to remove EADP constraints, however this again resulted in O1_2 and C3_2 going NPD, and the constraints were kept in the final refinement.

7$[BPh_4] \cdot (CHCl_3)_2$

The complex crystallises as the *bis*-dichloromethane solvate in the monoclinic space group $P2_1/n$ with $Z' = 1$. The mercapto-isobutanaol ligand (L) was positionally disordered over two sites S1_1 and S1_2, the latter being nearly positionally coincident with S2 (0.4 Å separation). Additionally, a disordered dichloromethane solvent molecule (only two components modelled) occupied the same positional space as the minor component of the mercapto-isobutanol ligand $L_{(min.)}$. Hence, two SUMP instructions were applied to refine the two-component L and dependent three-component $L_{(min.)}$-solvent disorders. To more accurately model $L_{(min.)}$, the SAME instruction was applied (chemically identical $L_{(maj.)}$), however the coincident disordered solvent complicated anisotropic refinement of $L_{(min.)}$ and it was left isotropic. Additionally, rigid bond and thermal restraints were applied to the solvent. The close proximity of disordered solvent to $L_{(min.)}$ also resulted in the methyl hydrogen atom H3C_2, constrained with an AFIX 137 code, to give a large shift error. The constraint was changed to AFIX 33, which allowed the refinement to con-

verge. A second dichloromethane solvent molecule was positionally disordered over the same site, and was modeled anisotropically, occupationally independent from the other disorders. A third dichloromethane solvent molecule was also positionally disordered about an inversion center, and after several unsatisfactory attempts to reasonably model the disorder, the SQUEEZE[214] routine from PLATON[215] was employed removing approximately 32 e^- from a volume of 61 $Å^3$. Thus, the void is tentatively assumed to contain a fractional occupation (0.76) of dichloromethane. Hydrogen atoms were added in a riding model at refined freely. Spurious Q-peaks were identified around $L_{(maj.)}$ towards the end of the refinement, suggesting a similar fractional occupation by a dichloromethane solvent molecule as for $L_{(min.)}$, however no attempt was made to model the solvent.

Table 2.5: Crystallographic data.

	3$[PF_6]_2 \cdot CH_2Cl_2$	**5**BPh_4	**7**$[BPh_4] \cdot (CH_2Cl_2)_2$
Empirical formula	$C_{76}H_{62}Cl_2F_{12}OP_6Pt_2S_2$	$C_{102}H_{91}BOP_4Pt_2S_2$	$C_{102}H_{93}BCl_4OP_4Pt_2S_2$
M_r $(g \cdot mol^{-1})$	1930.27	1921.73	2065.65
Crystal size (mm)	0.426 x 0.202 x 0.136	0.14 x 0.1 x 0.08	0.12 x 0.1 x 0.1
Crystal system	monoclinic	monoclinic	monoclinic
Space group	$C2/c$	$P2_1/c$	$P2_1/n$
a (Å)	17.696(2)	13.64020(10)	17.80128(13)
b (Å)	23.253(2)	35.8761(2)	24.33854(19)
c (Å)	21.300(2)	17.39980(10)	21.27309(15)
α (°)	90	90	90
β (°)	95.595(2)	95.0090(10)	95.7451(7)
γ (°)	90	90	90
V $(Å^3)$	8722.7(16)	8482.20(9)	9170.42(12)
Z	4	4	4
ρ_{calc} $(g \cdot cm^{-3})$	1.470	1.505	1.479
$\mu(CuK_\alpha)$ (mm^{-1})	3.487	7.632	7.999
$F(000)$	3784.0	3856.0	4091.0
2θ range (°)	2.9 to 56.8	5.662 to 148.438	6.172 to 144.256
Reflections collected/unique	77889/76832/10950	182028/180394/16995	147878/144655/18010
R_{int}	0.0382	0.0540	0.0617
Data/parameters/restraints	10950/499/146	16995/1132/143	18010/1104/46
Goodness-of-fit on F^2	1.232	1.042	1.132
Final R indices $[I > 2\sigma(I)]$	$R_1 = 0.0550, wR_2 = 0.1296$	$R_1 = 0.0259, wR_2 = 0.0584$	$R_1 = 0.0423, wR_2 = 0.0919$
R indices (all data)	$R_1 = 0.0616, wR_2 = 0.1323$	$R_1 = 0.0290, wR_2 = 0.0597$	$R_1 = 0.0471, wR_2 = 0.0942$
T_{min}/T_{max}	0.602/0.746	0.601/1.000	0.734/1.000
ρ_{max}/ρ_{min} $(e \cdot Å^{-3})$	2.57/-1.85	0.88/-1.89	1.11/-1.61

2.9.4 Synthesis

Synthesis of $[Pt_2(\mu\text{-}S)(\mu\text{-}S{-}C_3H_5OH)(PPh_3)_4][PF_6]_2$ (**3**$[PF_6]_2$)

To a stirring suspension of **1a** (120 mg, $7.98{\times}10^{-2}$ mmol) in methanol (25 mL) was added epibromohydrin (0.2 mL, 320 mg, 2.34 mmol) dropwise after which crushed triphenylphosphine (22.0 mg, $8.39{\times}10^{-2}$ mmol) was added. After stirring at room temperature for 24 hours, the clear pale-yellow solution was filtered to remove a trace amount of insoluble matter before the addition of a molar excess of ammonium hexafluorophosphate (50.0 mg, $3.07{\times}10^{-1}$ mmol), resulting in the formation of a pale-yellow precipitate, which was collected by vacuum filtration on a glass sintered frit, washed successively with distilled H_2O (3 x 20 mL) and diethyl ether (1 x 10 mL) before drying under vacuum to give pure **3**$[PF_6]_2$ as an off-white solid (107 mg, 72%). M.p. 266°C. *Anal.* Calc. for $C_{75}H_{66}F_{12}OP_6Pt_2S_2$: C, 48.65; H, 3.59%. Found: C, 48.50; H, 3.41%. Clear hexagonal plate-like crystals were obtained by vapor diffusion of diethyl ether into a dichloromethane solution. $^{31}P\{^1H\}$-NMR (121.49 MHz, $CDCl_3$): δ 19.2 [s, br, $^1J_{(PtP)}$ 3040 Hz]. ESIMS, *m/z* 780.64 $[M]^{2+}$ (100%), *m/z* 1706.24 $[M][PF_6]^+$ (18%).

Synthesis of $[Pt_2(\mu\text{-}Se)(\mu\text{-}Se{-}C_3H_5OH)(PPh_3)_4][PF_6]_2$ (**4**$[PF_6]_2$)

Epibromohydrin (0.1 mL, 160 mg, 1.17 mmol) was added dropwise to a cloudy brown suspension of **1b** (51.0 mg, $3.19{\times}10^{-2}$ mmol) in methanol (15 mL). Triphenylphosphine (10.0 mg, $3.81{\times}10^{-2}$ mmol) was immediately added, and the resulting mixture stirred at room temperature for 2 hours. Ammonium hexafluorophosphate (50.0 mg, $3.07{\times}10^{-1}$ mmol) was added to the clear red reaction solution, and a red brown solid collected by vacuum filtration on a glass sintered frit, which was washed successively with distilled H_2O (2 x 10 mL) and diethyl ether (1 x 10 mL) before drying under vacuum (41.4 mg, 67%). ESIMS, *m/z* 827.96 (calc. *m/z* 828.08) $[M]^{2+}$ (100%).

Synthesis of $[Pt_2(\mu\text{-}S)(\mu\text{-}S{-}C_6H_{10}OH)(PPh_3)_4][BPh_4]$ (**5**[BPh_4])

A cloudy orange suspension of **1a** (84.7 mg, $5.63{\times}10^{-2}$ mmol) and cyclohexene oxide (0.4 mL, 388 mg, 3.95 mmol) in methanol (25 mL) was stirred and brought to a gentle reflux for 5 hours, after which the reaction solution was clear and yellow in color. After cooling to room temperature, the reaction solution was filtered to remove a trace amount of insoluble matter before a molar equivalent of $NaBPh_4$ (19.3 mg, $5.64{\times}10^{-2}$ mmol) was added, prompting the immediate formation of a yellow precipitate. After the subsequent addition of distilled H_2O (10 mL) and stirring for 10 minutes, a yellow solid was collected by vacuum filtration on a glass sintered frit, washed with distilled H_2O (4 x 20 mL) and Et_2O (1 x 10 mL), before drying under vacuum to give pure **5** as a yellow powder (82.0 mg, 76%). Yellow plate-like crystals suitable for a single-crystal XRD experiment were grown from diffusion of diethyl ether into a chloroform solution. M.p. 141°C. *Anal.* Calc. for $C_{102}H_{91}BOP_4Pt_2S_2$: C, 63.75; H, 4.77%. Found: C, 63.38; H, 4.85%. ESIMS, *m/z* 1602.16 $[M]^+$ (100%). ^{1}H-NMR (600 MHz, $CDCl_3$): δ 7.46-6.88 [aromatic, 80H], 5.89 [d, 1H], 3.87 [m, br, 1H], 1.99 [d, br, 1H], 1.55 [d, br, 1H], 1.32 [m, br, 1H], 1.02 [m, 2H], 0.94 [d, br, 1H], 0.37 [dq, br, 1H], 0.21 [dq, 1H], -0.34 [d, br, 1H]. ^{13}C-NMR (150.91 MHz, $CDCl_3$): δ 164.9-121.6 [aromatic], 73.8, 57.7, 35.2, 34.2, 26.7, 24.8. ^{31}P{^{1}H}-NMR (242.95 MHz, $CDCl_3$): δ 26.9 [m, $^1J_{(PtP)}$ (*trans* RS^-) 3225 Hz], 26.7 [m, $^1J_{(PtP)}$ (*trans* S^{2-}) 2686 Hz], 22.5 [m, br, $^1J_{(PtP)}$ (*trans* RS^-) 2623 Hz], 22.4 [m, br, $^1J_{(PtP)}$ (*trans* S^{2-}) 3152 Hz]. ^{195}Pt{^{1}H}-NMR (129.02 MHz, $CDCl_3$): δ -4262 [dd, $^1J_{(PtP)}$ 3227, 2631 Hz, $^2J_{(PtPt)}$ 977 Hz], -4311 [dd,$^1J_{(PtP)}$ 3144, 2691 Hz].

Synthesis of $[Pt_2(\mu\text{-}S)(\mu\text{-}S{-}C_8H_8OH)(PPh_3)_4][BETI]$ (**6**[**BETI**])

To a suspension of **1a** (105 mg, $6.98{\times}10^{-2}$ mmol) in methanol (20 mL) was added styrene oxide (0.2 mL, 210 mg, 1.75 mmol) dropwise, and the resulting suspension was left to stir at r.t. for 24 hours. After filtering the clear yellow solution, a molar excess of lithium bis(pentafluoroethanesulfonyl)imide (BETI, 100 mg, $2.58{\times}10^{-1}$ mmol) was added prompting the formation of a yellow precipitate which was col-

lected by vacuum filtration on a glass sintered frit. The yellow solid was washed successively with distilled H_2O (3 x 20 mL) and diethyl ether (1 x 5 mL) before drying under vacuum to give pure **6**[BETI] (119 mg, 85%). M.p. 116°C. *Anal.* Calc. for $C_{84}H_{69}F_{10}NP_4Pt_2S_2$: C, 50.33; H, 3.47; N, 0.70%. Found: C, 51.22; H, 3.28; N, 0.66%. ^{13}C-NMR (150.91 MHz, $CDCl_3$): δ 142.7-109.8 (aromatic, BETI CF_n), 74.0, 66.7 (-ve DEPT), 60.7, 43.5 (-ve DEPT); $^{31}P\{^1H\}$-NMR (242.95 MHz, $CDCl_3$): δ 26.1 [m, $^1J_{(PtP)}$ 3216 Hz], 25.9 [m, $^1J_{(PtP)}$ 2640 Hz], 25.7 [m, $^1J_{(PtP)}$ 2595 Hz], 25.7 [m, $^1J_{(PtP)}$ 3229 Hz], 23.3 [ddd, $^2J_{(PP)}$ 18.7, $^4J_{(PP-trans)}$ 27, $^4J_{(PP-cis)}$ 3, $^1J_{(PtP)}$ 3307 Hz], 22.9 [ddd, br, $^2J_{(PP)}$ 19.5, $^4J_{(PP-trans)}$ 28, $^1J_{(PtP)}$ 3298 Hz], 22.5 [m, br, $^1J_{(PtP)}$ 2655 Hz], 22.1 [ddd, $^2J_{(PP)}$ 19.6, $^4J_{(PP-trans)}$ 27, $^4J_{(PP-cis)}$ 7, $^1J_{(PtP)}$ 2646 Hz]; $^{195}Pt\{^1H\}$-NMR (129.02 MHz, $CDCl_3$): δ -4278.8 [dd, $^1J_{(PtP)}$ 3233 (*trans* RS^-), 2631 (*trans* S^{2-}), $^2J_{(PtPt)}$ 930 Hz], -4305.9 [dd, $^1J_{(PtP)}$ 3230 (*trans* RS^-), 2593 Hz (*trans* S^{2-})], -4336.6 [dd, $^1J_{(PtP)}$ 3287 (*trans* RS^-), 2643 Hz (*trans* S^{2-})], -4368.0 [dd, $^1J_{(PtP)}$ 3299 (*trans* RS^-), 2661 (*trans* S^{2-}), $^2J_{(PtPt)}$ 860 Hz]. ESIMS, *m/z* 1624.28 (calc. *m/z* 1624.31) $[M]^+$ (100%).

Eppendorf reaction of $[Pt_2(\mu\text{-}Se)_2(PPh_3)_4]$ **1b** and styrene oxide

To an eppenforf vial containing **1b** (≈ 2 mg, 1.25×10^{-3} mmol) in methanol (0.5 mL) was added styrene oxide (≈ 0.05 mL, 55 mg, 4.58×10^{-1} mmol) and the resulting mixture was agitated and left to sit at room temperature for 5 hours after which a portion (≈ 0.05 mL) of the solution was removed and anlysed by ESIMS. ESIMS, *m/z* 1719.05 (calc. *m/z* 1719.20) $[M]^+$ (100%), *m/z* 1040.03 (calc. *m/z* 1040.19) $[PtSe(C_8H_8O)(C_8H_8OH)(PPh_3)_2]^+$ (30%).

Attempted synthesis of $[Pt_2(\mu\text{-}S)(\mu\text{-}S{-}C(CH_3)_2C(CH_3)_2OH)(PPh_3)_4]^+$

To a suspension of **1a** (≈ 2 mg, 1.33×10^{-3} mmol) in methanol (1 mL) in a 2 mL eppendorf vial was added one drop of 2,3-dimethyl-2,3-epoxybutane (≈ 0.05 mL, 39.05 mg, 3.90×10^{-1} mmol) and the resulting mixture shaken vigorously and allowed to sit at room temperature for 30 minutes, after which a small amount of solution

was examined by ESIMS. The reaction was repeated in a 10 mL roundbottom flask fitted with a condenser, heating gently until reflux temperature was reached. After 3 hours of refluxing, a small amount of solution (0.1 mL) was examined by ESIMS.

Synthesis of $[Pt_2(\mu\text{-}S)(\mu\text{-}S{-}CH_2C(CH_3)_2OH)(PPh_3)_4][BPh_4]$ (**7**$[BPh_4]$)

The cloudy orange suspension of **1a** (93.0 mg, $6.19{\times}10^{-2}$ mmol) and 2,2-dimethyloxirane (0.4 mL, 324.8 mg, 4.50 mmol) in methanol (20 mL) was stirred whilst gently heating to reflux temperature. After refluxing 40 minutes, the reaction solution was clear and yellow in color. The heating mantle was removed and the solution allowed to return to room temperature after which a molar equivalent of sodium tetraphenylborate was added (21.9 mg, $6.40{\times}10^{-2}$ mmol). After the addition of distilled H_2O (10 mL) and stirring at room temperature for an additional 20 minutes, a fine pale-yellow precipitate was collected by vacuum filtration on a glass sintered frit and washed successively with distilled H_2O (3 x 20 mL) and Et_2O (1 x 10 mL) before drying under vacuum to give pure **7**$[BPh_4]$ as a fine yellow solid (97.4 mg, 83%). Crystals suitable for an single-crystal XRD experiment were grown successfully from vapor diffusion of pentane into a chloroform solution of the salt. M.p. 258°C. *Anal.* Calc. for $C_{100}H_{89}BOP_4Pt_2S_2$: C, 63.36; H, 4.73%. Found: C, 63.27; H, 4.68%. ^{1}H-NMR (600 MHz, $CDCl_3$): δ 7.47-6.88 [*aromatic*, 80H], 2.31 [t, 2H, $^4J_{(PH)}$ 5.3 Hz], 2.29 [s, br, 1H], 0.68 [s, 6H]. ^{13}C-NMR (150.91 MHz, $CDCl_3$): δ 164.5-121.6 *aromatic*, 70.1, 53.4, 29.1. $^{31}P\{^1H\}$-NMR (242.95 MHz, $CDCl_3$): δ 24.5 (dd, br, $^1J_{(PtP)}$ (*trans* RS^-) 3290 Hz), 23.59 (dd, br, $^1J_{(Pt-P)}$ (*trans* S^{2-}) 2630 Hz) ESIMS, *m/z* 1576.12 $[M]^+$ (100%).

Attempted synthesis of $[Pt_2(\mu\text{-}S)(\mu\text{-}S{-}C_{12}H_8N_2OH)(PPh_3)_4]^+$ (**8**)

5,6-Epoxy-5,6-dihydro-[1,10]-phenanthroline (207 mg, 1.06 mmol) was added to a cloudy orange suspension of **1a** (107 mg, $7.13{\times}10^{-2}$ mmol) in methanol (20 mL) and the resulting suspension stirred at room temperature. After one hour a small amount of the orange-red solution was examined by ESIMS, and the reaction allowed to

continue. The reaction solution was examined again by ESIMS after 3 and 30 hours. Over this time duration the color of the reaction solution progressively changed to a dark red-orange color and clear. After 30 hours, the reaction solution was allowed to sit covered on the bench. ESIMS was again used to examine the reaction solution after three weeks and two months. After three weeks, the reaction solution was clear and very dark red in color.

Chapter 3

Nucleophilic ring-opening reactions of various activated cyclopropanes and an aziridine with $[Pt_2(\mu\text{-}S)_2(PPh_3)_4]$

3.1 Introduction

Cyclopropanes are quite interesting in that despite their relatively high energy and ring-strain, the C−C bonds, which resemble more closely the C=C double bond, are quite kinetically inert and tend to retain the cyclic structure.[216,217] Thus, ring-opening reactions of cyclopropanes by thiol nucleophiles is limited to activated cyclopropanes with electron withdrawing groups, often complemented by increased ring-strain in the cyclopropane.[218] For example, diactivated cyclopropanes like diallyl cyclopropane-1,1-dicarboxylate, have been used to synthesise polymer chains with thiol-ene click functionality.[219] Enhanced activation of the three membered ring can be achieved more readily with vicinal donor-acceptor groups, termed donor-acceptor (D-A) cyclopropanes,[220,221] ring-opening reactions of which are well represented in the literature.[217] The cyclopropanes chosen for this study are all activated in varying

degrees, the exception being bromomethyl cyclopropane.

Nucleophilic ring-opening reactions of aziridines by alkyl- and aryl-thiols has been extensively explored,[222] and in contrast to cyclopropanes, can typically proceed without the use of catalysts.[223] These reactions are often used as a convenient means of accessing novel β-amino sulfides, which have found use as catalysts,[224,225] in medicine[226] and drug design,[227] and as chemosensors.[228] Particularly interesting in β-amino sulfides are their propensity for heterobidentate coordination, a property which has seen them employed as chiral asymmetric catalysts in allylic substitution reactions.[229–231] Similar to epoxides, the site of nucleophilic attack by thiols on an asymmetric aziridine is generally the less hindered carbon,[232,233] and high regioselectivity can be achieved, often without the use of catalysts[223] or activated aziridines.[234] Increased reactions rates however have been achieved using catalysts such as strong acids,[235,236] Lewis acids,[237] and in water with tributylphosphine.[118]

Various activated cyclopropanes and an aziridine (Figure 3.1) were chosen to complement the initial examination of epoxide ring-opening with $[Pt_2(\mu\text{-}S)_2(PPh_3)_4]$

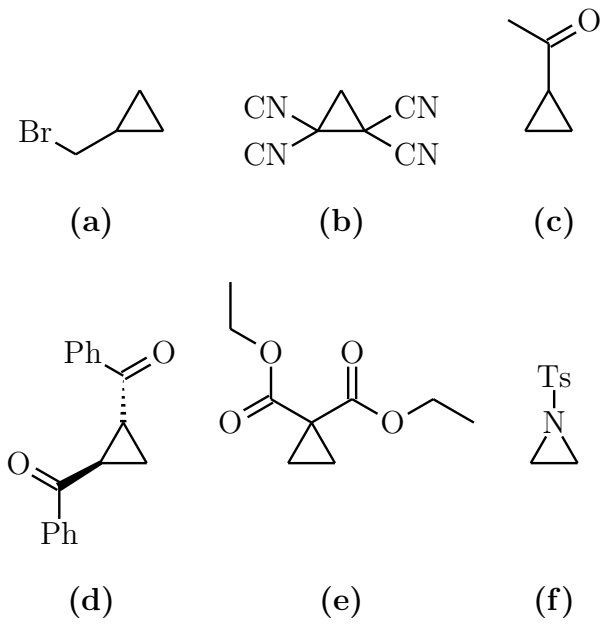

Figure 3.1: Cyclopropanes and aziridine to be examined: **(a)** (bromomethyl)cyclopropane, **(b)** 2,2,3,3-tetracyanocyclopropane, **(c)** cyclopropyl methyl ketone, **(d)** *trans*-1,2-dibenzoylcyclopropane, **(e)** diethyl cylopropane-1,2-dicarboxylate, **(f)** *N*-tosylaziridine.

(**1a**) discussed in Chapter 2. The degree of substitution on the ring-carbons of the epoxide was determined to be a significant factor for a successful reaction, and in some cases it was shown to dictate regioselectivity. For example when **1a** was reacted with 2,2-dimethyl oxirane the reaction appears to have only occurred at the sterically accessible ring-carbon, while the reaction with styrene oxide resulted in a mixture of structural isomers, indicating significant reactivity at the more substituted ring-carbon. An examination of **1a** with the selected cyclopropanes and aziridine will be interesting on several fronts, primarily it should provide a more robust description of the nucleophilicity in **1a**, considering the varying degree of activation in the chosen cyclopropanes. Furthermore, any successful reactions will complement the existing literature by opening up otherwise unexplored routes to novel thiolato derivatives of **1a**, species that are typically only accessible through the use of alkylating agents.

3.2 Bromomethylcyclopropane, alkylation and/or ring-opening

The nucleophilic sulfide centers of the Pt^{II} dimer $[Pt_2(\mu\text{-}S)_2(PPh_3)_4]$ **1a** readily undergo alkylation reactions, even with mild alkylating agents.[17,42b] Previously in this work, the μ-sulfide ligands of **1a** have also been shown to effect ring-opening of various epoxides. As (bromomethyl)cyclopropane, like the oxirane epibromohydrin, is an alkylating agent, a similar reaction is anticipated whereby the cyclopropane is tethered in close proximity to the underivatised sulfide in **1a** (Scheme 3.1). Although the cyclopropane ring is quite inert towards nucleophilic attack, especially without activating substituents, this geometric constraint could promote intramolecular ring-opening, as was observed in the oxirane analogue.

In the first examination of possible (bromomethyl)cyclopropane ring-opening by **1a**, mono-alkylation was observed after 72 hours at r.t. (Figure 3.2) and no evidence of the proposed ring-opened cyclopropane derivative around *m/z* 779.6. The isotope pattern of the cation at *m/z* 1558.27 closely matches a calculated pattern for the proposed alkylation product $[Pt_2(\mu\text{-}S)(\mu\text{-}S{-}CH_2C_3H_5)(PPh_3)_4]^+$ **10** (calc. *m/z* 1558.29).

To see if more forceful conditions would promote nucleophilic ring-opening of

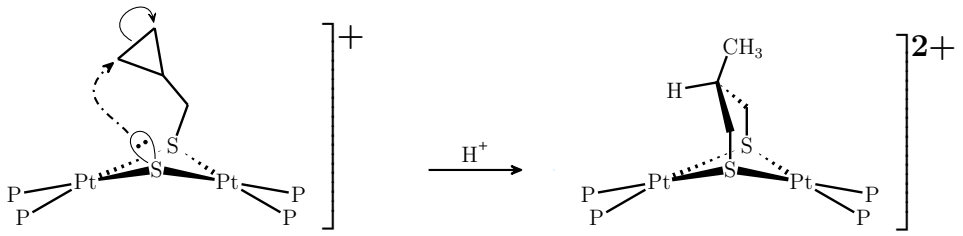

10, calc. *m/z* 1558.29 **28**, calc. *m/z* 779.65

Scheme 3.1: A possible intramolecular nucleophilic ring-opening reaction of the proposed tethered cyclopropane derivative $[Pt_2(\mu\text{-}S)(\mu\text{-}S{-}CH_2C_3H_5)(PPh_3)_4]^+$ **10** resulting in an overhead-bridged dication $[Pt_2(\mu\text{-}S{-}CH_2CHCH_3CH_2{-}\mu\text{-}S)(PPh_3)_4]^{2+}$ **28**, similar to the isolated complex **3** from the reaction of **1a** and epibromohydrin.

the cyclopropane, the reaction was repeated in refluxing ethanol, which appears to be a more robust solvent choice for reactions requiring extended periods at elevated temperatures, despite the sparing solubility of **1a** in the higher alcohols. After stirring and reaching reflux temperature (15 min.) the reaction solution became yellow and clear, indicative of monoalkylated derivatives of **1a**, as observed in this work and reported in the literature.[126] Indeed, ESIMS examination of the reaction solution confirmed a mass spectrum with a single cation at *m/z* 1558, assigned as **10**. After stirring and refluxing for an additional 65 hours, the reaction solution turned cloudy and slightly off-white in color. A bad stench was also evident, similar in nature to that of a short chain thiol.

Examination of the reaction solution by ESIMS affords a much changed spectrum, as additional cations are now present alongside the previously identified **10** at *m/z* 1431.16, 1665.22, and 2040.17 (Figure 3.3). More forcing conditions appears to have enhanced the alkylation of **1a** resulting in di-alkylation of both sulfide centers in the proposed $[Pt_2(\mu\text{-}S{-}CH_2C_3H_5)(PPh_3)_3Br]^+$ at *m/z* 1431.16 (Figure 3.4a), and in decomposition leading to trimetallic aggregates $[Pt_3(\mu_3\text{-}S)(\mu\text{-}S{-}CH_2C_3H_5)_3(PPh_3)_3]^+$ **29** (Figure 3.4b) and $[Pt_3(\mu_3\text{-}S)_2(PPh_3)_5Br]^+$ at *m/z* 1665.21 and 2040.17

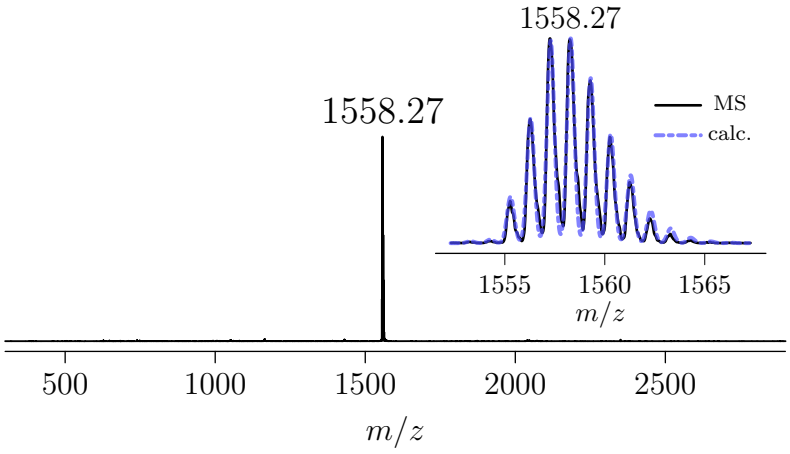

Figure 3.2: ESI mass spectrum of **1a** and (bromomethyl)cyclopropane in methanol after stirring for 72 hours at r.t. The inset is an isotope pattern of the observed peak at *m/z* 1558.27 and a calculated pattern for the proposed cation $[Pt_2(\mu\text{-}S)(\mu\text{-}S{-}CH_2C_3H_5)(PPh_3)_4]^+$ **10** (calc. *m/z* 1558.29). Capillary exit voltage 60 V.

respectively. Although typically requiring extreme conditions or strong alkylating agents, further alkylation of a cationic species $[Pt_2(\mu\text{-}S)(\mu\text{-}S{-}R)(PPh_3)_4]^+$ at the underivatised sulfide has been observed to occur.[18,42b] While halide ligand replacement by Br^- or I^- in these dications has been observed previously[18,123,132] and in this work, degradation of the dimer leading to multi-metallic aggregates is somewhat unusual. Typically these species are observed when significant forcing conditions are used[105] or when there is increased lability in one of the chalcogenide bridging ligands, such as in derivatives of **1a** with selenolate or tellurolate ligands.[78] Metal scrambling reactions, known to occur for derivatives of **1b**, can also lead to these multi-metallic aggregates.[73d] The structural motif of the proposed species **29** has been observed previously for trinuclear Pt^{II} complexes with thiolate[238] and tellurolate[78] ligands.

The use of more forcing conditions over an extended period has not been sufficient to promote any cyclopropane ring-opening. The excess bromomethylcyclopropane

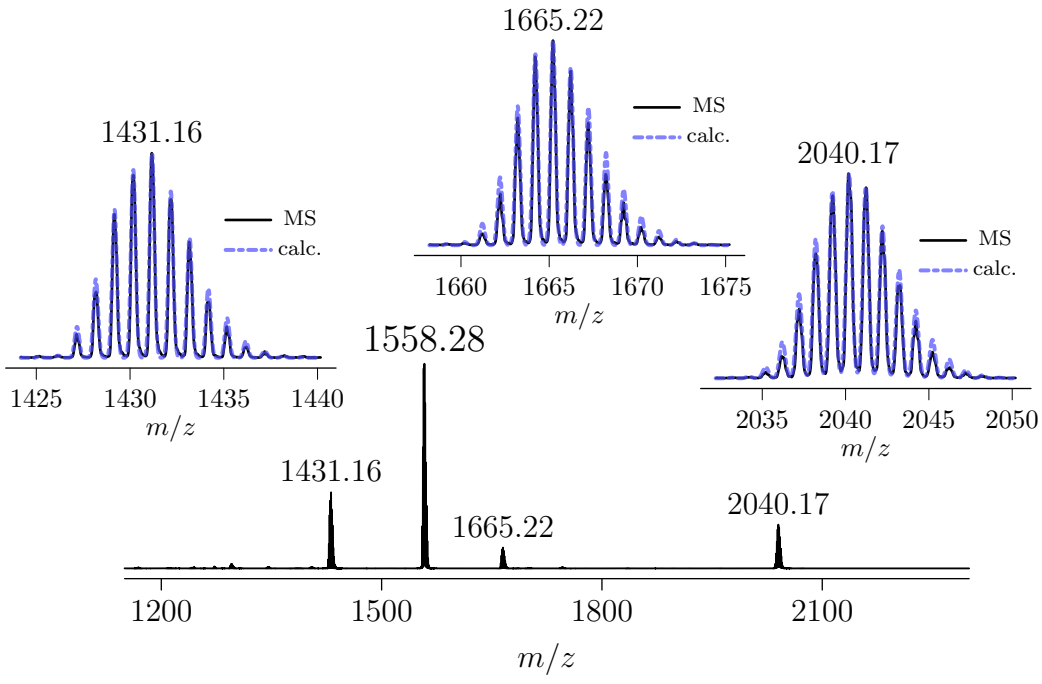

Figure 3.3: ESI mass spectrum of **1a** and bromomethylcyclopropane in ethanol after refluxing for 65 hours. The insets are isotope pattern comparisons of observed peaks and calculated patterns for (left) *m/z* 1431.16 and $[Pt_2(\mu\text{-}S{-}CH_2C_3H_5)_2(PPh_3)_3Br]^+$ (calc. *m/z* 1431.17), (center) *m/z* 1665.22 and $[Pt_3(\mu_3\text{-}S)(\mu\text{-}S{-}CH_2C_3H_5)_3(PPh_3)_3]^+$ (calc. *m/z* 1665.21), and (right) *m/z* 2040.17 and $[Pt_3(\mu_3\text{-}S)_2(PPh_3)_5Br]^+$ (calc. *m/z* 2040.21). Capillary exit voltage 150 V.

present in the reaction solution and use of forcing conditions might be competitively inhibiting any possible ring-opening reaction of the bound cyclopropane. To examine the effect of forcing conditions on only intramolecular ring-opening of the tethered cyclopropane in **10**, the reaction was repeated to isolate the tetraphenylborate salt. The complex $\mathbf{10}\cdot\mathrm{BPh_4}$ was then dissolved in a small amount of chloroform prior to refluxing in a methanolic solution for 64 hours. The ESI mass spectrum of the reaction solution again showed no evidence of cyclopropane ring-opening, with the only cation in the mass spectrum being **10**. The fragmentation of **10** was examined by employing a capillary exit voltage of 210 V, resulting in two additional cations in the mass spectrum at *m/z* 1295.119 and 1033.10 assigned as $[\mathbf{10} - \mathrm{PPh_3}]^+$ (calc. *m/z* 1295.20) and $[\mathbf{10} - 2\,\mathrm{PPh_3}]^+$ (calc. *m/z* 1033.11) respectively.

To further characterise the alkylated derivative **10**, a chloroform-*d* solution was examined by ^{1}H, ^{13}C, and ^{31}P{^{1}H}-NMR spectroscopy. The phosphorus spectrum (Figure 3.5) is indicative of an alkylated derivative of **1a**. The two central resonances at δ 24.8 and 24.0 each have ^{195}Pt satellites with $^{1}J_{(\mathrm{PtP})}$ couplings of 3250 and 2620 Hz respectively. The resonance at δ 24.8 ppm is assigned to the phosphines *trans* to the alkylated bridging $\mathrm{RS^-}$ ligand, as the significantly larger $^{1}J_{(\mathrm{PtP})}$ coupling of 3250 Hz reflects the reduced *trans* influence exerted by $\mathrm{RS^-}$ compared with $\mathrm{S^{2-}}$. While the multiplicities of the resonances are starting to resemble the *ddd* expected for each phosphine, the signal width is too broad to reliably estimate any $^{n}J_{(\mathrm{PP})}$ couplings.

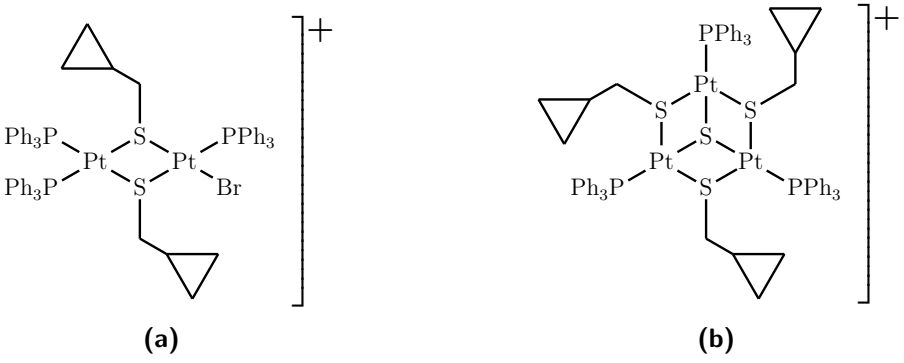

Figure 3.4: Proposed structures of **(a)** $[Pt_2(\mu\text{-}S{-}C_4H_7)_2(PPh_3)_3Br]^+$ (calc. *m/z* 1431.17) and **(b)** $[Pt_3\mu_3\text{-}S(\mu\text{-}S{-}C_4H_7)_3(PPh_3)_3]^+$ (calc. *m/z* 2040.21).

The protons in the cyclopropane ring of **10** are even more shielded than those of neat (bromomethyl)cyclopropane (δ 1.30 ppm CH, δ 0.76, 0.36 ppm CH_2) resonating upfield as broad multiplets at δ 0.07 and -0.21 ppm for the methylene protons, and δ 0.04 ppm for the methine proton. $^{3}J_{(\mathrm{PtH})}$ satellites or $^{4}J_{(\mathrm{PH})}$ couplings are not resolvable on the S-CH_2 protons, which appear as a broad multiplet at δ 2.31 ppm, also resonating upfield from (bromomethyl)cyclopropane (3.33 ppm). The multiplet however has a significantly broadened base, suggesting the presence of ^{195}Pt satellites. Such $^{3}J_{(\mathrm{PtH})}$ and $^{4}J_{(\mathrm{PH})}$ couplings have been observed previously for S-CH_2 protons in an alkylated derivative of **1a**.[175] The ^{13}C-NMR spectrum provided three expected resonances, appearing at δ 50.3 (assigned as S-CH_2), 13.1 (assigned as the methine carbon, DEPT-135), and 7.2 ppm (assigned as methylene carbons). These shifts, sans the S-CH_2 carbon, are very similar to those for the neat cyclopropane.

Crystals of **10** · [BPh_4] were grown from vapour diffusion of n-pentane into a chloroform solution. The complex crystallises in the orthorhombic space group $P2_12_12_1$ as the chloroform solvate. The BPh_4^- anion is present in the structure, confirming **10** is monocationic. The data appear to have spurious peaks in the difference map

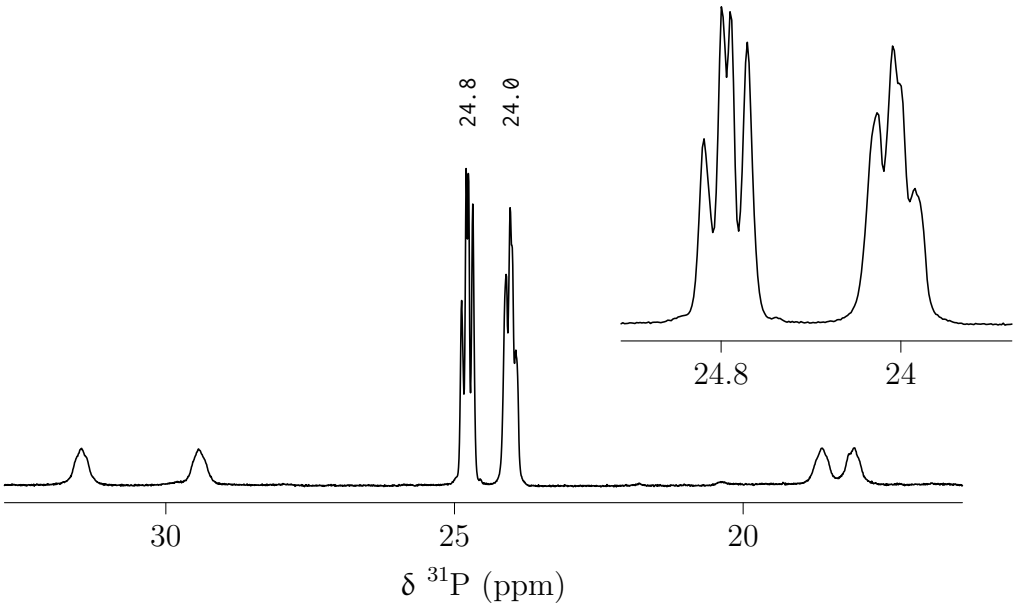

Figure 3.5: $^{31}P\{^{1}H\}$-NMR (242.95 MHz, $CDCl_3$) of **10**. The inset is an enhanced view of the multiplets at δ 24.8 and 24.0 ppm.

at chemically nonsensical locations, and although all non-hydrogen atoms can be refined anisotropically, convergence cannot be achieved without applying significant constraints. Fortunately, the core of the structure and the tethered cyclopropane ligand have sensible thermal parameters after refinement. The structure is presented in Figure 3.6 and selected bonds (Å) and angles (°) are in Table 3.1.

The structure is in a hinged configuration, as is typically observed for monoalkylated derivatives of **1a**, and has a Pt1-S2-S1-Pt2 dihedral angle of 137.5(2)°. The Pt-Pt separation is 3.320(1) Å which is consistent with a significantly hinged dimer. The large standard deviations in the bond distances for the mercapto-cyclopropane ligand preclude a detailed analysis, suffice to say they all appear shorter at around 1.50(3) Å consistent with the strained structure. The phosphines *trans* to the underivatised sulfide (S2) both have longer Pt-P bonds (2.308(4), 2.291(4) Å for P3,

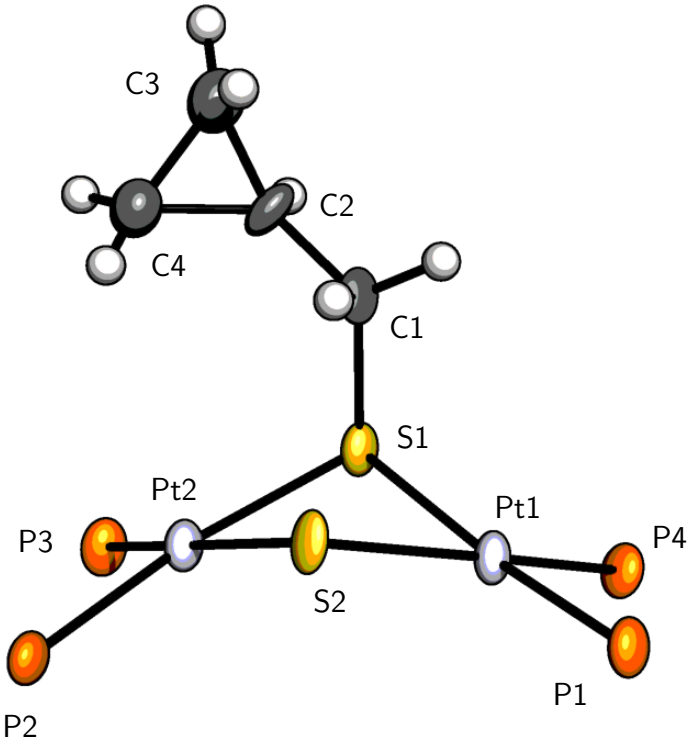

Figure 3.6: Crystal structure of **10**[BPh_4]·$CHCl_3$. The phenyl rings of the PPh_3 ligands, chloroform solvent, and BPh_4^- anion are omitted for clarity. Ellipsoids are displayed at 50% probability.

P4 respectively) than their counterparts *trans* to RS^- (2.286(4), 2.269(4) Å for P2, P4 respectively) reflective of the larger *trans* influence exerted by S2.

While alkylation of **1a** was achieved, the ring-opening of the cyclopropane was not observed to occur. Several attempts were made using forcing conditions on the initial reaction solution and on the isolated derivative **10** resulting in some unexpected multimetallic aggregates and dialkylated species. The alkylation product **10** was characterised and its structure unambiguously determined by single-crystal XRD. It is well know that olefinic complexes of Pt^{II} are reactive towards non-activated cyclopropanes, resulting in the corresponding platinacyclobutanes.[239] A suggestion for future work on **10** is to investigate the reactivity of the tethered cyclopropane with suitable Pt^{II} species, such as Zeise's dimer.[240]

Table 3.1: Selected bond lengths (Å), angles (°), and torsions (°) for $[Pt_2(\mu\text{-}S)(\mu\text{-}S{-}CH_2{-}CHC_2H_4)(PPh_3)_4][BPh_4]\cdot CHCl_3$ (**10**$[BPh_4]\cdot CHCl_3$).

Pt1-S2	2.320(4)	S2-Pt1-S1	81.37(14)
Pt1-S1	2.361(4)	P4-Pt1-S2	167.27(15)
Pt1-P4	2.291(4)	P4-Pt1-S1	87.55(16)
Pt1-P1	2.269(4)	P1-Pt1-S2	92.62(15)
Pt2-P2	2.286(4)	P1-Pt1-S1	170.30(16)
Pt2-S2	2.352(4)	P1-Pt1-P4	99.17(16)
Pt2-S1	2.349(4)	P2-Pt2-S2	85.90(14)
Pt2-P3	2.308(4)	P2-Pt2-S1	166.49(14)
S1-C1	1.830(19)	P2-Pt2-P3	101.79(17)
C2-C1	1.56(2)	S1-Pt2-S2	80.94(13)
C2-C4	1.50(3)	P3-Pt2-S2	171.29(15)
C2-C3	1.50(3)	P3-Pt2-S1	91.13(15)
		C1-S1-Pt2	102.1(7)
Pt1-S2-Pt2	90.58(12)	C4-C2-C1	117.7(18)
Pt2-S1-Pt1	89.65(14)	C4-C2-C3	60.1(14)
C1-S1-Pt1	99.0(6)	C3-C2-C1	115.1(18)

3.2.1 Cyclopropyl methyl ketone and *trans*-1,2-dibenzoylcyclopropane

As the previous reaction between **1a** and (bromomethyl)cyclopropane demonstrated, the non-polar character of the cyclopropane bonds heavily discourages the attack of nucleophilic species towards ring-opening reactions.[241] The next cyclopropanes examined, cyclopropyl methyl ketone and *trans*-1,2-dibenzoylcyclopropane, are both moderately activated with electron-withdrawing ketones.

Cyclopropyl methyl ketone was first screened in a micro-scale reaction with **1a** by ESIMS, giving negative results for any ring-opened derivative and showing mostly protonated starting material (**1a** + $[H]^+$). A second reaction using more forcing conditions (methanol reflux, 24 hours) was carried out and returned a similar mass spectrum, however a cation proposed as the ring-opened species $[Pt_2(\mu\text{-}S)(\mu\text{-}S{-}C_3H_6COCH_3)(PPh_3)_4]^+$ **30** was detected, albeit at a *very* low relative intensity (Figure 3.7).

It is known that Lewis acid catalysts in combination with forcing conditions have effected nucleophilic ring-opening reactions of electron-deficient cyclopropanes.[218] Lanthanum chloride and yttrium nitrate tetrahydrate were chosen as suitable cata-

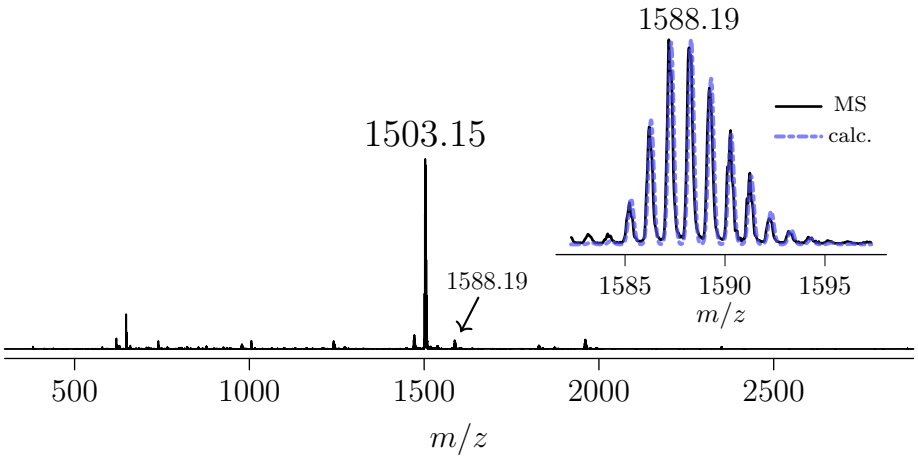

Figure 3.7: ESI mass spectrum of **1a** and cyclopropyl methyl ketone in methanol after refluxing for 24 hours. The inset is an isotope pattern comparison of the peak observed at *m/z* 1588.19 and a calculated pattern for the proposed ring-opened species $[Pt_2(\mu\text{-}S)(\mu\text{-}S{-}C_3H_6COCH_3)(PPh_3)_4]^+$ **30** (calc. *m/z* 1588.31). Capillary exit voltage 150 V.

lysts for this purpose as their lower protic acidity (Bronsted) would prevent attack by the highly nucleophilic sulfide centers of **1a**, and they have been determined to behave well in aqueous conditions.[242] The reaction of **1a** and cycloproyl methyl ketone was repeated twice, using a catalytic amount of each catalyst and forcing conditions. Both experiments were examined using ESIMS, returning negative results for any ring-opened derivates. Interestingly when using lanthanum chloride as the catalyst, instead of only protonated starting material in the mass spectrum, the proposed species $[Pt_2(\mu\text{-}S)_2(PPh_3)_4]Cl^+$ at *m/z* 1538 was present at around 30% relative intensity. This species has been detected before in various reactions with **1a**, and its nature and structure are still somewhat uncertain. Oxidising or acidic conditions along with excess chloride in solution or within the mass spectrometer are speculated to be responsible for its observation, and attempts to isolate this species have so far been unsuccessful.

A micro-scale eppendorf reaction of **1a** and *trans*-1,2-dibenzoylcyclopropane at room temperature was examined by ESIMS after several hours returning negative results for the presence of any cationic ring-opened species in the mass spectrum. A small scale reaction using more forcing conditions (ethanol reflux, 20 hours) was then carried out, also returning negative results as evidenced by ESIMS. Interestingly,

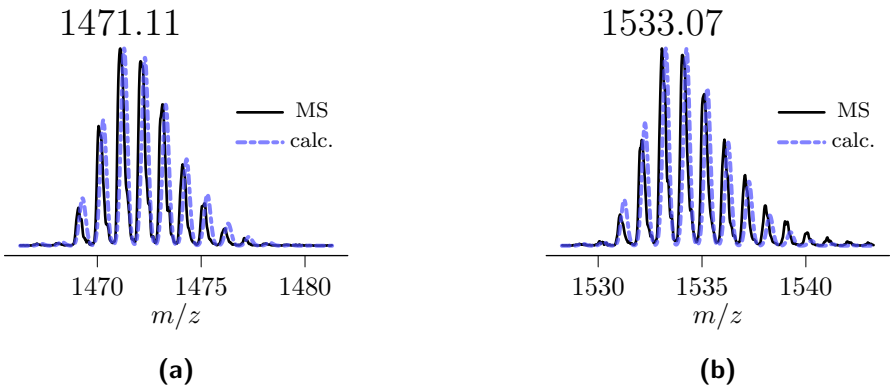

Figure 3.8: Isotope pattern comparisons for cations observed in the ESI mass spectrum of **1a** and *trans*-1,2-dibenzoylcyclopropane at **(a)** *m/z* 1471.11 and a calculated pattern for $[Pt_2(\mu\text{-}O)(\mu\text{-}OH)(PPh_3)_4]^+$ (calc. *m/z* 1471.29), and **(b)** at *m/z* 1533.07 and a calculated pattern for $[Pt_2(\mu\text{-}S)(\mu\text{-}S{-}OCH_3)(PPh_3)_4]^+$ (calc. *m/z* 1533.26). Capillary exit voltage 150 V.

along with protonated starting material **1a** + $[H]^+$ in the mass spectrum, a methoxy cation $[Pt_2(\mu\text{-}S)(\mu\text{-}S{-}OCH_3)(PPh_3)_4]^+$ at *m/z* 1533 and protonated oxo species $[Pt_2(\mu\text{-}O)_2(PPh_3)_4]H^+$ at *m/z* 1471 were tentatively identified.

While the potency of **1a** as a nucleophile has been well documented, the inability to effect ring opening in the species examined thus far exemplifies the high stability of these cyclopropanes.

3.3 Diethyl cyclopropane-1,1-dicarboxylate

Diethyl cyclopropane-1,1-dicarboxylate was next examined (Figure 3.1, **e**), a considerably more activated cyclopropane due to the 1,1-disubstituted carboxylate moieties. Initially, the cyclopropane was found not to engage in a ring-opening reaction with **1a** when screened by ESIMS in a micro-scale reaction at room temperature, evidenced by the absence any cationic species in the mass spectrum. The reaction was however found to occur sluggishly in refluxing methanol, as evidenced by detection of the proposed ring-opened species $[Pt_2(\mu\text{-}S)(\mu\text{-}S{-}C_2H_4CH(COOEt)_2)(PPh_3)_4]^+$ **11** in the ESI mass spectrum. Additionally, sodium and potassium aggregate ions of the cyclopropane were identified at *m/z* 395 and 411 respectively. Due to the long reaction time (80+ hours) and forcing conditions, significant transesterification was also observed (Figure 3.9), and the reaction was subsequently repeated using ethanol.

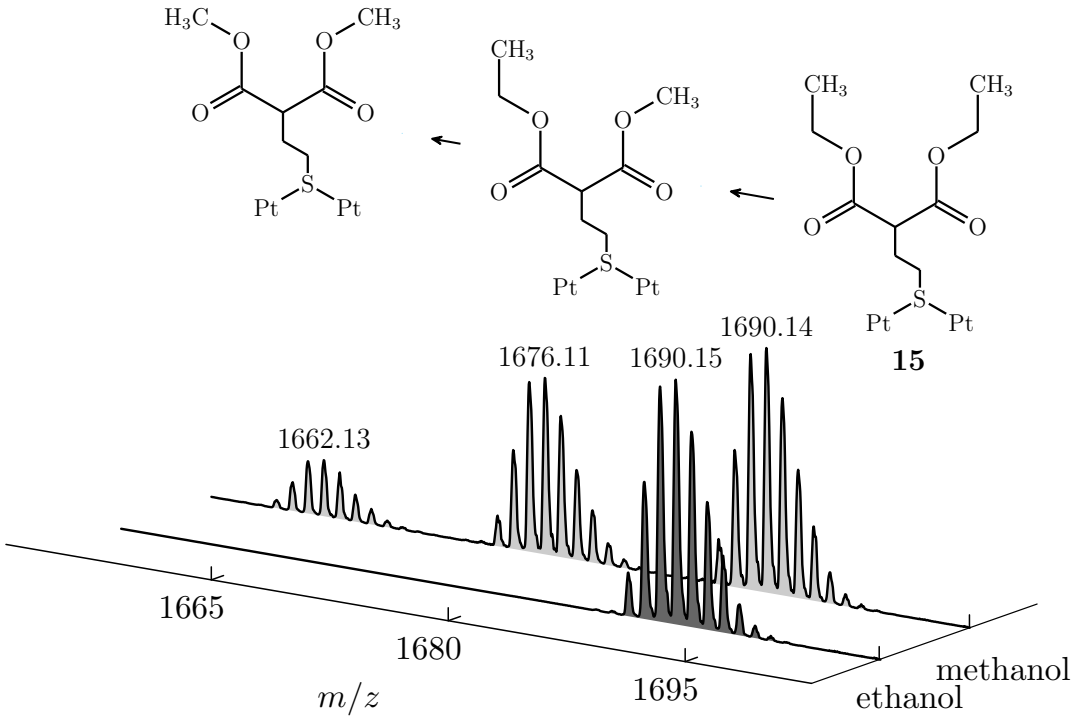

Figure 3.9: A comparsion of ESI mass spectra for the reaction of **1a** and diethyl cyclopropane-1,1-dicarboxylate in both methanol and ethanol, capillary exit voltage 60V. Shown above is a simplified representation of **11** undergoing one and two transesterification reactions (OEt → OMe) in methanol, corresponding to observed peaks at *m/z* 1676 and 1662 respectively.

After refluxing in ethanol for 80 hours, the ESI mass spectrum confirms one cation is present in the reaction solution at *m/z* 1690.12, and the observed data closely match a calculated isotope pattern for the proposed ring-opened derivative **11**. To investigate fragmentation of the cation **11**, the capillary exit voltage was increased to 240 V after 210 V was insufficient to effect significant fragmentation (Figure 3.10). The parent cation **11** and two fragmentation cations are present in the mass spectrum, assigned as triphenylphosphine loss cations $[\mathbf{11} - \mathrm{PPh_3}]^+$ and $[\mathbf{11} - 2\,\mathrm{PPh_3}]^+$ at *m/z* 1427.06 and 1165.01 respectively. The calculated isotope patterns for these fragmentation ions are a close match to the observed peaks in the mass spectrum. Unexpectedly, the fragmentation ion resulting from the loss of two PPh_3 ligands at *m/z* 1165 appears at a higher relative intensity than the fragmentation ion resulting from the loss of one (*m/z* 1427). This behaviour is typically not observed for these types of dimers, as coordinatively unsaturated Pt^{II} center in $[M - {}_2PPh_3]^+$ should be less stable.

The ring-opened derivative was isolated as the BETI salt and characterised by ^1H and $^{31}P\{^1H\}$-NMR spectroscopy. The phosphorus spectrum has two coincident

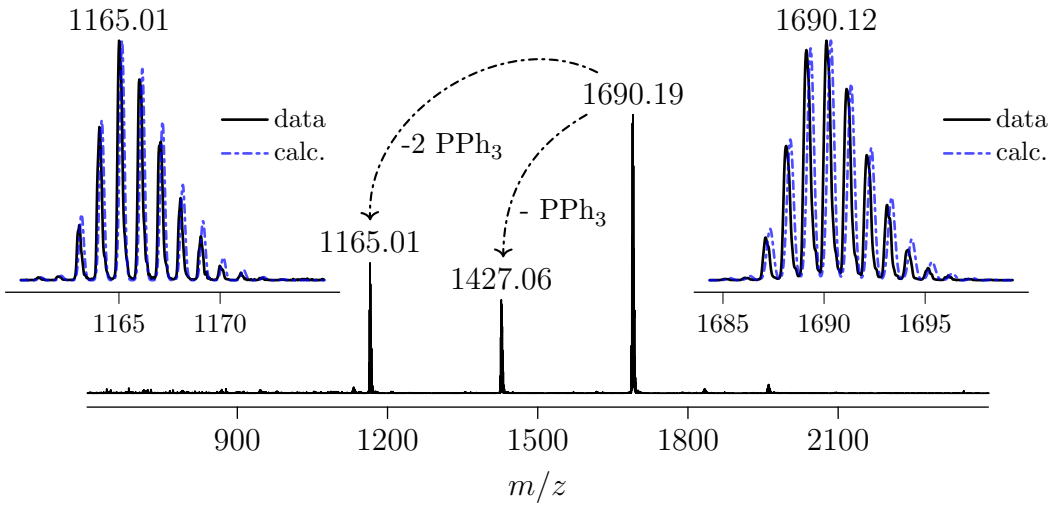

Figure 3.10: ESI mass spectrum of **1a** and diethyl cyclopropane-1,1-dicarboxylate acquired at an elevated capillary exit voltage of 240 V to induce fragmentation. The insets are calculated isotope patterns compared with observed peaks: (right) $[Pt_2(\mu\text{-}S)(\mu\text{-}S{-}C_2H_4CH(CO_2Et)_2)(PPh_3)_4]^+$ **11** calc. *m/z* 1690.34, (center) $[\mathbf{11} - \mathrm{PPh_3}]^+$ calc. *m/z* 1427.25, and (left) $[\mathbf{11} - 2\,\mathrm{PPh_3}]^+$ calc. *m/z* 1165.15.

resonances at δ 25.1 and 25.3 with $^{2}J_{(PtP)}$ couplings of 2600 and 3280 Hz respectively, the phosphorus environment *trans* to the underivatised sulfide assigned to δ 25.1 ppm.[56] In the ^{1}H-NMR spectrum, the shifts for the CH_2 and CH_3 protons are nearly identical to those in the neat cyclopropane[†]. The appearance of the methine proton at δ 2.87 ppm, and the methylene protons at δ 2.25 and 1.20 ppm provide additional evidence of cyclopropane ring-opening. The resonance at δ 2.25 ppm is assigned as the S−CH_2 protons, appearing as a broad multiplet in a similar spectral region to previously observed methylene protons in the ring-opened (bromomethyl)-cyclopropane derivative **10** (δ 2.31 ppm) and the ring-opened 2,2-dimethyloxirane derivative **7** (δ 2.31 ppm). In similar mono-alkylated derivative, $[Pt_2(\mu\text{-}S)(\mu\text{-}SCH_2\text{-}C(O)NHC(O)NHEt)(PPh_3)_4]PF_6$ in the literature, the S−CH_2 protons resonate at δ 2.85 ppm and $^{3}J_{(PtH)}$ and $^{4}J_{(PH)}$ couplings were resolvable.[175] For the S−CH_2 protons in **11**, the multiplet has a significantly broad appearance however no such couplings are resolvable.

Crystals of the bis(pentafluoroethanesulfonyl)imide salt **11**[BETI] were obtained by layered pentane on a chloroform solution. A single-crystal XRD experiment

[†] ^{1}H-NMR (400 MHz, $CDCl_3$) Enamine Ltd.

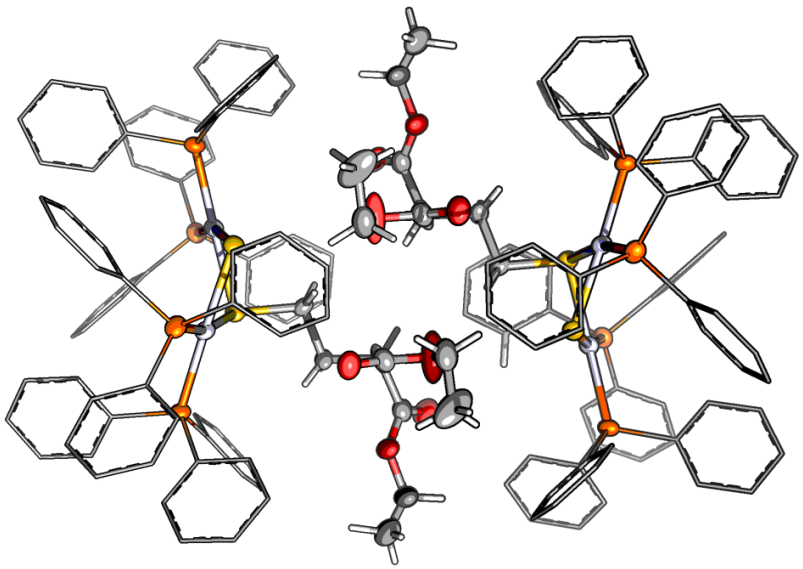

Figure 3.11: Crystal structure of **11**[BETI] showing the intelocked cations. Thermal ellipsoids at 50% occupancy.

was carried out providing after refinement the structure in Figure 3.12. Selected bond lengths and angles are given in Table 3.2. The complex crystalises in the orthorhombic *Ccce* space-group, and half of the cation is contained in the asymmetric unit as a $C2$ axis passes directly through the $\{Pt_2S_2\}$ ring, perpendicular to the S1-S1′ vector. The BETI anion in the unit cell is in very close proximity to an inversion position and is severely disordered. Additionally, a different $C2$ axis runs through the mercapto-dicarboxylate ligand, resulting in significant disorder that was modeled in the refinement. The high symmetry observed in the structure is a result of the unique crystal packing, whereby two cations of **11** are facially interlocked via the bulky mercapto-dicarboxylate ligands at 180° (Figure 3.11).

The structure of **11**[BETI] has typical features of a mono-alkylated derivative of **1a**. A significant dihedral angle between the Pt coordination planes of 137.0(1)° (Pt1-S1-S1a-Pt1a) and as a result, there is a moderately short Pt-Pt non-bonding

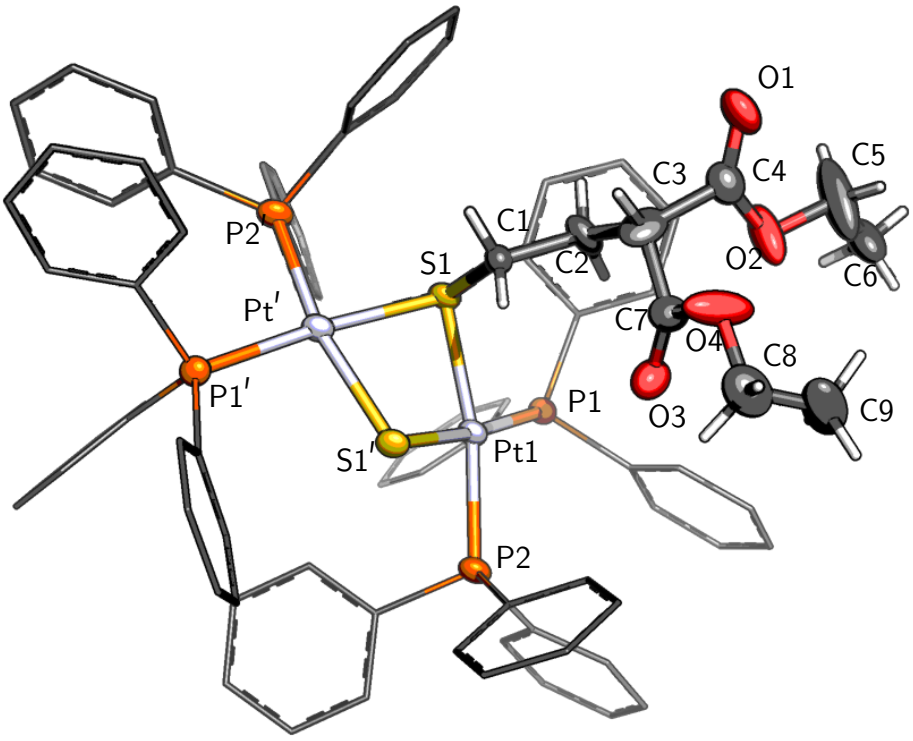

Figure 3.12: Crystal structure of **11**[BETI]. Thermal ellipsoids are shown at 50% occupancy. For clarity the disordered BETI counterion, solvent, and hydrogen atoms of PPh_3 ligands have been omitted for clarity. A stick motif has been employed to represent carbon atoms of the PPh_3 ligands. Atoms marked with (′) are generated with symmetry code $[\frac{1}{2} - x, -y, z]$.

separation of 3.133(1) Å. The coordination geometry about Pt1 is close to ideal square-planar, having a τ_4' value of 0.14.[141] Interestingly, the P-Pt bonds *trans* to the thiolate ligand RS^- are longer (2.288(3) Å) than those *trans* to the underivatised sulfide S^{2-} (2.270(2) Å). It must be noted that, due to the $C2$ symmetry element, these bonds are essentially averaged and as a result may deviate from the pure distances.

Table 3.2: Selected bond lengths (Å) and angles (°) for **11**[BETI]. Atom S1′ generated with symmetry code $[\frac{1}{2} - x, -y, z]$.

Pt1-P1	2.270(3)	P1-Pt1-S1a	174.68(9)
Pt1-S1	2.334(2)	P1-Pt1-S1	93.85(9)
Pt1-S1′	2.344(3)	P1-Pt1-P2	100.34(10)
Pt1-P2	2.288(3)	S1-Pt1-S1a	80.83(9)
S1-C1	1.83(2)	P2-Pt1-S1a	84.98(9)
O3-C7	1.23(3)	P2-Pt1-S1	165.49(10)
O1-C4	1.21(3)	Pt1-S1a-Pt1a	90.20(8)
C7-O4	1.30(4)	C1-S1-Pt1a	98.7(6)
C7-C3	1.47(5)	C1-S1-Pt1	107.7(7)
O2-C4	1.32(4)	O3-C7-O4	122(3)
O2-C5	1.41(4)	O3-C7-C3	124(3)
C1-C2	1.54(3)	O4-C7-C3	114(3)
C2-C3	1.50(6)	C4-O2-C5	116(3)
C9-C8	1.45(5)	C2-C1-S1	106.0(15)
C4-C3	1.52(4)	O1-C4-O2	127(3)
C6-C5	1.15(5)	O1-C4-C3	127(3)
O4-C8	1.46(5)	O2-C4-C3	106(3)
		C6-C5-O2	119(4)

3.4 1,1,2,2-Tetracyanocyclopropane

Previous attempts at ring-opening reactions with cyclopropyl methyl ketone and *trans*-1,2-dibenzoylcyclopropane were unsuccessful, and the diactivated diethyl cyclopropane-1,1-dicarboxylate resulted in ring-opening only when refluxing in ethanol for an extended period. The significantly activated 1,1,2,2-tetracyanocyclopropane (TCCP, Figure 3.1, **b**) was selected as the next prospective candidate for ring-opening with **1a**. Despite the increase in steric crowding around the tertiary carbon centers, a factor that resulted in a slowing of the ring-opening when **1a** was reacted with epoxides, the highly polar nitrile groups should enhance the susceptibility of the substituted ring-carbons towards nucleophilic attack. A recent computational examination of TCCP as a supramolecular synthon likened the cyclopropane to an electron-deficient bowl which readily engages in non-covalent bonding interactions with non-coordinating anions and π-electron or lone-pair donating molecules.[243] Indeed, the enhanced activation provided by the nitrile groups has been harnessed in the thermal condensation of modified tetracyanocyclopropanes to strongly electron-deficient tracyanosubstituted triazaphenalenes, which possess fascinating optoelectronic properties.[244] This serendipitously discovered reaction highlights the propensity of TCCP derivatives to undergo rapid intramolecular rearrangement reactions.

TCCP was synthesised by a modified procedure in the literature,[245] and the resulting clear red-brown crystalline material was confirmed by a single-crystal XRD experiment and melting point analysis. A small scale reaction was carried out using a slight molar excess of tetracyanocyclopropane and $[Pt_2(\mu\text{-}S)_2(PPh_3)_4]$ **1a** in methanol, which had the appearance of a dark red-orange solution with a significant amount of insoluble material after reacting for three hours at r.t. The color change to dark red is not typical for alkylated derivatives of **1a**, as solutions of these complexes tend to be yellow in color. Additionally, the presence of insoluble material in reactions of **1a** is typically observed when these reactions are sluggish or unsuccessful. A sample was taken from the suspension, centrifuged to separate any orange-red insoluble material present, and examined by ESIMS (Figure 3.13). The

main cation in the mass spectrum was identified as the cyclopropane ring-opened product $[Pt_2(\mu\text{-}S)(\mu\text{-}S{-}C(CN_2)CH_2CH(CN)_2)(PPh_3)_4]^+$ **31** at *m/z* 1646.38. The cation at *m/z* 1568 is more curious, and is tentatively assigned as a dicyano-methyl species $[Pt_2(\mu\text{-}S)(\mu\text{-}S{-}C(CN)_2)H(PPh_3)_4]^+$ **12**, presumably resulting from an intramolecular rearrangement of **31**. Both observed peaks closely match calculated isotope patterns for their respectively proposed species.

The orange-red insoluble material separated by centrifugation was dissolved in a small amount of $CHCl_3$ and diluted with methanol before examination by ESIMS (Figure 3.14). The cation at *m/z* 1568.33 proposed as **12** is preponderant, and peaks at *m/z* 784.65 and 1646.36 are assigned as $[\mathbf{12}][H]^{2+}$ (calc. *m/z* 784.63) and **31** respectively, both appearing at a lower relative intensity. Absent from the mass spectrum are any peaks around *m/z* 1503 related to protonated starting material **1a** or at *m/z* 1587 due to the alkylation of **1a** by chloroform, as is known to happen in chlorinated organic solvents.[42b] The isolation of **12** as a precipitate without the addition of a counterion is thus a little surprising, especially considering

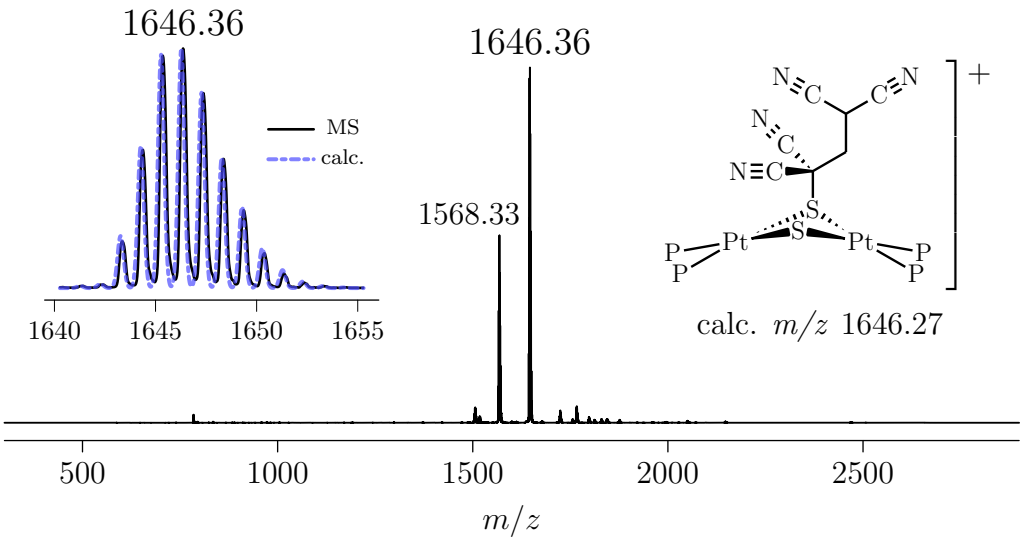

Figure 3.13: ESI mass spectrum of **1a** and tetracyanocyclopropane in methanol after stirring for 3 hours, sample taken from orange-red solution after separation of orange-red insoluble material. The left inset is an isotope pattern comparison of the observed peak at *m/z* 1646.36 and a calculated pattern for the cyclopropane ring-opened derivative $[Pt_2(\mu\text{-}S)(\mu\text{-}S{-}C(CN)_2CH_2CH(CN)_2)(PPh_3)_4]^+$ **31** (right inset, calc. *m/z* 1646.27). Capillary exit voltage 60 V.

that cationic derivatives of **1a** tend to be very soluble in methanol (and rarely ethanol). The excellent property of methanol that makes it a particularly suitable solvent for derivatives of **1a** is that metathesis with a suitable counterion often effects rapid precipitation. Additionally, the origin of **12** is also puzzling, and is proposed to be related to the initial cyclopropane ring-opening product **31**. Another possibility is that a small amount of bromomalonitrile is present in TCCP as an impurity from the synthetic workup, and is competitively alkylating **1a**. Evidence to the contrary would be the crystallinity of the TCCP sample, XRD experiment, and significantly higher melting point (220 cf. 65°). Unfortunately, both TCCP and bromomalonitrile could result in **12** when exposed to **1a**, complicating matters somewhat. For completion, it is suggested this reaction be carried out none the less.

The reaction of **1a** and tetracyanocyclopropane was repeated, using slightly more than a molar equivalent of the cyclopropane. A red-orange solid was isolated by precipitation from a translucent deep-red reaction solution after 20 hours. ESIMS was used to identify the solid as **12**, and fragmentation was investigated by increasing the capillary exit voltage to 210 V. The recorded spectrum is interesting in that the

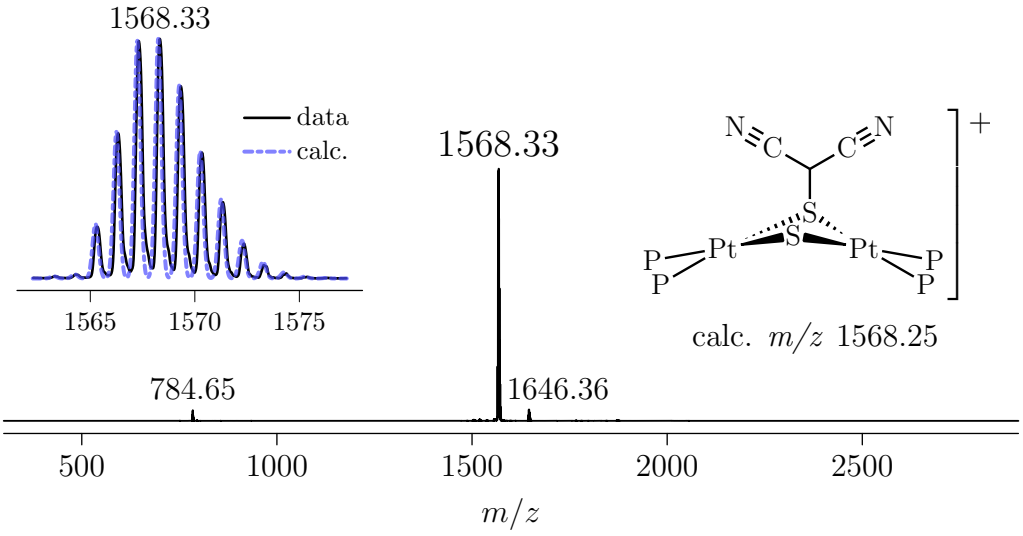

Figure 3.14: ESI mass spectrum of the orange-red precipiate from the reaction of **1a** and tetracyanocyclopropane in methanol. The left inset is an isotope pattern comparison of the peak observed at *m/z* 1568.33 and a calculated pattern for proposed $[Pt_2(\mu\text{-}S)(\mu\text{-}S{-}CH(CN)_2)(PPh_3)_4]^+$ **12** (right inset, calc. *m/z* 784.63). Capillary exit voltage 60 V.

main fragmentation pathway appears to be S-C bond activation, leaving the radical cation $[Pt_2(\mu\text{-}S)_2(PPh_3)_4]^{\bullet+}$ at m/z 1502.04 as the base peak of the spectrum and presumably the corresponding dicyanomethyl radical $^{\bullet}CH(CN)_2$. The relative stability of this radical has been ascribed to π-resonance stabilisation of the unpaired electron with the CN groups, evidenced by a relatively low C−H bond dissociation energy in malonitrile.[246] A computational examination of conformational space for the dicyanomethyl radical $^{\bullet}CH(CN)_2$ and $CH(CN)_2^-$ anion predicted planar geometries and C_{2v} symmetry for both species.[246] It is quite unusual to see S-C bond activation under fragmentation conditions for mono-alkylated derivatives of **1a**, even at elevated capillary exit voltages, and would be typically indicative of a weak S-C bond and/or the -C-R moiety being a stable leaving group.

To promote further fragmentation of the cations $[\mathbf{12}][H]^+$ and $[\mathbf{1a}]^{\bullet+}$, the cap-

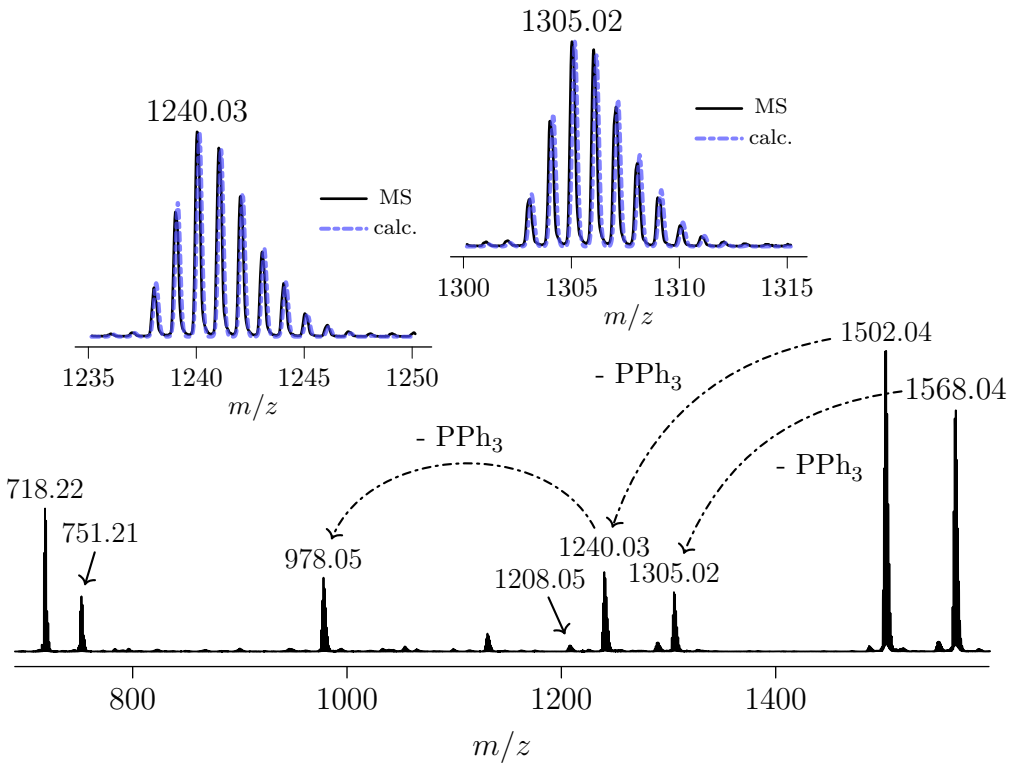

Figure 3.15: ESI mass spectrum of **12** in dichloromethane/methanol at a capillary exit voltage of 240 V. The insets are isotope pattern comparisons of peaks observed at m/z 1240 and m/z 1305 with calculated patterns for (left) $[Pt_2(\mu\text{-}S)_2(PPh_3)_3]^{\bullet+}$ [**1a** – PPh_3]$^{\bullet+}$ (calc. m/z 1240.14) and (right) $[Pt_2(\mu\text{-}S)(\mu\text{-}S{-}C(CN)_2)(PPh_3)_3][H]^+$ [**12** – PPh_3][H]$^+$ (calc. m/z 1305.16) respectively.

illary exit voltage was increased to 240 V (Figure 3.15). The radical cation $[\mathbf{1a}]^{\bullet+}$ fragments via the typical loss of one and two PPh_3 ligands evidenced by cations at *m/z* 1240.03 and 978.05 respectively. The only PPh_3 loss fragmentation cation observed for **12** is $[\mathbf{12} - PPh_3][H]^+$ at *m/z* 1305.02, with no evidence in the spectrum of a second PPh_3 ligand loss, which is interesting considering the elevated capillary exit voltage. The cyclometallated species $[(PPh_2\overline{C_6H_4)Pt}(PPh_3)]^+$ is observed at *m/z* 718.22 at an elevated relative intensity, typical of very forcing conditions in the spectrometer. There appear to be more mononuclear fragmentation ions in the spectrum appearing as a combinatorial pattern at *m/z* 751.21, due to their isotopic *m/z* distributions being nearly coincident.

Thus, they are tentatively assigned as $[PtSH(PPh_3)_2]^+$ and $[Pt\overline{SPPh_2}C_6H_4(PPh_3)]^+$, the latter proposed to contain a five-membered heterocycle (Figure 3.16 *a*), and both reflective of extreme fragmentation of **12**. Further evidence of the harsh fragmentation conditions is a peak at *m/z* 1208.05, of low relative intensity, again proposed to be a combinatorial pattern of two fragmentation ions, $[Pt_2(\mu\text{-}S)(PPh_3)_3]^{\bullet+}$ and the cyclometallated $[PPh_2\overline{C_6H_4}Pt_2(\mu\text{-}S)(PPh_3)_2]^+$ (Figure 3.16 *b*). These proposed ions are similar to previously reported Pt_2S triangular species[16,247] and would formally contain a Pt^I-Pt^I bond. Reductive elimination of sulfide in **1a** by CO has previously been used to achieve complexes of this type.[248]

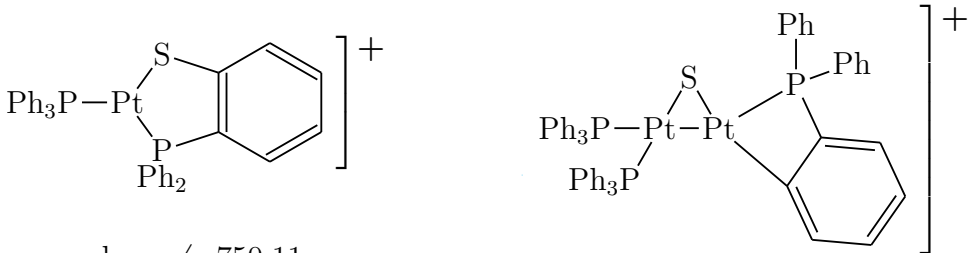

calc. *m/z* 750.11 **(a)**

calc. *m/z* 1207.17 **(b)**

Figure 3.16: Proposed cyclometallated fragmentation ions observed in Figure 3.15. **(a)** $[PtS(PPh_3)PPh_2(C_6H_4)]^+$, **(b)** $[(Ph_3P)_2Pt_2(\mu\text{-}S)PPh_2(C_6H_4)]^+$.

To gain additional structural insight into **12**, ^{1}H, ^{31}P{^{1}H}, and ^{195}Pt{^{1}H}-NMR spectroscopy experiments were carried out. No resonance for the $C(CN)_2H$ proton is identifiable in the ^{1}H-NMR spectrum. It is possibly located in the busy aromatic region, however the proton in bromomalonitrile resonates at δ 5.0 ppm. It seems unlikely any such $S-C(CN)_2H$ proton would resonate much further downfield, but this cannot be ruled out. The ^{31}P{^{1}H}-NMR spectrum in Figure 3.17 is consistent with two distinct phosphorus environments, as resonances at δ 30.7 and 23.1 ppm each have a set of platinum satellites with estimated $^{1}J_{(PtP)}$ couplings of 2830 and 2940 Hz respectively. In previously reported ^{31}P{^{1}H}-NMR spectroscopic data in the literature,[124d] and for systems observed in this work, mono alkylated and arylated derivatives of **1a** have $^{1}J_{(PtP)}$ couplings for phosphines *trans* to an underivatised sulfide typically around 2500-2700 Hz and 3200-3500 Hz for phosphines *trans* to thiolato ligands. These couplings are reflective of the relative *trans* influences[166] of the sulfide and thiolato ligands. Thus, the observed $^{1}J_{(PtP)}$ couplings of 2840 and

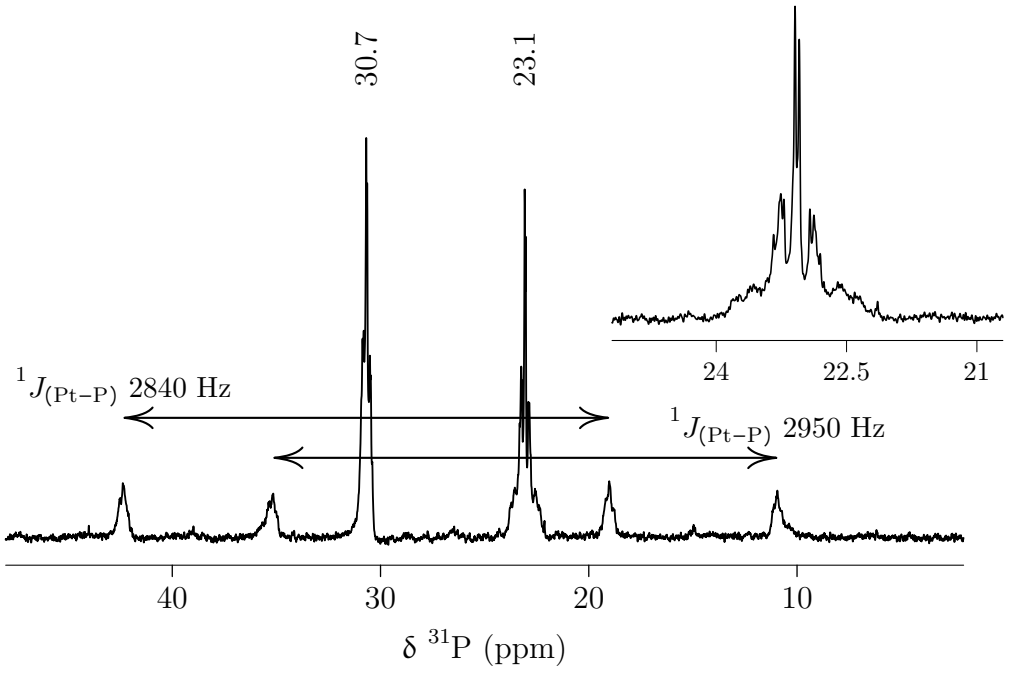

Figure 3.17: ^{31}P{^{1}H}-NMR (121.49 MHz, $CDCl_3$) of $[Pt_2(\mu\text{-}S)(\mu\text{-}S-C(CN)_2)(PPh_3)_4]$ **12**, $^{1}J_{(PtP)}$ SSCC are shown. The inset is an expansion of the multiplet at δ 23.1 displaying the broad peaks flanking the resonance assigned as a $^{3}J_{(PtP)}$ coupling of 120 Hz.

2950 Hz are difficult to assign due to their similar magnitude. What is certain is the *trans* influence for the bridging ligands, in comparison to previously reported structures, is both significantly weaker and stronger for the sulfide and thiolate ligands respectively in **12**. The resonance at δ 23.08 ppm however differs significantly, flanked by broad symmetrical peaks which are assigned as a $^{3}J_{(\mathrm{PtP})}$ coupling and estimated to have a magnitude of around 120 Hz. This coupling is also manifest in sloping asymmetric ^{195}Pt satellites, which was confirmed with the aid of a simulated spin system for **12** (*vide infra*).

Vicinal copulings to ^{195}Pt have been observed previously in ^{31}P-NMR spectra for bridging chloride complexs $[\mathrm{Pt}(\mu\text{-Cl})\mathrm{Cl}(\mathrm{PEt_3})]_2$ of 20 Hz,[249,250] in a *face-to-face* type dimer with terminal trifluoropropynyl ligands $[\mathrm{Pt}(\mathrm{C{\equiv}CCF_3})_2(\mathrm{dppm})]_2$ of 40 Hz,[251] and as little as 10 Hz for the bridging hydroxo species $[\mathrm{Pt_2}(\mu\text{-OH})_2(\mathrm{PMe_3})_4][\mathrm{NO_3}]_2$.[252] In the more similar thiolato- and selenato-bridged species of the type $[\mathrm{Pt_2}(\mu\text{-E}{-}\mathrm{R})_2(\mathrm{dppm})_2][\mathrm{BPh_4}]_2$ (E = S [R = Ph, C6H4Me-*p*]; Se [R = Ph]) these couplings were around 25-30 Hz.[253] Recently a $^{3}J_{(\mathrm{PtP})}$ coupling of 46 Hz was reported for a water-soluble phosphatriazaadamantane (PTA) derivative of **1a**.[254] Hence, the $^{3}J_{(\mathrm{PtP})}$ cou-

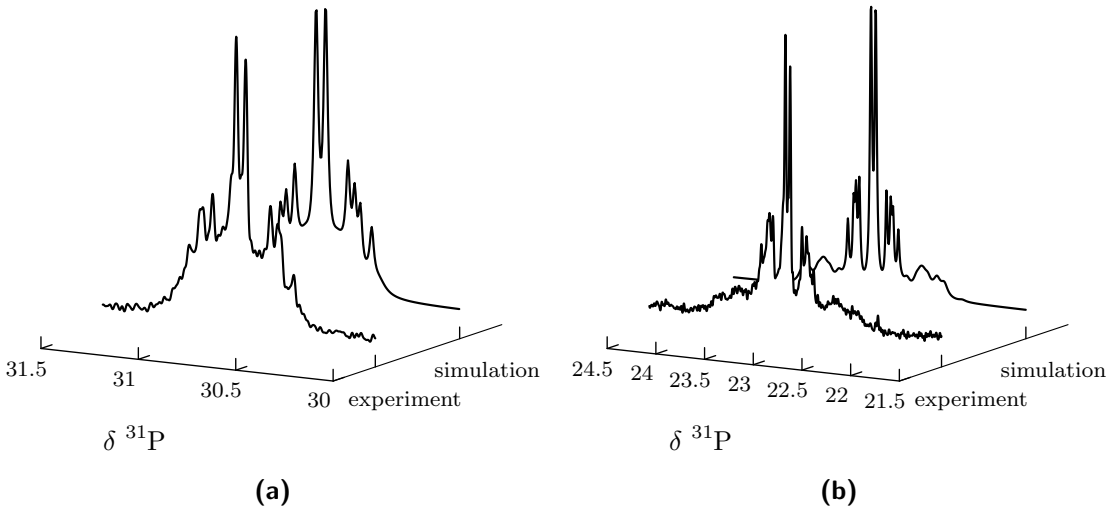

Figure 3.18: A comparison of the ^{31}P{^{1}H}-NMR spectrum for **12** and a simulated spin system: **(a)** δ 30.7 [P_a, $^{1}J_{(\mathrm{PtP})}$ 2830, $^{2}J_{(\mathrm{PP})}$ -20, $^{3}J_{(\mathrm{PtP})}$ 20, $^{4}J_{(\mathrm{PP})}$ *trans* 26, $^{4}J_{(\mathrm{PP})}$ *cis* -6 Hz], **(b)** 23.1 ppm [P_b, $^{1}J_{(\mathrm{PtP})}$ 2940, $^{3}J_{(\mathrm{PtP})}$ 120, $^{4}J_{(\mathrm{PP})}$ *cis* -9 Hz]. Complete spin system parameters in experimental.

pling of 120 Hz estimated for **12** appears to be unusually large. Considering the resonance at δ 30.69 does not have a significant $^{3}J_{(\mathrm{PtP})}$ coupling (ie. > 20 Hz), it seems reasonable to conclude $^{3}J_{(\mathrm{PtP})}$ coupling is related to a magnetic inequivalence in the dimer, although no similar dinuclear Pt^{II} complexes with a bridging $S{-}C(CN)_2$ ligand exist in the literature, precluding comparison. Both resonances in the spectrum are complicated multiplets due to $^{n}J_{(\mathrm{PP})}$ and $^{1,3}J_{(\mathrm{PtP})}$ coupling, however their overall similar appearance suggests the thiolate ligand is most likely adopting a symmetrical orientation and the system can be modelled as an $AA'BB'X$ system. As the second order character of the resonances precludes direct estimation of the $^{n}J_{(\mathrm{PP})}$ couplings, a simulated spin system was constructed using information from the experimentally acquired spectrum and making reasonable projections for unknowns. Figure 3.18 shows a comparison of the simulated spin system and the observed spectrum at both main resonances (δ 30.7 and 23.1 ppm). The caption contains the couplings used to construct the system. The isotopomers containing NMR active ^{195}Pt nuclei were sufficiently broadened to conform with the experimentally observed system. Overall, there is a nice agreement between the observed data and the spin system, suggesting the system is quite magnetically symmetric.

The ^{195}Pt NMR spectrum (Figure 3.19) of **12**, although a formally a *doublet of doublets*, appears as a *pseudo* triplet at δ -4025 resulting from chemically and magnetically equivalent ^{195}Pt centers and $^{1}J_{(\mathrm{PtP})}$ couplings that are very close in magnitude. Hence, the system can be treated as an $AA'X_2Y_2$ multiplet, and a simulated spin system is also displayed in Figure 3.19, constructed from the observed $^{1}J_{(\mathrm{PtP})}$ and $^{3}J_{(\mathrm{PtP})}$ couplings in the $^{31}P\{^{1}H\}$-NMR spectrum (Figure 3.17). As expected, the large $^{3}J_{(\mathrm{PtP})}$ coupling of 120 Hz observed in the phosphorus spectrum is identified in the $^{195}Pt\{^{1}H\}$-NMR spectrum which has a close agreement with the simulated multiplet. There appears to be a significant $^{2}J_{(\mathrm{PtPt})}$ coupling of around 980 Hz, as each multiplet peak in the resonance is flanked by satellites with an intensity corresponding to the isotopomer composed of two ^{195}Pt nuclei (11.4% of the sample). $^{2}J_{(\mathrm{PtPt})}$ couplings have been observed to vary significantly from 200 to

900 Hz,[154,168] and a $^{2}J_{(\mathrm{PtPt})}$ coupling of 970 Hz has been observed for one of the first known monoalkylated derivatives of **1a**.[58] Large $J_{(\mathrm{PtPt})}$ couplings (> 1 kHz) have been correlated with close Pt-Pt separations and are assumed to be indicative of the existence of a Pt-Pt bond, while the same is not true for $J_{(\mathrm{PtPt})}$ couplings < 1 kHz.[154]

Slow evaporation from a chloroform/pentane solution provided crystals of **12** suitable for an XRD experiment. The complex crystallises in the orthorhombic space group *Pbcm* as the *bis*-chloroform solvate $\mathbf{12}\cdot(\mathrm{CHCl_3})_2$ and has four molecules in the unit cell, with half of the molecule contained in the asymmetric unit (Figure 3.20). The absence of a counterion and trigonal-planar geometry of the C50 carbon heavily suggests **12** is a neutral species with a bridging thiolato-carbanion ligand. A mirror plane bisects the complex (symmetry operation $[x, y, \frac{1}{2} - z]$), and both sulfide centers and the carbanion moiety $\mathrm{C(CN)_2}^-$ reside on special positions. It is somewhat

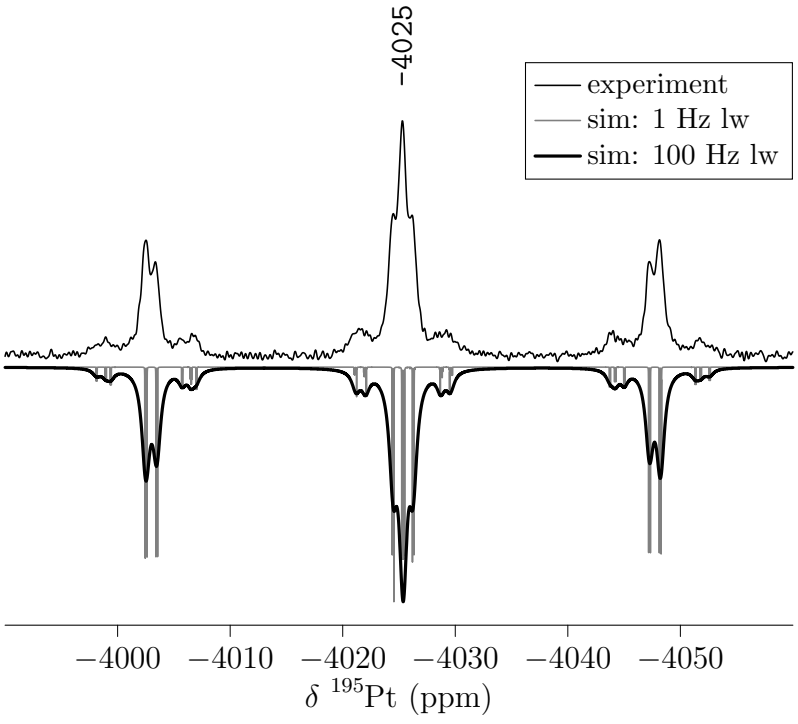

Figure 3.19: A comparison of (*top*) $^{195}\mathrm{Pt}\{^{1}\mathrm{H}\}$-NMR (121.09 MHz, $\mathrm{CDCl_3}$) spectrum of **12** and (*bottom*) a simulated $\mathrm{AA'X_2Y_2}$ spin system: δ -4025 ppm [$^{2}J_{(\mathrm{PtPt})}$ 980, $^{1}J_{(\mathrm{PtP})}$ (P_a) 2830, $^{1}J_{(\mathrm{PtP})}$ (P_b) 2940, $^{3}J_{(\mathrm{PtP})}$ (P_b) 120, $^{3}J_{(\mathrm{PtP})}$ (P_a) 20 Hz]. $\Delta\nu$ = 1,100 Hz linewidth.

unusual for $Z' = 0.5$ with a mirror plane symmetry element in triphenylphosphine derivatives of $\{Pt_2S_2\}$ type bridging dimers bisecting the Pt-Pt vector, and accordingly 4 independent PPh_3 groups have been modeled in the refined structure. More typical for highly symmetric derivatives of **1a** (when half of the dimer is in the asymmetric unit) are $C2$ axes perpendicular to the S-S vector and running through the center of the $\{Pt_2S_2\}$ core, as observed in the structures of **3** and **11**. The trigonal planar geometry of the carbanion at C50 is evident, with S1, C50, C51, and C52 all lying on a mirror plane and angles of nearly 120° for S1-C50-C52 (121.0(8)°) and C51-C50-C52 (119.2(10)°). Additional selected angles and bond distances are in Table 3.3.

The Pt-P bond *trans* to the underivatised sulfide is slightly shorter (Pt1-P1_2 2.277(2) Å) than the bond *trans* to the thiolato-carbanion ligand (Pt1-P1_1 2.388(1) Å). The Pt−S^{2-} bond is also shorter (Pt1-S2) at 2.330(2) Å compared to the Pt−SR^{-} bond 2.352(2) Å. The platinum center is slightly distorted from ideal square-planar

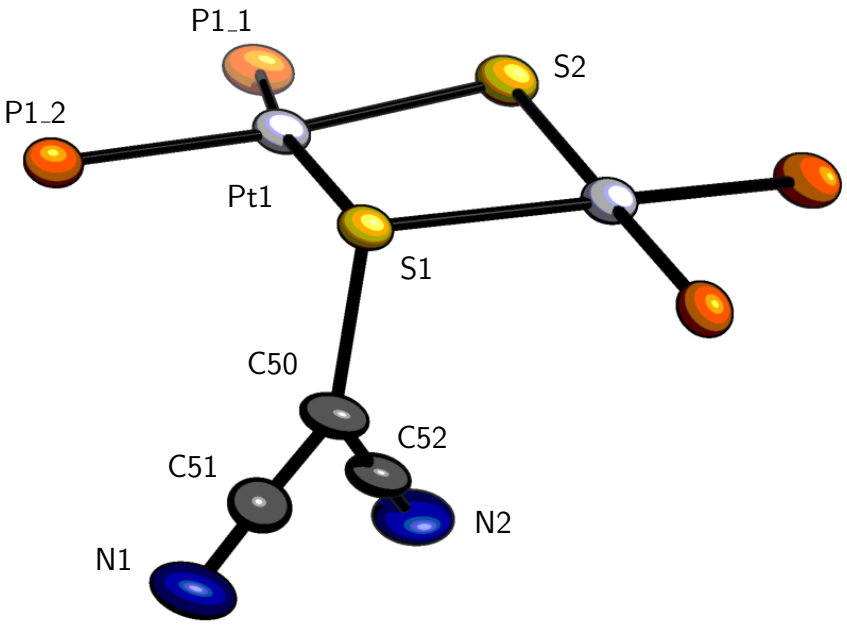

Figure 3.20: Crystal structure of $[Pt_2(\mu\text{-}S)(\mu\text{-}S{-}C(CN)_2)(PPh_3)_4]\cdot(CHCl_3)_2$ (**12**$\cdot(CHCl_3)_2$). Solvent molecules and phenyl rings of PPh_3 ligands are omitted for clarity. Thermal ellipsoids are displayed at 50% probability.

geometry, having a τ_4' parameter[141] of 0.17, and has a Pt-Pt separation of 3.538(1) Å with the symmetry generated Pt1′. The S1-C50 distance of 1.779(10) Å is shorter than a typical distance observed for other monoalklyated derivatives of **1a** (≈ 1.83 Å), and could be exhibiting some S=C double bond character. Notably, the folding dihedral angle of the core is slightly hinged θ_{hinge} = 169.04° and the thiolato ligand is protruding in an *endo* type configuration. This is a very unusual geometry, as previously reported structures of mono-alkylated derivatives of **1a** typically exhibit a significant hinge angle ($\theta_{hinge} \approx 140 \pm 10°$) and have the thiolato ligand oriented away from the hinge in an *exo* configuration. Dialkylated derivatives of **1a** are somewhat different in that θ_{hinge} is dependent on the configuration of the thiolato ligands.

For a *syn exo* arrangement the hinge angle can be quite acute $\theta = 140 \pm 20°$ but a wide range of angles exist, while for an *anti* arrangement $\theta_{hinge} = 180°$. A wider search of the CSD for mono- or di-alkylated $\{Pt_2S_2\}$ type phosphine dimers provided 66 matching structures, which are presented in Figure 3.21. Out of all the matching structures, only two had a similar *endo* configuration as observed in the **12**: A mono-alkylated perfluoropyridine dppp complex $[Pt_2(\mu\text{-}S)(\mu\text{-}S{-}C_5F_4N)\text{-}(dppp)_2]F$[105] (◒) and a dialkylated complex with chelating bis(diphenylphosphino)-

Table 3.3: Selected bond lengths (Å), angles (°), and torsions (°) for $[Pt_2(\mu\text{-}S)(\mu\text{-}S{-}C(CN)_2)(PPh_3)_4]\cdot(CHCl_3)_2$ (**12**$\cdot(CHCl_3)_2$). ⋆Generated with symmetry operation $[x, y, \frac{1}{2} - z]$.

Pt1-S1	2.3526(16)	S2-Pt1-S1	81.25(7)
Pt1-S2	2.3308(17)	P1_1-Pt1-S1	165.85(8)
Pt1-P1_1	2.288(2)	P1_1-Pt1-S2	87.25(8)
Pt1-P1_2	2.277(2)	P1_2-Pt1-S1	93.22(7)
S1-C50	1.779(10)	P1_2-Pt1-S2	170.32(8)
C50-C51	1.398(15)	P1_2-Pt1-P1_1	99.26(8)
C50-C52	1.396(16)	Pt1-S1-Pt1	97.52(9)
C51-N1	1.163(15)	C50-S1-Pt1	104.0(2)
C52-N2	1.161(16)	C50-S1-Pt1	104.0(2)
Pt1-S2-Pt1	98.75(10)	C52-C50-S1	121.0(8)
C51-C50-S1	119.8(9)	N1-C51-C50	177.5(13)
Pt1-S1-S2-Pt1⋆	169.0(1)	N2-C52-C50	178.0(12)
P1_2-S1-C50-C51	91(1)	C51-C50-C52	119.2(10)

dimethyltetrathiofulvalene phosphines and bridging benzenethiolate ligands in an *anti* configuration[255] (⧫). In the monoalkylated complex, the *endo* configuration was attributed to π-π interactions between the mercapto-perfluoropyridine ring and phenyl rings of the dppp ligands.[105] Incidentally, $^{1}J_{(\mathrm{PtP})}$ couplings for this species were typical, 2567 and 3412 Hz for dppp *trans* to S^{2-} and $NF_4C_5S^-$ respectively. Also similar in these structures (◒, ⧫) was the S···S-C angle of the *endo* thiolato ligand being substantially larger (147 and 149˚ respectively) than for typical mono- (80-110˚) or di-alkylated (110-125˚) species. In **12** this angle 117(1)˚ is larger than the vast majority mono-alklyated structures, and is comparable to the larger angles in dialkylated derivatives. The Pt-Pt separation dimension was chosen as it nicely clusters the mono-alkylated and dialkylated *syn-exo* derivatives. The trend in this group is clear, a more acute hinge dihedral is accompanied with a decrease in Pt-Pt separation and S···S-C angle. For the dialkylated derivatives configured *anti* the Pt-Pt separation is consistently long and the dihedral angle is at or very close to

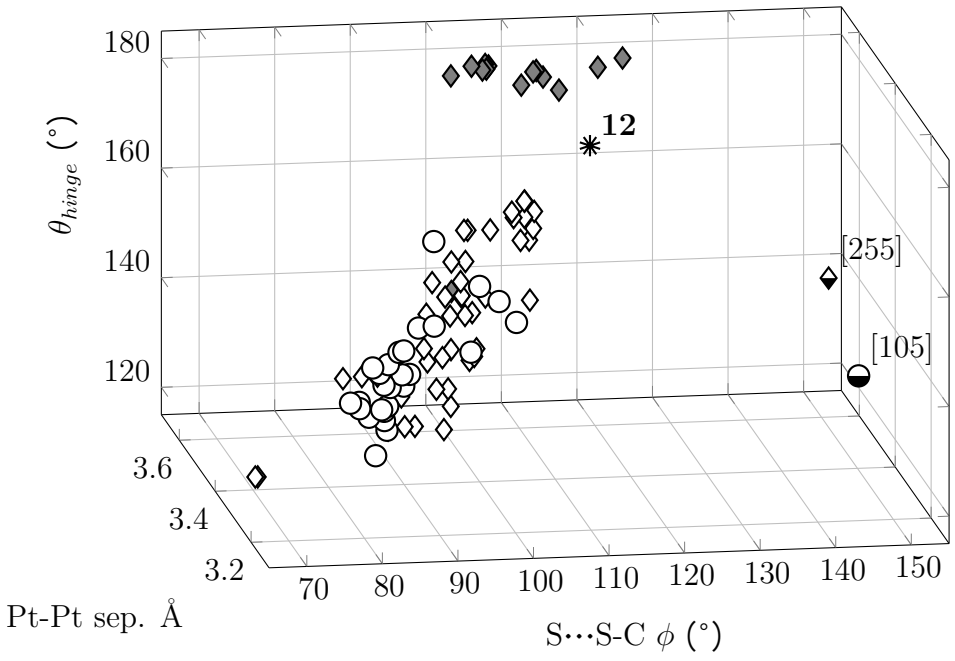

Figure 3.21: A scatter representation of S···S-C angle ϕ, Pt-Pt distance, and dihedral angle θ for structures of mono- and di-alkylated Pt^{II} phosphine dimers in the CSD. (*key*: ○ monoalkylated *exo*, ◒ monoalkylated *endo*, ◇ dialkylated *syn exo*, ⧫ dialkyl *anti* (θ = 180˚), ⧫ dialkyl *anti*(θ < 180˚) *endo*, and ✳ TCCP derivative **12**.)

180°, and some variation exists in the S···S-C angles. Considering these parameters, **12** lies in a somewhat unique space, in between the clusters of mono-alkylated and dialkylated *syn exo* and dialkylated *anti* derivatives.

A dichloromethane solvate **12** · CH_2Cl_2 was also characterised by a single-crystal XRD experiment. This solvate crystallises in the monoclinic $C2/c$ space group, with the sp^2 hybridised $C(CN)_2^-$ moiety at a slight dihedral angle to the S−S−C plane. The thiolate S atom is resting on a two-fold rotation axis which runs slightly offset to the S−S vector. Further complicating refinement of this structure are two-fold screw axes lying either side of the rotation axis, resulting in disordered solvent lying close to or on top of the $C(CN)_2^-$ moiety. Nonetheless, the core of the structure and thiolate ligand were refined anisotropically and are consistent with **12** · 2 $CHCl_3$. The dihedral angle of the $\{Pt_2S_2\}$ core is also slightly inverted with θ_{hinge} = 174(1)° and the geometry about the thiolato-carbon is also trigonal planar. Additionally, the Pt-P bond *trans* to the underivatised sulfide is shorter than the bond *trans* to the

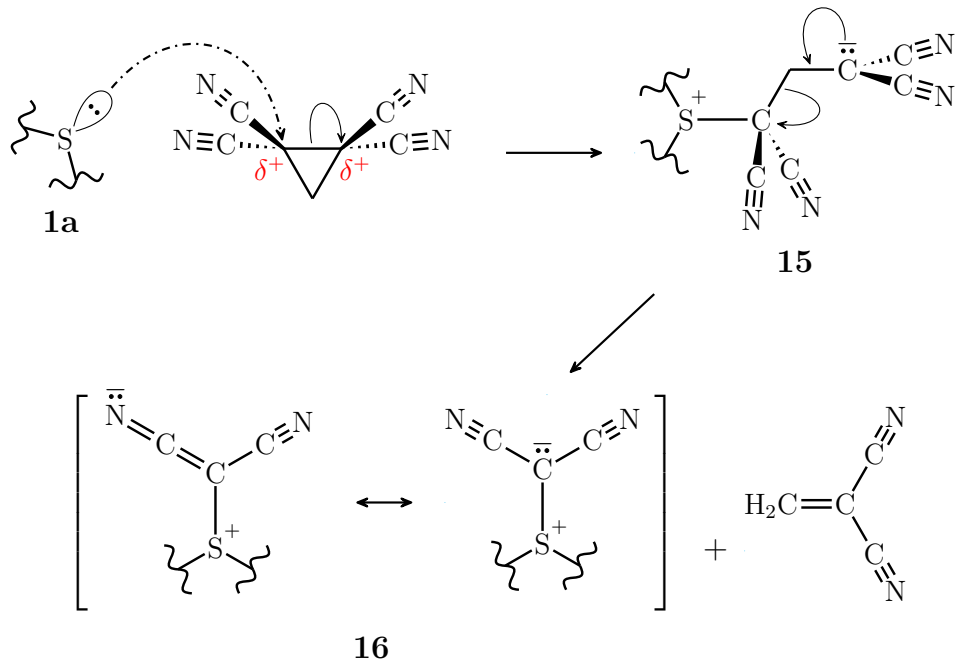

Scheme 3.2: Proposed scheme for the reaction of **1a** and 1,1,2,2-cyclopropane-tetracarbonitrile resulting in nucleophilic ring-opening of the cyclopropane followed by an intramolecular rearrangement and elimination of 1,1-dicyanoethylene to give $[Pt_2(\mu\text{-}S)(\mu\text{-}S{-}C(CN)_2)(PPh_3)_4]$ (**12**).

thiolato-carbanion ligand (2.274(2) and 2.295(2) Å respectively).

Although the thiol of the ligand S−$C(CN)_2$ in **12** formally has a charge of -1, the composition of the four-membered $\{Pt_2S_2\}$ ring to which it belongs of two Pt^{II} centers and an underivatised sulfide result in a partial positive charge and net neutral molecular charge. Hence, another way to consider the S−$C(CN)_2$ moiety is as a zwitterioinic sulfonium ylide. Despite the resulting dication $[\mathbf{12}]^{2+}$ from a typical ylide resonance, ie. $[R_2S^+-C^-] \longleftrightarrow [R_2S{=}C]$, not being detected by ESIMS, the S1-C50 bond length of 1.779(10) Å suggests partial π character. Additionally, the carbanion is afforded stabality through π-resonance of the nitrile groups (Scheme 3.2, resonance form of **32**).[256]

If the S−$C(CN)_2$ moiety is considered as a sulfonium ylide, the rearrangement to form **12** via the initial ring-opened tetracyanocyclopropane **31** is essentially a retro Johnson-Corey-Chaykovsky cyclopropanation.[257] Similar retro epoxidations involving sulfide and amine nucleophiles with activated epoxides such as tetracyanoethylene oxide or 2,2-dicyano-3,3-bis(trifluoromethyl)ethylene oxide have been utilised in the synthesis of various ketones and corresponding sulfonium and ammonium ylides in mild basic conditions.[258] In a recent examination of modified tetracyanocyclopropanes, nucleophilic attack resulted in ring-opening of the cyclopropane and a dicyanomethylidene derivative was obtained after an intramolecular rearrangement.[259] The mechanism of this rearrangement was proposed to involve C−C bond activation (Scheme 3.3), and the same dicyanomethylidene product was obtained when phosphine, thiol, and sulfanyl nucleophiles were employed. However when triphenylphosphine was used, attempts to detect the λ^5-phosphorane leaving group $Ph_3P{=}C(CN)_2$ were unsuccessful, and no such attempts were attempted to detect the corresponding sulfonium ylide when thiol and sulfanyl nucleophiles were used.[259]

The proposed rearrangement in Scheme 3.2, could be facilitated by a basic reaction solution and strongly electron-withdrawing nitrile groups. It would also appear the initially ring-opened species **31** has a stronger proton affinity than **12**, evidenced by its ionisation efficiency in the methanolic reaction solution. The ESIMS fragmen-

tation of **12** into the radical cation of **1a** is consistent with a moderately weak S-C bond in **12** and gives more weight to the treatment of the S−C(CN)$_2$ moiety as a sulfonium ylide. To see if a slightly acidic reaction solution would promote stability of the initial ring-opened product **31** and suppress the rearrangement reaction, a micro-scale reaction was carried out between **1a** and tetracyanocyclopropane in methanol/acetonitrile with a small amount of formic acid added. An ESIMS examination of the reaction solution after 5 minutes provided evidence to the contrary, with the only two ionisable species in solution identified as **12**[H]$^+$ and **12**[H]$_2{}^{2+}$ at *m/z* 1568.11 and 784.56 respectively.

The initial ESIMS investigation of TCCP and **1a** revealed a successful ring-opening reaction of the activated cyclopropane to give **31**, and serendipitous discovery of **12**. Subsequent characterisation of **12** by heteronuclear NMR spectroscopy provided evidence of a system with magnetically equivalent phosphines *trans* to S^{2-} and *trans* to RS^-, and in contrast to previously reported mono-alkylated derivatives of **1a**, the $^1J_{(PtP)}$ couplings were very close in magnitude hampering assignment. A single crystal X-ray diffraction experiment unambiguously determined **12** to be a neutral species with a bridging mercapto-carbanion ligand. It is proposed the initial ring-opening reaction of TCCP by **1a** results in **31** which undergoes an intramolecular rearrangement resulting in **12**.

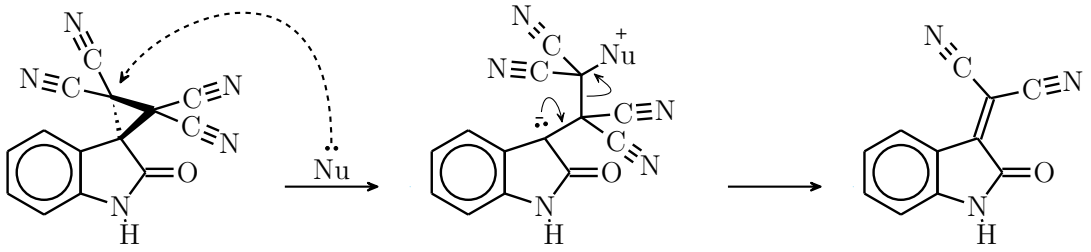

Scheme 3.3: A proposed rearrangement from the literature,[259] showing a nucleophilic ring-opening reaction of a modified tetracyanocyclopropane followed by an intramolecular rearrangment resulting in a dicyanomethylidene derivative. For the phosphine nucleophile PPh_3, attempts at detecting the phosphonium ylide leaving group $Ph_3P{=}C(CN)_2$ were unsuccessful.

3.5 *N*-Tosylaziridine

To compliment the nucleophilic ring-opening reactions of various epoxides and cyclopropanes by $[Pt_2(\mu\text{-}S)_2(PPh_3)_4]$ **1a** in this work, *N*-tosylaziridine was synthesised using a procedure from the literature[260] and screened for reactivity with **1a** in a micro-scale reaction in methanol. Sufficient evidence for the existence of a cationic ring-opened derivative was provided by ESIMS (Figure 3.22). At a low capillary exit voltage there is notably an absence of **1a**, either protonated or oxidised, representing a clean reaction. The ionisation efficiency of **1** is excellent as the sulfide centers are readily protonated. A cation at *m/z* 1701.39, tentatively assigned as $[Pt_2(\mu\text{-}S)(\mu\text{-}S{-}C_2H_4NH{-}Ts)(PPh_3)_4]^+$ **13** (Ts = tosyl), appears to be the result of aziridine ring-opening. The reaction was repeated at a larger scale and the proposed **13** isolated with ammonium hexafluorophosphate. ESIMS was again used to confirm the successful isolation of **13**$[PF_6]$ before inducing fragmentation in the cation, resulting in characteristic triphenylphosphine loss (Figure 3.23).

Interestingly, **13** has a somewhat increased resistance to fragmentation when compared with ring-opened derivatives previously examined in this work (180 - 210

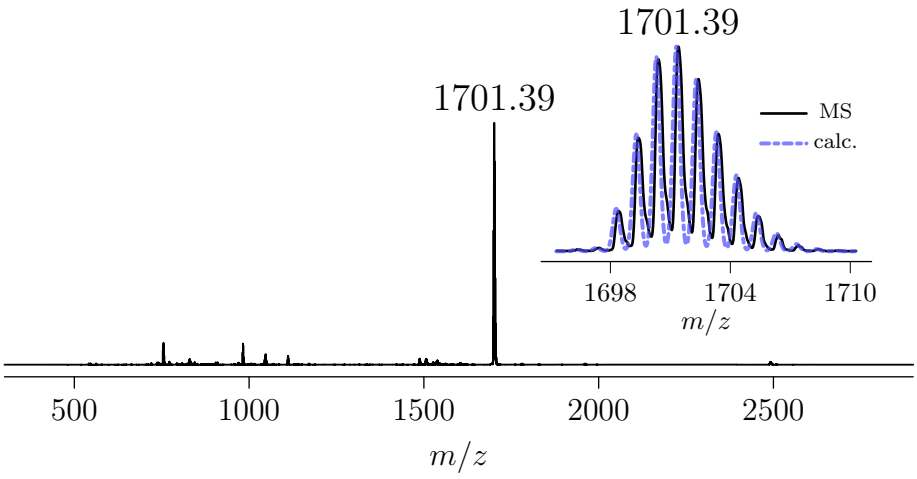

Figure 3.22: ESI mass spectrum of $[Pt_2(\mu\text{-}S)_2(PPh_3)_4]$ and *N*-tosylaziridine in methanol after 3 hours. The inset is an isotope pattern comparison of the peak observed at *m/z* 1701 and a calculated pattern for the proposed species $[Pt_2(\mu\text{-}S)(\mu\text{-}S{-}C_2H_4NH{-}Ts)(PPh_3)_4]^+$ (Ts = tosyl, calc. *m/z* 1701.29). Capillary exit voltage 60 V.

V capillary exit usually induces PPh_3 fragmentation). A capillary exit voltage of 210 V was insufficient in fragmenting triphenylphosphine from the parent cation at a significant relative intensity, and these ions increased in intensity only when a voltage of 240 V was employed.

To further characterise the derivative, a $^{31}P\{^{1}H\}$-NMR spectroscopy experiment was carried out giving the spectrum in Figure 3.24, which has features typical of alkylated derivatives of **1a**. The central ^{31}P resonances are coincident at δ 25.45 ppm, each having a pair of ^{195}Pt satellites with $^{1}J_{(PtP)}$ coupling constants of 2591 and 3232 Hz. These couplings compare favorably with those previously reported for alkylated derivatives of **1a**.[36] The smaller coupling constant of 2591 Hz is assigned to the phosphorus environment *trans* to the underivatised sulfide, which is presumed to exhibit a larger *trans*-influence compared to the thiolate ligand. The larger coupling of 3232 Hz is thus assigned to the phosphorus environment *trans* to the thiolate ligand. The central resonance is a symmetrical multiplet with significant second order character, and thus any $^{n}J_{(PP)}$ or $^{3}J_{(PtP)}$ couplings were unable to be reliably estimated. There appears to be an impurity in the spectrum at δ 9.9 ppm, and a

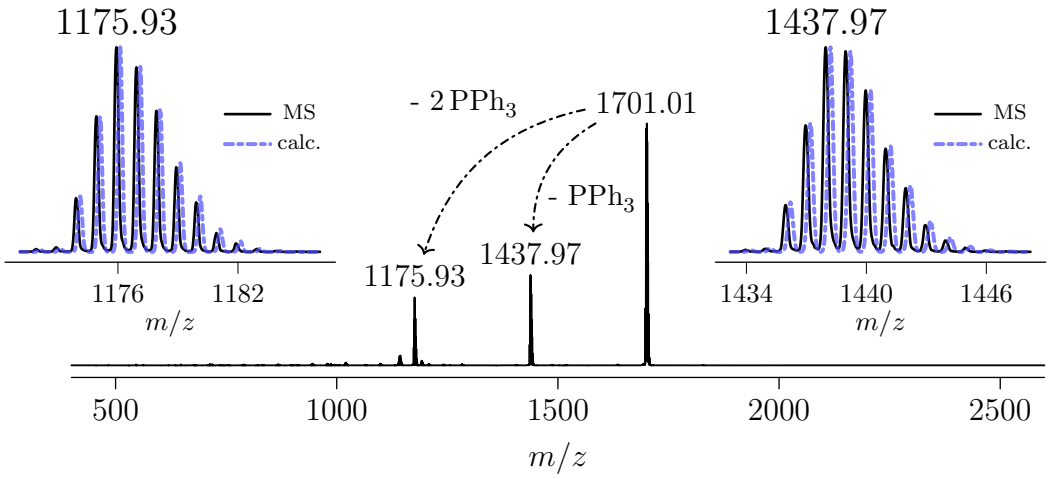

Figure 3.23: ESI mass spectrum of $[Pt_2(\mu\text{-}S)(\mu\text{-}S{-}C_2H_4NH{-}Ts)(PPh_3)_4][PF_6]$ in CH_2Cl_2/methanol at an increased capillary exit voltage of 240 V to induce fragmentation. Isotope pattern comparisons of (left inset) the peak observed at *m/z* 1175 and a calculated pattern for $[M - 2\,PPh_3]^+$ (calc. *m/z* 1176.11) and (right inset) the peak observed at *m/z* 1437 and a calculated pattern for $[M - PPh_3]^+$ (calc. *m/z* 1438.21).

$^1J_{(\mathrm{PtP})}$ coupling of around 3200 Hz suggests may be a mononuclear Pt complex with a thiolate ligand.[261]

Crystals of **13**[PF_6] were obtained via vapor diffusion of diehtyl ether into a chloroform solution, and a single-crystal XRD experiment was carried out to unambiguously determine the structure of the complex. **13** cyrstallises in $P\bar{1}$ as the *tris*-chloroform solvate and has two independent molecules in the unit cell. The cationic nature of **13** is confirmed with the presence of a hexafluorophosphate anion, which is disordered over two sites. Three structural disorders for the thiolate moiety S−C_2H_4−NH−Ts have been modeled in the final refinement (ψ_1, 50; ψ_2, 30; ψ_3, 20% occupancy Figure 3.26) and the primary disorder ψ_1 is shown in Figure 3.25.

Two of the disorders $\psi_{1,2}$ involve coincident C1 and C2 atoms, and are essentially rotamers of the tosyl aryl ring, distinguished by the C4-C3-S3-N1 torsions (ϕ) of 142 and 126° respectively. ψ_3 is a full positional disorder of the thiolate-sulfonamide moiety S−C_2H_4−NH−Ts, in which the thiolate S is coincident with the

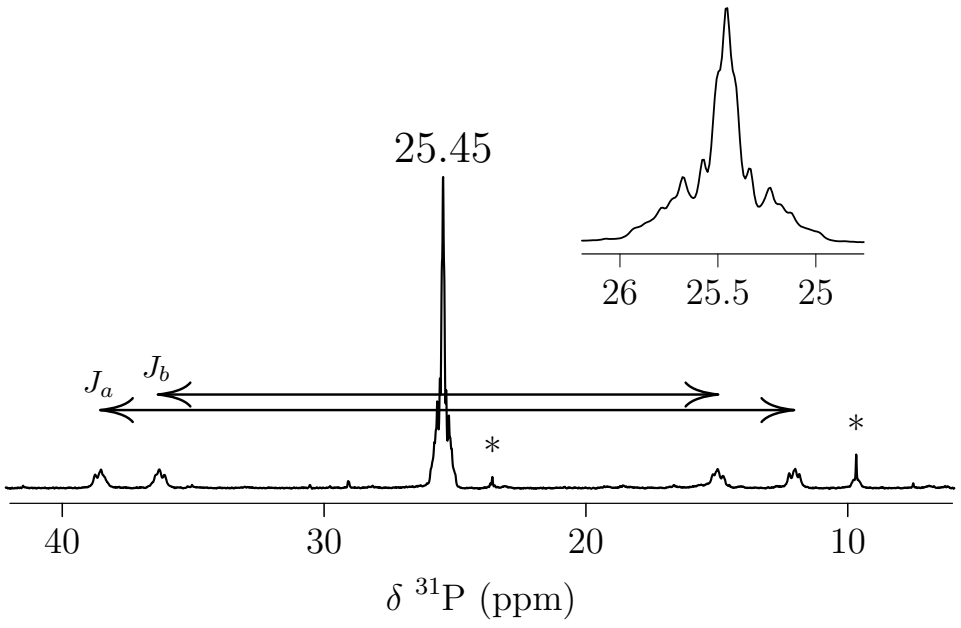

Figure 3.24: $^{31}P\{^1H\}$-NMR (121.49 MHz, $CDCl_3$) of **13**·[PF_6].Coincident resonances at δ 25.5 ppm (*inset*) have $^1J_{(\mathrm{PtP})}$ coupling constants of 3232 and 2591 Hz (J_a, J_b respectively). Peaks marked * are an impurity.

underivatised sulfide of $\psi_{1,2}$, and ψ_3 has a torsion ϕ of 123°. Essentially, $\psi_{1,2}$ and ψ_3 are rotamers about the torsion S-C1-C2-N1 (χ), with $\chi_{1,2}$ and χ_3 -78 and 64° respectively. Newman projections along the S3-C3 bond for all disorders are shown in Figure 3.27.

It is somewhat unfavorable for the aryl ring to be coplanar with one of the S=O

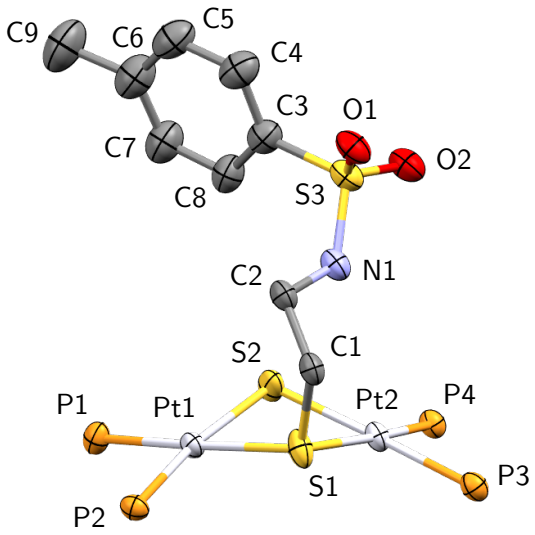

Figure 3.25: The crystal structure of $[Pt_2(\mu\text{-}S)(\mu\text{-}S{-}C_2H_4NH{-}Ts)(PPh_3)_4][PF_6]\cdot CHCl_3$ (**13**$[PF_6]\cdot CHCl_3$), showing the primary disorder ψ_1. Omitted for clarity are phenyl rings of the PPh_3 ligands, hydrogen atoms, PF_6 anion, chloroform solvent, and disorders of the $S{-}C_2H_4NH{-}Ts$ moeity.

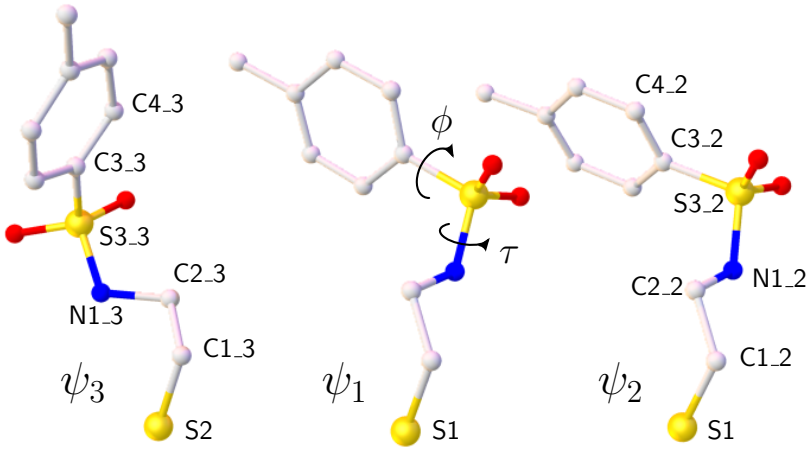

Figure 3.26: A comparison of the three modeled disorders in the crystal structure of $[Pt_2(\mu\text{-}S)(\mu\text{-}S{-}C_2H_4NH{-}Ts)(PPh_3)_4][PF_6]\cdot CHCl_3$ **13**$[PF_6]\cdot CHCl_3$. The central disorder ψ_1 has the torsion angles ϕ and τ defined.

bonds in arylsulfonamides, as early computational[262] and crystallographic studies[263] found a significant preference for ϕ of around 90° with the aromatic *p*-orbital bisecting the O=S=O angle. A more recent and comprehensive examination of published structures in both the CSD and PDB with arylsulfonamide substituents also found this preference.[264] Despite this observed preference, computational studies of benzensulfonamide ($PhSO_2NH_2$) revealed a relatively low barrier for rotation about ϕ (S-C bond) of < 2 kcal $\cdot$ mol^{-1}.[265] Not surprisingly, there is significant deviation of ϕ from 90° for secondary aromatic sulfonamides when halogen substituents are introduced to the aryl ring.[266]

The Pt−SR bond distances for the thiolate ligand S1-Pt1 2.362(2) Å and S1-Pt2 2.340(1) Å are longer than the underivatised sulfide S2-Pt1 2.323(1) Å and S2-Pt2 2.328(1) Å. The Pt−P bonds *trans* to the thiolate ligand Pt1-P1 and Pt2-P4 are 2.250(2) and 2.280(1) Å respectively, while bonds *trans* to the underivatised sulfide Pt1-P2 and Pt2-P3 are 2.306(1) and 2.292(1) Å respectively. These distances are mostly consistent with a higher *trans* influence[166] of the underivatised sulfide ligand, however the Pt2-P3 bond is slightly shorter than Pt2-P4, possibly a product of the disorder ψ_3, in which the thiolate sulfur occupies the same position (S2) as the underivatised sulfide in the primary disorders.

The hinge angle of the $\{Pt_2S_2\}$ core in **13**[PF_6] (θ_{hinge}) is 148.9°, consistent with previously observed θ for alkylated derivatives of **1a**. Overall, the bond lengths in

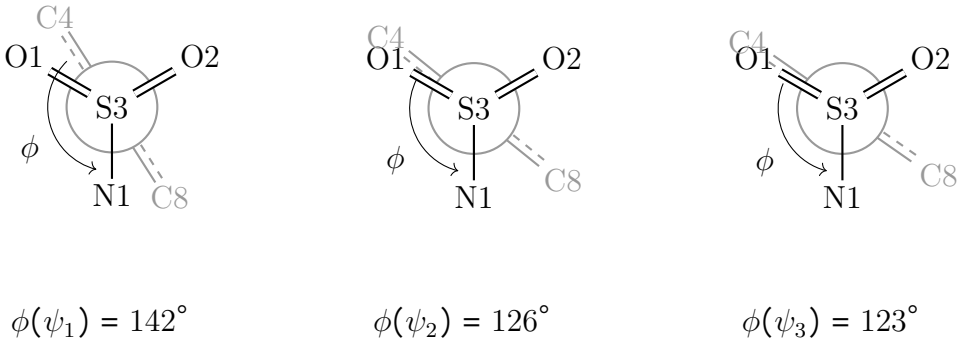

Figure 3.27: Newman projections along the S3-C3 bond in the crystal structure of $[Pt_2(\mu\text{-}S)(\mu\text{-}S{-}C_2H_4NH{-}Ts)(PPh_3)_4][PF_6]\cdot CHCl_3$ (**13**[PF_6]$\cdot CHCl_3$). The torsion angle ϕ of C4-C3-S3-N1 is shown for the three disorders.

13[PF_6] are consistent with the observed chemical shifts and $^1J_{(PtP)}$ recorded in the $^{31}P\{^1H\}$-NMR experiment, and compare favorably to previously reported examples of alkylated derivatives of **1a**.[123,175] All hydrogens were included with a riding model, even though the data were sufficient to identify most aryl proton positions in the difference map. Unsurprisingly, half of the methylene protons and both sulfonamide amine protons were not able to be located this way, and the secondary amide was initially treated as sp^2 hybridised by the riding model.

A study of sulfonamides by Brameld *et al.*[264] found a significant relationship between the torsion angle τ (C−S−N−C) and the pyramidality of the nitrogen atom, quantified by the distance $d_{(N\rightarrow|)}$ between the nitrogen and the plane passing through each ligand. Based on this relationship and considering the torsion angles τ of 69, 75, and 71° in the crystal structure (Figure 3.28), a more sp^3 hybridised nitrogen would be predicted, with $d_{(N\rightarrow|)} \approx 0.25 - 0.3$ Å. In addition, the study by Brameld *et al.* found the nitrogen lone pair, assumed to lie on a vector parallel to d, tends to adopt an antiperiplanar geometry ±20° with respect to the S−C bond in a vast majority of structures.

This preference for the amine lone pair was explored in a density functional theory (DFT) computational study of sulfonyl and phosphoryl systems using natural bonding orbital (NBO) analysis to propose reciprocal hyperconjugation about the central atom as a driving factor behind observed geometries in these species.[267]

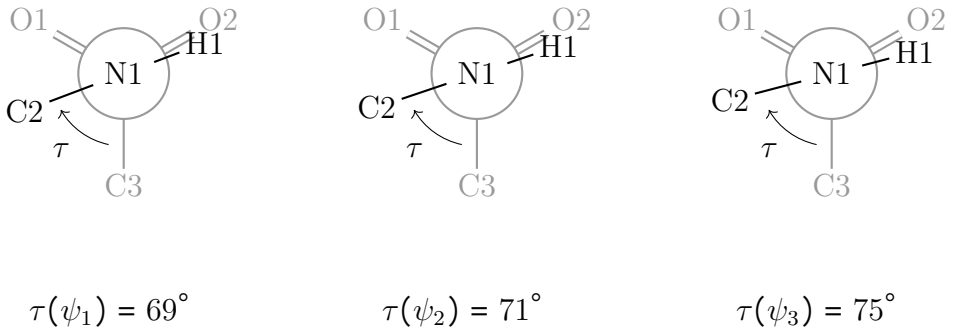

Figure 3.28: Newman projections along the N1-S3 bond in the crystal structure of [Pt_2(μ-S)(μ-S−C_2H_4NH−Ts)(PPh_3)$_4$][PF_6]·$CHCl_3$ (**13**[PF_6]·$CHCl_3$), showing the torsion angle τ of C3-S3-N1-C2 in the three disorders.

For sulfonamide systems, this would consist of a nitrogen lone pair to S=O and S−C antibonding orbital interactions ($n_N \rightarrow \sigma^*$), and these interactions maximised when the nitrogen lone pair bisects the O=S=O angle and is antiperiplanar to the S−C bond. Very recently, a computational study expanded upon this idea using NBO analysis and potential energy surfaces (PES) to examine conformations about the N−S bond in simple sulfonamides and sulfamides.[268] It was proposed that the geometry about the N−S bond is significantly influenced by an anomeric effect of the nitrogen lone pair on the S=O and S−N antibonding orbitals in sulfonamides. Additionally, sulfur K-edge XAS has been used to reveal little S_{3p} contribution to S-N π-bonding,[269] a result that is consistent with quantum chemical calculations showing a relatively low rotational barrier for τ (S-N bond) of < 5 kcal $\cdot$ mol^{-1}.[265]

Table 3.4: Selected bond lengths (Å), angles (°), and torsions (°) for $[Pt_2(\mu\text{-}S)(\mu\text{-}S{-}C_2H_4NH{-}Ts)(PPh_3)_4][PF_6] \cdot CHCl_3$ (**13**$[PF_6] \cdot CHCl_3$).

P1-Pt1-P2	98.79(5)	Pt1-P1	2.2500(15)
P1-Pt1-S2	92.28(5)	Pt1-P2	2.3063(12)
P1-Pt1-S1	174.39(5)	Pt1-S2	2.3228(12)
P2-Pt1-S2	168.85(5)	Pt1-S1	2.3621(14)
P2-Pt1-S1	86.71(5)	Pt2-P3	2.2924(13)
S2-Pt1-S1	82.20(5)	Pt2-P4	2.2804(15)
P3-Pt2-S2	87.61(5)	Pt2-S2	2.3282(15)
P3-Pt2-S1	169.45(5)	Pt2-S1	2.3408(13)
P4-Pt2-P3	98.70(5)	S2-C1_3	1.74(3)
P4-Pt2-S2	173.67(5)	S1-C1_1	1.800(7)
P4-Pt2-S1	91.19(5)	C1_1-C2_1	1.514(9)
S2-Pt2-S1	82.55(5)	C2_1-N1_1	1.454(8)
Pt1-S2-Pt2	93.63(5)	N1_1-S3_1	1.633(6)
C1_2-S2-Pt1	112.0(8)	S3_1-O1_1	1.443(7)
C1_2-S2-Pt2	130.8(8)	S3_1-O2_1	1.433(6)
Pt2-S1-Pt1	92.29(5)	S3_1-C3_1	1.774(10)
C1_1-S1-Pt1	113.7(2)		
C1_1-S1-Pt2	109.3(2)	Pt1-S1-S2-Pt2 (θ_{hinge})	148.96(7)
C2_1-C1_1-S1	117.1(5)	C1_1-C2_1-N1_1-S3_1	-145.4(6)
N1_1-C2_1-C1_1	111.3(6)	C1_2-C2_2-N1_2-S3_2	-154.5(7)
C2_1-N1_1-S3_1	120.9(6)	C1_3-C2_3-N1_3-S3_3	160.4(18)
N1_1-S3_1-C3_1	107.9(5)	C3_1-S3_1-N1_1-C2_1 (τ_{ψ_1})	69.3(8)
O1_1-S3_1-N1_1	105.6(8)	C3_2-S3_2-N1_2-C2_2 (τ_{ψ_2})	71.4(11)
O1_1-S3_1-C3_1	110.0(8)	C3_3-S3_3-N1_3-C2_3 (τ_{ψ_3})	75(2)
O2_1-S3_1-N1_1	107.3(7)	N1_1-S3_1-C3_1-C4_1 (ϕ_{ψ_1})	142.3(11)
O2_1-S3_1-O1_1	119.3(8)	N1_2-S3_2-C3_2-C4_2 (ϕ_{ψ_2})	126.0(19)
O2_1-S3_1-C3_1	106.2(7)	N1_3-S3_3-C3_3-C4_3 (ϕ_{ψ_3})	123(2)

It would appear that any such $n_N \rightarrow \sigma^*_{S-O}$ or $n_N \rightarrow \sigma^*_{S-C}$ hyperconjugation would be maximised by a nitrogen lone pair oriented such that it is antiperiplanar to the S−C bond. Indeed the $n_N \rightarrow \sigma^*_{S-C}$ stabilisation in this orientation has been calculated to be around 10 kcal $\cdot$ mol^{-1} for acyclic sulfonamides.[270] A more specific study on secondary sulfonamide substituents from over 1300 structures in the CSD revealed an overwhelming majority of structures adopt a C−N−S−C torsion angle τ of 65 - 80°.[271] A Newman projection along the N1-S3 bond is shown for all ψ in Figure 3.28, showing the torsion angle C3-S3-N1-C2 (τ).

In a recent quantum chemical study of sulfonamides, a strong inverse correlation (R^2 = 0.987) was found between the length of the N−S bond in cyclic sulfonamides and the *s*-character of the nitrogen contribution to the N−S bond, and hence, the hybridisation of the nitrogen atom.[270] Based on this relationship and N−S bond lengths in the crystal structure (≈1.63 Å), a conservative estimate of ≈ 25% nitrogen *s*-character would be expected in the N−S bond and the nitrogen lone pair to adoption of a more sp^3 hybridised conformation.

To examine the proton conformation in the secondary sulfonamide of **13** further, a constrained geometric optimisation was carried out for all disorders (ψ). The starting geometries were taken from the refined molecular geometry, fixing atomic positions of heteroatoms and hydrogens of the triphenylphosphine ligands. In all optimisations, the sulfonamide amine adopted a more pyramidal geometry as the proton migrated towards the underivatised sulfide center concomitant with an elongation in the N−H bond, suggesting the existence of a significant noncovalent interaction. Figure 3.29 shows a double y-axis plot of relative energy against the change in S···H-N distance for the optimisation steps of ψ_1.

Intramolecular N-H···S hydrogen bonds of thiol metalloligands are prevalent in the literature,[272,273] especially for iron containing porphyrins[274] and proteins such as ferrodoxins[275] and rubredoxins.[276] These interactions are suspected of contributing significantly to the redox chemistry and coordination environment of the metal in these systems. In a recent computational examination of N-H···S hydrogen bonding

between dimethylamine and dimethylsulfide, noncovalent interactions (NCI) theory[157,160,277] was used to complement FTIR data and confirm the propensity of sulfide as a hydrogen bonding acceptor of comparable strength to dimethyl ether.[278]

Due to the position adopted by the sulfonamide proton with respect to the underivatised sulfide ligand, NCI theory was used to investigate a potential hydrogen bonding interaction with the underivatised sulfide center. The Reduced Density Gradient s is plotted against the electronic density ρ times the sign of the second eigenvalue of the Hessian matrix (λ_2) in Figure 3.30. The latter parameter λ_2 is representative of attractive ($\lambda_2 < 0$) and repulsive ($\lambda_2 > 0$) interactions in the electronic density tail, where the gradient vanishes. The plot indicates a noncovalent interaction between the underivatised sulfide and sulfonamide N-H proton at around -0.02 sign(λ_2)ρ. A repulsive interaction around 0.03 sign(λ_2)ρ is identified as the center of the $\{Pt_2S_2\}$ ring. These assignments were made by color-mapping sign(λ_2)ρ on the RDG isosurface in a 3D graphical representation.

The adoption of a coordination geometry with significant pyramidality by the sulfonamide amine is consistent with predictions in the literature based on the N−S bond lengths and τ torsion angles in **13**. The concomitant migration of the sulfonamide amine proton towards the underivatised sulfide, in addition to agreeing

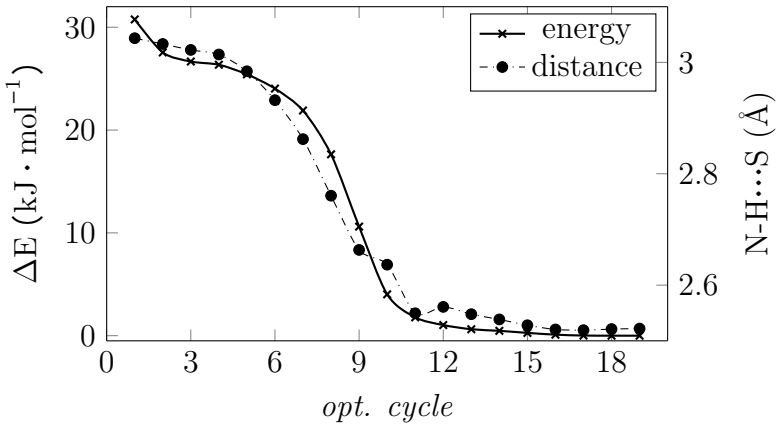

Figure 3.29: Relative energy ($kJ \cdot mol^{-1}$) vs. N-H···S distance (Å) for the constrained proton-optimization of $[Pt_2(\mu\text{-}S)(\mu\text{-}S{-}C_2H_4NH{-}Ts)(PPh_3)_4]^+$ at the 6-31++G**/ωB97X-D3 level of theory. Molecular geometry taken from **13**$[PF_6] \cdot CHCl_3$, disorder ψ_1.

with the previously discussed energetically favored amine hybridisation, reflects the moderate acidity secondary sulfonamide amines are known to have[263] and associated propensity to engage in intramolecular hydrogen bonding.[266] The underivatised sulfide in monoalkylated derivatives of **1a** has been shown to exhibit potent nucleophilicity, provided steric congestion and electrostatic repulsion of the cationic derivative are not prohibitive.[56] These obstacles are more relevant for potential intermolecular interactions with the underivatised sulfide, and would appear to be mitigated in **13** as the intramolecular proximity of the donor and acceptor species is facilitated by a moderately constrained $\{Pt_2S_2\}$ core.

The calculated distance between N1 and the plane formed by S3,H1,C2 in the optimised ψ is 0.28, 0.34, and 0.37 Å, and agrees nicely with predicted $d_{(N\rightarrow|)}$ based on the C−S−N−C torsion angles τ in the crystal structure of **13**$[PF_6]$.[264] Furthermore, this adoption of more sp^3 hybridised geometry by the nitrogen is consistent with the shorter S−N bond distances and suggests an increased s character of the nitrogen lone pair.[264]

In $\psi_{1,2}$ the proton migration and adoption of pyramidally by the sulfonamide amine results in the nitrogen lone pair bisecting the O=S=O sulfonyl angle and

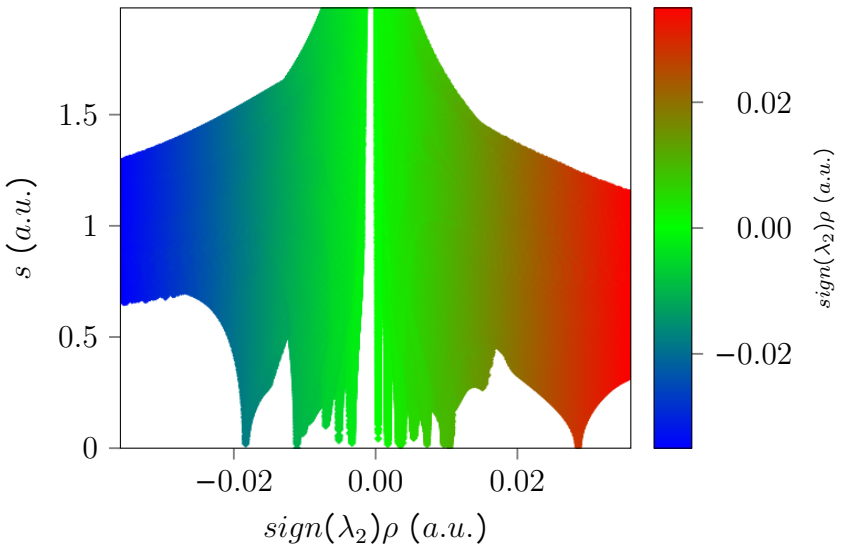

Figure 3.30: The reduced density gradient s $(a.u.)$ is plotted against $sign(\lambda_2)\rho$ $(a.u.)$ for the proton-optimised structre $[Pt_2(\mu\text{-}S)\text{-}(\mu\text{-}S{-}C_2H_4NH{-}Ts)(PPh_3)_4]^+$, ψ_1 disorder.

antiperiplanar to the S−C bond of the aryl ring (Figure 3.31). These geometric features align nicely with energetically preferred conformations in sulfonamide systems, based on frequency of recorded structures in the CSD and quantum chemical rationalisations of $n_N \rightarrow \sigma^*$ interactions *supra infra*. Interestingly, the proton migration towards the underivatised sulfide acceptor in disorder ψ_3 results in the N−H instead partially bisecting the sulfonyl angle, and the nitrogen lone pair at a less favored angle almost antiperiplanar to the S=O bond (Figure 3.31).

An additional consideration when discussing potential pyramidally of the sulfonamide nitrogen is nitrogen inversion, which has been shown to be expedited in tertiary amines with bulky ligands that sterically destabilise and promote $sp^3 \rightarrow sp^2$ hybridisation of the nitrogen.[279] However, the barrier for nitrogen inversion is known to increase with the electronegativity of heteroatom substituents.[279] Additionally, a larger s character of nitrogen lone pair is correlated with an increased inversion barrier, as the transition state for inversion is an ideal planar sp^2 geometry with the lone pair in a pure p-orbital.[279] Retarding of nitrogen inversion via intramolecular hydrogen bonding interactions has been shown to occur in small ring systems[280,281] and more recently in larger marcrocycles in which steric crowding and hindered

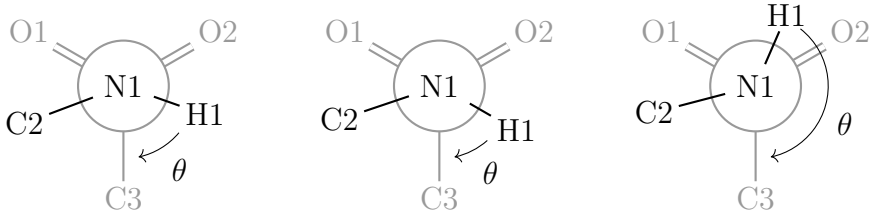

ψ_1 *opt.*		ψ_2 *opt.*		ψ_3 *opt.*	
θ	49.9°	θ	41.3°	θ	141.8°
$d_{(N\rightarrow\vert)}$	0.28 Å	$d_{(N\rightarrow\vert)}$	0.34 Å	$d_{(N\rightarrow\vert)}$	0.37 Å
$d_{(S2-N1)}$	3.43 Å	$d_{(S2-N1)}$	3.43 Å	$d_{(S2-N1)}$	3.67 Å
$d_{(S2-H1)}$	2.53 Å	$d_{(S2-H1)}$	2.52 Å	$d_{(S2-H1)}$	2.72 Å
S2-H1-N1	147.4°	S2-H1-N1	147.7°	S2-H1-N1	153.8°

Figure 3.31: Newman projections along the N1-S3 bond in the proton optimised disorders (ψ) of $[Pt_2(\mu\text{-}S)(\mu\text{-}S{-}C_2H_4NH{-}Ts)(PPh_3)_4]^+$ (**13**). The torsion anlge C3-S3-N1-H1 θ, distances $d_{(N\rightarrow\vert)}$, $d_{(S2-N1)}$, and $d_{(S2-H1)}$ and angle S2-H1-N1 are shown for each ψ.

rotation additionally contributed.[282]

The sulfonamide moiety in **13**[PF_6] presents a unique example in that a rigid Pt−μ-SR−Pt thiolate anchor constrains the substituent above the {Pt_2S_2} ring, sandwiched between triphenylphosphine ligands, which presumably influence N−S and N−C rotation. The influence of the basic sulfide ligand as a hydrogen bond acceptor appears to also be significant, manifest in calculated minima for the sulfonamide amine proton. However, it has been demonstrated for sulfonamides there is usually a sizeable discrepancy between calculated low-energy conformations in the gas phase and geometries observed in crystal structures,[271,283] as crystal packing, inter- and intra-molecular interactions play significant roles in the geometries adopted.

3.6 Ethylene sulfide

Episulfides are another three-membered heterocycle that have been well studied[284] and are known to undergo ring-opening reactions readily, often more so than their lighter chalcogen relatives due to the weaker, less polar S-C bond.[285] The internal ring strain in episulfides has also been shown to be lower than in both cyclopropanes and oxiranes. Nucleophilic ring-opening reactions of episulfides result in the expected β-substituted mercaptans, however this can also give olefins via desulfurisation.[286] Additionally, the ease of nucleophilic ring-opening enjoyed by episulfides is reflected in facile self-polymerisation reactions that have been observed to occur,

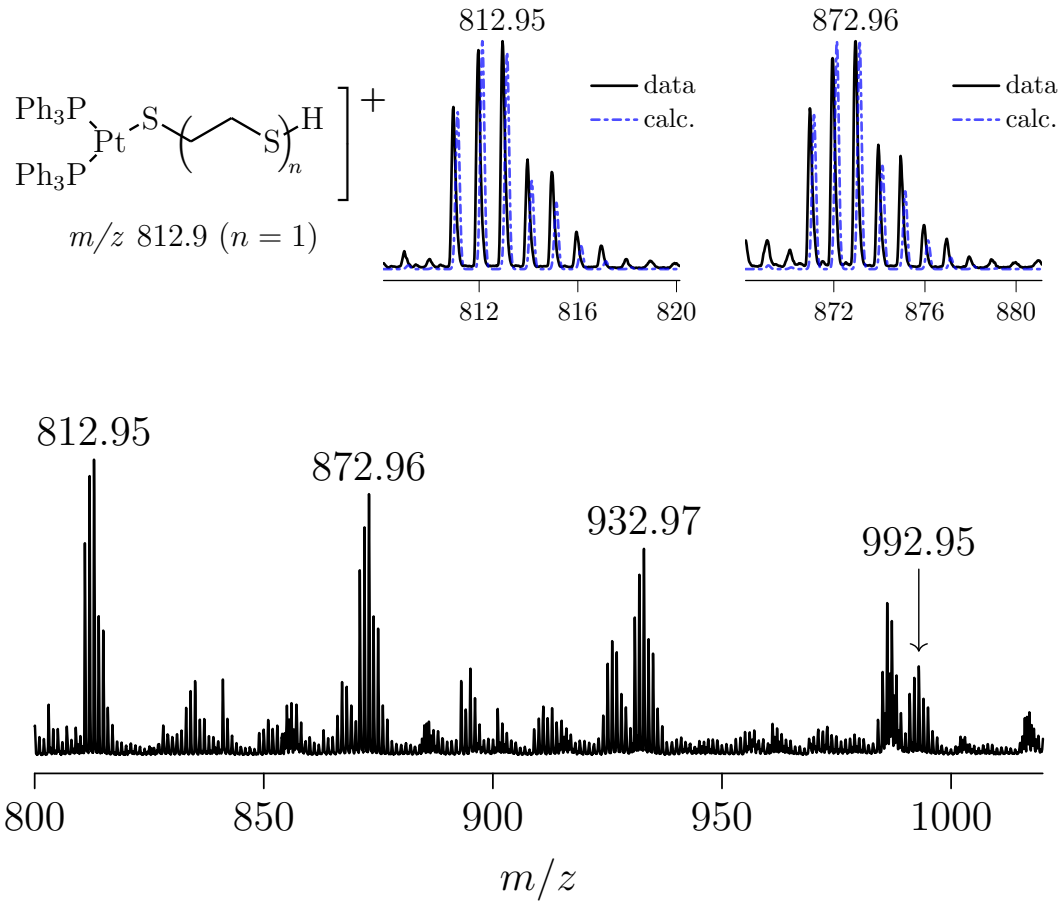

Figure 3.32: ESI mass spectrum of **1a** and ethylene sulfide, capillary exit voltage 90 V. The top left inset is a general structure for the proposed ions. The top center and right insets are isotope pattern comparisons for n = 1, 2 and peaks observed at *m/z* 812.9 and 872.9 respectively.

often without initiators.[284]

The only episulfide examined for ring-opening with **1a** was ethylene sulfide, the simplest episulfide (SC_2H_4), which polymerises slowly into an insoluble white solid when stored at room temperature. A small-scale reaction was carried out between **1a** and ethylene sulfide in methanol at room temperature. After two hours, the reaction solution was slightly off-white and had an unpleasant odor. The ESI mass spectrum was indicative of substantial decomposition and absent of any ring-opened derivative (the monoalkylated $S-C_2H_4SH$ or the overhead-bridged dication). A very densely populated region of medium to hight relative intensity cations around m/z 400-1000 was examined in close detail (Figure 3.32). Of the very few platinum containing ions in the spectrum, only the cationic series tentatively assigned as mononuclear $[(Ph_3P)_2PtS(C_2H_4SH)_n]^+$ (n = 1-4) cations were able to be identified. Although the proposed structure of these cations in Figure 3.32 (*top left inset*) is open-chain with a terminal thiol, equally likely is bidentate coordination through terminal thiolates resulting in a neutral complex which ionises through protonation. The complex $[(Ph_3P)_2PtSC_2H_4S]$ is known,[287] as are various derivatives (Figure 3.33 *a*).[288,289] Also known are dications of the type $cis-[P_2Pt(SC_2H_4)_3]^{2+}$ containing crown trithioether ligands and terminal phosphines (*b*).[290,291] These *pseudo* 5-coordinate Pt^{II} dications have a slightly distorted square-planar arrangement about the metal with the third thioether approaching axially at a slightly longer distance (2.65 cf. 2.35 Å).

However, the ion series tentatively identified in the mass spectrum of **1a** and ethylene sulfide are proposed to be transient species, possibly generated via poly-

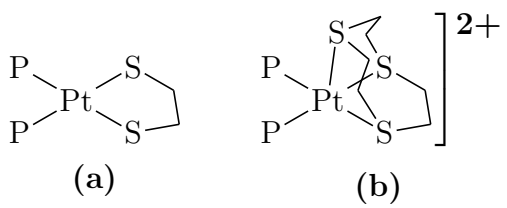

Figure 3.33: **(a)** A general structure of the *cis*-Pt neutral thiother chelate; **(b)** General geometric arrangement of *cis*-Pt trithioether dications. P is mono- or bi-dentate phosphane.

mer fragmentation within the spectrometer. As such, their structure was tentatively depicted as a long-chain thiol (Figure 3.32 *top left inset*), however the series could very well conserve a square-planar coordination geometry about the Pt^{II} center via terminal thiolates. Due to the appearance of the reaction solution and evidence of polymeric species in the mass spectrum, it was concluded ring-opening was occurring concomitant with degradation of the dimer and polymerisation, as is common for ethylene sulfide.[286] No further attempts were made to investigate additional episulfides, however due to the rich chemistry enjoyed by the three membered heterocycle, further investigations of nucleophilic ring-opening reactions between **1a** (and the selenide analogue **1b**) and episulfides are warranted.

3.7 Experimental

3.7.1 General

Cyclopropanes (bromomethyl)cyclopropane, cyclopropyl methyl ketone, *trans*-1,2-dibenzoylcyclopropane, and diethyl cyclopropane-1,2-dicarboxylate were obtained from Sigma. 2,2,3,3,-tetracyanocyclopropane[245] and *N*-tosylaziridine[260] were synthesised by procedures in the literature. Ethylene sulfide was commercially acquired (Sigma). All reactions were carried out in ambient conditions. Reagent or laboratory grade solvents were used without purification.

3.7.2 Computational

Geometry optimisation and single point energy DFT calculations were carried out using the molecular geometry obtained from the crystal structure of $[Pt_2(\mu\text{-}S)(\mu\text{-}S{-}C_2H_4NH{-}Ts)(PPh_3)_4][PF_6]$ (**13**$[PF_6]$) with the Q-Chem 4.2 software package[292] using the ωB97X functional[293] with DFT-D3 long-range dispersion correction by Grimme *et al.*[201,202] The platinum atoms were treated with the LANL2DZ effective core potential and basis set.[294] All other atoms were treated with the Pople split valence double-ζ basis set 6-31++G**, with diffuse and polarisation functions for all atoms.[295–301] The reduced density gradient (RDG) and sign$\lambda_2(\rho)$ cube files were generated using the Multiwfn toolkit,[205] which was constrained with a modified grid that encompassed the specific area of chemical interest. VMD[302] was used to combine the molecular geometry with RDG isosurface and colormap with sign$\lambda_2(\rho)$ to identify areas of interest. A python script, using the matplotlib module,[206] was created to output the NCI plot of RDG vs. sign$\lambda_2(\rho)$.

3.7.3 Single crystal XRD experiments

The structures were solved using intrinsic phasing from the SHELXT-2018/2[208] package and refined using SHELXL-2018/3[209] with full-matrix least-squares on F^2, all carried out in Olex2.[210] Unless otherwise stated, all non-hydrogen atoms were

refined anisotropically and hydrogen atoms added with a riding model. Crystallographic data are tabulated in Table 3.6.

10$[BPh_4] \cdot CHCl_3$

X-ray diffraction data were collected on a Rigaku Oxford Diffraction XtaLAB-Synergy-S single crystal diffractometer with a PILATUS 200 K hybrid pixel array detector using Cu Kα radiation (λ = 1.54184 Å) at 100.0(4). The intensity data were processed with the CrysAlis PRO[207] software suite and multi-scan empirical absorption corrections were applied using spherical harmonics, implemented in the SCALE3 ABSPACK scaling algorithm. The structure solves routinely however after the refinement proceeds several large density peaks in the difference map ($\approx$ 5 $e \cdot Å^{-3}$) were located in chemically nonsensical positions, suggesting twinning.

11[BETI]

Yellow parallelepiped crystals suitable for an X-ray diffraction experiment were obtained by slow evaporation of a chloroform solution layered with pentane. X-ray diffraction data were collected on a Rigaku Oxford Diffraction XtaLAB-Synergy-S single crystal diffractometer with a PILATUS 200 K hybrid pixel array detector using Cu Kα radiation (λ = 1.54184 Å) at 99.9(6) K. The intensity data were processed with the CrysAlis PRO[207] software suite and multi-scan empirical absorption corrections were applied using spherical harmonics, implemented in the SCALE3 ABSPACK scaling algorithm. As $Z' = 0.5$, half a BETI anion is required for charge balance. However, the BETI anion was found to be extremely disordered having a $C2$ axis pass perpendicularly through it and several attempts to model it were unsuccessful. The SQUEEZE routine[214] was used to model unresolved electron density.

12 $\cdot (CHCl_3)_2$

Red prismatic cyrstals were obtained by slow evaporation of a chloroform solution. Data were recorded (100.01 K) using a Bruker APEX-II CCD diffractometer with Mo K_α radiation $\lambda = 0.71073$. The complex crystallises in the orthorhombic space group *Pbcm* as the di-chloroform solvate **12** $\cdot 2\,CHCl_3$ and has four independent molecules in the unit cell, with half a molecule contained in the asymmetric unit. Due to the mirror symmetry bisecting the dimer, significant positional disorder was present in both triphenylphosphine ligands in the ASU. The PPh_3 ligands were treated as residues and refined with SIMU and SAME restraints applied. A large density peak of 3.34 e $\cdot$ Å^{-3} remained after the final refinement cycle 0.6 Å from Pt1.

13$[PF_6] \cdot CHCl_3$

Orange-red crystals were obtained from vapor diffusion of diethyl ether into a chloroform solution. X-ray diffraction data were collected at 99.9(4) K on a SuperNova Dual AtlasS2 diffractometer fitted with Cu Kα radiation (λ = 1.54184 Å). The intensity data were processed with the CrysAlis PRO[207] software suite and multi-scan empirical absorption corrections were applied using spherical harmonics, implemented in the SCALE3 ABSPACK scaling algorithm. The complex crystallises in the triclinic centrosymmetric space group $P\bar{1}$ with two independent molecules in the unit cell, associated PF_6 anions, and chloroform of crystallisation. After several refinement cycles, a 3-component disorder was evident in the *N*-tosyl ligand. The disordered components were assigned to residues with the RESI instruction and the SAME, DELU, and RIGU restraints were applied. The SUMP instruction was used along with additional free variables to model the disorder.

3.7.4 Synthesis

Synthesis of $[Pt_2(\mu\text{-}S)(\mu\text{-}S{-}C_4H_7)(PPh_3)_4][BPh_4]$ (**10**$[BPh_4]$)

After the addition of a molar exccess of (bromomethyl)cyclopropane (0.4 mL, 557 mg, 4.16 mmol) to a cloudy orange suspension of **1a** (109 mg, $7.25{\times}10^{-2}$ mmol) in methanol (30 mL), the reaction suspension was stirred and gradually heated to reflux temperature. After 20 minutes, the reaction solution gradually turned clear and yellow, and the heating mantle was promptly turned off. After stirring for an additional 30 minutes, the room temperature clear yellow reaction solution was filtered to remove a trace amount of insoluble matter. To the clear yellow filtrate was added a molar equivalent of $NaBPh_4$ (25.8 mg, $7.54{\times}10^{-2}$ mmol), prompting the immediate formation of a pale-yellow precipitate. Distilled H_2O (15 mL) was

Table 3.5: Crystallographic data for **13**$[PF_6]\cdot CHCl_3$

Empirical formula	$C_{82}H_{73}Cl_3F_6NO_2P_5Pt_2S_3$
M_r ($g\cdot mol^{-1}$)	1890.56
Crystal size (mm)	0.260 x 0.341 x 0.126
Crystal system	triclinic
Space group	$P\bar{1}$
a (Å)	14.2811(3)
b (Å)	14.3903(3)
c (Å)	19.3606(4)
α (°)	92.6987(19)
β (°)	103.5715(19)
γ (°)	100.6726(19)
V ($Å^3$)	3783.66(15)
Z	2
ρ_{calc} ($g\cdot cm^{-3}$)	1.659
$\mu(CuK_\alpha)$ (mm^{-1})	9.440
$F(000)$	1871.0
2θ range (°)	7.022 to 140.104
Reflections collected/unique/$[I > 2\sigma(I)]$	40634/40581/11791
R_{int}	0.0347
Data/parameters/restraints	14003/1195/741
Goodness-of-fit on F^2	1.036
Final R indicies $[I > 2\sigma(I)]$	R_1 = 0.0344, wR_2 = 0.0731
R indicies (all data)	R_1 = 0.0475, wR_2 = 0.0801
T_{min}/T_{max}	0.812/0.946
ρ_{max}/ρ_{min} ($e\cdot Å^{-3}$)	1.32/-1.20

added and the suspension was stirred for 20 minutes to complete precipitation. The pale-yellow solid was then collected by vacuum filtration on a glass sintered frit and successively washed with distilled H_2O (3 x 20 mL) and Et_2O (2 x 10 mL) before drying under vacuum to give pure **10**[BPh_4] as a pale-yellow solid (78 mg, 59%). M.p. 234°C. *Anal.* Calc. for $C_{100}H_{87}BP_4Pt_2S_2$: C, 63.96; H, 4.67%. Found: C, 63.62; H, 4.69%. ESIMS, *m/z* 1558.27 $[M]^+$ (100%). $^{31}P\{^1H\}$-NMR (242.95 MHz, $CDCl_3$): δ 24.8 [m, br, $^1J_{(PtP)}$ 3250 Hz], 24.0 [m, br, $^1J_{(PtP)}$ 2620 Hz]. ^{1}H-NMR (600.17 MHz, $CDCl_3$) 7.48-6.89 [aromatic], 2.31 [m, br, 2H], 0.07 [m, br, 2H], 0.04 [m, br, 1H], -0.21 [m, br, 2H]. ^{13}C-NMR (150.91 MHz, $CDCl_3$): δ 165.0-121.6 [aromatic], 50.3 [S-CH_2, -ve DEPT-135], 13.2 [CH], 7.2 [CH_2, -ve DEPT-135].

Reflux of (**10**[BPh_4])

The pale-yellow solid **10**[BPh_4] (68.2 mg, 3.63×10^{-2} mmol) was dissolved in chloroform (0.5 mL) and diluted with methanol (10 mL) until the clear yellow solution became slightly translucent. The translucent yellow solution was stirred and refluxed for 24 hours, after which ESI mass spectra provided no evidence of cyclopropane ring-opening.

Attempted synthesis of $[Pt_2(\mu\text{-S})(\mu\text{-S}{-}CH_2CH_2CH_2COCH_3)(PPh_3)_4]^+$ (**30**)

(No catalyst) A molar excess of Cyclopropyl methyl ketone (0.25 mL, 212 mg, 2.52 mmol) was added dropwise to a stirred yellow-orange suspension of **1a** (23.7 mg, 1.58×10^{-2} mmol) in ethanol (15 mL), and the resulting mixture refluxed for 24 hours. ESIMS, *m/z* 1503.15 (calc. *m/z* 1503.25) **1a**$[H]^+$ (100%), *m/z* 1588.19 (calc. *m/z* 1588.31) $[M]^+$ (5%).

($LaCl_3\cdot 7H_2O$, 0.235 eq.) To a cloudy orange suspension of **1a** (22.4 mg, 1.49×10^{-2} mmol) in methanol (20 mL), a molar excess of cyclopropyl methyl ketone (0.3 mL, 255 mg, 3.03 mmol) and lanthanum chloride (1.3 mg, 3.5×10^{-3} mmol) were added and the resulting mixture refluxed for 24 hours. ESIMS, *m/z* 1503.05 (calc. *m/z* 1503.25) **1a**$[H]^+$ (100%), *m/z* 1538.04 (calc. *m/z* 1538.21) $[Pt_2(\mu\text{-S})_2(PPh_3)_4]Cl^+$

(33%).

($Y(NO_3)_3 \cdot 4\,H_2O$, 0.335 eq.) Yttrium nitrate tetrahydrate (1.2 mg, 4.2×10^{-3} mmol) and a molar excess of cyclopropyl methyl ketone (0.3 mL, 255 mg, 3.03 mmol) were added to a cloudy orange suspension of **1a** (18.9 mg, 1.26×10^{-2} mmol) in methanol (25 mL) and the resulting mixture refluxed for 24 hours. ESIMS, *m/z* 1503.10 (calc. *m/z* 1503.25) **1a**$[H]^+$ (100%), *m/z* 1538.03 (calc. *m/z* 1538.21) $[Pt_2(\mu\text{-}S)_2(PPh_3)_4]Cl^+$ (20%).

Attempted synthesis of $[Pt_2(\mu\text{-}S)(\mu\text{-}S{-}CH_2CH(COPh)CH_2(COPh))(PPh_3)_4]^+$

To a cloudy orange suspension of **1a** (22.4 mg, 1.49×10^{-2} mmol) in methanol (15 mL) was added a molar excess of *trans*-1,2-dibenzoylcyclopropane (13.7 mg, 5.47×10^{-2} mmol) and the reaction suspension was refluxed for 72 hours while stirring, after-which the reaction solution was examined by ESIMS.

Synthesis of $[Pt_2(\mu\text{-}S)(\mu\text{-}S{-}C_2H_4CH(CO_2C_2H_5)_2)(PPh_3)_4][BETI]$ (**11**[BETI])

A molar excess of Diethyl cyclopropane-1,1-dicarboxylate (0.5 mL, 527 mg, 2.83 mmol) was added dropwise to a stirring yellow-orange suspension of **1a** (88.6 mg, 5.89×10^{-2} mmol) in ethanol (40 mL) and the resulting mixture refluxed for 80 hours. The clear yellow-orange solution was filtered to remove a trace amount of insoluble matter and lithium bis(pentafluoroethanesulfonyl)imide (150 mg, 3.87×10^{-1} mmol) was added effecting a yellow precipitate which was collected by vacuum filtration in a glass sintered frit. The yellow solid was washed successively with distilled H_2O (3 x 20 mL) and Et_2O (1 x 5 mL) before drying under vacuum to give pure **11**[BETI] as a fine yellow solid (77 mg, 63%). Yellow parallelepiped crystals of the complex were obtained from a chloroform solution layered with pentane. M.p. 140°C. *Anal.* Calc. for $C_{85}H_{75}F_{10}NO_8Pt_2S_4$: C, 49.30; H, 3.65; N, 0.68%. Found: C, 49.82; H, 3.71; N, 0.71%. ESIMS, *m/z* 1690.19 (calc. *m/z* 1690.34) $[M]^+$ (100%). ^{1}H-NMR (600.17 MHz, $CDCl_3$): δ 7.02-7.41 [aromatic, PPh_3], 4.17 [m, 4H], 2.87 [t, 1H, $^3J_{(HH)}$ 6.89 Hz], 2.25 [m, br, 2H], 1.24 [t, 6H, $^3J_{(HH)}$ 7.23 Hz], 1.20 [m, 2H]. ^{31}P$\{^1$H$\}$-NMR

(242.95 MHz, $CDCl_3$): δ 25.1 [m, br, $^2J_{(PtP)}$ 2600 Hz], 25.3 [m, br, $^2J_{(PtP)}$ 3280 Hz].

Synthesis of $[Pt_2(\mu\text{-}S)(\mu\text{-}S{-}C(CN)_2)(PPh_3)_4]$ (**12**)

Tetracyanocyclopropane (12 mg, $8.5{\times}10^{-2}$ mmol) was added to a suspension of **1a** (115 mg, $7.65{\times}10^{-2}$ mmol) in methanol (15 mL) and stirred at room temperature for 1 hour. The clear red-orange solution was filtered to remove trace amounts of insoluble matter before distilled H_2O (15 mL) was added slowly, resulting in the formation of a red-orange precipitate which was collected by vacuum filtration on a glass sintered frit and washed successively with distilled H_2O (2 x 10 mL) and diethyl ether, before drying under vacuum to give **12** as a red-orange solid (79 mg, 66%). M.p. 151°C. *Anal.* Calc. for $C_{75}H_{60}N_2P_4Pt_2S_2$: C, 57.47; H, 3.86; N, 1.79%. Found: C, 59.00; H, 3.83; N, 1.78%. Red parallelepiped crystals were obtained by slow evaporation from a chloroform solution layered with pentane. ^{1}H-NMR ^{31}P{^{1}H}-NMR (121.49 MHz, $CDCl_3$): δ 30.69 [m, $^1J_{(PtP)}$ 2830 Hz], 23.08 [m, $^1J_{(PtP)}$ 2940 Hz, $^3J_{(PtP)}$ 120 Hz]. ^{195}Pt{^{1}H}-NMR (129.02 MHz, $CDCl_3$): δ -4025 [dd, $^1J_{(PtP)}$ 2940, $^1J_{(PtP)}$ 2830, $^2J_{(PtPt)}$ 980, $^3J_{(PtP)}$ 120 Hz]. ESIMS, (*m/z* , *r.i.*), *m/z* 1568.09 (calc. *m/z* 1568.24) [**12** + H]$^+$ (100%).

Synthesis of $[Pt_2(\mu\text{-}S)(\mu\text{-}S{-}C_2H_4NH{-}Ts)(PPh_3)_4][PF_6]$ (**13**[PF_6])

To a cloudy orange suspension of **1a** (148 mg, $9.84{\times}10^{-2}$ mmol) in methanol (20 mL), *N*-tosylaziridine (70.0 mg, $3.55{\times}10^{-1}$ mmol) was added. The reaction solution was stirred at r.t. for one hour before the clear orange solution was filtered to remove trace amounts of insoluble matter. A molar excess of ammonium hexafluorophosphate (50 mg, $3.1{\times}10^{-1}$ mmol) was added, prompting the formation of a yellow precipitate. Distilled H_2O (10 mL) was added to complete precipitation, before isolation of the yellow solid by vacuum filtration on a glass sintered frit, and successive washing of the solid by distilled H_2O (2 x 20 mL) and diethyl ether (1 x 5 mL). The yellow solid was then dried under vacuum to give pure **13**[PF_6] (135 mg, 74%). M.p. 128°C. *Anal.* Calc. for $C_{81}H_{72}F_6NO_2P_5Pt_2S_3$: C, 52.68; H, 3.93; N,

0.76%. Found: C, 53.27; H, 3.92; N, 1.06%. Crystallisation from vapor diffusion of diethyl ether into a chloroform solution gave orange-red parallelepipeds. $^{31}P\{^{1}H\}$-NMR (121.49 MHz, $CDCl_3$) δ 25.45 [m, $^{1}J_{(PtP)}$ 3232, 2591 Hz]. ESIMS, *m/z* 1701.01 $[M]^+$ (100%).

Attempted ring-opening reaction of **1a** and ethylene sulfide

A cloudy orange-yellow suspension of **1a** (16 mg, 1.1×10^{-2} mmol) in methanol (5 mL) was stirred. A molar excess of ethylene sulfide (0.2 mL, 2.0 mmol) was added dropwise after filtering through cotton wool to remove white insoluble material present in the commercial sample. After stirring for 2 hours, the reaction solution appeared off-white and cloudy with a visible off-white precipitate. A sample was taken for ESIMS analysis providing evidence of significant decomposition of the starting complex **1a**.

Table 3.6: Crystallographic data.

	11[BETI]	**12**$\cdot(CHCl_3)_2$	**10**[BPh_4]$\cdot CHCl_3$
Empirical formula	$C_{85}H_{75}F_{10}NO_8Pt_2S_4$	$C_{77}H_{61}N_2P_4S_2Pt_2Cl_6$	$C_{101}H_{88}BCl_3P_4Pt_2S_2$
M_r ($g \cdot mol^{-1}$)	1946.92	1805.07	1997.05
Crystal size (mm)	0.12 x 0.10 x 0.08	0.24 x 0.15 x 0.04	0.14 x 0.08 x 0.08
Crystal system	orthorhombic	orthorhombic	orthorhombic
Space group	$Ccce$	$Pbcm$	$P2_12_12_1$
a (Å)	26.7454(2)	17.8385(6)	31.3098(5)
b (Å)	25.5058(2)	17.0427(6)	19.9508(3)
c (Å)	25.30520(10)	23.3329(8)	13.8946(2)
α (°)	90	90	90
β (°)	90	90	90
γ (°)	90	90	90
V ($Å^3$)	17262.3(2)	7093.6(4)	8679.3(2)
Z	8	4	4
ρ_{calc} ($g \cdot cm^{-3}$)	1.304	1.476	1.528
$\mu(CuK_\alpha)$ (mm^{-1})	7.456	4.140	8.303
$F(000)$	6744.0	3105.0	3992.0
2θ range (°)	5.926 to 148.654	2.282 to 56.564	7.178 to 148.822
Reflections collected/unique	120612/8767	106548	65526/17267
R_{int}	0.0501	0.0680	0.0695
Data/parameters/restraints	8767/474/0	9014/752/984	17267/994/15
Goodness-of-fit on F^2	1.236	1.007	1.070
Final R indices [$I > 2\sigma(I)$]	$R_1 = 0.0443, wR_2 = 0.1001$	$R_1 = 0.0564, wR_2 = 0.1471$	$R_1 = 0.0770, wR_2 = 0.1926$
R indices (all data)	$R_1 = 0.0458, wR_2 = 0.1007$	$R_1 = 0.0768, wR_2 = 0.1656$	$R_1 = 0.0824, wR_2 = 0.1962$
T_{min}/T_{max}	0.641/1.000	0.658/0.965	0.511/1.000
ρ_{max}/ρ_{min} ($e \cdot Å^{-3}$)	1.24/-1.24	3.34/-2.46	5.88/-3.14

Chapter 4

Functionalising $[Pt_2(\mu\text{-}S)_2(PPh_3)_4]$ via substitution

4.1 Introduction

In previous work by Henderson,[42c] it was observed that arylation of $[Pt_2(\mu\text{-}S)_2(PPh_3)_4]$ **1a** with pyridinium alkylating agent *N*-methyl-2-chloropyridinium iodide (**14**[I]) did not result in the expected dicationic derivative $[Pt_2(\mu\text{-}S)(\mu\text{-}S{-}C_6H_7N)(PPh_3)_4]^{2+}$ (**2**), rather the known[71] bridging iodo complex $[Pt_2(\mu\text{-}S)(\mu\text{-}I)(PPh_3)_4]^{+}$ (**15**) was isolated. Upon a closer investigation of this reaction by ESIMS, the analogous bridging chloride species $[Pt_2(\mu\text{-}S)(\mu\text{-}Cl)(PPh_3)_4]^{+}$ (**33**) was also observed, and it was proposed the initially formed dicationic derivative **2** was susceptible to substitution reactions, presumably as the zwitterionic bridging ligand *N*-methyl-2-mercaptopyridinium formed in the alkylation of **1a** was an excellent leaving group (Scheme 4.1).[42c] Hence, to unlock the proposed utility of **2** as a synthon towards

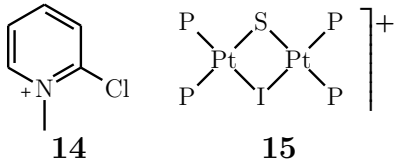

14 **15**

Figure 4.1: Structure of *N*-methyl-2-chloropyridinium cation **14** and bridging-iodo complex **15**.

substituted derivatives, a pyridinium salt with a suitable non-coordinating anion was needed as the strong proclivity of the soft iodide anion for Pt^{II} precluded any further substitution reactions. In the initial work by Henderson,[42c] a metathetic reaction of the commercially available iodide salt **14**[I] with sodium tetraphenylborate was successfully employed to remove iodide, and upon reaction of **14**[BPh_4] with **1a** and then ammonia, a novel bridging-amido complex [Pt_2(μ-S)(μ-NH_2)(PPh_3)$_4$][BPh_4] was isolated.

The work carried out and described in this chapter is a continuation of this chemistry, with a particular emphasis on two fronts: preparing a suitable pyridinium salt, ideally with a weakly coordinating anion such that a choice of counterion is available for substituted derivatives later in the synthetic workup, and to explore a variety of potential candidates ligands L for insertion into a μ_2 coordination within the {Pt_2(μ-S)(μ-L)} dimer (Scheme 4.1). In particular for thiolate ligands, this method has the potential to access unique and highly-tuned derivatives of **1a** that would otherwise be inaccessible or require harsh or exotic alkylating agents.

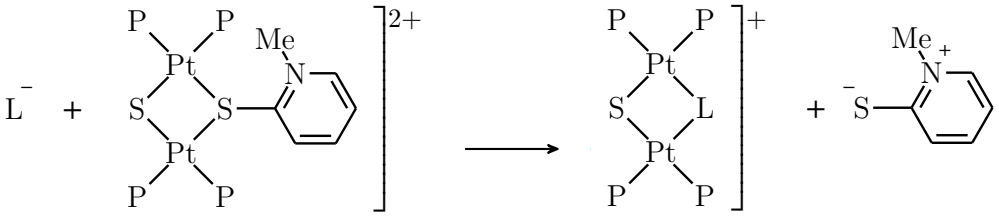

2

Scheme 4.1: Proposed scheme for insertion of anionic ligand L^- into **2**.

4.2 Pyridinium salts

The commercially available iodide salt of *N*-methyl-2-chloropyridinium (**14**) was deemed unsatisfactory for synthesising $[Pt_2(\mu\text{-}S)(\mu\text{-}S{-}C_6H_7N)(PPh_3)_4]^{2+}$ (**2**) due to the free iodide anion readily forming the incredibly inert μ-iodide complex $[Pt_2(\mu\text{-}S)(\mu\text{-}I)(PPh_3)_4]^{+}$ (**15**). Initially, a metathesis reaction of **14**[I] with sodium tetraphenylborate was carried out to give **14**[BPh_4], as was done previously in the literature.[42c] Upon ESIMS examination of several micro-scale test reactions between **1a** and **14**[BPh_4], it was determined trace amounts of iodide remained in the BPh^- salt, evidenced by the presence of **15** at low but consistent relative intensities. Alternative routes to **14** with a non-coordinating anion were next explored to completely eliminate iodide from the work-up, the most successful of which involved *N*-methylation of 2-chloropyridine with very strong methylating agents. Dimethylsulfate produced **14**[CH_3SO_4] as a hygroscopic waxy white solid which was used either directly as an aqueous solution or metathetically isolated with counterions BPh_4^- and PF_6^- to give their respective salts as stable white solids. Additionally, the tetrafluoroborate salt **14**[BF_4] was analogously synthesised using trimethyloxonium tetrafluoroborate.

Initial ESIMS examinations of a freshly prepared micro-scale solutions of **1a** and salts of **14** suggested that a mixture of **2** and **33** cations were present in solution in a roughly similar proportion, assuming a similar ionisation efficiency. The relative intensity of **2** was observed to vary with increasing capillary exit voltage, and at voltages above 120V the signal for **2** was absent in collected spectra. This behaviour is somewhat unusual for dicationic derivatives of **1a** for which a reduction in the relative intensity of the ion signal and fragmentation of triphenylphosphine are typically observed when increasing capillary exit voltage. Charge reduction of multiply charged systems by aggregating with additional counterions or electrochemical reduction is a well known phenomena in ESIMS,[80] and this behaviour has been observed previously for dicationic derivatives of **1a**.[29a] In the case of **2**, charge reduction was presumably occurring via enhanced substitution of Cl^- to form **33** or by loss of the zwitterionic ligand and a concomitant 2e reduction process to form a neutral

species with a Pt^{I}-Pt^{I} bond and a triangular $\{Pt_2(\mu\text{-}S)\}$ core. The large relative intensity of **33** was initially surprising, considering the smaller and harder chloride anion should be a very poor bridging ligand and that only a slight molar excess of chloride should be present in solution. Although ESIMS can typically give reliable information regarding relative concentrations of similar cationic species,[72] care must be taken when examining species that have significantly different ionisation efficiencies or redox behaviour.

After concentrating the reaction solution under vacuum, a subsequent $^{31}P\{^{1}H\}$-NMR spectroscopy examination of the methanolic reaction solution revealed a somewhat different speciation than was observed in the mass spectrum. Two species appeared to be present as evidenced by four resonances, each with the expected ^{195}Pt satellites. However unlike the reasonably equal relative intensities observed by ESIMS, the preponderant species (δ 27.2 and 25.3) was conservatively estimated by integration to be approximately 45 times more prevalent in solution. These res-

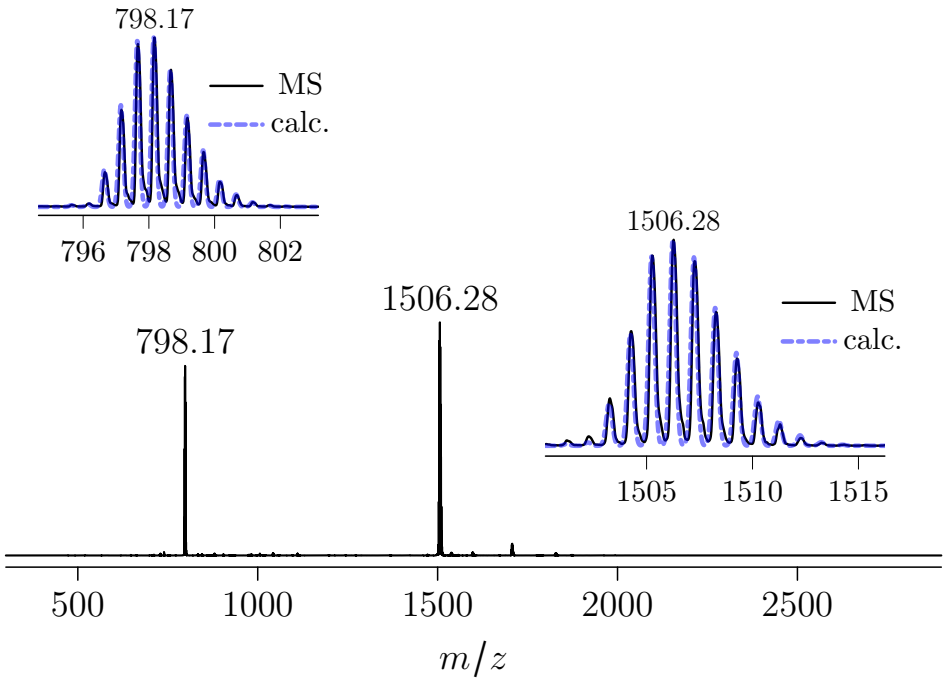

Figure 4.2: ESI mass spectrum of $[Pt_2(\mu\text{-}S)_2(PPh_3)_4]$ (**1a**) and **14**$[CH_3SO_4]$ in methanol. The insets are comparisons of peaks observed at *m/z* 798.17 and 1506.28 and calculated isotope patterns for $[Pt_2(\mu\text{-}S)(\mu\text{-}S{-}C_6H_7N)(PPh_3)_4]^{2+}$ **2** and $[Pt_2(\mu\text{-}S)(\mu\text{-}Cl)(PPh_3)_4]^{+}$ **33** respectively. Capillary exit voltage 60 V.

onances were assigned to **2**, based on the estimated $^{1}J_{(\mathrm{PtP})}$ coupling constants of 2608 and 3757 Hz respectively. The larger $^{1}J_{(\mathrm{PtP})}$ was assigned to the phosphines *trans* to the thiolato-pyridnium ligand, assuming a much weaker *trans* influence than the underivatised sulfide. In comparison, the bridging chloride cation **33** was assigned to the resonances at δ 28.2 and 19.4 ppm with estimated $^{1}J_{(\mathrm{PtP})}$ coupling constants of 2618 and 4423 Hz respectively. Again, the very large $^{1}J_{(\mathrm{PtP})}$ coupling of 4423 Hz was assigned to the phosphines *trans* to Cl^{-}, epitomizing the very weak *trans* influence expected for the harder chloride ligand. Large $^{1}J_{(\mathrm{PtP})}$ coupling constants of 3994, 3997, and 4143 Hz have been observed for other Pt^{II} dimers with bridging chloride ligands *trans*-$[Pt_2(\mu\text{-}Cl)_2(S{-}R)_2P_2]X_2$ (R, P, X = EtPh, PPr^{n}_{3}, BF_4; HPh, PPr^{n}_{3}, BF_4; MePh, PMe_2Ph, SO_3F respectively).[303] Assignments of **2** and **34** were made on the account of the significantly different resonance pair separation (Δν much larger for the mixed-bridged **33**) and a much larger $^{1}J_{(\mathrm{PtP})}$ for the phosphines *trans* to Cl^{-}. The preponderance of **2** in solution was not entirely surprising considering the relative instability of the μ_2-chloride ligand in **33**, and the non-negligible concentration of chloride ions along with charge reduction processes within the mass spectrometer presumably results in greater substitution rates for

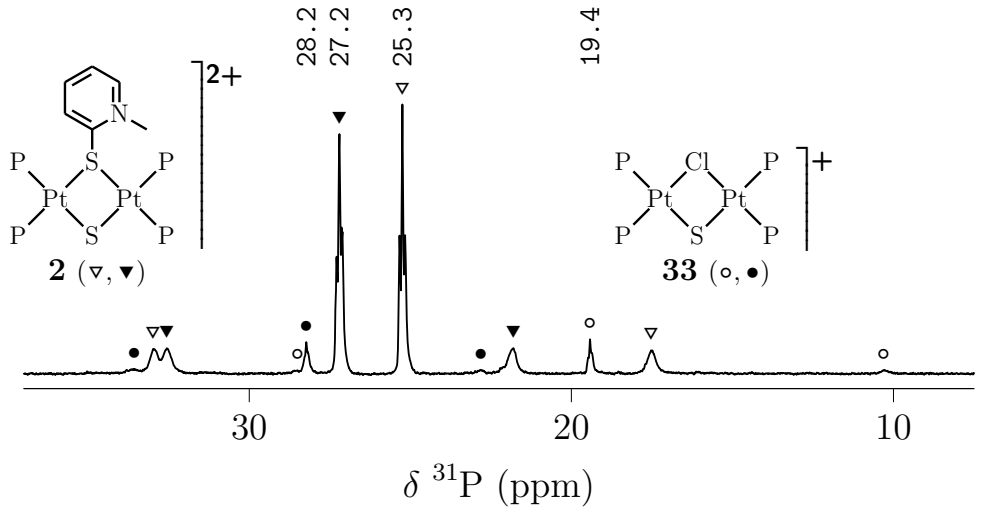

Figure 4.3: $^{31}P\{^{1}H\}$-NMR (242.95 MHz) of **1a** and **14**$[CH_3SO_4]$ in methanol. Proposed structures for $[Pt_2(\mu\text{-}S)(\mu\text{-}S{-}C_7H_6N)(PPh_3)_4]^{2+}$ **2** and $[Pt_2(\mu\text{-}S)(\mu\text{-}Cl)(PPh_3)_4]^{+}$ **33** are assigned to resonances in the spectrum.

the mercapto-pyridinium ligand giving a somewhat misleading representation of **33** by ESIMS. To examine the effect of increasing [Cl^-], a slight molar excess of LiCl was added to the methanolic solution and the $^{31}P\{^1H\}$-NMR spectrum recorded once more. The resonances of **33** increased only slightly in area, confirming the poor bridging ability of the hard chloride anion and no attempt was made to isolate **33**.

Initially, we attempted to synthesize and isolate $[Pt_2(\mu\text{-}S)(\mu\text{-}Br)(PPh_3)_4]^+$ (**16**) as an intermediate by exposing **2** to an excess of bromide. Theoretically this cation would possess the ideal properties of being both isolable yet sufficiently reactive to undergo bromide substitution when exposed to stronger nucleophiles. Although this multi-step approach would increase the complexity of the work-up, having a solid intermediate enabled more precise control over stoichiometry in the final substitution step. When ESIMS was used to examine micro-scale reactions between a freshly prepared solution of **2** and bromide (LiBr), the excess bromide in the reaction solution appeared insufficient to drive the substitution reaction fully to completion as evidenced by cations assigned as $[Pt_2(\mu\text{-}S)(\mu\text{-}S{-}C_6H_7N)(PPh_3)_4]^{2+}$ **2** at *m/z* 798

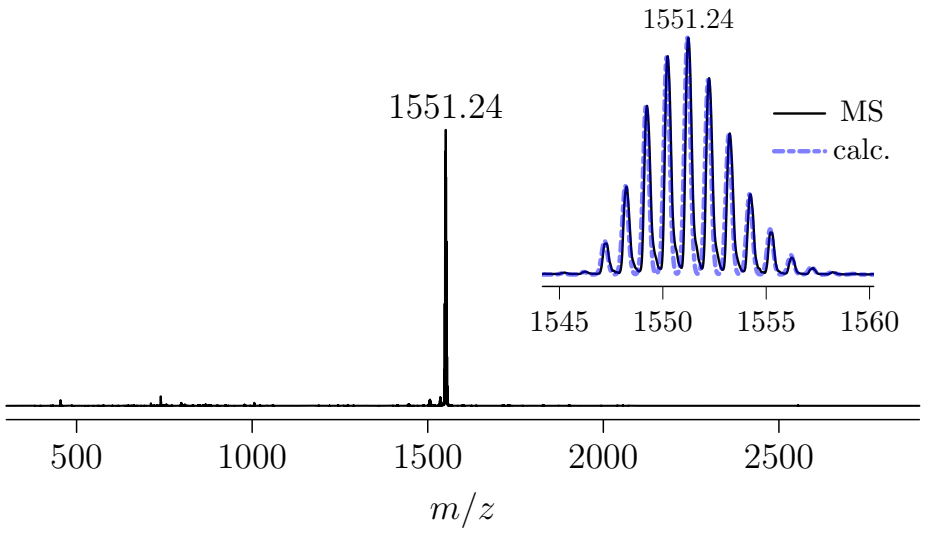

Figure 4.4: ESI mass spectrum of **16**[BPh_4] in a dichloromethane-methanol solution. The inset is a comparison of the peak observed at *m/z* 1551.24 and a calculated isotope pattern for the proposed cation $[Pt_2(\mu\text{-}S)(\mu\text{-}Br)(PPh_3)_4]^+$ (**16**, calc. *m/z* 1551.19). Capillary exit voltage 60 V.

and $[Pt_2(\mu\text{-}S)(\mu\text{-}Cl)(PPh_3)_4]^+$ **33** at *m/z* 1506 accompanying the base peak at *m/z* 1551 $[Pt_2(\mu\text{-}S)(\mu\text{-}Br)(PPh_3)_4]^+$ **16**. Despite this observed difficulty in the micro-scale, several attempts were made to isolate **16** macroscopically. Upon carrying out the initial macroscopic synthesis of **16**, employing the aqueous methylsulfate solution of **14**, it was observed by ESIMS that a large molar excess of lithium bromide was indeed sufficient to drive substitution towards **16**, with signals for the cations **2** and **33** absent in the spectrum. However, the excess bromide was also able to act as a suitable counterion for **16**, evidenced by significant precipitation in the reaction solution upon stirring in ambient conditions for 30 minutes. ESIMS of the red-orage precipitate confirmed **16** as the only ionisable species present. **16**$[BPh_4]$ was successfully isolated in a subsequent synthesis by a more prompt addition of the BPh_4^- counterion. ESIMS was used to examine the isolated solid, confirming the predominant ionisable cation was the mixed-bridged $[Pt_2(\mu\text{-}S)(\mu\text{-}Br)(PPh_3)_4]^+$ **16** at *m/z* 1551. A calculated isotope pattern for **16** was in strong agreement with the observed peak (Figure 4.4). The sample was examined in negative-ion mode to confirm the presence of the BPh_4^- counterion.

$^{31}P\{^1H\}$-NMR was next employed to characterise **16**$[BPh_4]$ (Figure 4.5), with

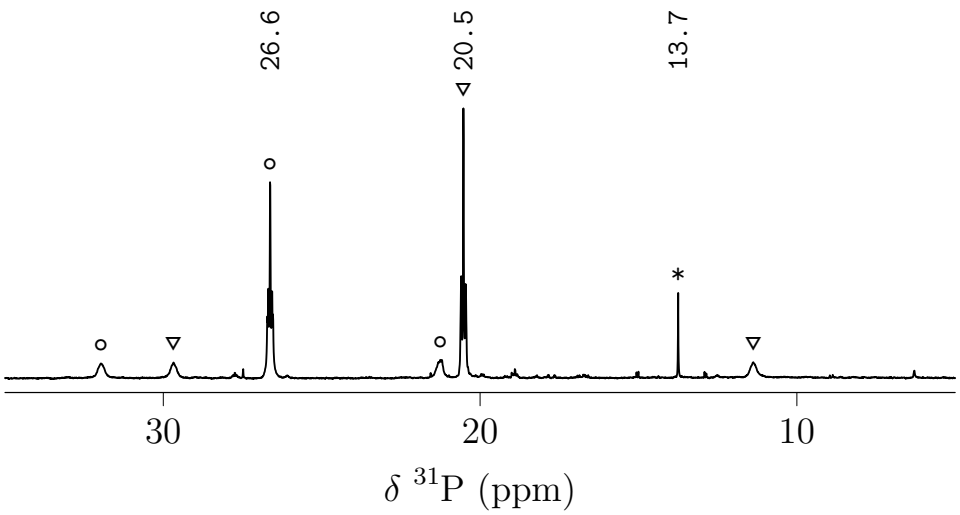

Figure 4.5: $^{31}P\{^1H\}$-NMR (242.95 MHz) of **16**$[BPh_4]$ in acetone/chloroform-*d* solution. The resonance marked * at δ 13.7 ppm is an impurity, proposed to be *cis*-$[PtBr_2(PPh_3)_2]$.

the experiment carried out on an acetone-chloroform-*d* solution as the complex was sparingly soluble in neat chloroform. The provided spectrum (Figure 4.5) contained the characteristic features of a mixed-bridged $\{Pt_2(\mu\text{-}S)(\mu\text{-}L)\}$ dimer, displaying two significantly separated resonances at δ 26.6 and 20.5 ppm, each with characteristic ^{195}Pt satellites. Estimated $^{1}J_{(PtP)}$ coupling constants were 2603 and 4447 Hz respectively. The much larger coupling was assigned to the phosphines *trans* to the μ_2-bromide ligand, which has a significantly weaker *trans* influence than the underivatised sulfide. In the complex $[Pt_2(\mu\text{-}Br)_2(PPh_3)_4][BF_4]_2$, $^{1}J_{(PtP)}$ was also large at 3747 Hz.[304] An impurity in the spectrum resonating at δ 13.7 ppm was tentatively identified as the mono-nuclear *cis*-$[PtBr_2(PPh_3)_2]$. The $^{1}J_{(PtP)}$ coupling constant of 3640 Hz is similar to that of 3614 Hz reported in the literature, although the chemical shift varies slightly from the reported 14.3 ppm, presumably due to solvent effects as the literature reference was collected in neat $CDCl_3$.[304] Both resonances of **16** appear as *pseudo* triplets suggesting the fluxionality of the $\{Pt_2(\mu\text{-}S)(\mu\text{-}Br)\}$

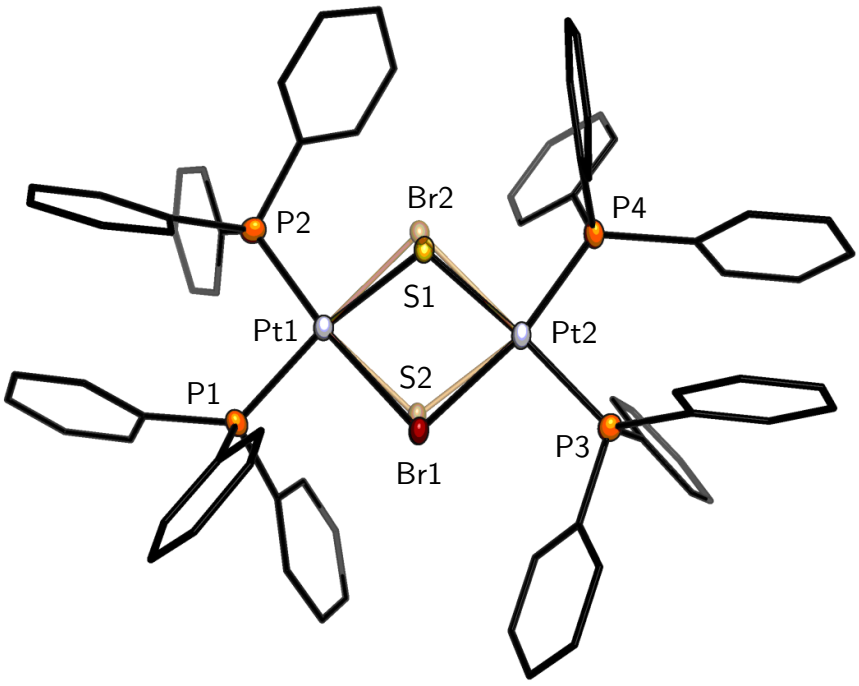

Figure 4.6: Crystal structure of **16**$[BPh_4]\cdot CH_3CN$. BPh_4^- anion and solvent have been omitted and phenyl rings of PPh_3 ligands are displayed as sticks for clarity. Disordered core atoms Br2 and S2 are shown with a reduced opacity. Thermal ellipsoids at 50% probability.

core is sufficiently slow such that magnetic resolution of $^{2}J_{(\mathrm{PP})}$ *cis* and $^{4}J_{(\mathrm{PP})}$ *cis* and *trans* couplings can occur.

Slow evaporation from an acetonitrile solution of **16**[BPh_4] produced orange prismatic crystals of sufficient quality for an X-ray diffraction experiment. The complex crystallises in the triclinic space group $P\bar{1}$ as the acetonitrile solvate. The presence of a single BPh_4^- anion confirms the monocationic charge of **16**. A positional disorder in the core of **16** was modelled, with the primary component having a refined occupation of approximately 77%. The Pt^{II} centers in **16** exhibit the expected square-planar geometry, with Pt1 slightly more ideal than Pt2 quantified by τ_4' parameters[141] of 0.09 and 0.13 respectively. The dihedral angle hinging the dimer is slightly puckered at 158.9(2)°, and the Pt-Pt separation is 3.544(1) Å consistent with a reasonably planar {Pt_2(μ-S)(μ-Br)} core. The Pt-Br bonds (Pt1-Br1 2.496(1) Å, Pt2-Br1 2.548(1) Å) are significantly longer than the Pt-S bonds (Pt1-S1 2.311(4) Å, Pt2-S1 2.312(5) Å). Accordingly, the P-Pt bonds *trans* to the underivatised sulfide (P2-Pt1 2.286(1) Å, P4-Pt2 2.307(1) Å) are longer than those *trans* to bromide

Table 4.1: Selected bond lengths (Å) and angles (°) for the crystal structure of **16**[BPh_4] · CH_3CN.

Pt1-Br1	2.4959(11)	S1-Pt1-Br1	83.69(11)
Pt1-S1	2.311(4)	S2-Pt1-Br2	82.1(3)
Pt1-Br2	2.595(5)	P1-Pt1-Br1	168.69(3)
Pt1-S2	2.350(12)	P1-Pt1-S1	85.07(11)
Pt1-P1	2.2559(8)	P1-Pt1-Br2	82.01(15)
Pt1-P2	2.2861(8)	P1-Pt1-S2	163.3(3)
Pt2-Br1	2.5489(9)	P1-Pt1-P2	99.71(3)
Pt2-S1	2.312(5)	P2-Pt1-Br1	91.56(3)
Pt2-Br2	2.497(6)	P2-Pt1-S1	175.02(12)
Pt2-S2	2.329(11)	P2-Pt1-Br2	172.87(16)
Pt2-P4	2.3069(8)	P2-Pt1-S2	96.7(3)
Pt2-P3	2.2534(8)	S1-Pt2-Br1	82.49(10)
S2-Pt2-Br2	84.7(3)	P3-Pt2-Br2	86.14(15)
P4-Pt2-Br1	85.18(3)	P3-Pt2-S2	169.3(3)
P4-Pt2-S1	163.80(13)	P3-Pt2-P4	101.47(3)
P4-Pt2-Br2	161.87(17)	Pt1-Br1-Pt2	89.28(2)
P4-Pt2-S2	88.9(3)	Pt1-S1-Pt2	100.16(12)
P3-Pt2-Br1	173.17(3)	Pt2-Br2-Pt1	88.22(14)
P3-Pt2-S1	91.24(11)	Pt2-S2-Pt1	98.5(4)

(P1-Pt1 2.256(1) Å, P3-Pt2 2.253(1) Å). Selected bonds and angles from the crystal structure of **16**$[BPh_4]\cdot CH_3CN$ are contained in Table 4.1.

It was serendipitously noticed that when **1a** was reacted with the hexafluorophosphate salt of *N*-methyl-2-chloropyridinium **14** and left to stand overnight, a red insoluble precipitate resulted. This was not the case for the methylsulfate or tetrafluoroborate salts of **14**, for which red methanolic solutions of **35** were found to be stable by ESIMS for a substantial amount of time (> 1 year) standing in ambient conditions. The red precipitate of **2**$[PF_6]_2$ dissolved very slowly into chloroform-*d* giving a deep red solution. $^{31}P\{^1H\}$-NMR of the dication was indicative of bridging ligands with significantly different *trans* influences and a moderately symmetrical arrangement about the $\{Pt_2(\mu\text{-}S)(\mu\text{-}SR)\}$ core (Figure 4.7). The more shielded δ 26.5 resonance was assigned as the phosphines *trans* to the underivatised sulfide due to the $^1J_{(PtP)}$ coupling constant of 2584 Hz. This is around the expected range of 2500 - 2700 Hz for triphenylphosphine *trans* to S^{2-}, and is substantially smaller than the $^1J_{(PtP)}$ coupling constant of 3756 Hz estimated for δ 24.9. The morphology of the resonances suggests a symmetrical conformation of the pyridinium ligand approxi-

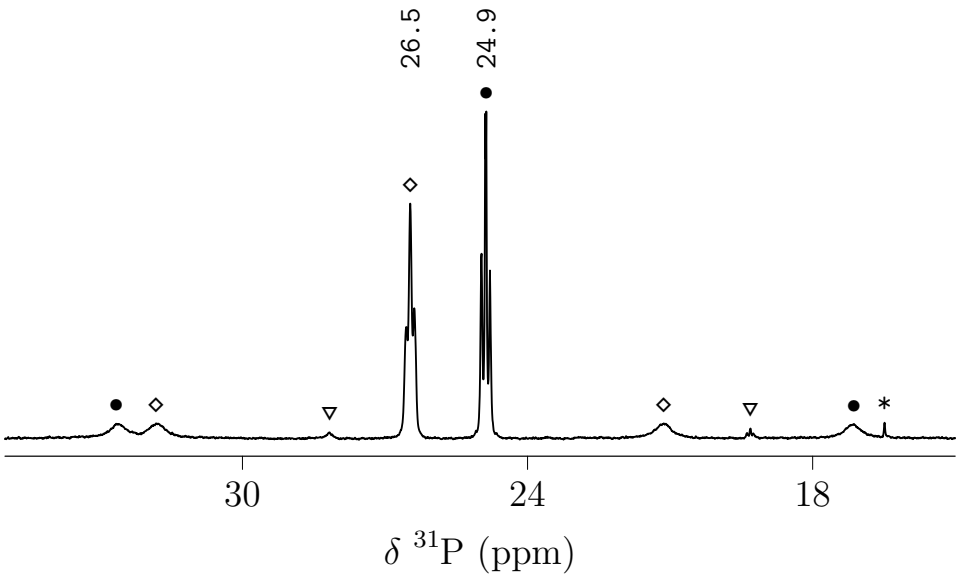

Figure 4.7: $^{31}P\{^1H\}$-NMR (242.95 MHz, $CDCl_3$) of **2**$[PF_6]_2$. The resonances marked ▽ at δ 28.2 and 19.3 ppm assigned as **33**. The resonance marked * is an unassigned impurity.

mating an ABX spin system, although the broadness of these resonances precludes estimation of any $^{n}J_{(PP)}$ couplings. The bridging chloride species **33** appears to be present as a trace impurity, evidenced by resonances at δ 28.1 and 19.3 ppm.

To further characterise **36**, a $^{195}Pt\{^{1}H\}$-NMR experiment was next carried out. The recorded spectrum has a single resonance at δ -4232 with the expected *doublet of doublet* multiplicity, and a close agreement with the $^{1}J_{(PtP)}$ coupling constants estimated in the $^{31}P\{^{1}H\}$-NMR spectrum ($^{1}J_{(PtP)}$ 2602, 3758 Hz). There appears to be a significant $^{2}J_{(PtPt)}$ coupling (≈ 1 kHz), however the broadness of the resonance (FWHM = 350 Hz) precludes meaningful estimation. The chemical shift observed for **2** is comparable to monoalkylated derivatives of **1a** examined in Chapter 2.

Clear red plates of **2**$[PF_6]_2$ of suitable quality for an X-ray diffraction experiment were obtained after slow evaporation of a dichloromethane solution. The com-

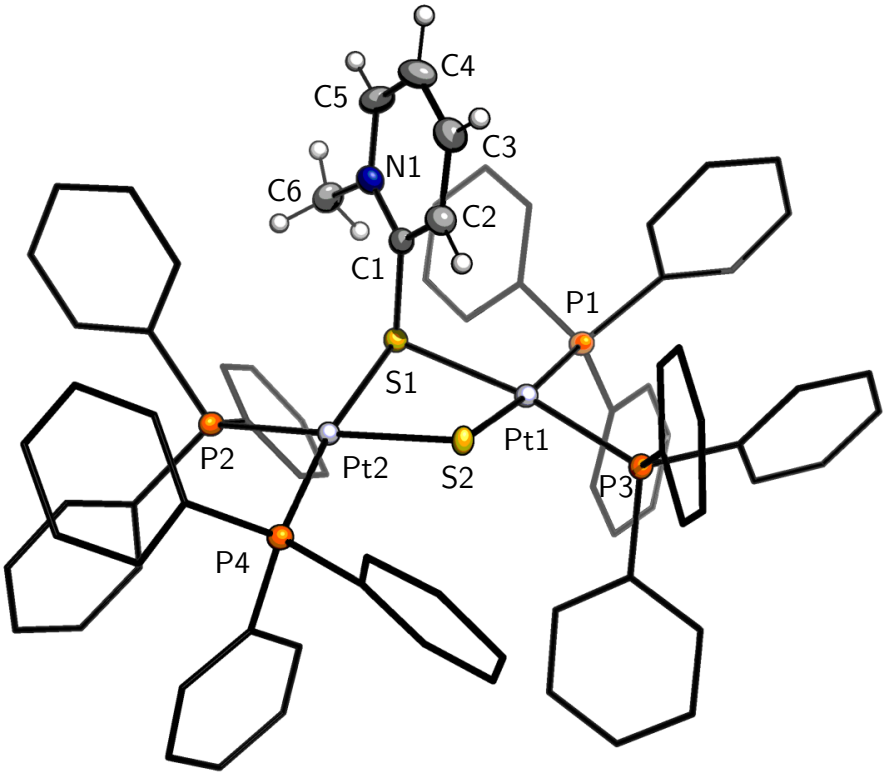

Figure 4.8: Crystal structure of **2**$[PF_6]_2 \cdot (CH_2Cl_2)_2$. The PF_6^- counterions and dichloromethane solvent have been omitted and phenyl rings of PPh_3 ligands represented as sticks for clarity. Thermal ellipsoids at 50% probability.

plex crystallises as the *bis*-dichloromethane solvate in the monoclinic space group $P2_1/c$, and has two independent PF_6 counterions present balancing the charge. Selected bond lengths and angles are in Table 4.2. The coordination geometry of the platinum(II) centers in **2** approach ideal square-planar geometry quantified by τ_4' parameters[141] of 0.13 and 0.12 for Pt1 and Pt2 respectively. The torsion Pt1-S1-S2-Pt2 of 150.04(5)° imparts a moderate hinge to the dimer, however the Pt-Pt separation is still moderately large at 3.418(1) ÅṪhe mercapto-pyridinium ligand is configured such that the plane of the ring is slightly deviating towards Pt1, approximated as 9.7(4)° by the S2-S1-C1-C2 torsion, and the methyl group of the mercapto-pyridinium ligand is facing away from the $\{Pt_2(\mu\text{-S})(\mu\text{-SR})\}$ core.

A brief search of the CSD for dinuclear Pt^{II} phosphine complexes bridged by an arylated thiol ligand[†] (μ-SAr) reveals an average S-C bond length of 1.792 Å. The S1-C1 bond of 1.773(5) Å in **2**, although slightly shorter, suggests the ligand

[†]CSD codes: LEZQAK, LEZQEO, NAZPIN, NUTMAQ, QUGHEG, TIXLUK, TIXMAR, TIXMEV, WOCDEZ, WOCDID, YILMIQ.

Table 4.2: Selected bond lengths (Å) and angles (°) for the crystal structure of $\mathbf{2}[PF_6]_2\cdot(CH_2Cl_2)_2$.

Pt1-P1	2.3002(11)	S2-Pt1-S1	82.81(4)
Pt1-P3	2.2813(11)	P2-Pt2-S1	90.40(4)
Pt1-S1	2.3909(11)	P4-Pt2-P2	97.08(4)
Pt1-S2	2.3263(10)	P4-Pt2-S1	171.50(4)
Pt2-P2	2.3218(11)	P4-Pt2-S2	89.47(4)
Pt2-S1	2.4069(10)	S2-Pt2-P2	171.83(4)
Pt2-P4	2.2693(11)	S2-Pt2-S1	82.75(4)
Pt2-S2	2.3127(10)	Pt2-S2-Pt1	94.92(4)
S1-C1	1.773(5)	Pt1-S1-Pt2	90.86(4)
C3-C2	1.381(7)	C1-S1-Pt1	101.77(16)
C3-C4	1.389(8)	C1-S1-Pt2	108.47(15)
C2-C1	1.398(7)	C2-C3-C4	118.6(5)
C5-C4	1.370(8)	C3-C2-C1	121.2(5)
C5-N1	1.355(7)	N1-C5-C4	121.2(5)
C6-N1	1.485(6)	C5-C4-C3	119.6(5)
N1-C1	1.365(6)	C5-N1-C6	117.2(4)
P1-Pt1-S1	94.98(4)	C5-N1-C1	121.2(4)
P1-Pt1-S2	174.49(4)	C1-N1-C6	121.6(4)
P3-Pt1-P1	97.14(4)	C2-C1-S1	124.7(4)
P3-Pt1-S1	167.67(4)	N1-C1-S1	117.2(4)
P3-Pt1-S2	85.31(4)	N1-C1-C2	118.1(4)

is coordinated in the zwitterionic thiol configuration. Additionally, the short N1-C1 and N1-C5 bonds of 1.365(6) and 1.354(6) Å and roughly equal C-C bonds in the pyridinium ring further suggest adoption of this form. As far as we are aware, this is the first crystallographic example of a 2-mercapto-*N*-alkylpyridinium ligand coordinated in a μ_2 arrangement. The Pt-S bonds for the mercapto ligand are substantially longer (Pt1-S1 2.391(1) Å, Pt2-S1 2.407(1) Å) than those of the underivatised sulfide (Pt1-S2 2.326(1) Å, Pt2-S2 2.313(1) Å). These bond distances are consistent with the observed $^{1}J_{(\mathrm{PtP})}$ coupling constants, and the assignment of the thiolato ligand having a very weak *trans* influence.

It was determined $[Pt_2(\mu\text{-S})(\mu\text{-Cl})(PPh_3)_4]^+$ **33** could not be synthesized directly from the mononuclear precursor *cis*-$[PtCl_2(PPh_3)_2]$ **37** and a half-molar equivalent of Na_2S, which instead gave only **1a** and unreacted **37** as observed by ESIMS. Thus moving forward, predominantly the aqueous methylsulfate solution and tetrafluoroborate salts of the **14** cation were employed, as these non-coordinating counterions did not effect immediate precipitation of cationic species in methanol solution (cf. tetraphenylborate and to a certain extent PF_6^-) and hence were able to be displaced by chosen counterions later in the synthetic work-up.

4.3 Thiol substitution

Various thiols (Figure 4.9) were subsequently explored as potential substitution candidates with **2** to give the corresponding derivatives as proposed in Scheme 4.1. Typically thiols were deprotonated with pyridine or triethylamine (TEA) prior to reaction with freshly prepared methanolic solutions of **2**.

ESIMS was employed as a screening tool to quickly examine micro-scale test reactions of thiols *N*-acetylcysteamine, 2-mercapto-1-methylimidazole, and 2-aminothiophenol with **2** which quickly revealed clean mass spectra containing single cations of the corresponding substituted derivative (Figure 4.10). These reactions were similarly successful when repeated macroscopically (as evidenced by ESIMS of the isolated solid), and the resulting derivatives $[Pt_2(\mu\text{-}S)(\mu\text{-}S{-}C_2H_4{-}NH{-}C(=O)CH_3)(PPh_3)_4]BF_4$ (**38**[BF_4]), $[Pt_2(\mu\text{-}S)(\mu\text{-}S{-}C_3H_2N_2{-}CH_3)(PPh_3)_4]$BETI (**17**[BETI]) and $[Pt_2(\mu\text{-}S)(\mu\text{-}S{-}C_6H_4NH_2)(PPh_3)_4]BF_4$ (**39**[BF_4]) were isolated respectively. Interestingly, fragmentation was observed in **17**[BETI] at a mild capillary exit voltage of 150V. Cations at *m/z* 1321.34 and 1059.20 resulting from the loss of one and two PPh_3 ligands were present at a relative intensity of 6 and 5% respectively. For comparison, the cations **38** and **39** did not undergo fragmentation unit a capillary voltage of 210V was employed.

Upon examination of these novel systems by $^{31}P\{^1H\}$-NMR, an unusual spectrum was recorded for **17**[BETI] in which four distinct resonances were present at δ 10.4, 14.3, 16.9, and 19.7 ppm (Figure 4.11). This was in contrast to both **38**[BF_4] and **39**[BF_4], for which the $^{31}P\{^1H\}$-NMR spectra each contained only two resonances,

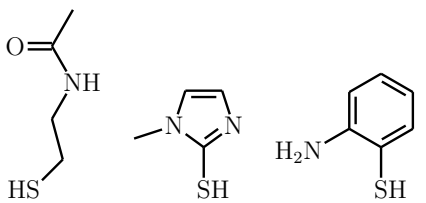

(a) **(b)** **(c)**

Figure 4.9: *N*-acetylcysteamine **(a)**, 2-mercapto-1-methylimidazole **(b)**, and 2-aminothiophenol **(c)**.

as is typical for mono-alkylated and -arylated derivatives of **1a** where there are two magnetically inequivalent sets of phosphines.

The unusual spectrum of **17** could be compared to that of $[Pt_2(\mu\text{-}S)(\mu\text{-}S{-}C_8H_8OH)(PPh_3)_4]$BETI **6**[BETI], the ring-opened styrene oxide derivate of **1a** characterised in Chapter 2, in which four separate resonances were observed for one of the isomers. In the case of **6**[BETI] however, the spectral window spanning the resonances was much narrower ($\Delta\nu \approx 2$ ppm cf. ≈ 10 ppm for **17**), and some resonances were well resolved multiplets such that ${}^{n}J_{(PP)}$ coupling constants could be estimated. These observed unique spectral features for **6**[BETI] were proposed to be a product of the increased steric strain imparted on the $\{Pt_2S_2\}$ core by the bulky thiolato ligand. In the spectrum of **17**, the significantly broader resonances and larger spectral window hint not necessarily at a ligand with steric bulk, rather at an unusual coordination geometry imparted by the mercapto-methylimidazole ligand. The resonances also appear at a much higher field than those of **6**[BETI] (δ 22 - 23

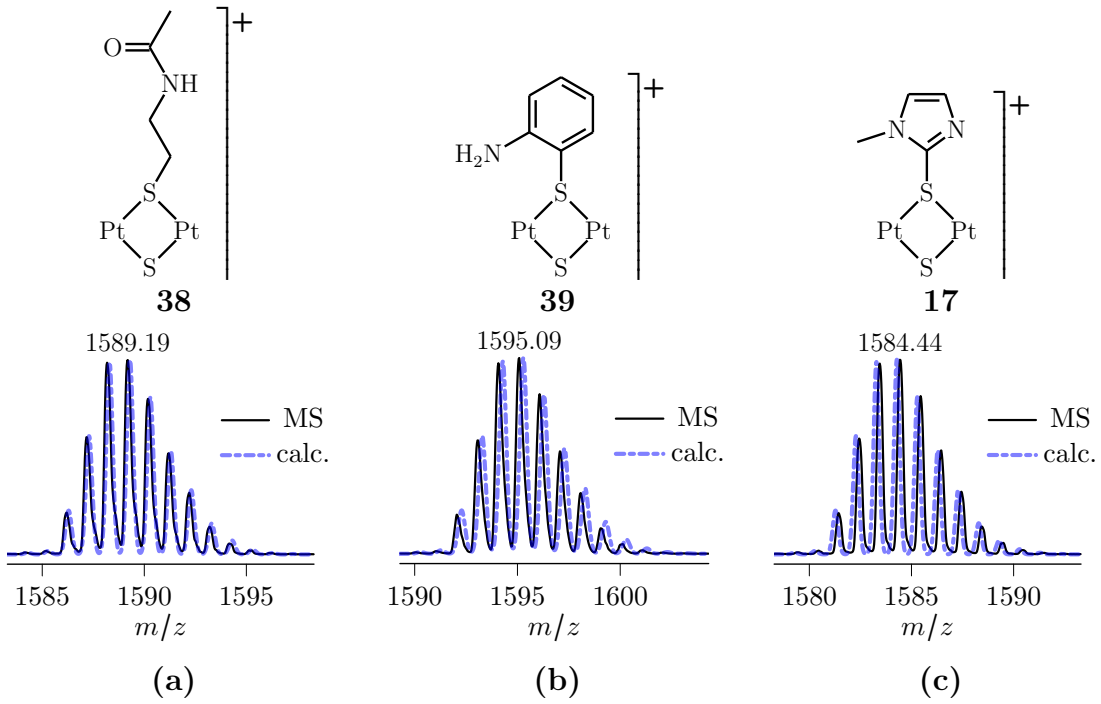

Figure 4.10: Isotope pattern comparisons of base peaks (ESIMS capillary exit voltage 60 V) from the reactions of **40** with **(a)** *N*-acetylcysteamine, **(b)** 2-aminothiophenol, and **(c)** 2-mercapto-1-methylimidazole with calculated patterns for **38**, **39**, and **17** respectively. Proposed structures for the cations are shown above, PPh_3 ligands omitted for clarity.

ppm), **38**[BF_4] (δ 25 ppm), or **39**[BF_4] (δ 27 and 29 ppm) indicating more shielded phosphines. The estimated $^1J_{(PtP)}$ coupling constants for **17**[BETI] are consistent with two phosphines *trans* to a bridging sulfide ligand (2633 and 2632 Hz) and two phosphines *trans* to a ligand with a much weaker *trans*-influence (3535 and 3645 Hz). The large discrepancy in the later pair of SSCCs is noteworthy, indicating ligands with moderately different *trans* influences, further hinting at an unusual coordination in the complex.

To compliment the $^{31}P\{^1H\}$-NMR spectroscopic data, a $^{195}Pt\{^1H\}$-NMR spectroscopy experiment was carried out on **17**[BETI] (Figure 4.12). The spectrum is quite unique for a derivative of **1a** in that the Pt^{II} centers appear to be in significantly different magnetic environments resonating at δ -4525 and -4727 ppm. As was observed with the $^{31}P\{^1H\}$-NMR resonances, these also appear at a higher field than resonances of mono-alkylated derivatives of **1a** (around δ -4200 - -4300 ppm). Both resonances exhibit *doublet-of-doublet* multiplicity with $^1J_{(PtP)}$ couplings agreeing closely with those estimated in the $^{31}P\{^1H\}$-NMR spectrum. The low field resonance δ -4525 appears to be slightly broader (FWHM 440 Hz cf. 420 Hz) and

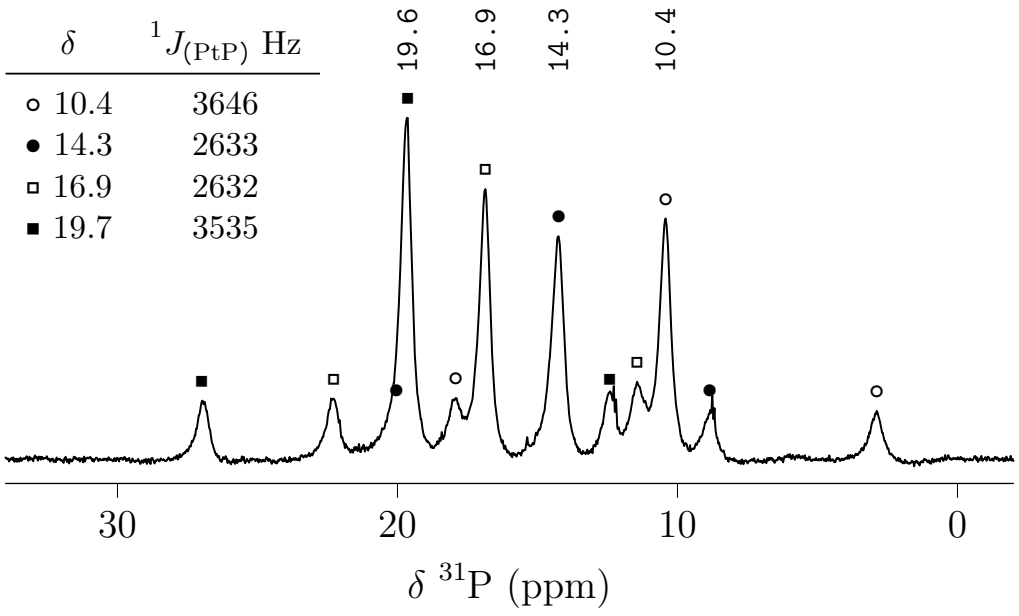

Figure 4.11: $^{31}P\{^1H\}$-NMR (242.95 MHz, $CDCl_3$) of [Pt_2(μ-S)(μ-S−$C_3H_2N_2$−CH_3)(PPh_3)$_4$]BETI **17**[BETI]. $^1J_{(PtP)}$ satellites are marked with the same symbol as the main resonance.

has estimated $^{1}J_{(\mathrm{PtP})}$ 2640 and 3648 Hz while δ -4727 has estimated $^{1}J_{(\mathrm{PtP})}$ 2649 and 3525 Hz. There appears to be no significant Pt-Pt coupling, evidenced by the absence of $^{2}J_{(\mathrm{PtPt})}$ satellites or significantly broadened bases of the multiplets, possibly indicating a large Pt-Pt separation. However, the base of each multiplet covers approximately 900 Hz, which is approximately the largest magnitude observed for $^{2}J_{(\mathrm{PtPt})}$ in derivatives of **1a** examined in Chapters 2 and 3.

The information provided by the ^{195}Pt{^{1}H}-NMR spectrum strongly suggests a transformation in the coordination arrangement has occurred in the {Pt_2(μ-S)-(μ-SR)} core upon the substitutive addition of 2-mercapto-1-methylimidazole to **2**. One possibility is an expansion to a 6-membered Pt-S-C-N-Pt-S heterocycle, with the mercapto-methylimidazole ligand S$^{\cap}$N coordinating across the Pt centers. The increased shielding observed in both ^{195}Pt{^{1}H}-NMR and ^{31}P{^{1}H}-NMR spectra is consistent with the formation of a heterocycle, and the significantly different $^{1}J_{(\mathrm{PtP})}$ coupling constants of 3648 and 3525 Hz are consistent with phosphines *trans* to N and SR^{-} respectively. The nitrogen of the methylimidazole would be expected to have a weaker *trans* influence than that of a thiolate. Additionally, the lower field

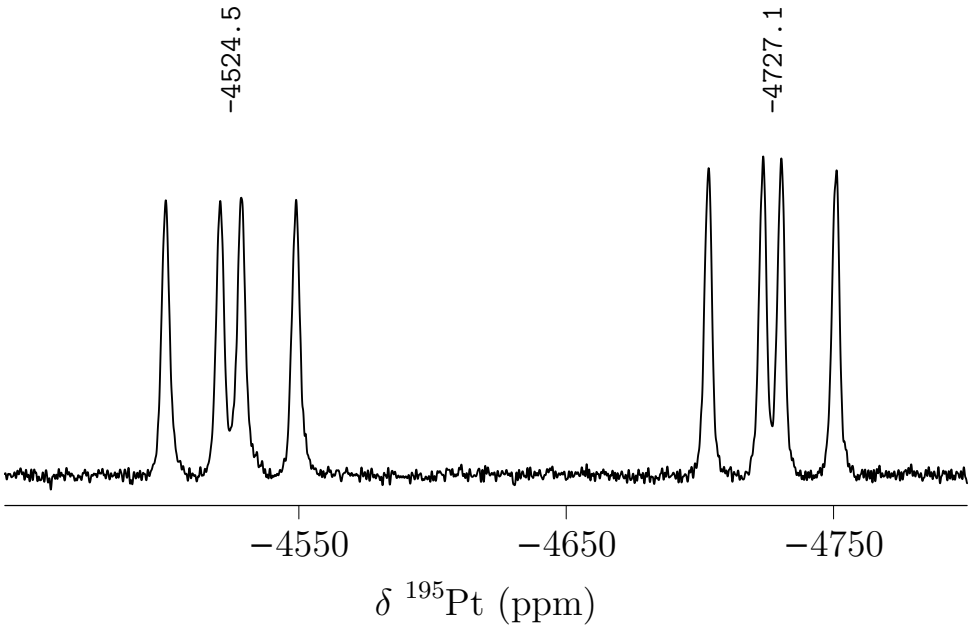

Figure 4.12: ^{195}Pt{^{1}H}-NMR (129.02 MHz, $CDCl_3$) spectrum of **17**[BETI].

resonance in the $^{195}Pt\{^{1}H\}$-NMR spectrum (δ -4525) appearing broader is consistent with coordination to a nitrogen, and could be a manifestation of quadrupolar coupling to ^{14}N.[305] ^{195}Pt chemical shifts are also known to be very sensitive to the bound ligands, and typcially Pt^{II} centers of composition P_2PtSN have been shown to resonate at a higher frequency than those of P_2PtS_2.[154,167]

To unambiguously characterise **17**[BETI], a single-crystal X-ray diffraction experiment was carried out on orange parallelepiped crystals grown from vapour diffusion of diethyl ether into a chloroform solution of the complex (Figure 4.13). **17**[BETI] crystallises in the triclinic space group $P\bar{1}$ with two independent molecules in the asymmetric unit. Upon closer inspection, the ASU molecular pair are non-superimposable mirror images. Although **17** has no formal stereocenter, chirality is

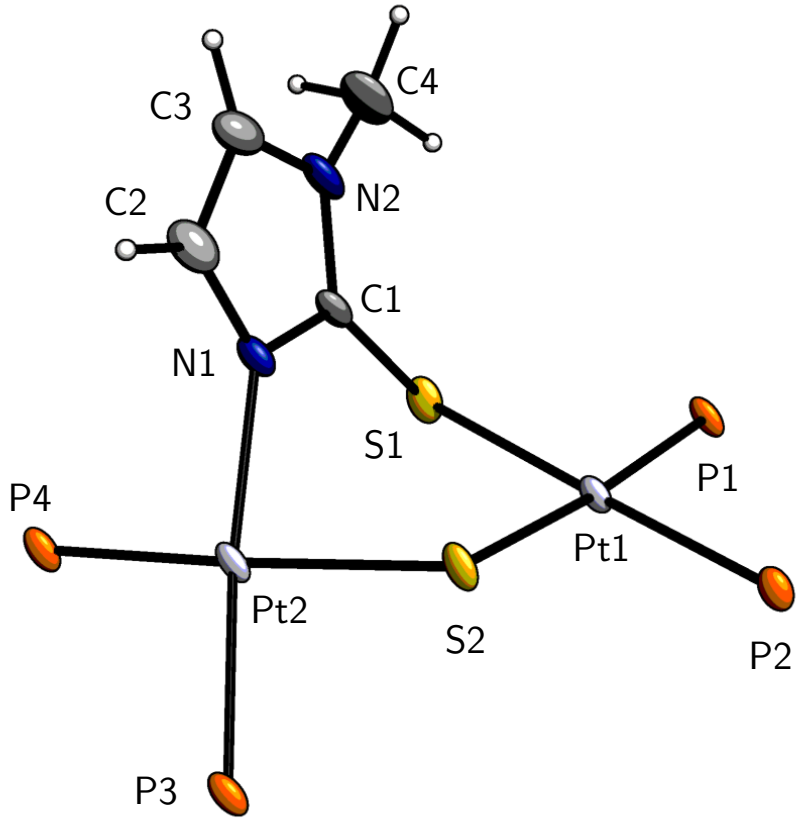

Figure 4.13: Crystal structure of **17**[BETI]. The BETI anion and phenyl rings of the PPh_3 ligands are omitted for clarity. Thermal ellipsoids displayed at 50% probability.

introduced when the 2-mercapto-1-methylimidazole ligand S$^{\cap}$N coordinates bridging the Pt^{II} centers modifying the molecular curvature of the 6-membered heterocycle. This type of chirality has been described as 'inherent' in the literature,[306,307] and has been used to describe systems such as substituted corannulenes.[308] Two independent molecules of the BETI anion cofirm the cationic charge of **17**. The asymmetry introduced by the coordination of 2-mercapto-1-methylimidazole and expansion to a 6-membered heterocycle results in twisting of the complex such that the least-squares plane composed of each square-planar platinum center reside at an angle of 123.54° for Pt1-Pt2 and 124.16° for Pt1A-Pt2A. The Pt-S-Pt angles for the underivatised sulfide ligand are now much more obtuse at 109.16(6)° for Pt1-S2-Pt2

Table 4.3: Selected bond lengths (Å) and angles (°) for the crystal structure of **17**[BETI].

Pt2-S2	2.3371(14)	P3-Pt2-S2	84.87(5)
Pt2A-S2A	2.3402(14)	P3A-Pt2A-S2A	84.93(5)
Pt2-P3	2.2675(15)	P3-Pt2-P4	99.33(5)
Pt2A-P3A	2.2637(15)	P3A-Pt2A-P4A	99.14(5)
Pt2-P4	2.2905(15)	P4-Pt2-S2	170.50(5)
Pt2A-P4A	2.3000(15)	P4A-Pt2A-S2A	171.56(5)
Pt2-N1	2.052(5)	N1-Pt2-S2	86.61(13)
Pt2A-N1A	2.042(4)	N1A-Pt2A-S2A	87.49(13)
Pt1-S2	2.3276(13)	N1-Pt2-P3	168.98(14)
Pt1A-S2A	2.3330(13)	N1A-Pt2A-P3A	170.02(13)
Pt1-P2	2.2882(14)	N1-Pt2-P4	90.14(13)
Pt1A-P2A	2.2736(15)	N1A-Pt2A-P4A	89.23(13)
Pt1-P1	2.3069(14)	S2-Pt1-S1	95.93(5)
Pt1A-P1A	2.3025(14)	S2A-Pt1A-S1A	95.10(5)
Pt1-S1	2.4000(14)	P2-Pt1-S2	83.62(5)
Pt1A-S1A	2.4069(15)	P2A-Pt1A-S2A	85.96(5)
S1-C1	1.727(6)	P2-Pt1-P1	99.08(5)
S1A-C1A	1.735(6)	P2A-Pt1A-P1A	97.46(5)
N1-C1	1.330(7)	P2-Pt1-S1	178.36(5)
N1A-C1A	1.325(7)	P2A-Pt1A-S1A	178.79(5)
N1-C2	1.376(7)	P1-Pt1-S2	175.76(5)
N1A-C2A	1.376(7)	P1A-Pt1A-S2A	175.89(5)
N2-C3	1.369(8)	P1-Pt1-S1	81.28(5)
N2A-C3A	1.362(7)	P1A-Pt1A-S1A	81.46(5)
N2-C1	1.359(7)	Pt1-S2-Pt2	109.15(6)
N2A-C1A	1.357(7)	Pt1A-S2A-Pt2A	110.46(6)
N2-C4	1.465(8)	C1-S1-Pt1	103.7(2)
N2A-C4A	1.452(8)	C1A-S1A-Pt1A	103.6(2)

and 110.46(6)° for Pt1A-S2A-Pt2A. The Pt-Pt separation is quite large compared to mono-alkylated derivatives of **1a** with a 4-membered ring (Figure 3.21), spanning 3.801(1) Å for Pt1-Pt2 and 3.838(1) Å for Pt1A-Pt2A. There is a significant difference in the square-planar coordination geometry for each platinum center, quantified by the τ_4' parameter[141] where ideal square-planar is 0 and ideal tetrahedral is 1. Pt1 and Pt1a (P_2PtS_2 coordination sphere) both have τ_4' parameters of 0.04 compared with 0.13 and 0.15 for Pt2 and Pt2A respectively (P_2PtSN coordination sphere). Selected bonds and angles for both independent molecules in the ASU are tabulated in Table 4.3, and mostly agree very closely such that only dimensions from one molecule will be discussed hereafter. The Pt-P distances for phosphines *trans* to S^{2-} are longer at 2.307(2) and 2.290(1) Å than those *trans* to N (2.267(2) Å) and SR (2.288(1) Å), consistent with the stronger *trans* influence exhibited by the underivatised sulfide. The Pt2-N1 distance of 2.052(5) Å is shorter than 15 structures

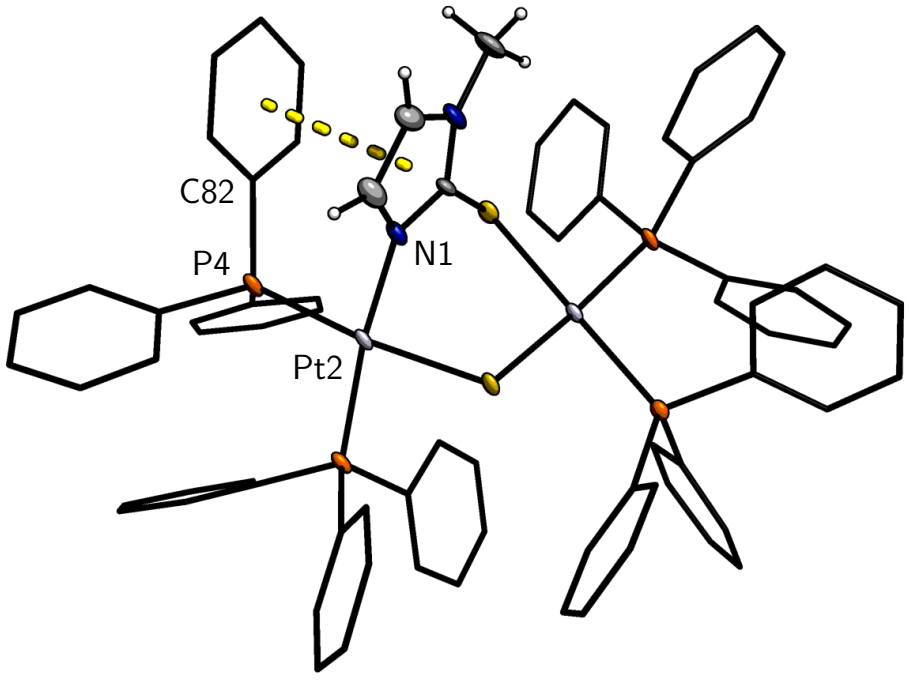

Figure 4.14: Crystal structure of **17**[BETI] showing the π-π interaction (dashed yellow line) between the methylimidazole ligand and a phenyl ring of the P4 PPh_3 ligand. BETI anion omitted and phenyl rings of PPh_3 ligands represented as sticks for clarity. Thermal ellipsiods shown at 50% probability.

from the CSD (mean 2.094 Å, σ 0.016 Å)[†] of square-planar Pt^{II} complexes with either a tertiary or cyclic amine ligand. The S1-C1 bond (1.728(6) Å) is significantly shorter than S-C bonds of arylated derivatives of **1a** (*see discussion* **2**$[PF_6]_2$ XRD, *vide supra*), but agrees nicely with 360 mercapto-imidazole structures in the CSD (mean 1.724 Å). There appears to be a significant π-π interaction between the imidazole ring and a phenyl ring of a PPh_3 ligand (Figure 4.14). The rings are nearly in stacked configuration with a centroid-centroid distance of 3.51 Å, well within the accepted range for such interactions,[309] and they are slightly tilted from parallel by 18.5°.

17 represents the first example of a Pt-S-C-N-Pt-S heterocycle in the literature, although many Pt^{II} complexes are known with 2-mercapto-1-methylimidazole as a terminal or bridging ligand.[310] A related Pd^{II} complex $[Pd_2(\mu_{NS}\text{-},\eta\text{-L})_2Cl_2(PMe_3)_2]$ (L = 2-mercapto-1-methylimidazole)[311] has been reported where two mercapto-imidazole ligands are S$^{\cap}$N coordinated resulting in an 8-membered Pd-S-C-N-Pd-S-C-N heterocycle. A similar Pt^{II} species has also been reported, although in more of a stacked conformation with a close Pt-Pt separation of 3.019(1) Å, and 2-mercapto-benzimidazole ligands.[312] The rapid and predictable nature of these substitution reactions of **2** with thiols are noteworthy, and are a strong candidate for further examination with additional thiols, phosphines, and other suitable nucleophiles.

[†]CSD codes: VIBXAG, ROBHOF, JAGMOX, JOGMIR, JAGMEN, JAGMAJ, JAGLUC, JAGLOW, JAGLAI, JAGKUB, HOSYEV, HOSYAR, FERQUR, EJAMAJ

4.4 Experimental

4.4.1 General

N-methyl-2-chloropyridinium tetrafluoroborate **14**[BF_4] was synthesised *via* alkylation of 2-chloropyridine (Sigma) by the BF_4 salt of trimethyloxonium (Sigma) following a procedure in the literature.[313,314] Similarly, **14**[CH_3SO_4] was synthesized by alkylating 2-chloropyridine with dimethylsulfate (Sigma) in petroleum spirits. 2-aminothiophenol, *N*-acetylcysteamine, and 2-mercapto-1-methylimidazole were obtained from Sigma. All reactions were carried out in ambient conditions. Reagent or laboratory grade solvents were used without purification.

4.4.2 Single crystal XRD experiments

Crystallographic data are tabulated in Table 4.4.

16[BPh_4]$\cdot CH_3CN$

X-ray diffraction data were collected at 99.9(4) K on a SuperNova Dual AtlasS2 diffractometer fitted with Cu Kα radiation (λ = 1.54184 Å). The intensity data were processed with the CrysAlis PRO[207] software suite and multi-scan empirical absorption corrections were applied using spherical harmonics, implemented in the SCALE3 ABSPACK scaling algorithm. The structure was solved with the SHELXT-2018/2 structure solution program[208] using intrinsic phasing and refined with full-matrix least-squares on F^2 using SHELXL-2018/3.[209] All non-hydrogen atoms were refined anisotropically, and C-bound hydrogen atoms were included using a riding model in calculated positions. A small void was treated with the SQUEEZE[214] routine of PLATON[215] to remove approximately 6 e from a volume of 50 $Å^3$ per formula unit. A positional disorder for the central bridging S and Br atoms was refined using the second free variable. A SIMU restraint was applied to these atoms to provide more reasonable temperature parameters as the atoms Br1, S2 and S1, Br2 were lying in very close proximity. Additionally, an EADP constraint was

applied to S2 to prevent the atom from going NPD in the final refinement cycles.

2$[PF_6]_2 \cdot (CH_2Cl_2)_2$

X-ray diffraction data were collected on a Rigaku Oxford Diffraction XtaLAB-Synergy-S single crystal diffractometer with a PILATUS 200 K hybrid pixel array detector using Cu Kα radiation (λ = 1.54184 Å) at 111.04(11) K. The intensity data were processed with the CrysAlis PRO[207] software suite and multi-scan empirical absorption corrections were applied using spherical harmonics, implemented in the SCALE3 ABSPACK scaling algorithm. The structure was solved with the SHELXT-2018/2 structure solution program[208] using intrinsic phasing and refined with full-matrix least-squares on F^2 using SHELXL-2018/3.[209] All non-hydrogen atoms were refined anisotropically and hydrogen atoms included in calculated positions using a riding model. A positional disorder in a dichloromethane solvent molecule was modeled using the second free variable, and hydrogen atoms were omitted. A large peak in the difference map (5.2 e $\cdot$ Å^{-3}) was located 1.16 Å from Pt1 and treated as spurious electron density.

17[BETI]

X-ray diffraction data were collected at 120 K on a Bruker APEX-II CCD diffractometer[211] using Mo Kα radiation (λ = 0.71073 Å) using a combination of ω- and φ-scans of 0.5°. Multi-scan empirical absorption corrections were applied using SADABS[212] (Bruker 2016). The structure was solved with the SHELXT-2018/2 structure solution program[208] using intrinsic phasing and refined with full-matrix least-squares on F^2 using SHELXL-2018/3.[209] All non-hydrogen atoms were refined anisotropically and hydrogen atoms included in calculated positions using a riding model. After the refinement was finished, several peaks in the difference map of around 3-4 e $\cdot$ Å^{-3} remained, all within 1 Å from Pt centers, and were treated as spurious electron density.

4.4.3 Synthesis

N-methyl-2-chloropyridinium[BF_4] (**14**[BF_4])

To a suspension of trimethyloxonium tetrafluoroborate (0.88 g, 5.96×10^{-3} mol) in dichloromethane (50 mL) was added 2-chloropyridine (0.72 g, 6.34×10^{-3} mol) and the mixture stirred at room temperature for 24 hours. Methanol (5 mL) was added and the clear colorless solution stirred for 10 minutes before removing the solvent under vacuum. The resulting white crystalline material was washed with petroleum spirits and dried under vacuum to give a white powder (1.23 g, 96%). ESIMS (positive ion) *m/z* 128.05, 100%. ^{1}H-NMR (600 MHz, CD_3OD): δ 9.01 [dd, 1H, $^3J_{(HH)}$ 6.1, $^4J_{(HH)}$ 1.4 Hz], 8.54 [td, 1H, $^3J_{(HH)}$ 8, $^4J_{(HH)}$ 1.6 Hz], 8.25 [dd, 1H, $^3J_{(HH)}$ 8.2, $^4J_{(HH)}$ 1 Hz], 8.00 [m, 1H], 4.40 [s, 3H]. ^{13}C-NMR (150.91 MHz, CD_3OD): δ 149.1, 148.1, 130.8, 127.2, 48.0.

2-chloro-*N*-methylpyridinium methylsulfate **14**[CH_3SO_4]

To a clear colorless solution of dimethyl sulfate (2.20 mL, 2.93 g, 2.32×10^{-2} mol) in pet. spirits (20 mL) was added 2-chloropyridine (4.40 mL, 5.28 g, 4.65×10^{-2} mol). The resulting clear colorless solution was refluxed for 9 hours while stirring. After allowing to cool and sit, a translucent white solid formed. The solvent was decanted and the waxy translucent white solid crushed before the addition of diethyl ether (50 mL). The suspension was stirred for 30 minutes with gentle heating before decanting diethylether and left to sit uncovered. Distilled H_2O (50 mL) was then added to the white translucent solid, quickly dissolving the solid and resulting in a clear colorless solution. An addition 20 mL of diethyl ether was then added and the resulting mixture stirred vigorously for 30 minutes before the collection of the aqueous layer, around 50 mL. ESIMS (positive ion) *m/z* 128.08, 100%.

Synthesis of BPh_4^- and PF_6^- salts

Metathesis reactions of an aqueous solution of **14**[CH_3SO_4] with $NaBPh_4$ or NH_4PF_6 resulted in immediate precipitation of the respective salt as a white solid. ESIMS (positive ion) *m/z* 128.06, 100%.

General preparation of $[Pt_2(\mu\text{-}S)(\mu\text{-}S{-}C_6H_7N)(PPh_3)_4][X]_2$ (**2**$[X]_2$)

To a stirred suspension of $[Pt_2(\mu\text{-}S)_2(PPh_3)_4]$ **1a** in methanol a slight molar excess of *N*-methyl-2-chloropyridinium[X] **14**[X] (X = BF_4, PF_6, CH_3SO_4) was added and the mixture stirred for 15 minutes giving a clear read solution. ESIMS: (positive ion) *m/z* 797.89 $[M]^{2+}$ 100.0%, *m/z* 1505.80 $[Pt_2(\mu\text{-}S)(\mu\text{-}Cl)(PPh_3)_4]^+$ 35.4%, *m/z* 1681.8 $[M + BF_4]^+$ 8.6%. $^{31}P\{^1H\}$-NMR (242.95 MHz, methanol) 26.3 [m, $^1J_{(PtP)}$ 2590 Hz], 24.3 [m, $^1J_{(PtP)}$ 3750 Hz].

Synthesis of $[Pt_2(\mu\text{-}S)(\mu\text{-}Br)(PPh_3)_4]BPh_4$ (**16**$[BPh_4]$)

To a clear red solution of **2**[CH3SO4]2 (**1a** 111.8 mg, 7.44×10^{-2} mmol, work-up as described section 4.4.3) in methanol (25 mL) was added a large excess of lithium bromide (60 mg, 6.91×10^{-1} mmol) while stirring at ambient conditions resulting in a pink-orange solution. After 5 minutes sodium tetraphenylborate (29 mg, 8.47×10^{-2} mmol) immediately effecting a pink-orange precipitate which was collected by vacuum filtration on a glass sintered frit and washed successively with distilled H_2O (2 x 20 mL), ethanol (1 x 10 mL) and diethyl ether (1 x 10 mL) before drying under vacuum to give **16**[BPh4] as a pink-orange solid (117.8 mg, 85%). Deep red-orange crystals suitable for XRD were acquired from slow evaporation of an acetonitrile solution. *Anal.* Found: C, 60.93; H, 4.46%. $C_{96}H_{80}BBrP_4Pt_2S$ requires: C, 61.64; H, 4.31%. ESIMS (positive ion) *m/z* 1551, $[M]^+$ 100%; *m/z* 1506, $[Pt_2(\mu\text{-}S)(\mu\text{-}Cl)(PPh_3)_4]^+$ 5%. $^{31}P\{^1H\}$-NMR (242.95 MHz, acetone/$CDCl_3$): δ 26.6 [m, $^1J_{(PtP)}$ *trans* S^{2-} 2603 Hz], 20.5 [m, $^1J_{(PtP)}$ *trans* Br^- 4447 Hz].

Synthesis of $[Pt_2(\mu\text{-}S)(\mu\text{-}S{-}C_6H_7N)(PPh_3)_4][PF_6]_2$ (**2**$[PF_6]_2$)

A clear red solution of **2**[PF6]2 (**1a** 155 mg, 1.03×10^{-1} mmol, work-up section 4.4.3) in methanol (30 mL) was stirred for 12 hours in ambient conditions resulting in the formation of an insoluble red precipitate which was collected by vacuum filtration and washed successively with distilled H_2O (3 x 20 mL), ethanol (1 x 5 mL), and diethyl ether (5 mL) before drying under vacuum to give a red powder (163 mg,

84%). Slow evaporation of a dichloromethane solution provided suitable crystals for an XRD experiment. *Anal.* Found: C, 49.69; H, 3.62; N, 0.93%. $C_{78}H_{67}NP_6Pt_2S_2$ requires: C, 49.66; H, 3.58; N, 0.74%. $^{31}P\{^1H\}$-NMR (242.95 MHz, $CDCl_3$) 26.5 [m, $^1J_{(PtP)}$ *trans* S^{2-} 2584], 24.9 [m, $^1J_{(PtP)}$ *trans* S−pyr 3756 Hz]. $^{195}Pt\{^1H\}$-NMR -4232 [dd, br, $^1J_{(PtP)}$ 2602, 3758 Hz].

Synthesis of $[Pt_2(\mu\text{-}S)(S{-}C_3H_2N_2CH_3)(PPh_3)_4]$BETI (**17**[BETI])

To a stirred clear red solution of **2**[CH3SO4]2 (**1a** 98.9 mg, $6.58{\times}10^{-2}$ mmol, work-up section 4.4.3) in methanol (25 mL) was added TEA (0.05 mL) before 2-mercapto-1-methylimidazole (23.9 mg, $2.09{\times}10^{-1}$ mmol) resulting in a clear orange solution. After 15 minutes, lithium bis(pentafluoroethanesulfonyl)imide (Li[BETI], 323 mg, $8.50{\times}10^{-1}$ mmol) was added and the resulting solution stirred for 20 minutes before precipitation of a yellow-orange solid was induced by the addition of distilled H_2O (10 mL). The precipitate was collected by vacuum filtration and washed successively with distilled H_2O (2 x 20 mL) and diethyl ether (1 x 10 mL) before drying under vacuum to give a fine yellow-orange solid (99 mg, 77%). Orange parallelepiped crystals of **17**[BETI] were grown from vapour diffusion of diethyl ether into a chloroform solution of the salt. *Anal.* Found: C, 48.32; H, 3.28; N, 2.23%. $C_{80}H_{63}F_{10}N_3O_4Pt_2S_4$ requires: C, 48.91; H, 3.33; N, 2.14%. ESIMS (positive ion) *m/z* 1584.44, $[M]^+$ 100%; *m/z* 792.74, $[M+H]^{2+}$ 16%; *m/z* 1965.44, $[M+H+BETI]^+$ 7%. $^{31}P\{^1H\}$-NMR (242.95 MHz, $CDCl_3$): δ 19.7 [s, br, $^1J_{(PtP)}$ *trans* S−R^- 3535], 16.9 [s, br, $^1J_{(PtP)}$ *trans* S^{2-} 2632], 14.3 [s, br, $^1J_{(PtP)}$ *trans* S^{2-} 2633], 10.4 [s, br, $^1J_{(PtP)}$ *trans* N 3646 Hz]. $^{195}Pt\{^1H\}$-NMR (129.02 MHz, $CDCl_3$): δ -4524 [dd, br, $^1J_{(PtP)}$ 2640, 3648], -4727 [dd, br, $^1J_{(PtP)}$ 2649, 3525 Hz].

Synthesis of $[Pt_2(\mu\text{-}S)(\mu\text{-}S{-}C_6H_4NH_2)(PPh_3)_4]BF_4$ (**39**[BF_4])

To a clear red solution of **2**[BF4]2 (**1a** 107.5 mg, $7.15{\times}10^{-2}$ mmol, work-up section 4.4.3) in methanol (20 mL) was added TEA (0.05) and 2-aminothiophenol (9.5 mg, $7.59{\times}10^{-1}$ mmol) while stirring at ambient conditions immediately resulting in

a yellow clear solution. After additional stirring for 2 hours, sodium tetrafluoroborate (50 mg, 4.55×10^{-1} mmol) and distilled H_2O (10 mL) were added effecting a yellow precipitate which was collected by vacuum filtration and washed successively with distilled H_2O (2 x 20 mL) and diethyl ether (1 x 5 mL) before drying under vacuum to give a yellow solid (85 mg, 71%). Suitable crystals for an XRD experiment were obtained by vapour diffusion of diethyl ether into a chloroform solution. *Anal.* Found: C, 55.69; H, 3.67; N, 1.01%. $C_{78}H_{66}BF_4NP_4Pt_2S_2$ requires: C, 55.69; H, 3.95; N, 0.83%. ESIMS (positive ion) *m/z* 1595.09, $[M]^+$ 100%. $^{31}P\{^1H\}$-NMR (242.95 MHz, $CDCl_3$): δ 29.2 [m, $^1J_{(PtP)}$ *trans* S^{2-} 2678], 26.7 [m, $^1J_{(PtP)}$ *trans* SR^- 3233 Hz].

Synthesis of $[Pt_2(\mu\text{-}S)(\mu\text{-}S{-}CH_2CH_2NHC(=O)CH_3)(PPh_3)_4]BF_4$ (**38**$[BF_4]$)

To a clear red solution of **2**[BF4]2 (**1a** 96.2 mg, 6.40×10^{-2} mmol, work-up section 4.4.3) in methanol (20 mL) was added TEA (0.05 mL) and *N*-acetylcysteamine (ρ = 1.21 g $\cdot$ mol^{-1}, 0.01 mL, 11.2 mg, 9.40×10^{-2} mmol) while stirring at ambient conditions resulting in a bright-yellow clear solution. After 30 minutes, sodium tetrafluoroborate (60 mg, 5.46×10^{1} mmol) and distilled H_2O (10 mL) was added and the resulting yellow precipitate collected by vacuum filtration, washed successively with distilled H_2O (2 x 20 mL) and diethyl ether (1 x 10 mL), and dried under vacuum to give a yellow solid (68 mg, 63%). XRD quality crystals were obtained from diffusion of diethyl ether into a chloroform solution. *Anal.* Found: C, 54.11; H, 4.16; N, 0.96%. $C_{76}H_{68}BF_4NOP_4Pt_2S_2$ requires: C, 54.45; H, 4.09; N, 0.84%. ^{1}H-NMR (600.17 MHz, $CDCl_3$): δ 7.38-7.05 [aromatic], 6.40 [t, br, NH, $^3J_{(HH)}$ 6.2 Hz], 2.86 [m, 2H], 2.17 [m, br, 2H], 1.84 [s, br, CH_3]. ^{13}C-NMR (150.91 MHz, $CDCl_3$): δ 170.0, 134.8-127.7 [aromatic], 40.7, 39.2, 23.3. $^{31}P\{^1H\}$-NMR (242.95 MHz, $CDCl_3$): δ 25.4 [m, br, $^1J_{(PtP)}$ *trans* SR^- 3276], 25.0 [m, br, $^1J_{(PtP)}$ 2599 Hz]. $^{195}Pt\{^1H\}$-NMR (129.02 MHz, $CDCl_3$): δ -4369 [dd, $^1J_{(PtP)}$ 2601, 3279, $^2J_{(PtPt)}$ 932 Hz].

Table 4.4: Crystallographic data.

	16$[BPh_4] \cdot CH_3CN$	**2**$[PF_6]_2 \cdot 2\,CH_2Cl_2$	**17**[BETI]
Empirical formula	$C_{98}H_{83}BBrNP_4Pt_2S$	$C_{80}H_{69}Cl_4F_{12}NP_6Pt_2S_2$	$C_{80}H_{65}F_{10}N_3O_4P_4Pt_2S_4$
M_r $(g \cdot mol^{-1})$	1911.49	2054.28	1964.65
Crystal size (mm)	0.1 x 0.08 x 0.04	0.12 x 0.10 x 0.04	0.26 x 0.15 x 0.15
Crystal system	triclinic	monoclinic	triclinic
Space group	$P\bar{1}$	$P2_1/c$	$P\bar{1}$
a (Å)	15.1192(3)	21.88060(13)	17.2214(19)
b (Å)	16.8920(4)	12.75254(9)	17.499(2)
c (Å)	17.7172(4)	28.3426(2)	27.876(3)
α (°)	109.762(2)	90	108.032(2)
β (°)	102.421(2)	96.2985(6)	95.491(2)
γ (°)	99.151(2)	90	107.680(2)
V $(Å^3)$	4025.41(17)	7860.80(9)	7441.9(14)
Z	2	4	4
ρ_{calc} $(g \cdot cm^{-3})$	1.577	1.736	1.754
$\mu(CuK_\alpha)$ (mm^{-1})	8.355	10.094	4.033
$F(000)$	1900.0	4040.0	3872.0
2θ range (°)	7.008 to 147.888	7.092 to 144.868	1.572 to 56.838
Reflections collected/unique	44005/15794	63261/15020	142088/37163
R_{int}	0.0435	0.0449	0.0796
Data/parameters/restraints	15794/987/12	15020/970/0	37163/1929/0
Goodness-of-fit on F^2	1.021	1.094	1.032
Final R indices $[I > 2\sigma(I)]$	$R_1 = 0.0292, wR_2 = 0.0672$	$R_1 = 0.0367, wR_2 = 0.0880$	$R_1 = 0.0463, wR_2 = 0.1055$
R indices (all data)	$R_1 = 0.0388, wR_2 = 0.0711$	$R_1 = 0.0399, wR_2 = 0.0894$	$R_1 = 0.0773, wR_2 = 0.1227$
T_{min}/T_{max}	0.444/1.000	0.480/1.000	0.587/0.746
ρ_{max}/ρ_{min} $(e \cdot Å^{-3})$	1.14/-1.20	5.15/-1.39	3.98/-1.96

Chapter 5

Synthesis of mixed-bridged chalcogenide complexes

5.1 Introduction

The propensity for the dicationic μ-thiolato-pyridinium complex $[Pt_2(\mu\text{-}S)(\mu\text{-}S{-}C_6H_7N)(PPh_3)_4]^{2+}$ **2** to engage in substitution reactions with suitable thiols has been thoroughly explored in the previous chapter. Employing **2** in accessing chalcogenide mixed-bridged complexes of the type $[Pt_2(\mu\text{-}S)(\mu\text{-}E{-}R)(PPh_3)_4]$ (E = Se, Te) was next investigated as, if successful, would open up a novel and predictable route towards accessing these rare systems (Scheme 5.1). Of the few reported dinuclear Pt^{II} complexes with mixed-chalcogen bridging ligands in the literature are *trans*-

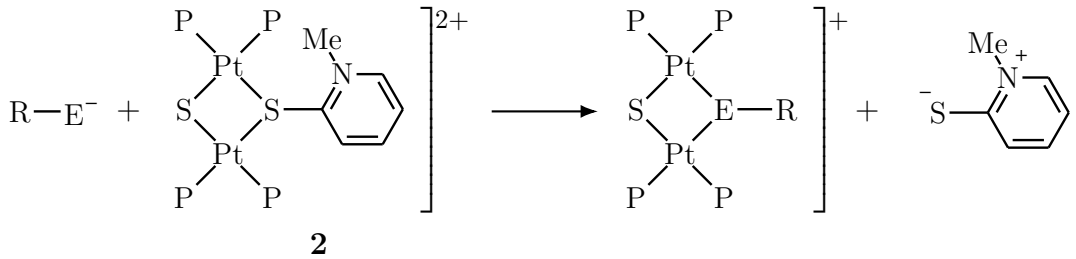

Scheme 5.1: Proposed substitution reaction of $[Pt_2(\mu\text{-}S)(\mu\text{-}SR)(PPh_3)_4]^+$ **2** and chalcogenolate anion $R{-}E^-$ resulting in a mixed-bridged derivative (E = Se, Te).

$[(PPr^n_3)_2Pt_2Cl_2(\mu\text{-}S{-}Bu^t)(\mu\text{-}Se{-}Bz)]$ **41**,[315] trimetallic aggregate $[(Ph_3PPt)_3(\mu\text{-}S{-}CH_3)_3(\mu_3\text{-}Se)]^+$ **42**,[238] and from our previous work[78] $[Pt_2(\mu\text{-}S)(\mu\text{-}Se)(PPh_3)_4]$ **23** and a series of mixed-bridged di- and tri-nuclear species. These are the mono-arylated series $[Pt_2(\mu\text{-}E^1)(\mu\text{-}E^2{-}Ar)(PPh_3)_4]^+$ **43** ($E^1 \neq E^2$ = S, Se; Ar = Ph *or* E^1 = S, E^2 = Te; Ar = Ph, C_6H_4OEt) and trimetallic aggregates $[(Ph_3PPt)_3(\mu\text{-}E^1{-}Ar)_3(\mu_3\text{-}E^2)]^+$ **44** (E^1Ar, E^2 = TePh, Se (**44a**); TeC_6H_4OEt, Se (**44b**); SePh, S (**44c**); TeC_6H_4OEt, S (**44d**)). The propensity of the heavier chalcogens to form multinuclear aggregates precluded the isolation of any mixed-bridged dinuclear systems, the only isolated species being $[(Ph_3PPt)_3(\mu\text{-}TePh)_3(\mu_3\text{-}Se)]^+$ **44a**, which was structurally characterised.[78]

In the course of exploring substitution reactions of **2** with various thioureas in the previous chapter, it was observed some disubstituted derivatives such as *N*-phenyl-*N'*-ethylmethoxy and *N*-phenyl-*N'*-methylthiourea resulted in regenerating starting complex $[Pt_2(\mu\text{-}S)_2(PPh_3)_4]$ **1a** when reacted with **2**. Indeed desulfurisation of thiourea is well known and has been exploited in various reactions, for example in the synthesis of episulfides.[316] More specifically, activation of the S−C bond in disubstituted thioureas have been observed upon coordination of diphenylthiourea in forming ruthenium clusters[317] and in the condensation of mononuclear palla-

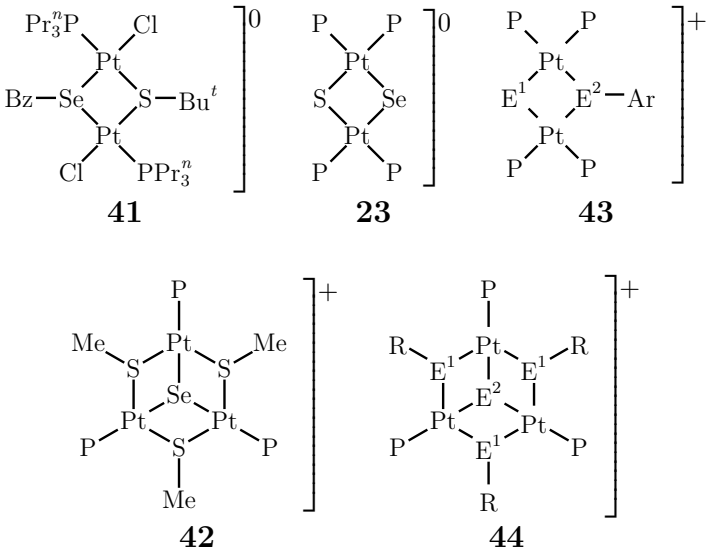

Figure 5.1: Mixed-bridged complexes from the literature. P = PPh_3, E = chalcogenide atoms.

dium(II)[318] and platinum(II)[106] species into dinuclear μ-S bridged complexes [Pd_2-(μ-S)(μ-dppm)$_2$(Tu)$_2$] (Tu = *N*,*N*′-*o*-tolylthiourea) and [Pt_2(μ-S)(μ-S−C(O)NMe_2)-(PPh_3)$_4$]BPh_4 (tetramethylthiourea in refluxing methanol) respectively.

The literature on selenoureas is scant in comparison to the sulfur analogue, due in part to more difficult preparations and instability of the resulting compounds.[319,320] The longer Se=C and shorter N−C bonds[321] of selenourea (cf. thiourea), consistent in various selenourea derivatives,[322] suggest a similar propensity for N lone pair delocalisation conferring resonance stability to the selenol zwitterion.[323] Hence, substitution reactions with dinuclear **2** akin to those observed for various thiolates are possible. Coordination may also similarly effect Se=C activation, resulting in the mixed-bridged [Pt_2(μ-S)(μ-E)(PPh_3)$_4$]$^+$ **23**. To complement selenourea, substitution reactions of **2** with aryl selenolates and tellurolates prepared from the corresponding diaryl dichalcogenides will also be examined. Reducing agents like sodium borohydride[324] and hydrazine hydrate[325] are typically employed to prepare the anions *in situ*. A substitution reaction with any such ArE^- species and **2** would be expected to proceed as rapidly and predictably as a thiolate, with the additional tractability conferred by a cationic derivative. That is to say, unlike the neutral mixed-bridge **23** which would most likely suffer similar solubility issues as **1a** and **1b**, hampering full characterisation.

5.2 Selenourea

Selenourea is known to coordinate to Pt^{II} as both a neutral terminal[326,327] and Se$^{\cap}$N bidentate dianionic[328] ligand, the latter being quite rare evidenced by one reported structure in the literature. Accordingly, there are no reported Pt^{II} dimers with monoanionc or neutral selenourea coordinated as a bridging ligand. The only similar structures in the literature are neutral *N*,*N*′-dimethylselenourea (dmsu) bridging two mononuclear platinum(II) fragments [{(dmsu)PtX_2}$_2$(μ-dmsu)] (X = Cl, Br), which were tentatively identified by TGA, IR, and ^{1}H-NMR.[329]

With the goal of generating a mixed-bridged complex with a mono-anionc selenourea $[Pt_2(\mu\text{-S})(\mu\text{-Se}{-}C(=NH)NH_2)(PPh_3)_4]^+$, or, in the case of Se−C activation, $[Pt_2(\mu\text{-S})(\mu\text{-Se})(PPh_3)_4]$ (**23**), a micro-scale reaction between a solution of **2** in methanol with a catalytic amount of triethylamine (TEA) and selenourea was carried out. Examination of the reaction by ESIMS after 5 minutes gave the spectrum in Figure 5.2. Along with several ions of lower relative intensity, the base peak at *m/z* 1551.04 was assigned as the mixed-bridged **23** + H^+, and has a close

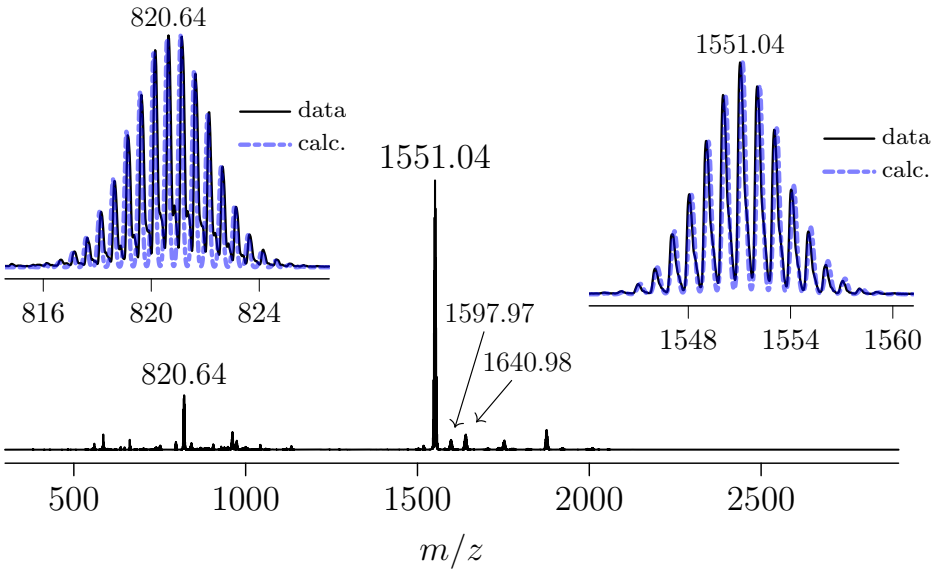

Figure 5.2: ESI mass spectrum of **2** and selenourea in methanol after 5 minutes, capillary exit voltage 60 V. The insets are comparisons of the peaks observed at *m/z* 820 and 1551 with calculated isotope patterns for $[Pt_2(\mu\text{-Se})(\mu\text{-Se}{-}CN_2H_4)(PPh_3)_4]^{2+}$ (calc. *m/z* 820.58) and $[Pt_2(\mu\text{-S})(\mu\text{-Se})(PPh_3)_4] + H^+$ (calc. *m/z* 1551.19) respectively.

agreement with a calculated isotope pattern for the proposed species. Interestingly, the bridging selenide parent complex **1b** was assigned to a peak observed at *m/z* 1597.97. More evidence of Se−C bond activation in the selenourea was found in the proposed cation/dication species $[Pt_2(\mu\text{-Se})(\mu\text{-Se}{-}C(=NH)NH_2)(PPh_3)_4]^+$ **45a** and $[Pt_2(\mu\text{-Se})(\mu\text{-Se}{=}C(NH_2)_2)(PPh_3)_4]^{2+}$ **45b** at *m/z* 1640.98 and 820.64 respectively. A neutral bridging selenone has been assigned to the latter species, although it is quite possibly coordinated in a monoanionic form viz. **45a** + H^+. Tentative evidence to the contrary was found in identification of the ion pair [**45b**]$MeSO_4^+$ at *m/z* 1752.97, typically observed when the underlying dication does not result from protonation and a suitable counterion is present.[80] The source of $MeSO_4$ was the workup of **2**, which involved arylating the staring complex $[Pt_2(\mu\text{-S})_2(PPh_3)_4]$ (**1a**) with 2-chloro-*N*-methylpyridinium methylsulfate.

Although moderately promising, the micro-scale reaction solution was allowed to sit overnight in ambient conditions, and was examined once more by ESIMS after 12 hours (Figure 5.3). The spectrum did not substantially change, however a new

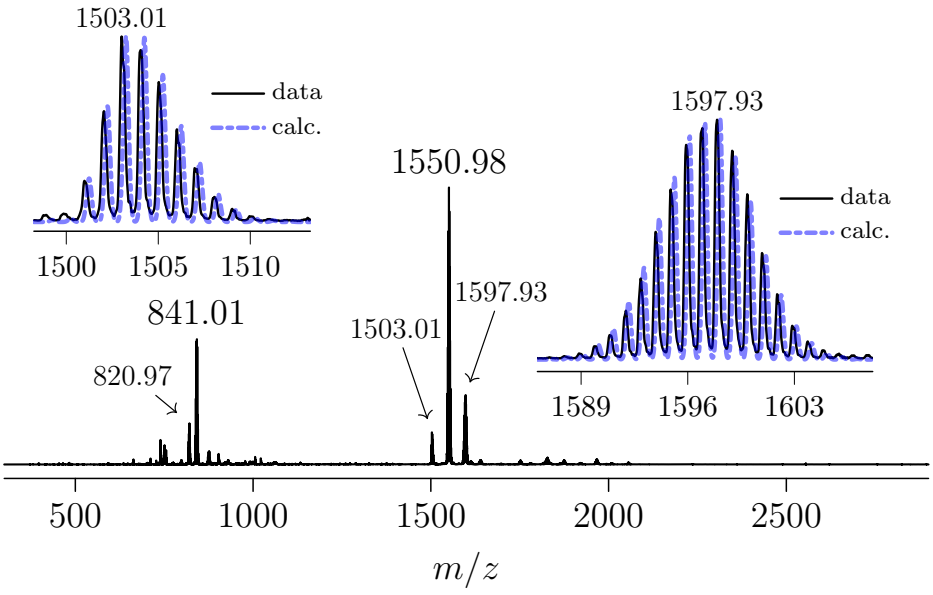

Figure 5.3: ESI mass spectrum of **2** and selenourea in methanol after 12 hours, capillary exit voltage 60 V. The insets are comparisons of the peaks observed at *m/z* 1503.01 and 1597.93 with calculated isotope patterns for **1a** + H^+ and **1b** respectively.

cation appeared at *m/z* 841.01, **1a** + H^+ was now present at *m/z* 1503.01, and the peak at *m/z* 1597.93, assigned as oxidised **1b**, had increased in relative intensity. The relative ease with which the selenide dimer **1b** oxidises relative to **1a** has been observed previously.[78] The emergence of **1a** is very interesting and suggests sulfide transfer is taking place presumably concomitant with selenourea Se−C activation. The peak at *m/z* 841.01 was identified as monocationic, and was tentatively assigned as $[(Ph_3P)_2PtSe{-}C(=NH)NH] + H^+$ **46** (calc. *m/z* 841.10). However, several possibilities exist for selenourea coordination in **46**: as either a mono or bis terminal neutral selenone, as a mono or bis terminal monoanion, or as a dianion Se$^\cap$N chelate (proposed), similar to the known *N*,*N*′-diphenylselenourea complex.[328] No conclusive evidence was observed for the existence of a neutral selenone ligand, either in the terminal chloride cation $[(Ph_3P)_2Pt(S{=}C(NH_2)_2)Cl]^+$, bis diselenone $[(Ph_3P)_2Pt(Se{=}C(NH_2)_2)_2]^{2+}$, or its proton loss monocation. To see if **46** would form directly from the mononuclear starting material *cis*-$[(Ph_3P)_2PtCl_2]$, a separate micro-scale reaction was carried out in methanol with a catalytic amount of TEA. After 5 minutes, ESIMS confirmed the appearance of the same cation at *m/z* 841.17 as the base peak, and essentially the only ionisable species in the reaction solution. Tentative

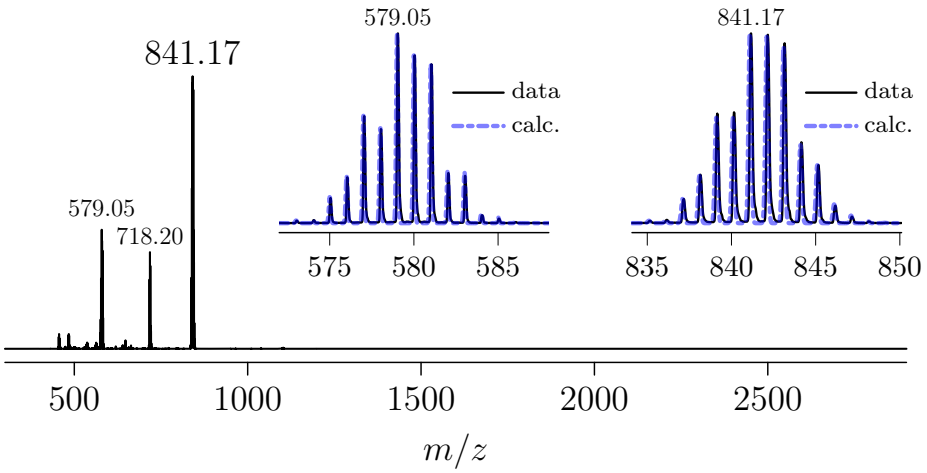

Figure 5.4: ESI mass spectrum of *cis*-$[(Ph_3P)_2PtCl_2]$ and selenourea in methanol/TEA, showing fragmentation at a capillary exit voltage of 210 V. The insets are comparisons of the peaks observed at *m/z* 579.05 and 841.17 and calculated isotope patterns for the species **46** - PPh_3 + H^+ and **46** + H^+ respectively.

evidence for a monoanionic coordination of selenourea was provided by the observation of a peak at m/z 1719.18, proposed to be the aggregate ion $[2\,\mathrm{M}\text{ - }\mathrm{Cl}]^+$ for M = $[(Ph_3P)_2Pt(Se{-}C(=NH)NH_2)Cl]$, at a very low relative intensity. When a fragmentation capillary exit voltage of 210V was applied, triphenylphosphine loss from the parent (**46** - PPh_3 + H^+, m/z 579.05) and cyclometallated $[(Ph_3P)PtPC_6H_4Ph_2]^+$ (m/z 718.20) cations were observed (Figure 5.4), the latter a known fragmentation species.[137]

To further probe the dynamic reaction, the solution of **2** and selenourea was allowed to sit in ambient conditions for a further 60 hours (72 hours total) after which a final examination by ESIMS was carried out (Figure 5.5). A much changed spectrum resulted, evidenced by an absence of the mixed-bridged species **23** along with **1a** + H^+ and **1b** cations. At around m/z 500-600 are several smaller monocationic species that, based on their isotope patterns, did not appear to contain any sele-

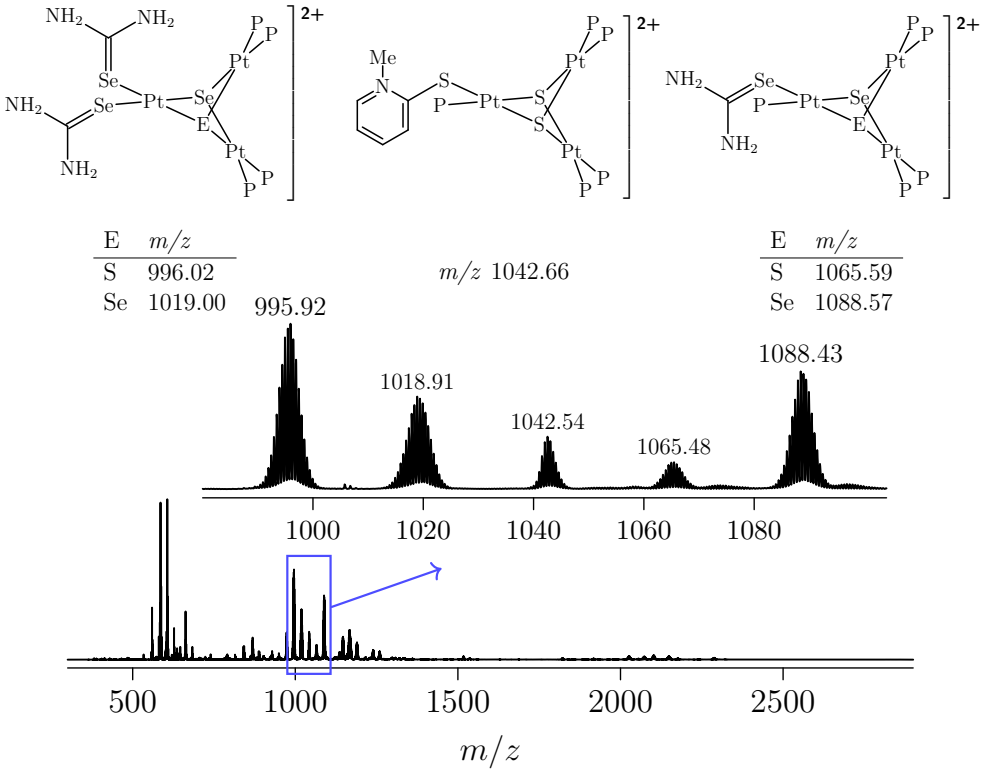

Figure 5.5: ESI mass spectrum of **2** and selenourea in methanol after 72 hours, capillary exit voltage 60 V. The middle inset is an expanded view of the spectrum. The top inset are the proposed structures (P = PPh_3) and calculated m/z .

nium or platinum, and were not assigned. The most notable region of the spectrum was around m/z 1000 (Figure 5.5 *inset*) where several large dications had appeared tentatively identified as trimetallic μ_3-S,Se complexes with neutrally coordinated selenourea ligands. The exception was the ion at m/z 1042, which was assigned as a trimetallic μ_3-S with a neutral mercapto-pyridinium ligand $[(Ph_3P)_4Pt_2(\mu_3\text{-}S)\text{-}Pt(PPh_3)S{-}C_6H_7N]^{2+}$. The ions observed at a slightly higher m/z of 1100-1200 were also dicationic and appeared to contain several polyisotopic elements, however no assignments were made.

Although the desired mixed-bridged derivative **23** results from the reaction of **2** and selenourea, there appears to be substantial concomitant deselenisation. The observation of $[Pt_2(\mu\text{-}Se)(\mu\text{-}Se{=}C(NH_2)_2)(PPh_3)_4]^{2+}$ and not the presumed initial substitution product $[Pt_2(\mu\text{-}S)(\mu\text{-}Se{=}C(NH_2)_2)(PPh_3)_4]^{2+}$ suggests deselenisation may be preferred to substitution, or the latter cation is more unstable with respect to Se−C activation. Regardless, the detection of both **1a** and **1b** as the reaction proceeded indicates sulfide transfer was occurring, possibly via thiourea substitution with unreacted **2** or selenide exchange with **23** (Scheme 5.2). The latter aslo rationalises the observation of **1b**, and would be enhanced by nucleophilic attack of a neutral species on selenourea or thiourea. The proclivity of the selenide system

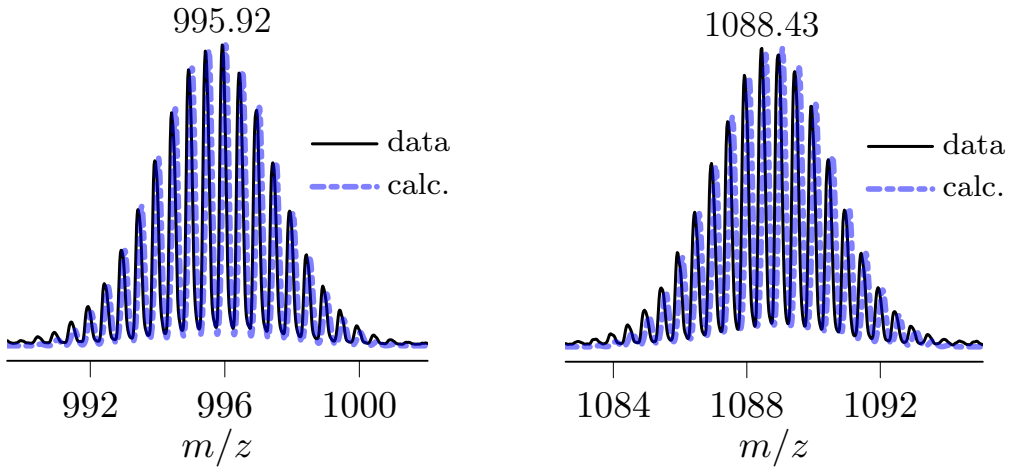

Figure 5.6: Comparisons of the peaks observed in Figure 5.5 at m/z 995.92 and 1088.43 with calculated isotope patterns for proposed dications in Figure 5.5 (*top inset*).

1b to engage in multi-metallic aggregate formation is well established,[44,124a] and is inherently more dynamic with respect to the sulfide analogue **1a** due to a high potential for "metal scrambling", a process by which metals and associated ligands can swap coordination sites.[330,331] Thus, the emergence of a diverse homo- and hetero-chalcogenide bridged trimetallic dications as the reaction proceeds is not entirely unexpected. Selenourea is assumed as a terminal ligand in these large mixed μ_3 bridge species, however it is possible this is instead thiourea neutrally coordinated and a homogeneous selenide core. Due to the dynamic behaviour observed in this reaction, a macroscopic synthesis was not attempted. For the mononuclear selenourea ligated complex **46**, the micro-scale reaction appeared to not suffer from polychalcogenide aggregation after sitting for several days in ambient conditions. As such, it is recommended for further investigation.

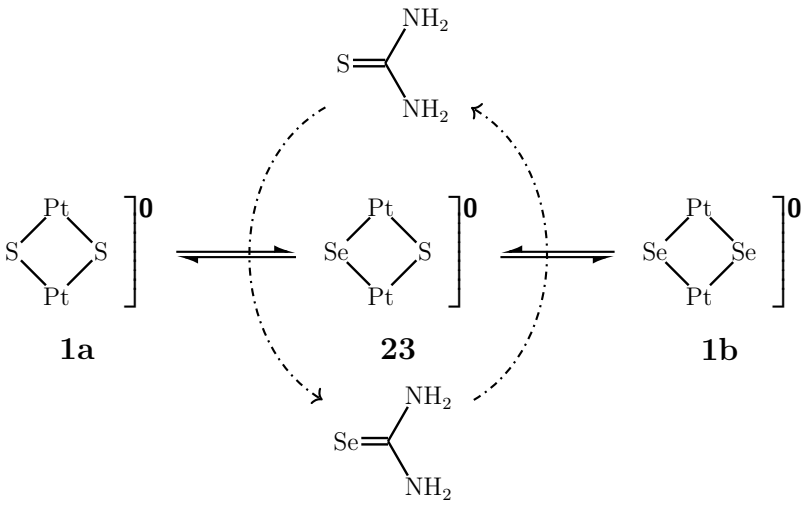

Scheme 5.2: A proposed scheme for generation of both sulfide **1a** and selenide **1b** dimers from the mixed-bridged complex **23** via thiourea/selenourea exchange. PPh_3 ligands omitted for clarity.

5.3 Diphenyl diselenide

Hydrazine was selected to reduce the diselenide for several reasons including ease of handling the dihydrochloride salt, compatibility with methanolic solutions (cf. sodium borohydride), and efficacy as an oxygen scavenger.[332] Considering all reactions were carried out under ambient conditions, the last quality is perhaps the most important as selenolate and thiolate species are sensitive with respect to oxidation. Diphenyl diselenide was reduced by a hydrazine solution and added to a freshly prepared clear red solution of **2**$[BF_4]_2$ which rapidly changed color to yellow-orange, and was immediately examined by ESIMS providing the spectrum in Figure 5.7 The promising detection of the mixed-bridge cation at m/z 1627 was tempered with the observation of cations at m/z 1501 and 1514, the former of significant relative intensity, tentatively assigned as bridging hydrazine $[Pt_2(\mu\text{-}S)(\mu\text{-}N_2H_3)(PPh_3)_4]^+$ **21** and bridging methylazo $[Pt_2(\mu\text{-}S)(\mu\text{-}N_2CH_3)(PPh_3)_4]^+$ **22** complexes respectively. A

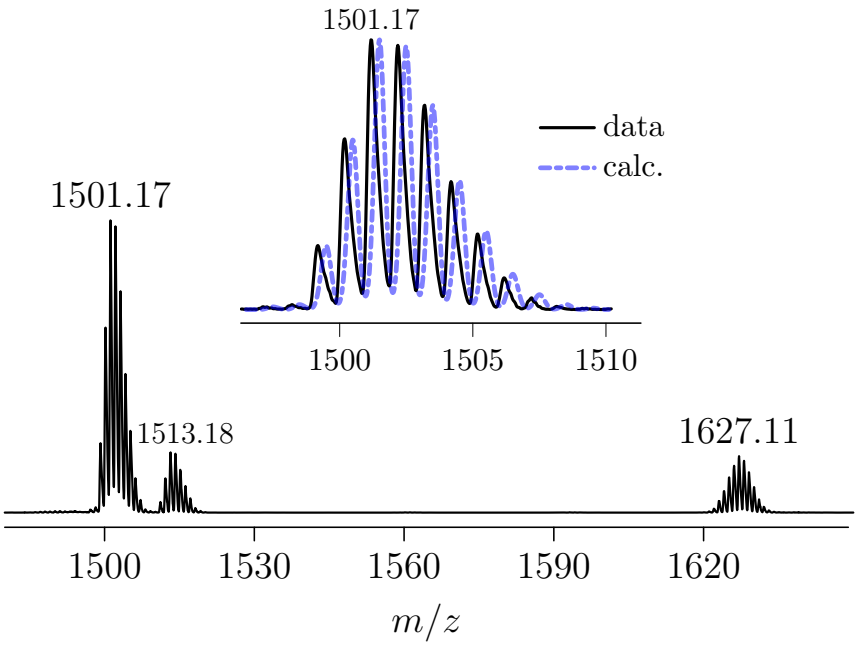

Figure 5.7: ESI mass spectrum of the micro-scale reaction between hydrazine reduced diphenyl diselenide and **2** in methanol, cropped to show significant cations. The inset is a comparison of the observed peat at m/z 1501 and a calculated isotope pattern for the proposed μ-hydrazido complex $[Pt_2(\mu\text{-}S)(\mu\text{-}N_2H_3)(PPh_3)_4]^+$ (calc. m/z 1501.30). Capillary exit voltage 90 V.

separate experiment was carried out attempting to isolate and characterise **21** (*vide infra*).

After letting the micro-scale reaction sit at ambient conditions for 12 hours, it was examined by ESIMS once more revealing a much changed spectrum which contained only the ion tentatively assigned as the mixed-bridged cation $[Pt_2(\mu\text{-}S)(\mu\text{-}Se{-}Ph)(PPh_3)_4]^+$ **18** at *m/z* 1627. The proposed hydrazido cation **21a** has disappeared completely, the peak at *m/z* 1513 tentatively assigned as **21b** still remains at a very low relative intensity. Although there appears to be several lower-mass ions present, these appear not to be composed of polyisotopic elements, and assignment was not carried out. It is noteworthy the absence of any multi-metallic PtSe aggregate formation, suggesting reasonable solution stability of the cationic mono-arylated derivative **18**. Fragmentation of the cation was investigated by raising the capillary exit voltage to 180V, which did not effect any triphenylphosphine loss (Figure 5.8). Only mild fragmentation was observed when at a voltage of 210V, as evidenced by the very low relative intensity of the PPh_3 loss cations at *m/z* 1364.92 (7% r.i.) and 1102.89 (5% r.i.) for the loss of one and two phosphines respectively.

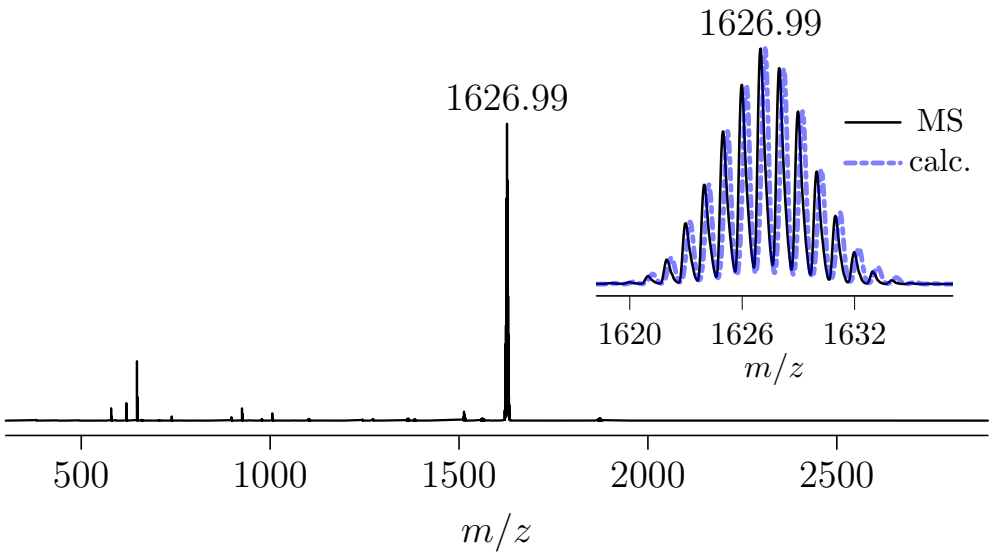

Figure 5.8: ESI mass spectrum of **2** and reduced Ph_2Se_2 in methanol after 12 hours. The inset is an isotope pattern comparison of the peak observed at *m/z* 1627 and a calculated pattern for the proposed cation $[Pt_2(\mu\text{-}S)(\mu\text{-}Se{-}Ph)(PPh_3)_4]^+$, **18**, calc. *m/z* 1627.22. Capillary exit voltage 180V.

After isolating **18** macroscopically with sodium tetrafluoroborate $^{31}P\{^{1}H\}$ and $^{195}Pt\{^{1}H\}$-NMR spectra were recorded. The $^{31}P\{^{1}H\}$-NMR has two distinct resonances at δ 30.3 and 24.7 ppm that are significantly separated in frequency. The latter resonance has a $^{1}J_{(PtP)}$ coupling of 3312 Hz and is assigned to the phosphines *trans* to the aryl selenolate ligand. The low field resonance has the smaller $^{1}J_{(PtP)}$ coupling of 2652 Hz and is assigned to the phosphines *trans* to the underivatised sulfide. The resonance multiplets share a *pseudo* quartet appearance, suggesting an ABX spin system and a symmetrical magnetic environment about the S-Se vector of the $\{Pt_2SSe\}$ core. There is no direct evidence of *trans* or *cis* $^{2}J_{(SeP)}$ coupling, the former expected to be larger in magnitude[333] and has been found to be 18 Hz in the mononuclear dianionic selenourea complex $[(Ph_3P)_2PtSe{-}C(=NPh)NPh]$,[328] around 45 Hz in monocationic diselenolate complexes of the type $[Pt(SeR)_2(P^{\cap}P)]$ (R = Ph, 2-pyridyl; $P^{\cap}P$ = dppm, dppe, dppp),[333] and 60 Hz in dinuclear complexes $[Pt_2Cl_2(\mu\text{-SeBz})_2(PR_3)_2]$ ($PR_3 = PPr^{n}_3$, PEt_3, $PMePh_2$).[315] Considering the relative abundance of ^{77}Se (7.6%) and significant chemical shift anisotropy imparted on the complex by the 14.1 T magnet, any ^{77}Se satellites in the spectrum would be expected to have a broad lineshape. The multiplet δ 24.7 ppm does indeed appear

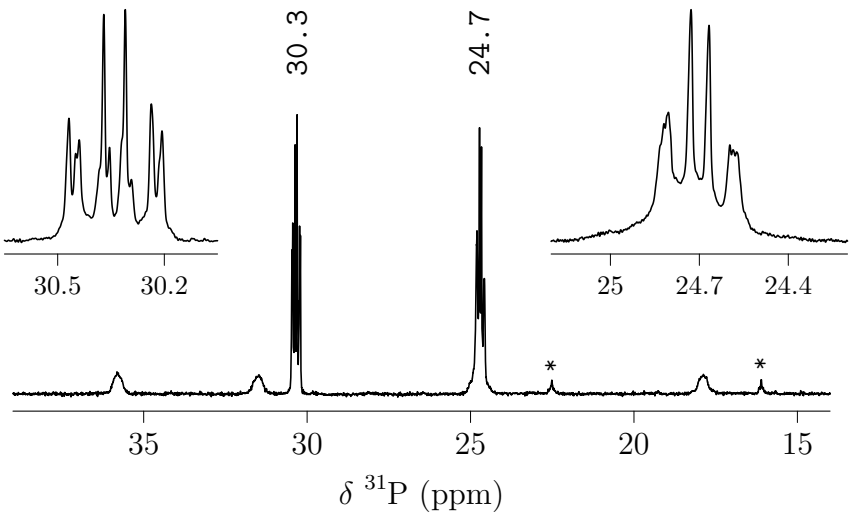

Figure 5.9: $^{31}P\{^{1}H\}$-NMR (242.95 MHz, $CDCl_3$) of the **18**$[BF_4]$.The peaks marked * are an impurity, and are tentatively assigned as the μ-methylazo complex **22**.

to be broader than the low field resonance (Figure 5.9 *insets*), due in part to coincidence with a ^{195}Pt satellite. The two resonances at δ 22.5 and 16.1 ppm are assigned as an impurity, possibly resulting from the proposed methylazo species **21b**, which was observed by ESIMS in the isolated BF_4^- salt of **18** at very low relative intensity. The resonances of the impurity were of insufficient intensity to confidently identify any ^{195}Pt satellites.

A ^{195}Pt{^{1}H}-NMR experiment was next carried out, giving the expected *doublet of doublet* multiplicity for the ^{195}Pt nuclei resonating at δ -4424.8 ppm (Figure 5.10). Although ^{195}Pt NMR data were not reported for the arylated analogue $[Pt_2(\mu\text{-}S)(\mu\text{-}S{-}Ph)(PPh_3)_4]^+$, a comparison can be made with the diaryl thioether bis(**1a**) complex $[(Ph_3P)_4Pt_2(\mu\text{-}S)(\mu\text{-}S{-}C_6H_4{-}S{-}C_6H_4{-}\mu\text{-}S)(\mu\text{-}S)Pt_2(PPh_3)_4]^{2+}$ in which the ^{195}Pt nuclei resonate at δ -4263 ppm. This observation is consistent with the known trend in ^{195}Pt chemical shifts, that as a periodic group is descended, δ goes towards a higher field (more negative).[154,167] $^1J_{(PtP)}$ couplings of 2654 and 3306 Hz compare favorable with those observed in the ^{31}P{^{1}H}-NMR spectrum. A large $^2J_{(PtPt)}$ coupling of 940 Hz is also estimated, indicating significant spin density transfer for the bridging sulfide and selenolate ligands.[58] As with the ^{31}P{^{1}H}-NMR

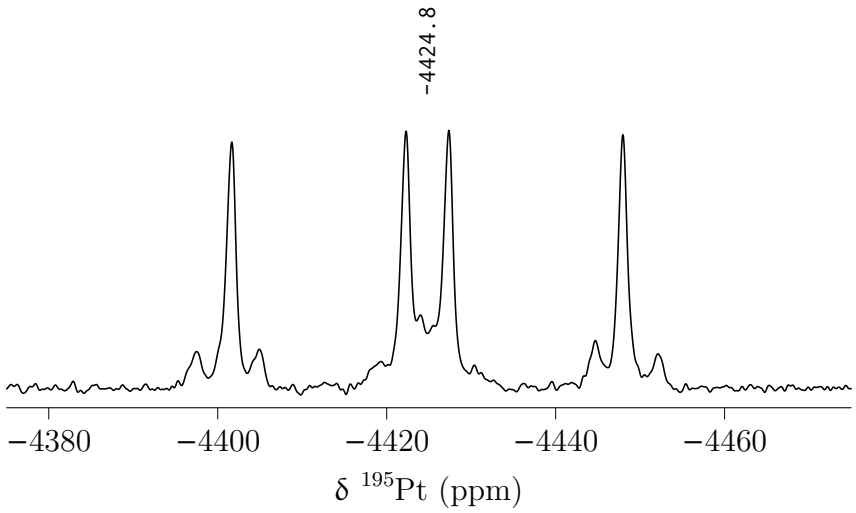

Figure 5.10: ^{195}Pt{^{1}H}-NMR (129.02 MHz, $CDCl_3$) of the mixed-bridged system $[Pt_2(\mu\text{-}S)(\mu\text{-}Se{-}Ph)(PPh_3)_4]^+$. $^1J_{(PtP)}$ couplings result in a doublet of doublet pattern, and the multiplet is further split by a $^2J_{(PtPt)}$ coupling of 940 Hz.

experiment, no direct evidence of any $^{1}J_{(\mathrm{PtSe})}$ coupling appears to be present in the spectrum. Such a coupling has been determined to have a positive sign, and may be large in magnitude.[154,334] However, considering only two isotopomers (roughly 4%) of the sample has both NMR-active ^{195}Pt and ^{77}Se nuclei (Figure 5.11), and the previously discussed issues observing $^{2}J_{(\mathrm{SeP})}$ above, the absence of this coupling is also not surprising.

Yellow-orange irregular shaped crystals of **18**[BF_4] were grown from slow diffusion of diethyl ether into a chloroform solution (Figure 5.12). The complex **18**[BF_4]$\cdot$ 3 $CHCl_3$ crystallises in the monoclinic space group $P2_1/m$ and has two independent molecules in the unit cell. Selected bonds and angles are tabulated in Table 5.1. The BF_4^- anion is present confirming the cationic nature of **18**. The dimer is bisected by a mirror plane running throuh S1, Se1, and the aryl ring of the selenide. Such a mirror plane was also observed in the crystal structure of the symmetric thiolato derivative of **1a** [Pt_2(μ-S)(μ-S−C(CN)$_2$)(PPh_3)$_4$] **12**. To the best of our knowledge, it is the first structurally characterised mixed-(sulfide,selenol)bridged Pt^{II} dimer. As expected, the Se1-C1 bond (1.931(9) Å) is substantially longer than S-C bonds in similar Pt^{II} dimers (S-C, μ = 1.759 Å for 23 structures in CSD) and compares favorably with the few selenol examples in the literature of SePh coordinated to a Pt^{II} center (Se-C, μ = 1.942 Å, 15 structures in CSD). The arylated derivative of **1b**, [Pt_2-(μ-Se)(μ-SePh)(PPh_3)$_4$]PF_6, has a substantially longer Se-C bond of 2.018(9) Å.[124f] An unusually long S-C distance of 1.995(8) Å is also observed in the very similar tri-

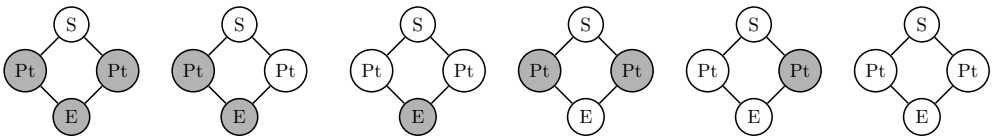

Se	0.9	3.4	3.3	10.6	41.3	40.5%
Te	0.8	3.1	3.1	10.6	41.6	40.8%

Figure 5.11: Composition of isotopomers for mixed-bridged complexes [Pt_2(μ-S)(μ-E−R)(PPh_3)$_4$]$^+$ (E = Se, Te) showing NMR active (^{77}Se, ^{125}Te, ^{195}Pt, *grey*) and inactive (*white*) nuclei in the {Pt_2(μ-S)(μ-E)} core.

phenylphosphine derivative $[Pt_2(\mu\text{-}S)(\mu\text{-}S{-}Ph)(PPh_3)_4]PF_6$.[63] However this complex crystallised in the space group $C2/c$ with $Z' = 0.5$ and a 2-fold rotation axis passing through the $\{Pt_2S_2\}$ core. Thus, the bridging thiolato and sulfide atoms were nearly positionally coincident presumably complicating estimation of the S-C distance.

The nearly flat $\{Pt_2SSe\}$ core in **18** (torsion Pt1-Se1-S1-Pt1′ = 178.58°) is slightly inverted as the Se-C ligand is in an *endo* configuration. An inverted or *endo* geometry for the thiolate ligand is unusual for mono-alkylated or arylated derivatives of **1a**, and was observed in the TCCP ring-opened derivative **12** which also had moderately flat $\{Pt_2S_2\}$ ring, with a hinge torsion of 169° (*see discussion* chapter 3). Examples are scant in the CSD for mono-alkylated or arylated derivatives of **1b**, the only two being $[Pt_2(\mu\text{-}Se)(\mu\text{-}Se{-}Ph)(PPh_3)_4]PF_6$[124f] and $[Pt_2$-

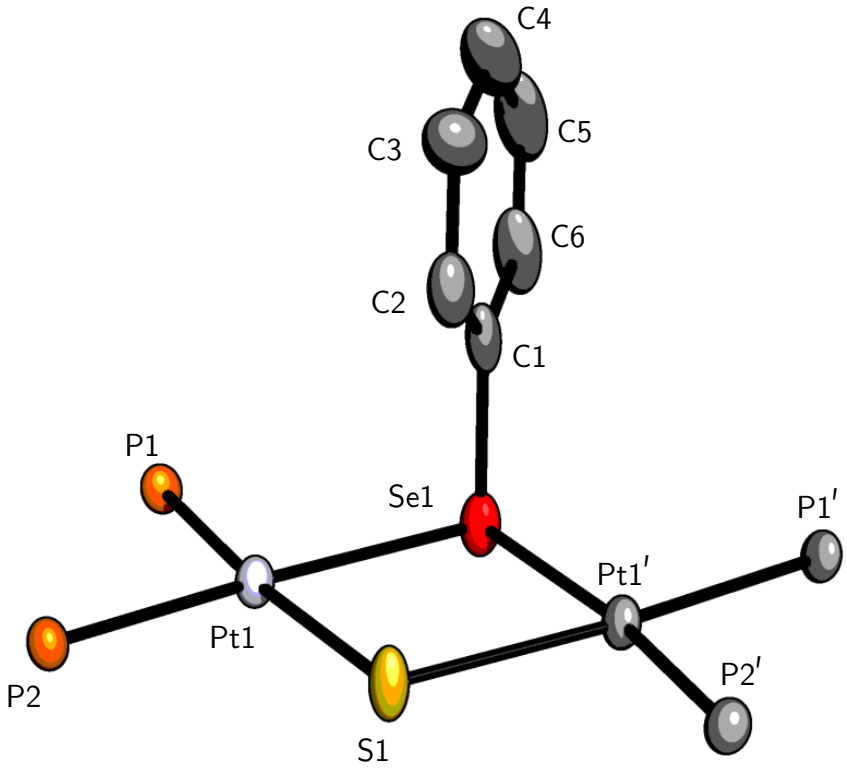

Figure 5.12: Crystal structure of **18**$[BF_4]\cdot(CHCl_3)_2$. Primed atoms are generated by symmetry operation $[+x, \frac{1}{2} - y, +z]$. Phenyl rings of PPh_3 ligands, BF_4^- counterion, and chloroform solvent omitted for clarity. Thermal ellipsoids displayed at 50% occupancy.

(μ-Se)(μ-Se−CH_3)(PPh_3)$_4$]PF_6.[73d] These structures have hinge torsions of 164.87 and 133.55° respectively, and both selenolate ligands are in the *exo* configuration. The mono-arylated derivative [Pt_2(μ-S)(μ-S−Ph)(PPh_3)$_4$]PF_6 was also significantly hinged at 146.3° and *exo*.[63] The only other arylated derivatives of **1b** in the literature are di-arylated with the selenato ligands in an *anti* configuration and hinge dihedral angles of 180° or very close. Two di-alkylated derivatives of **1b** with overhead bridges ([P_2Pt(μ-Se−$(CH_2)_n$−μ-Se)PtP_2]$^{2+}$, n = 2, 4; P = PPh_3) have significant dihedral hinge angles of 121.07 and 146.86° respectively.[335] There is a large Pt1-Pt1′ separation of 3.658(1) Å in **18**, a product of the very flat geometry in the {Pt_2SSe} core, and interesting considering the large $^2J_{(PtPt)}$ coupling of 940 Hz observed. The Pt1-Se1 bond is accordingly longer (2.446(1) Å) than the Pt1-S1 bond (2.345(1) Å), however the Pt1-P2 and Pt1-P1 bonds are essentially identical (2.286(1) and 2.286(1) Å respectively). The Pt^{II} center has an ideal square-planar geometry, quantified by a τ_4' parameter[141] of 0.13.

Table 5.1: Selected bond lengths (Å) and angles (°) for the crystal structure of **18**[BF_4]·$(CHCl_3)_2$. Pt′ generated by symmetry operation $[+x, \frac{1}{2}-y, +z]$.

Pt1-Se1	2.4464(6)	P2-Pt1-Se1	93.69(4)
Pt1-P2	2.2856(13)	P2-Pt1-S1	174.01(5)
Pt1-S1	2.3446(12)	P2-Pt1-P1	98.19(5)
Pt1-P1	2.2861(13)	S1-Pt1-Se1	80.32(4)
Se1-C1	1.931(9)	P1-Pt1-Se1	167.24(4)
C2-C1	1.401(14)	P1-Pt1-S1	87.79(5)
C2-C3	1.394(14)	Pt1-Se1-Pt1′	96.79(3)
C1-C6	1.405(13)	C1-Se1-Pt1	96.73(18)
C5-C4	1.41(2)	Pt1-S1-Pt1′	102.56(7)
C5-C6	1.387(18)	C3-C2-C1	119.7(10)
C4-C3	1.378(19)	C2-C1-Se1	122.1(7)
C2-C1-C6	121.2(9)	C3-C4-C5	120.8(10)
C6-C1-Se1	116.7(8)	C5-C6-C1	118.2(12)
C6-C5-C4	120.6(10)	C4-C3-C2	119.5(12)

5.4 Diaryl ditellurides and 2

The previous substitution reaction between $[Pt_2(\mu\text{-}S)(\mu\text{-}S{-}C_6H_7N)(PPh_3)_4]^{2+}$ **2** and hydrazine-reduced diphenyl diselenide was successful in generating the mixed-bridged species $[Pt_2(\mu\text{-}S)(\mu\text{-}Se{-}Ph)(PPh_3)_4]^{+}$ **18** under ambient conditions. Although it appears a bridging hydrazine species **21a** is generated in addition to the $PhSe^-$ selenol, this species is transient and converts to the more stable **18** after several hours in solution. The heavier chalcogen tellurium has similar analogues in diaryl ditelluride species that exhibit a greater reactivity due to the longer and weaker Te-Te bond,[336] and greater propensity to form multimetallic aggregates with platinum group metals.[74c] The diaryl ditellurides Ar_2Te_2 ($Ar = Ph^-$, $EtOC_6H_4^-$) were examined previously with both **1a** and **1b** resulting in ESIMS identification of mixed-bridged derivatives $[Pt_2(\mu\text{-}E)(\mu\text{-}Te{-}Ar)(PPh_3)_4]^{+}$ (E = S, Se), although isolation of these novel mixed-bridged tellurol species proved elusive.[78] In addition to these systems, ESIMS provided evidence of larger aggregates of high nuclearity such as the trimetal-

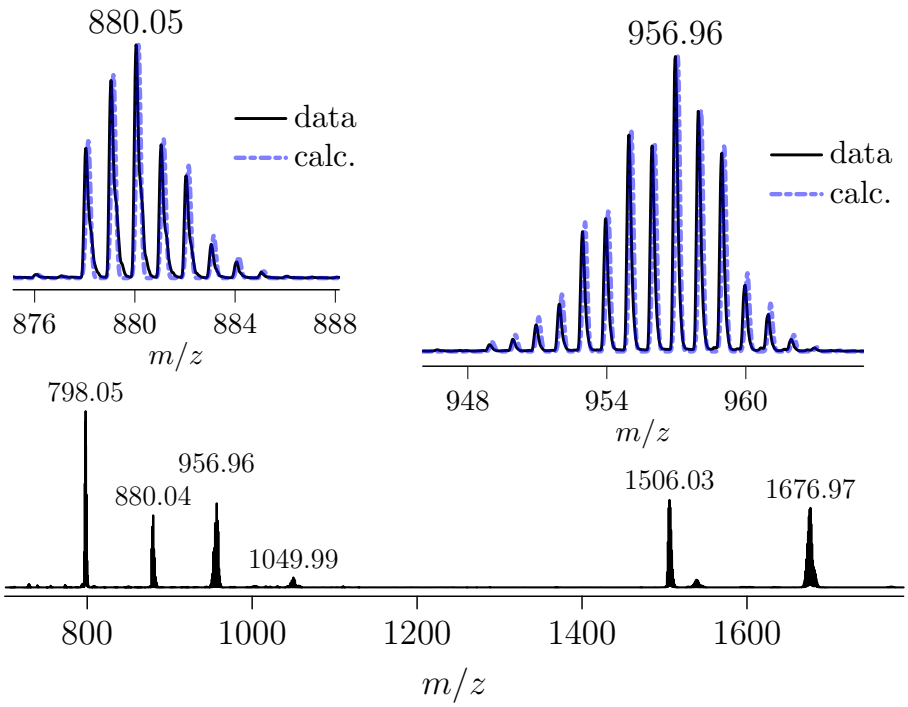

Figure 5.13: ESI mass spectrum of Ph_2Te_2 in a hydrazine hydrate solution and **2** in methanol. Capillary exit voltage 90 V. The insets are isotope pattern comparisons of peaks observed in the spectrum (*m/z* 880.94, 956.96) and proposed cations in Figure 5.14 (*a* and *c* ($[(Ph_3P)_2PtSTePh]^+$) respectively).

lic complex $[(Ph_3PPt)_3(\mu\text{-}TePh)_3\mu_3\text{-}Se]^+$ **44a**.

Diphenyl ditelluride was investigated first on a micro-scale, following a similar procedure as the synthesis of **18**. The ditelluride was first reduced with a hydrazine solution prior to substitution with a freshly prepared solution of **2** in methanol. The reaction was probed using ESIMS after 10 minutes (Figure 5.13). The desired substitution of $PhTe^-$ into the Pt^{II} dimer is present in the mass spectrum at *m/z* 1677, $[Pt_2(\mu\text{-}S)(\mu\text{-}Te{-}Ph)(PPh_3)_4]^+$ **47**, along with **2** at *m/z* 798 and **33** at *m/z* 1506. Observation of these species in conjunction with the target cation is excellent to see in these micro-scale reactions, as fine control over stoichiometry is more challenging and their identification indicates additional reactant/time are needed for completion. However, several mononuclear cations are present around *m/z* 880 - 1050, and appear to indicate degradation of the $\{Pt_2(\mu\text{-}S)(\mu\text{-}SR)\}$ core in **2** or the $\{Pt_2(\mu\text{-}S)(\mu\text{-}TeR)\}$ core in **47**, especially considering the gentle capillary exit voltage of 90V employed, typically not sufficient to induce fragmentation of these cationic dimers. The cation $[(Ph_3P)_2Pt(S{-}C_6H_7N)Cl]^+$ is tentatively identified at *m/z* 880, presumably resulting from the scission of the core in **2**. The square-planar geometry of the mononucelar Pt^{II} fragment stabilised by a terminal chloride. The ion *m/z* 956 is proposed to be $(\eta^2\text{-}STe{-}Ph)^-$ coordinated to a platinum diphos center $[(Ph_3P)_2PtL]^+$. Another possibility for L is $(\kappa^2\text{-}O_2Te{-}Ph)^-$, although this seems

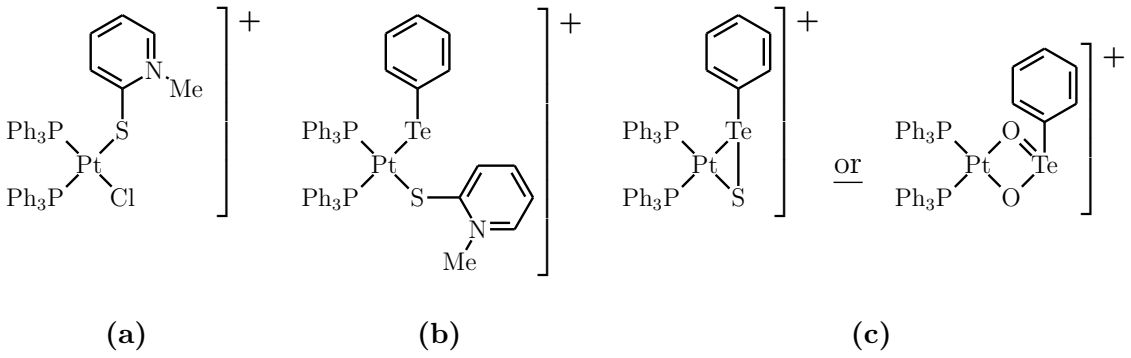

Figure 5.14: Proposed structures of mononuclear Pt^{II} species observed in Figure 5.13. **(a)** $[(Ph_3P)_2Pt(SC_6H_7N)Cl]^+$ (*calc. m/z* 880.14), **(b)** $[(Ph_3P)_2Pt(SC_6H_7N)(TePh)]^+$ (*calc. m/z* 1050.12), **(c)** *two possible structures*: $[(Ph_3P)_2PtSTePh]^+$ (*calc. m/z* 957.06) or $[(Ph_3P)_2Pt(\mu\text{-}O)_2(TePh)]^+$ (*calc. m/z* 957.08).

less likely due to Te being a very soft coordination center. These proposed species share an almost identical mass and isotope pattern, complicating assignment. Presumably the cation at *m/z* 956 is a product of ring scission of **47**, resulting in a $PhTeS^-$ type anionic terminal or bridging ligand for the transient species.

Such $RTeS^-$ species have been isolated[337] although no examples exist in the literature for this ligand terminally coordinated to a metal center. In our previous work, it was however observed by ESIMS as a transient species proposed to be in a thiolate-bridged coordination viz. $[Pt_2(\mu\text{-}S)(\mu\text{-}S{-}TePh)(PPh_3)_4]^+$, the result of nucleophilic attack of **1a** on diphenyl ditelluride.[78] Oxidation of the tellurolate can also not be ruled out. Benzenetelluric acid is known,[338,339] and a rare example of a metallated tellurinic acid had been isolated as a bridging ligand coordinated to two Zn^{II} centers.[340] The formation of this reported species involved reduction of the ditelluride by Zn^{I} followed by oxidation of the bridging tellurolate to tellurinic acid. An ion of much lower relative intensity at *m/z* 1049 is tentatively identified as the proposed species observed at *m/z* 880 with a tellurolate fragment $PhTe^-$ terminally

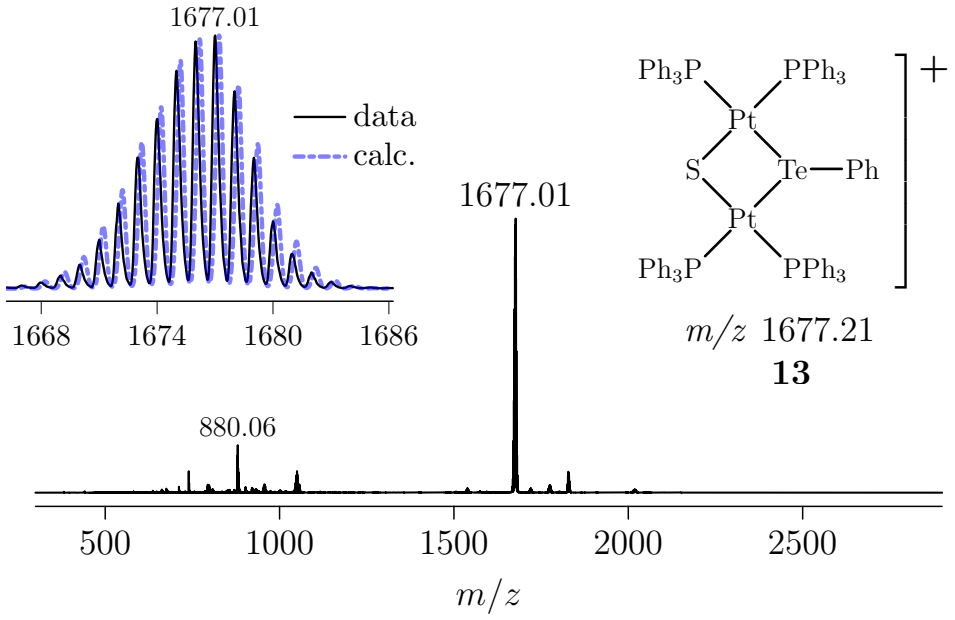

Figure 5.15: ESI mass spectrum of Ph_2Te_2 and **2** in methanol, capillary exit voltage 90 V. The left inset is an isotope pattern comparison for $[Pt_2(\mu\text{-}S)(\mu\text{-}Te{-}Ph)(PPh_3)_4]^+$ (calc. *m/z* 1677.21, *right inset*, **47**) and the observed peak at *m/z* 1677.01.

coordinated instead of chloride, *viz.* ($[(Ph_3P)_2Pt(SC_6H_7N)TePh]^+$.

Interestingly, a more successful generation of the target mixed-bridged $[Pt_2(\mu\text{-}S)(\mu\text{-}Te{-}Ph)(PPh_3)_4]^+$ **47** was observed when diphenyl ditelluride was reacted directly (not reduced) with the intermediate species **2**. Although it did not appear to be a qualitatively "clean" synthesis by ESIMS analysis (Figure 5.15), the micro-scale reaction appeared to contain fewer degradation species than when hydrazine was employed in reduction of the ditelluride. Unfortunately, when the reaction was repeated macroscopically the resulting precipitate suffered from significant impurities and no further attempts were made to isolate **47**. It must be noted, when reacting diphenyl diselenide directly (not reduced) with **2**, the mixed-bridged cation was not detected by ESIMS. While these initial reactions provided promising results by ESIMS towards a mixed-bridged system, a subsequent micro-scale reaction between the *p*-ethoxyphenyl analogue di-4-ethoxyphenyl ditelluride and **2** achieved similar success, and was successfully isolated when the reaction was carried out macroscopically.

A micro-scale reaction between reduced di-4-ethoxyphenyl ditelluride and **2** in methanol was examined by ESIMS, and detection of the mixed-bridged species $[Pt_2(\mu\text{-}S)(\mu\text{-}Te{-}C_6H_4{-}OEt)(PPh_3)_4]^+$ **48** was tentatively confirmed by the appearance of a monocation at *m/z* 1721. Additionally identified at a low relative intensity in the spectrum was a monocation at *m/z* 2150.7 tentatively assigned as $[(Ph_3PPt)_3(\mu\text{-}Te{-}C_6H_4{-}OEt)_3\mu_3\text{-}S]^+$ **44d**, a species that was observed in a reaction between **1a** and di-4-ethoxyphenyl ditelluride in our previous work.[78] The spectrum also contained the previously observed cation at *m/z* 1501, assigned as the mixed-bridged hydrazido species **21a**. Additionally, several large polyisotopic cations were present appearing to contain tellurium, all at a low relative intensity (< 2% r.i.), and were not assigned. Significant fragmentation only occurred when the capillary exit voltage reached 240V, consistent with **18** which also resisted fragmentation at lower voltages. Interestingly, when fragmentation was observed for **19**, the cation at *m/z* 1458.9 assigned as $[M - PPh_3]^+$, had a significantly lower relative intensity than the

cation at m/z 1195.9 assigned as [M - 2PPh$_3$]$^+$ (16.4 cf. 80.2% r.i.).

The reaction was repeated on a macroscopic scale and the cation isolated with sodium tetrafluoroborate to give **48**[BF$_4$] which was subsequently characterised by ^{31}P{^{1}H}, and ^{195}Pt{^{1}H}-NMR spectroscopy. The ^{31}P{^{1}H}-NMR spectrum reveals a less clean synthesis than the diphenyl diselenide analogue **18**, possibly related to propensity of tellurium to form multimetallic aggregates as observed in the ESI mass spectrum of **19**. A similar broadening of the resonance *trans* to the tellurolate ligand at δ 20.2 ppm is also observed. Unlike the ^{31}P{^{1}H}-NMR spectrum of **18** (Figure 5.9), there is no ^{195}Pt satellite coincidence, and the observed broadness is ascribed to ^{125}Te coupling (^{125}Te $I = \frac{1}{2}$, 7.07% abundant, see isotopomers of **19** Figure 5.11). The $^1J_{(\mathrm{PtP})}$ couplings of 3080 and 2820 Hz are much closer in magnitude than those observed for the selenolate analogue **18**, however the larger coupling is still assigned to the phosphines *trans* to the aryl tellurolate ligand. Thus, the $^1J_{(\mathrm{PtP})}$ coupling of 2820 Hz assigned to the phosphines *trans* to the underivatised sulfide (δ 29.1 ppm) is quite large, and reflective of a reduction in *trans*

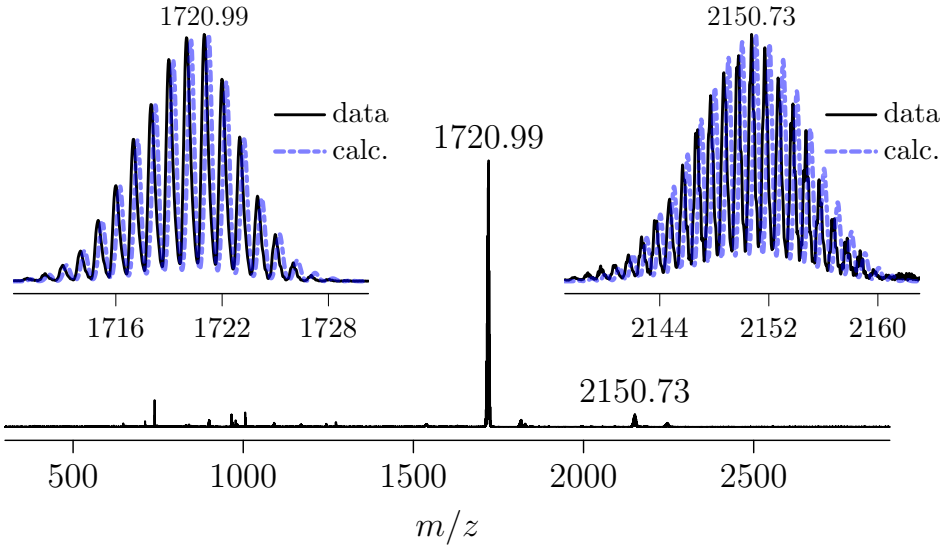

Figure 5.16: ESI mass spectrum of **2** and a hydrazine hydrate solution of di-4-ethyoxyphenyl ditelluride after 12 hours stirring in ambient conditions, capillary exit voltage 90 V. The insets are comparisons of the observed peaks at m/z 1720.99 and 2150.7 and calculated isotope patterns for the proposed mixed-bridged species **19** and trimetallic [(Ph$_3$P-Pt)$_3$(μ-Te−C$_6$H$_4$OEt)$_3$(μ$_3$-S)]$^+$ **44d** respectively.

influence of the bridging sulfide and larger *s* character in the Pt-P bond. Conversely, the $^{1}J_{(\mathrm{PtP})}$ coupling of 3080 Hz is quite small in comparison to the analogous coupling in **18**, or in thiolato-derivatives of **1a** which are around 3200 Hz, and suggests a comparative increase in the *trans* influence exerted by the tellurolate ligand. A $^{1}J_{(\mathrm{PtP})}$ coupling of 3030 Hz was recorded for a similar triphenylphosphine Pt^{II} dimer with bridging tellurolate ligands ($MeOC_6H_4{-}Te^{-}$) *trans*-$[(Ph_3P)_2Pt_2Cl_2(Te{-}C_6H_4\text{-}OEt)_2]$.[341] The difference in resonating frequencies ($\Delta\nu$) is more pronounced at ca. 9 ppm than in **18**, indicative of significant deshielding and shielding for the phosphines *trans* to the underivatised bridging sulfide and bridging tellurloate ligands respectively. The morphology of the resonance multiplicities (Figure 5.17 *insets*) are very similar to those observed in **18** and likewise suggest an ABX spin system, implying symmetry about the center of the $\{Pt_2(\mu\text{-}S)(\mu\text{-}TeR)\}$ core.

To gain additional structural insight into **19** a $^{195}Pt\{^{1}H\}$-NMR spectroscopy experiment was carried out (Figure 5.18). Isotopomers of **19** with ^{125}Te and at least one ^{195}Pt nucleus make up 3.9% of the sample, and accordingly no $^{1}J_{(\mathrm{PtTe})}$ coupling

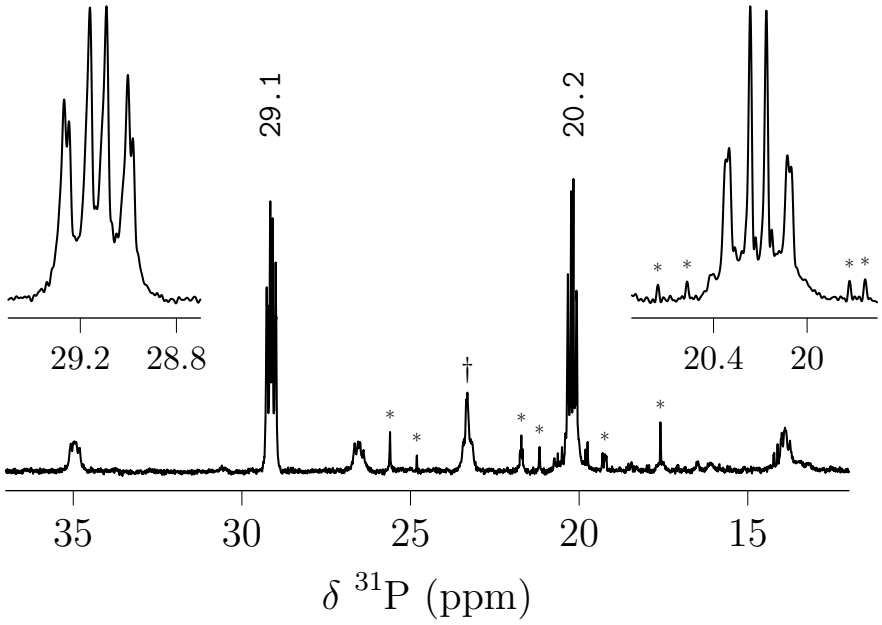

Figure 5.17: $^{31}P\{^{1}H\}$-NMR (242.95 MHz, $CDCl_3$) spectrum of **19**$[BF_4]$. The insets are enhanced views of the resonances at δ 29.1 and 20.2 ppm. The peak marked (†) is an impurity coincident with at ^{195}Pt satellite. Other impurities are marked with (*).

was observed. This coupling should be quite large, estimated to be around 1300 Hz in mononuclear Pt^{II} complexes $[Pt(Te_2(^iPr_2P)_2N)_2]$.[342] The ^{195}Pt nuclei resonate coincidentally at δ -4769 ppm with the expected *doublet of doublet* multiplicity. The estimated $^1J_{(PtP)}$ couplings of 2840 and 3073 Hz agree nicely with those in the $^{31}P\{^1H\}$-NMR spectrum. A $^2J_{(PtPt)}$ of 572 Hz is estimated for **19**, much smaller than that observed for **18**, and suggesting a greater Pt-Pt separation. The resonating frequency for **19** is in agreement known trends for chemical shifts of Pt^{II} complexes, appearing at higher fields as a periodic group is descended.[154,167,333]

Orange-red parallelepiped crystals of **19**$[BF_4]$ were grown from layered propan-2-ol on a chloroform solution, and the structure was unambiguously characterised by a single-crystal X-ray diffraction experiment (Figure 5.19). The structure crystallises as the bis(2-propanol) solvate in the triclinic space group $P\bar{1}$ and has two molecules in the unit cell ($Z' = 1$). A single BF_4^- counterion in the asymmetric unit confirms the monocationic nature of **19**. Unlike the selenolate derivative **18**, the torsion dihedral angle Pt2-Te1-S1-Pt1 is more hinged at 160.99(4)° and the tellurolate ligand is in an *exo* orientation from the dihedral. The observed hinged configuration is also in contrast to the planarity of the $\{Pt_2Te_2\}$ ring in dimers of the type $[Pt_2(\mu\text{-}Te)_2P]$ (P = $(PPh_3)_4$;[74c] $(PEt_3)_4$;[74a] $(dppe)_2$[343]) and $[Pt_2(\mu\text{-}Te{-}C_3$-

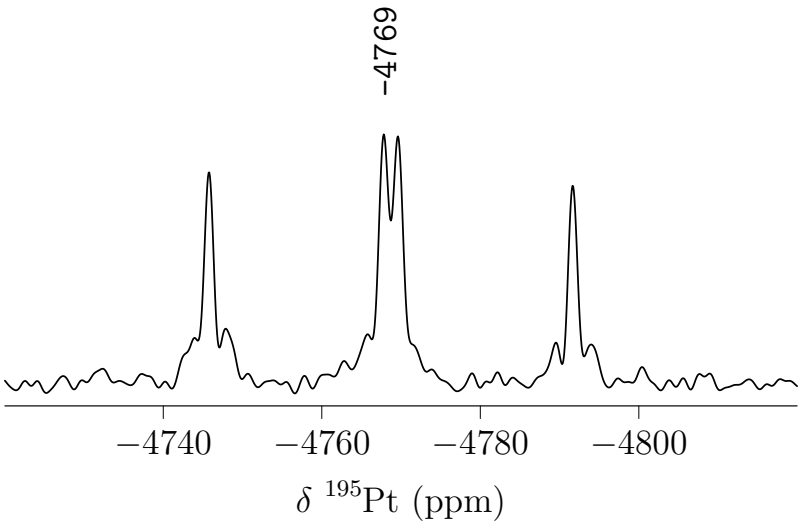

Figure 5.18: $^{195}Pt\{^1H\}$-NMR (129.02 MHz, $CDCl_3$) spectrum of **19**$[BF_4]$.

(3-Me)H_6N)$_2$(dppe)$_2$](BPh$_4$)$_2$.[344] The Te-Pt bonds are substantially longer than the Pt-Se bonds (2.446(1) Å) in **18** at 2.594(1) and 2.607(1) Å for Pt1-Te1 and Pt2-Te1 respectively (Table 5.2). The S-Pt bonds are also longer than in **18** at 2.359(1) and 2.357(1) Å cf. 2.344(1) Å.

Accordingly, the Pt2-Pt1 separation of 3.738(1) Å is also longer than in **18** (3.658(1) Å) despite the moderate hinge dihedral angle and near planarity observed for the mixed-bridged selenol system. The Pt-P bonds *trans* to the underivatised sulfide (2.281(1), 2.284(1) Å) are substantially shorter than those *trans* to the tel-

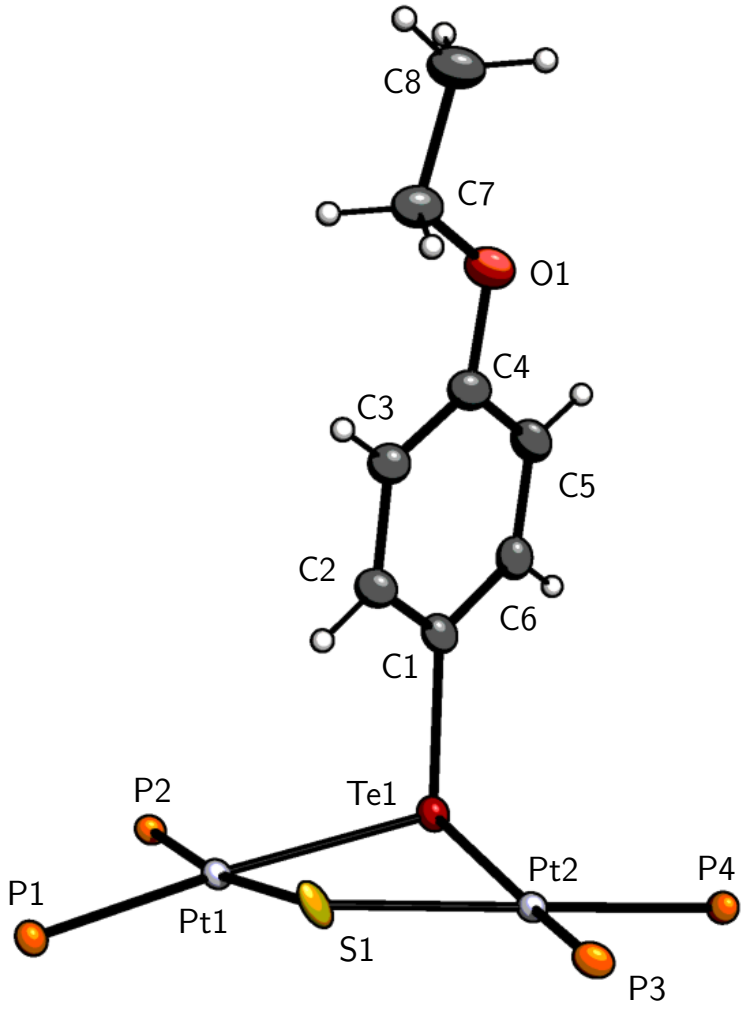

Figure 5.19: Crystal structure of **19**[BF_4]·(^{i}PrOH)$_2$. The solvent, BF_4^- anion, and phenyl rings of the PPh_3 ligands omitted for clarity. Thermal ellipsoids displayed at 50% occupancy.

lurolate (2.308(1), 2.302(1) Å). The square-planar geometry of both platinum centers appears to be distorted by the larger tellurolate ligand, evidenced by Te-Pt-P angles (93.03(3) and 93.24(3)° for Te1-Pt2-P4 and Te1-Pt1-P2 respectively) larger than S-Pt-P angles (89.12(4) and 87.54(4)° for S1-Pt2-P3 and S1-Pt1-P1 respectively). The τ_4' parameters[141] of 0.14 and 0.17 for Pt1 and Pt2 respectively show moderate distortion from square-planar in the latter. The Te1-C1 bond of 2.120(5) Å is slightly shorter than the mean ($\mu = 2.138$ Å) of 20 similar Pt-Te-C(aryl) structural moieties (15 structures) in the CSD.

The 4-ethoxyphenyl-tellurolate ligand is not oriented symmetrically about the $\{Pt_2STe\}$ core, and is slightly tilted by 14.7(4)° through the S1-Te1-C1-C2 torsion. Upon a close inspection of the packing arrangement in the unit cell, there appears to be a bifurcated intermolecular non-covalent interaction between the centrosymmetric cations consisting of a π-π and O···π component (Figure 5.20). The π-π interaction is between the electron rich 4-ethoxyphenyl ring and a phenyl ring of P2′ in a parallel displaced arrangement having an interplanar angle of 12.47°. The centroid-centroid distance of 4.339 Å is longer than typically encountered for sig-

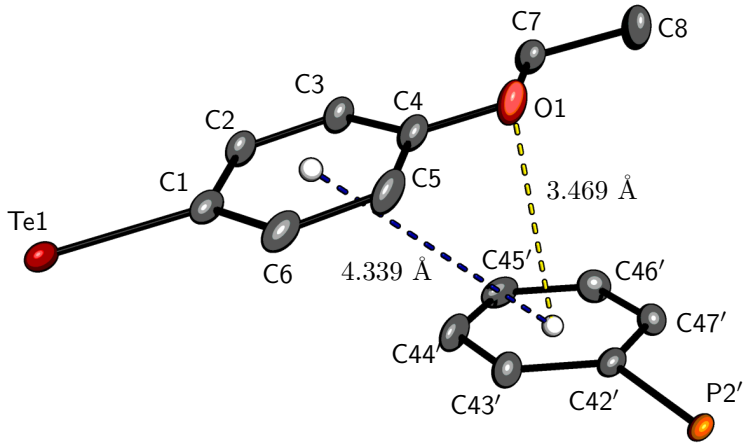

Figure 5.20: A cropped view of the crystal structure of **19**[BF_4]·(^{i}PrOH)$_2$ showing the intermolecular π-π (*blue*) and O-π (*yellow*) contacts between the tellurolate-ethoxyphenyl ligand, O1, and a phenyl ring of P2′, inversion symmetry $[1-x, 1-y, 1-z]$. Thermal ellipsoids at 50% probability.

nificant parallel displaced π-π interactions (3-4 Å),[309] but is well within the range observed for weaker such interactions,[345] especially those stabilising macromolecular crystal packing arrangements.[346] Additionally, there appears to be a significant O···π interaction between the ethoxy O1 and the same phenyl ring of P2′. These interactions are not as well described in the literature as other π- non-covalent interactions,[347] and result from a reduced electronic density on the oxygen such that a stabilising interaction with the π-cloud of an aryl ring can exist. O1 is positioned 3.469 Å above and 7.5° off a normal of the centroid of the phenyl ring C42′-C47′. Although the distance is slightly longer than the sum of van der Waals radii (3.22 Å), the observed parameters are consistent with the previously described O···π interactions.[347]

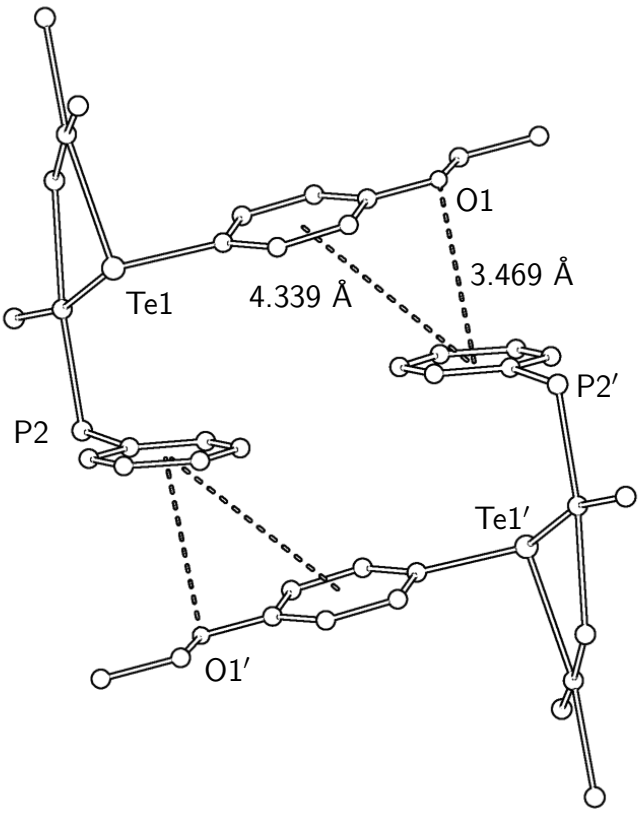

Figure 5.21: A cropped depiction of the crystal packing arrangement in **19**[BF_4] · (^{i}PrOH)$_2$ showing dashed π-π and O1···π intermolecular interactions.

Table 5.2: Selected bond lengths (Å), angles (°), and torsions (°) for the crystal structure of **19**$[BF_4] \cdot ({}^{i}PrOH)_2$.

Te1-C1	2.120(5)	Pt2-Te1-C1	94.0(1)
S1-Pt2	2.359(1)	Pt2-S1-Pt1	104.87(4)
S1-Pt1	2.357(1)	Pt2-Te1-Pt1	91.87(1)
Te1-Pt1	2.5949(4)	Te1-Pt2-P4	93.03(3)
Te1-Pt2	2.6074(5)	P4-Pt2-P3	98.61(4)
Pt2-P4	2.284(1)	P3-Pt2-S1	89.12(4)
Pt2-P3	2.308(1)	P1-Pt1-S1	87.54(4)
Pt1-P1	2.302(1)	P1-Pt1-P2	99.31(4)
Pt1-P2	2.281(1)	P2-Pt1-Te1	93.24(3)
Pt2-Pt1	3.7382(5)	S1-Pt1-Te1	79.89(3)
C1-C2	1.399(6)	S1-Pt2-Te1	79.61(3)
C1-C6	1.398(8)	Pt1-Te1-C1	100.2(1)
C2-C3	1.394(7)	C7-O1-C4	116.0(4)
C3-C4	1.391(8)	O1-C4-C3	124.4(5)
C4-C5	1.408(7)	Te1-C1-C6	118.3(3)
C5-C6	1.386(7)	Te1-C1-C2	122.8(4)
C4-O1	1.359(6)		
O1-C7	1.431(6)	Pt2-Te1-S1-Pt1	160.99(4)
C7-C8	1.502(7)	S1-Te1-C1-C2	14.7(4)

5.5 Hydrazine

After the serendipitous observation by ESIMS of the proposed bridging hydrazine species $[Pt_2(\mu\text{-}S)(\mu\text{-}N_2H_3)(PPh_3)_4]^+$ **21** in the workup of selenol and tellurol substitution reactions with **2**, a separate experiment was carried out to isolate and characterise **21**. There are several examples in the literature of dimetallic Pt^{II} complexes bridged by hydrazine ligands, such as the $Pt{-}NH_2{-}NH_2{-}Pt$ moiety, reported as bridging a dinuclear dimer **49a**,[348] and bridging two Pt^{II} mononuclear fragments **49b**.[349] Several complexes have also been reported with a bridging hydrazido ligand $R_2N{-}NH^-$ in $[Pt_2(\mu\text{-}NH{-}NH_2)_2(P^{\frown}P)]^{2+}$ **51** ($P^{\frown}P$ = dppm, dppp, dppb)[350] and mixed-bridged $[Pt_2(\mu\text{-}OH)(\mu\text{-}NH{-}NRR')dppp]^{2+}$ **52** (R = R′ = Me; R = Ph, R′ = H).[351] Less closely related bridging pyrazolato complexes of the type $[Pt_2Ar_2(\mu\text{-}Cl)(\mu\text{-}N{-}N)(PR_3)_2]^+$ (Ar = Ph or *p*-C_6H_4OMe; N-N = pyrazolate, 3,5-dimethylpyrazolate, or 3,4,5-trimethylpyrazolate; PR_3 = tertiary phosphine) **50** X = Cl have also been reported.[352] A similar series of chalcogenide-bridged pyrazolato complexes $[Pt_2Cl_2(\mu\text{-}ER')(\mu\text{-}N{-}N)(PR_3)_2]$ (E = O, S, Se, Te; R′ = alkyl or aryl, N-N = pyrazolate;

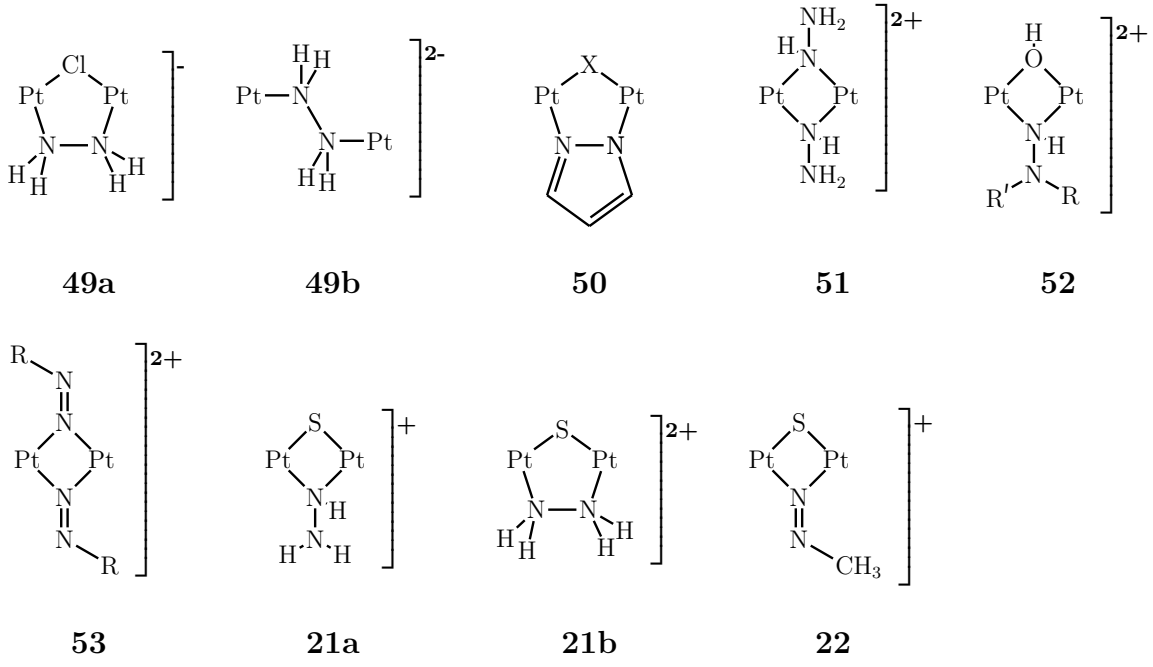

Figure 5.22: Structures referenced from the literature, and proposed structures for the observed cations at *m/z* 1501 (**21**) and 1513 (**22**).

PR_3 = tertiary phosphine) **50** X = ER' are also known.[353]

A freshly prepared hydrazine solution was added dropwise into a stirred clear-red solution of **2** in methanol resulting in a rapid change of color to pale-yellow while remaining clear. The reaction was monitored by ESIMS after 10 minutes giving the spectrum in Figure 5.23, confirming the reaction proceeds rapidly and quantitatively generates the preponderant cation at m/z 1501, tentatively proposed as the hydrazido derivative **21**. Although the dication of **2** at m/z 798 was not detected at a significant intensity (r.i. < 1%), the species $[Pt_2(\mu\text{-}S)(\mu\text{-}Cl)(PPh_3)_4]^+$ appears to be present, evidenced by a small deviation in the observed spectrum from the calculated isotope pattern of **21** around m/z 1506 (Figure 5.23 *right inset*). The protonated hydrazido dication, **21** + H^+, is also observed at m/z 751 at a low relative intensity. It must be noted, doubly oxidised $[Pt_2(\mu\text{-}S)_2(PPh_3)_4]^{2+}$ ($\mathbf{1a}^{2+}$) has a very similar m/z ($\Delta m/z \approx 0.03$) and isotope pattern, although the presence of

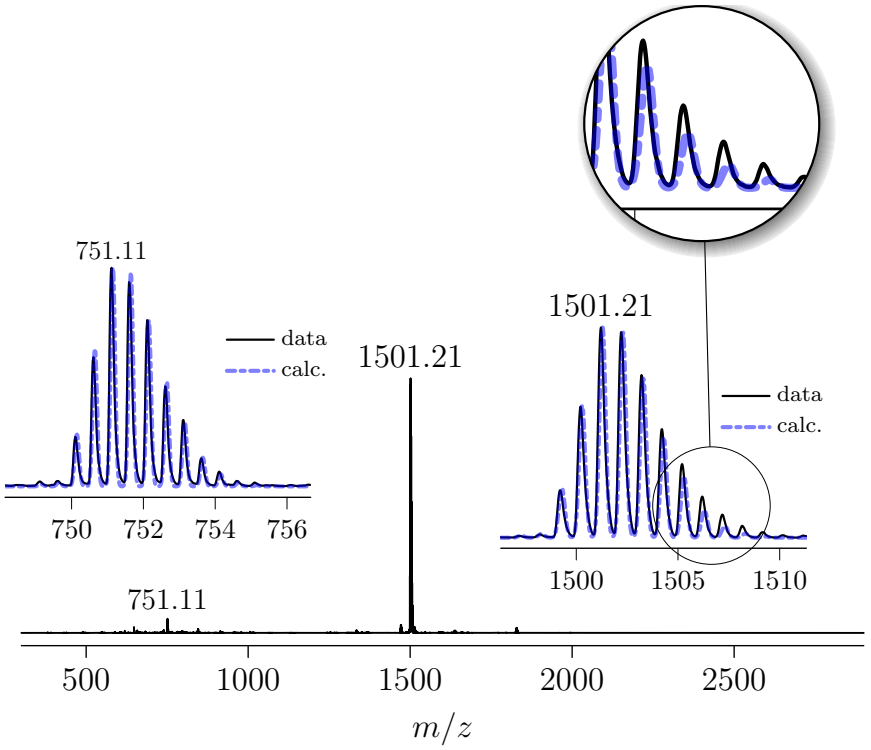

Figure 5.23: ESI mass spectrum of **2** and hydrazine hydrate, capillary exit 90 V. The insets are comparisons of peaks observed in the spectrum at m/z 751 and m/z 1501 and calculated isotope patterns for (*left*) $[Pt_2(\mu\text{-}S)(\mu\text{-}N_2H_4)(PPh_3)_4]^{2+}$ and (*right*) $[Pt_2(\mu\text{-}S)(\mu\text{-}N_2H_3)(PPh_3)_4]^+$ (**21**).

this species seems unlikely considering the reducing environment and conversion of **1a** in the reaction workup to **2**. Considering the mild ionising conditions employed, the data suggest **21** has a bridging hydrazido ligand $(\mu\text{-NH}{-}\text{NH}_2)^-$ (**21a**) which can be protonated, presumably at the free NH_2 group, to give the dication.

Alternatively, the bridging $NH_2{-}NH_2$ configuration of **21b** is also possible, however dicationic species typically appear at much higher relative intensities under such gentle conditions. The cation at *m/z* 1514, tentatively assigned as a bridging methylazo species $[Pt_2(\mu\text{-S})(\mu\text{-N=NCH}_3)(PPh_3)_4]^+$ **22**, appears at a much lower relative intensity than when initially observed in Figure 5.7. This proposed species is similar to the reported bridging phenylazo complexes $[Pt_2(\mu\text{-N=N}{-}R)_2(PPh_3)_4]^{2+}$ (**53**, R = Ar)[354] and μ-N=NH azo complex (**53**, R = H).[355] In the latter complex, synthesised from *cis*-$[(Ph_3P)_2PtCl_2]$ and hydrazine in ethanol, a bridging $NH{-}NH_2^-$ ligand was discounted by examination of ν_{NH} absorptions.[355b] Both the arylazo and μ-N=NH species readily engage in hydrogenation when exposed to olefins, resulting in the evolution of N_2 and a mononucler platinum(II)-hydrido $[(Ph_3P)_3PtH]^+$ species.[354,355]

The reaction solution was investigated further by increasing the capillary exit

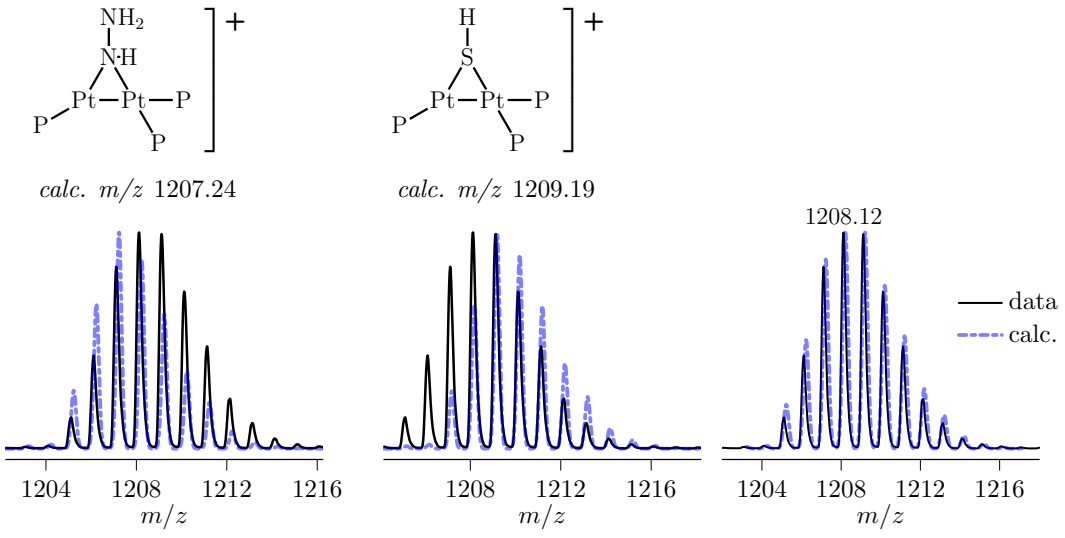

Figure 5.24: An isotope pattern comparison of the fragmentation cation observed at *m/z* 1208.12 (capillary exit voltage 210V) and (*left*) $[Pt_2(\mu\text{-NH}{-}NH_2)(PPh_3)_3]^+$, (*center*) $[Pt_2(\mu\text{-SH})(PPh_3)_3]^+$, and (*right*) a 57:43 combination respectively.

voltage to 210V. Notably, the triphenylphosphine loss cations, typically observed as the dominant fragmentation species for derivatives of $[Pt_2(\mu\text{-}S)_2(PPh_3)_4]$ **1a**, are instead predominantly observed concomitant with the loss of one bridging ligand (μ-S^{2-} or $(\mu\text{-}NH{-}NH_2)^-$). In the first isolated μ-amino mixed-bridged complex $[Pt_2(\mu\text{-}S)(\mu\text{-}NH_2)(PPh_3)_4]^+$, a similar fragmentation behaviour was observed in the loss of μ-NH_2, presumed to be as NH_3, in addition to PPh_3 loss.[42c] As can be seen in Figure 5.24, calculated isotope patterns for both $[Pt_2(\mu\text{-}NH{-}NH_2)(PPh_3)_3]^+$ (**54b** calc. m/z 1207.24) and $[Pt_2(\mu\text{-}SH)(PPh_3)_4]^+$ (**54a** calc. m/z 1209.18) provide only partial

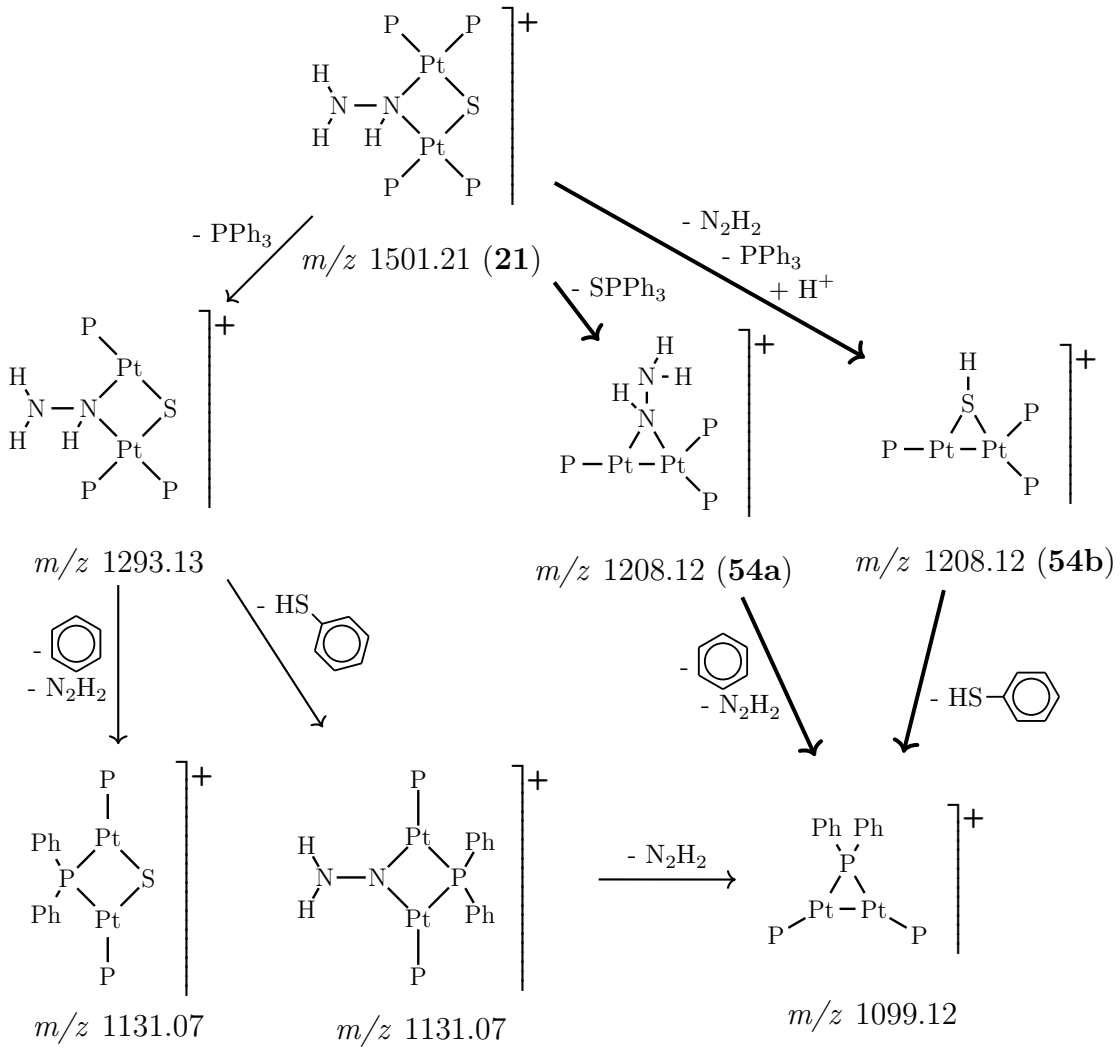

Scheme 5.3: Proposed fragmentation pathways for **21**. Given m/z correspond to the observed peak from which ion assignments were made. Bold arrows indicate dominant path, P = PPh_3.

agreement with the observed isotope pattern at m/z 1208.12. Hence, this peak was successfully modelled as a superposition of **54b** and **54a** in a proportion slightly favoring the former cation. Triphenylphosphine loss from the parent cation **21** is still observed at m/z 1293.13, however at a significantly reduced relative intensity with respect to the combined signal of **54** (3.5 cf. 13.6% r.i. respectively). Also notable in the spectrum is a cation at m/z 718, assigned as the mononuclear cyclometallated $[(Ph_3P)PtPPh_2C_6H_4]^+$, a species that is often observed in harsh fragmentation conditions for mono- and di-nuclear Pt^{II} triphenylphosphine complexes[174,356] and is indicative of complete scission and μ-ligand loss of the parent dimer **21**.

The capillary exit voltage was further increased to 240V to promote additional fragmentation, and an immediate change was observed in the recorded spectrum

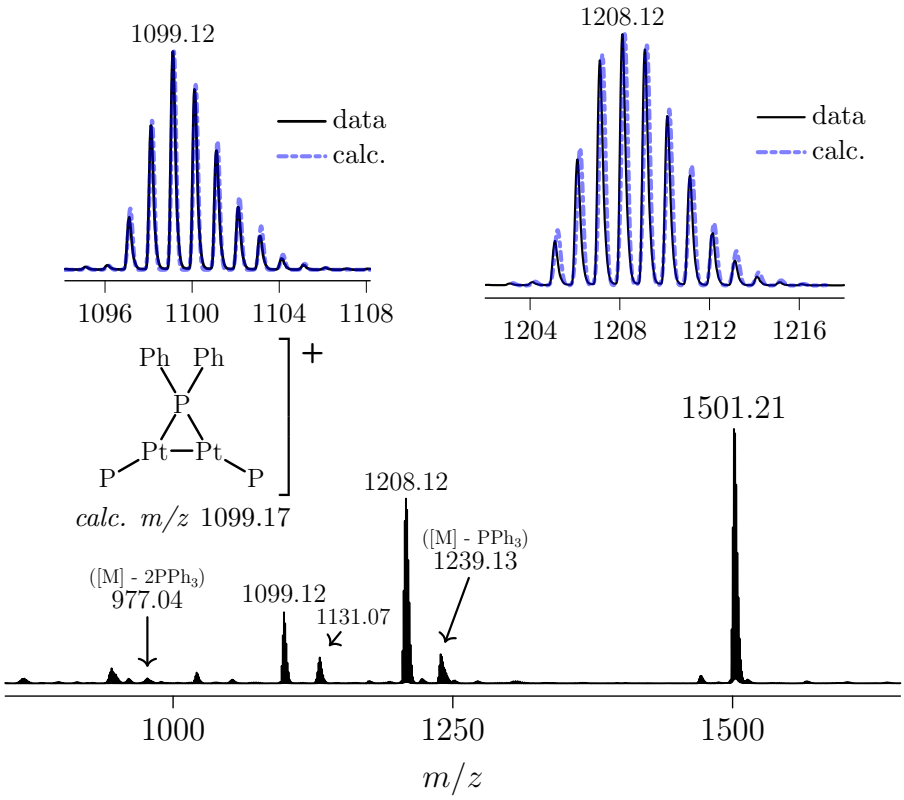

Figure 5.25: ESI mass spectrum of **2** and hydrazine hydrate in methanol, capillary exit voltage 240 V. The insets are comparisons of observed peaks at m/z 1099.12 and 1208.12 and calculated isotope patterns for (*left*) $[Pt_2(\mu\text{-}PPh_2)(PPh_3)_2]^+$ and a combined pattern for $[Pt_2(\mu\text{-}NH{-}NH_2)(PPh_3)_3]^+$ and $[Pt_2(\mu\text{-}SH)(PPh_3)_3]^+$ (*approx.* 63:37) respectively.

with the cations at *m/z* 1099.12 and 1137.07 increasing in relative intensity to 30 and 10% respectively (Figure 5.25). The former is tentatively assigned as $[(Ph_3P)_2\text{-}Pt_2(\mu\text{-}PPh_2)]^+$ (calc. *m/z* 1099.17) and is proposed to result from P-C activation and loss of $C_6H_5^+$, presumably concomitant with $\mu\text{-}L^-$, from fragment ions **54** such that **54b** loses benzene and N_2H_2 while **54a** loses thiophenol. These types of $[Pt_2\mu\text{-}P]^+$ complexes with μ-diphenylphosphido ligands are well known.[357] The cation at *m/z* 1131.07 appears to also be a composite of nearly coincident cations, tentatively assigned as $[Pt_2(\mu\text{-}S)(\mu\text{-}PPh_2)(PPh_3)_2]^+$ (calc. *m/z* 1131.14) and $[Pt_2(\mu\text{-}N_2H_2)(\mu\text{-}PPh_2)(PPh_3)_2]^+$ (calc. *m/z* 1129.19). A model composed of approximately 3:1 agrees sufficiently with the observed isotope pattern (Figure 5.26). Further evidence that the cation at *m/z* 1208.12, tentatively assigned as a composite of **54b** and **54a**, does indeed consist of overlapping ions is manifest in a morphologically different isotope pattern from the pattern observed at a capillary exit voltage of 210V. A model constructed with a ratio of approximately 63:37 for **54b**:**54a** agrees sufficiently with the observed pattern, indicating a comparatively higher stability for the **54b**

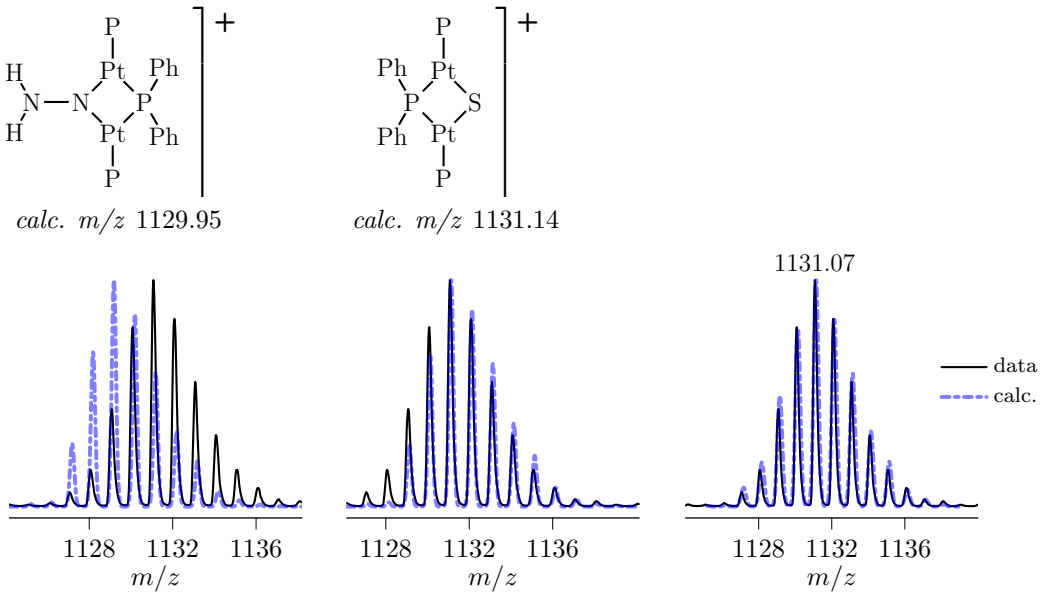

Figure 5.26: A comparison of the cation observed at *m/z* 1131.07 in Figure 5.25 and calculated isotope patterns for *left* $[Pt_2(\mu\text{-}N{-}NH_2)(\mu\text{-}PPh_2)(PPh_3)_2]^+$, *center* $[Pt_2(\mu\text{-}S)(\mu\text{-}PPh_2)(PPh_3)_2]^+$, and *right* a 1:3 combination respectively. P = PPh_3.

at elevated capillary exit voltages. Several possibilities exist for the structure of the cations in **54**.

Considering the unusual behaviour of **21** under fragmentation conditions, it seems a reasonable proposition that the observed μ-L ligand loss from the {Pt_2-(μ-S)(μ-N_2H_3)} core of **21** results in reductive Pt-Pt bond formation for the cations $[Pt_2(\mu\text{-L})(PPh_3)_3]^+$ (L = S + H^+ **54a**, NH−NH_2 **54b**). Such Pt^I-Pt^I complexes are known,[14,17] and have been observed previously in reductive elimination reactions of **1a** derivative $[Pt_2(\mu_3\text{-S})_2Co(Cl)_2(PPh_3)_4]^+$ with CO.[28] Alternatively, fragmentation loss of L could result in a bridging hydride species of the type $[Pt_2(\mu\text{-L})(\mu\text{-H})(PPh_3)_3]^+$ (L = S (**54a**), N−NH_2 or NH−NH (**54b**)). Interestingly, the parent cation **21** appears not to undergo near-complete fragmentation at an elevated capillary exit voltage of 240V, evidenced by the base peak still being $[M]^+$, purporting a moderate stability of the mixed-bridged cation in these conditions. The very low intensity of triphenylphosphine loss cations ([M] - $n$$PPh_3$: n = 1, m/z 1239.21; 2, m/z 977.11) is unusual, and considering the predominantly observed fragmentation cations, suggests the core of **21** is acutely susceptible towards reductive elimination

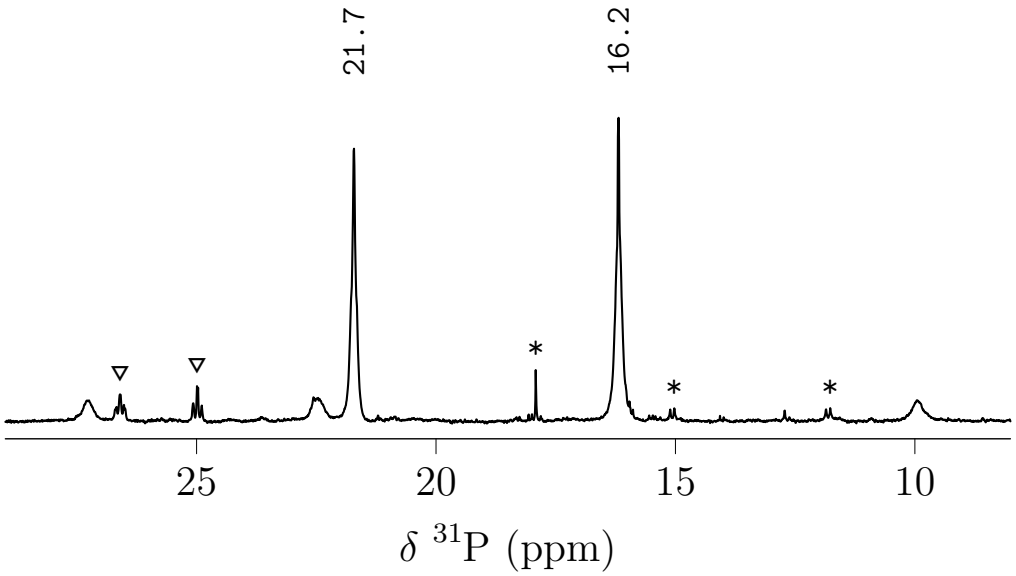

Figure 5.27: $^{31}P\{^1H\}$-NMR (242.95 MHz, $CDCl_3$) spectrum of **21**[BPh_4]. Resonances marked ▽ are $[Pt_2(\mu\text{-S})(\mu\text{-S}{-}C_6H_7N)(PPh_3)_4]^{2+}$ **2**, unassigned impurities are marked ⋆.

(μ-S^{2-} presumably lost as triphenylphosphine sulfide and likewise N_2H_3 as diazene) concomitant with terminal phosphine loss.

To further characterise **21**, a chloroform-*d* solution of the BPh_4^- salt was examined by $^{31}P\{^1H\}$ and $^{195}Pt\{^1H\}$-NMR spectroscopy. The $^{31}P\{^1H\}$-NMR spectrum appears typical for derivatives of **1a** with a $\{Pt_2(\mu\text{-}S)(\mu\text{-}L)\}$ core (L ≠ S), having two resonances δ 16.2 and 21.7 significantly separated in frequency ($\Delta\nu \approx 5.5$ ppm). Unlike the mixed-bridged derivatives **18** and **19**, the resonances appear as sharp singlets with a broad base suggesting rapid equilibration of magnetic environments. Each resonance is accompanied by ^{195}Pt satellites, the larger $^1J_{(PtP)}$ coupling constant (3042 Hz) assigned to the phosphines *trans* to the hydrazido ligand (δ 16.2) which has a smaller *trans* influence than the underivatised sulfide ($^1J_{(PtP)}$ 2692 Hz assigned to phosphines *trans* S^{2-} δ 21.7). The coupling constant of 3042 Hz compares favorably with similar μ-hydrazido complexes $[Pt_2(\mu\text{-}NH{-}NH_2)_2(P^{\cap}P)](BF_4)_2$ with chelating phosphines ($P^{\cap}P$ = dppp, 2803 Hz; dppb, 2847 Hz).[350] In the μ-phenylhydrazido complex $[Pt_2(\mu\text{-}NHNHPh)(dppp)_2](BF_4)_2$ a similar value for $^1J_{(PtP)}$ of 2860 Hz was reported.[351]

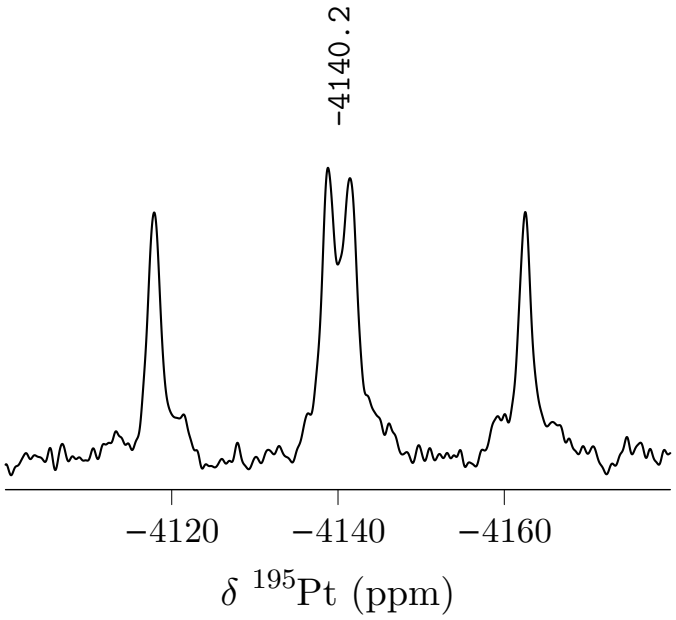

Figure 5.28: $^{195}Pt\{^1H\}$-NMR (129.02 MHz, $CDCl_3$) spectrum of **21**[BPh_4].

A close agreement for the coupling constant is also found in the amido bridged complex $[Pt_2(\mu\text{-}NH_2)(PMePh_2)_4]^+$ of 3053 Hz.[358] A favorable comparison to **21** can also be found in the mixed-bridged complex $[Pt_2(\mu\text{-}S)(\mu\text{-}NH_2)(PPh_3)_4]^+$, in which the phosphines resonated at δ 17.8 and 21.1 ppm with $^1J_{(PtP)}$ coupling constants of 3313 and 2610 Hz for P *trans* to μ-NH_2 and μ-S ligands respectively.[42c] A small amount of starting complex **2** was identified in the spectrum, consistent with the observation of $[Pt_2(\mu\text{-}S)(\mu\text{-}Cl)(PPh_3)_4]^+$ by ESIMS. Although there was no direct observation of the dication $[Pt_2(\mu\text{-}S)(\mu\text{-}S{-}C_6H_7N)(PPh_3)_4]^{2+}$ **2**, the bridging chloride species is typically observed when examining solutions of **2**, especially at elevated capillary exit voltages.

The $^{195}Pt\{^1H\}$-NMR spectrum of **21** showed one resonance at δ -4140.2 with the expected *doublet of doublet* multiplicity (Figure 5.28). The estimated $^1J_{(PtP)}$ coupling constants of 3052 and 2707 Hz compare favorably with those estimated from the $^{31}P\{^1H\}$-NMR spectrum. Additionally, a $^2J_{(PtPt)}$ coupling constant of around 900 Hz is tentatively estimated. The data appear moderately noisy, possibly a product of the broad resonance (FWHM ≈ 220 Hz), and as such $^2J_{(PtPt)}$ was estimated with the aid of Lorentzian fit functions. Regardless, a large $^2J_{(PtPt)}$ strongly suggests a four-membered $\{Pt_2(\mu\text{-}S)(\mu\text{-}N)\}$ core for **21**. A Pt-Pt separation of 3.751(1) Å was reported for the pyrazolato-bridged complex $[Pt_2Ph_2(\mu\text{-}Cl)(\mu\text{-}pz)(PMe_2Ph)_2]$ (**50**),[352] and, although not characterised structurally by XRD, the ^{195}Pt nuclei in the hydrazine-bridged complex $[Pt_2(\mu\text{-}Cl)(\mu\text{-}N_2H_4)Cl_4]^-$ (**49a**) with a similar $\{Pt_2(\mu\text{-}Cl)(\mu\text{-}NN)\}$ five-membered core showed no evidence of $^2J_{(PtPt)}$ coupling.[348] The lower field $\delta(^{195}Pt)$ of **21** compared to mono-alkylated derivatives of **1a** such as $[Pt_2(\mu\text{-}S)(\mu\text{-}S{-}C_6H_{10}OH)(PPh_3)_4]^+$ **5** (δ -4260, -4310 ppm) and $[Pt_2(\mu\text{-}S)(\mu\text{-}S{-}C_8H_8OH)(PPh_3)_4]^+$ **6** (δ -4278, -4306, -4336, -4368 ppm) is consistent with a $[PtP_2NS]$ coordination sphere.

5.6 Experimental

5.6.1 General

N-methyl-2-chloropyridinium tetrafluoroborate was synthesised *via* alkylation of 2-chloropyridine (Sigma) by the BF_4 salt of trimethyloxonium (Sigma) following a procedure in the literature.[313,314] The diaryl ditelluride $(p{-}EtOC_6H_4)_2Te_2$ was synthesised from tellurium tetrachloride following procedures in the literature.[359,360] Diphenyl ditelluride (Sigma), diphenyl diselenide (Sigma), selenourea (Sigma), and hydrazine dihydrochloride (BDH) were used as received. All reactions were carried out in ambient conditions. Reagent or laboratory grade solvents were used without purification.

5.6.2 Single crystal XRD experiments

X-ray diffraction data were collected on a Rigaku Oxford Diffraction XtaLAB-Synergy-S single crystal diffractometer with a PILATUS 200 K hybrid pixel array detector using Cu Kα radiation (λ = 1.54184 Å) at 113.8(2) K (**19**[BF_4]) and 114.5(7) K (**18**[BF_4]). The intensity data were processed with the CrysAlis PRO[207] software suite and multi-scan empirical absorption corrections were applied using spherical harmonics, implemented in the SCALE3 ABSPACK scaling algorithm. The structures were solved (**19**[BF_4] SHELXS-2008[213] using direct methods and **18**[BF_4] SHELXT-2018/2[208] using intrinsic phasing) and refined using SHELXL-2018/3[209] with full-matrix least-squares on F^2, all carried out in Olex2.[210] All non-hydrogen atoms were refined anisotropically and H atoms were included using a riding-model. Crystallographic data are tabulated in Table 5.3.

18[BF_4]$\cdot(CHCl_3)_3$

The complex crystallises in the space group $P2_1/m$ with $Z' = 0.5$ as the *tris*-chloroform solvate. In the asymmetric unit, one-half solvent molecule is disordered and lies on the mirror plane bisecting the formula unit (symmetry operation: $+x, \frac{1}{2}-y, +z$).

It was refined isotropicaly, fixing the occupancy of chlorine atoms and without the inclusion of hydrogen atoms. The other solvent molecule in the ASU was substantially disordered and could not be modelled sensibly, thus for the final refinement it was treated with the SQUEEZE[214] method of PLATON,[215] which removed 63 electrons from a void of 196 $Å^3$. The remaining largest residual peaks appear to predominantly be spurious electron density about the platinum and selenium centers.

19$[BF_4]\cdot(i\text{-PrOH})_2$

The complex crystallises in the space group $P\bar{1}$ with $Z' = 1$ and two molecules of propan-2-ol per formula unit. One molecule of solvent was positionally disordered over the same site, and was left isotropic and Refinement of the cation, anion, and solvent gave $R_1 = 0.0347$ with a large residual peak of 5.98 $e\cdot Å^{-3}$, located 0.79 Å from the underivatised sulfide S1. The difference map in Figure 5.29 shows the location of the density peak with respect to a plane passing through S1-Te1-C1 which bisects the $\{Pt_2(\mu\text{-S})(\mu\text{-TeR})\}$ core. Due to the chemically non-sensical position of

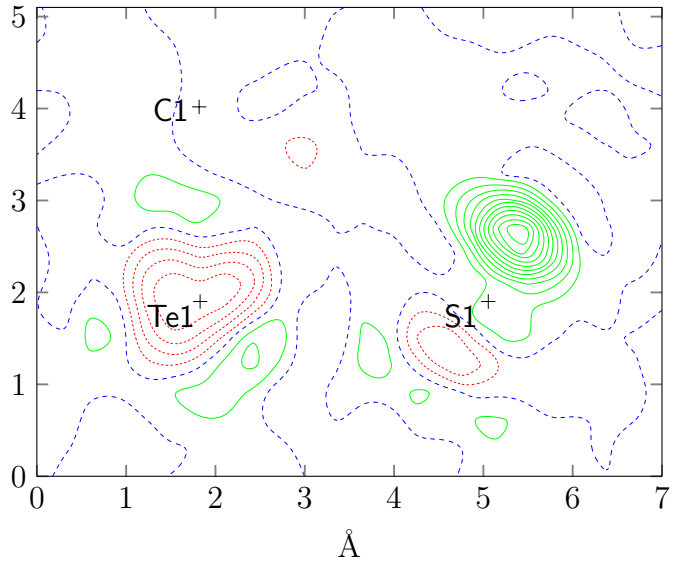

Figure 5.29: Final difference electron density map for **19**$[BF_4]\cdot(CHCl_3)_3$ at the center of the $\{Pt_2(\mu\text{-S})(\mu\text{-TeR})\}$ core, showing the S1-Te1-C1 plane. Countour levels at 0.5 $e\cdot Å^{-3}$, green is +ve (max 6 $e\cdot Å^{-3}$), red is -ve (min -1.5 $e\cdot Å^{-3}$).

the large density peak, the ADDSYM[361] routine of PLATON[215] was used to rule out a higher symmetry.

Table 5.3: Crystallographic data.

	19$[BF_4]\cdot(i\text{-}PrOH)_2$	**18**$[BF_4]\cdot(CHCl_3)_3$
Empirical formula	$C_{86}H_{77}BF_4O_3P_4Pt_2STe$	$C_{79}H_{65}BCl_3F_4P_4Pt_2SSe$
M_r $(g\cdot mol^{-1})$	1919.00	1832.55
Crystal size (mm)	0.3 x 0.08 x 0.04	0.2 x 0.1 x 0.05
Crystal system	triclinic	monoclinic
Space group	$P\bar{1}$	$P2_1/m$
a (Å)	13.41986(11)	12.54258(17)
b (Å)	16.15440(11)	23.5723(3)
c (Å)	18.83900(14)	14.20973(18)
α (°)	97.8454(6)	90
β (°)	94.7522(6)	104.3290(13)
γ (°)	104.6792(7)	90
V $(Å^3)$	3884.312(5)	4070.52(10)
Z	2	2
ρ_{calc} $(g\cdot cm^{-3})$	1.641	1.495
$\mu(CuK_\alpha)$ (mm^{-1})	11.045	9.124
$F(000)$	1884.0	1794.0
2θ range (°)	6.834 to 144.252	6.42 to 144.964
Reflections collected/unique/$[I > 2\sigma(I)]$	68168/65945/15276	33763/33742/8083
R_{int}	0.0401	0.0493
Data/parameters/restraints	15276/0/904	8083/0/453
Goodness-of-fit on F^2	1.045	1.027
Final R indices $[I > 2\sigma(I)]$	R_1 = 0.0347, wR_2 = 0.0907	R_1 = 0.0382, wR_2 = 0.0977
R indices (all data)	R_1 = 0.0350, wR_2 = 0.0910	R_1 = 0.0439, wR_2 = 0.1010
T_{min}/T_{max}	0.237/1.000	0.697/1.000
ρ_{max}/ρ_{min} $(e\cdot Å^{-3})$	5.98/-1.74	1.66/-1.70

Synthesis of *N*-methyl-2-chloropyridinium tetrafluoroborate

To a suspension of trimethyloxonium tetrafluoroborate (0.88 g, 5.6×10^{-3} mol) in dichloromethane (50 mL) was added 2-chloropyridine (0.72 g, 6.3×10^{-3} mol) and the mixture stirred at room temperature for 24 hours. Methanol (5 mL) was added and the clear colorless solution stirred for 10 minutes before removing the solvent under vacuum. The resulting white crystalline material was washed with petroleum spirits and dried under vacuum to give *N*-methyl-2-chloropyridinium tetrafluoroborate as a white powder (1.23 g, 96%). ESIMS (positive ion) *m/z* 128.05, 100%. ^{1}H-NMR (600 MHz, CD_3OD): δ 9.01 [dd, 1H, $^{3}J_{(HH)}$ 6.1, $^{4}J_{(HH)}$ 1.4 Hz], 8.54 [td, 1H, $^{3}J_{(HH)}$ 8, $^{4}J_{(HH)}$ 1.6 Hz], 8.25 [dd, 1H, $^{3}J_{(HH)}$ 8.2, $^{4}J_{(HH)}$ 1 Hz], 8.00 [m, 1H], 4.40 [s, 3H]. ^{13}C-NMR (150.91 MHz, CD_3OD): δ 149.1, 148.1, 130.8, 127.2, 48.0.

General method for preparation of methanolic $[Pt_2(\mu\text{-}S)(\mu\text{-}S{-}C_6H_7N)(PPh_3)_4][BF_4]_2$ (**2**$[BF_4]_2$) solution

To a stirred suspension of $[Pt_2(\mu\text{-}S)_2(PPh_3)_4]$ **1a** in methanol a slight molar excess of *N*-methyl-2-chloropyridinium tetrafluoroborate was added and the mixture stirred for 15 minutes giving a clear red solution. Solution was reduced under vacuum prior to examination by $^{31}P\{^{1}H\}$-NMR spectroscopy. ESIMS: (positive ion) *m/z* 797.89 $[M]^{2+}$ 100.0%, *m/z* 1505.80 $[Pt_2(\mu\text{-}S)(\mu\text{-}Cl)(PPh_3)_4]^{+}$ 35.4%, *m/z* 1681.8 $[M+BF_4]^{+}$ 8.6%. $^{31}P\{^{1}H\}$-NMR (242.95 MHz, methanol) 26.3 [m, $^{1}J_{(PtP)}$ 2590 Hz], 24.3 [m, $^{1}J_{(PtP)}$ 3750 Hz].

General method for preparation of hydrazine solution

Powdered sodium hydroxide (33.5 mg, 8.38×10^{-1} mmol) was dissolved in a small amount of distilled H_2O (1 mL) and added to a solution of hydrazine dihydrochloride (8.2 mg, 7.8×10^{-2} mmol) dissolved in methanol (5 mL). The clear colorless solution was promptly used for either reducing diaryl dichalcogenides or directly added to a solution of **2**$[BF_4]_2$.

Reaction of **2** with selenourea

In an eppendorf vial with methanol (0.5 mL), a solution of **2**$[BF_4]_2$ (≈ 0.05 mL, 0.2 mg, 1×10^{-4} mmol) in methanol was added. A small amount of triethylamine (TEA) (< 0.05 mL) was added along with selenourea (2 mg, 2×10^{-2} mmol) and the resulting mixture agitated. The reaction solution was examined by ESIMS after sitting at ambient conditions for 5 minutes, 12 hours, and 72 hours.

Reaction of *cis*-$[PtCl_2(PPh_3)_2]$ and selenourea

A solution of *cis*-$[PtCl_2(PPh_3)_2]$ (≈ 5 mg, 6×10^{-3} mmol) in 0.5 methanol was prepared in an eppendorf vial and to it added selenourea (≈ 1 mg, 8×10^{-3} mmol) and TEA (< 0.05 mL). The eppendorf vial was agitated briefly and left to sit at ambient conditions for 5 minutes before analysis by ESIMS.

Synthesis of $[Pt_2(\mu\text{-S})(\mu\text{-Se}{-}Ph)(PPh_3)_4]BF_4$ (**18**$[BF_4]$)

Diphenyldiselenide (43.1 mg, 1.38×10^{-1} mmol) was added to a freshly prepared solution of hydrazine, dissolving readily and promptly changing color from orange to colorless, before addition drop wise to a clear red solution of **2**$[BF_4]_2$ (141 mg, 7.98×10^{-2} mmol) resulting in a rapid change of color to yellow-orange, still clear. The solution was stirred for 12 hours at room temperature, after which additional sodium tetrafluoroborate (50.0 mg, 4.55×10^{-1} mmol) and distilled H_2O (5 mL) were added to effect a pale-orange precipitate which was collected by vacuum filtration, washed with distilled H_2O (2 x 20 mL) and diethyl ether (2 x 10 mL) before drying under vacuum to give pure **18**$[BF_4]$ as a pale-orange solid (98.5 mg, 72%). ESIMS (positive ion) *m/z* 1626.99, 100%. $^{31}P\{^1H\}$-NMR (242.95 MHz, $CDCl_3$): δ 30.3 [m, $^1J_{(PtP)}$ 2652 Hz], 24.7 [m, $^1J_{(PtP)}$ 3312 Hz]. $^{195}Pt\{^1H\}$-NMR (129.02 MHz, $CDCl_3$): δ -4424.8 [dd, $^1J_{(PtP,trans-S)}$ 2654, $^1J_{(PtP,trans-SePh)}$ 3306, $^2J_{(PtPt)}$ 940 Hz]. *Anal.* Found: C, 54.67; H, 3.84%. $C_{78}H_{65}BF_4Pt_2SSe$ requires: C, 54.65; H, 3.82%. Suitable crystals for a single-crystal X-ray diffraction experiment were grown from slow diffusion of diethyl ether into a chloroform solution.

Reaction of **2** with Ph_2Te_2

Ph_2Te_2 reduced with hydrazine hydrate In an eppendorf vial with methanol (0.5 mL), a solution of **2**$[BF_4]_2$ (≈ 0.05 mL, 0.2 mg, 1×10^{-4} mmol) in methanol was added. A solution of diphenyl ditelluride (≈ 0.05 mL, 0.1 mg, 2×10^{-4} mmol) was reduced by hydrazine solution before addition. The eppendorf vial was allowed to stand at ambient conditions for 10 minutes before examination by ESIMS.

No reducing agent used A similar reaction was carried out using a solution of diphenyl ditelluride in methanol. The eppendorf solution was examined by ESIMS after sitting at ambient conditions for 10 minutes.

Synthesis of $[Pt_2(\mu\text{-S})(\mu\text{-Te}-p-C_6H_4OEt)(PPh_3)_4]BF_4$ (**19**$[BF_4]$)

Di-4-ethoxyphenyl ditelluride (37.5 mg, 7.54×10^{-2} mmol) was added to a freshly prepared solution of hydrazine, dissolving readily and promptly changing color from deep-orange to very pale-yellow, before addition drop wise to a clear red solution of **2**$[BF_4]_2$ (115 mg, 6.52×10^{-2} mmol) resulting in a rapid change of color to yellow-orange, still clear. The solution was stirred for 12 hours at room temperature, after which a molar excess of sodium tetrafluoroborate (56 mg, 5.1×10^{-1} mmol) and distilled H_2O (5 mL) were added to effect a deep-orange precipitate which was collected by vacuum filtration, washed with distilled H_2O (2 x 20 mL) and diethyl ether (2 x 10 mL) before drying under vacuum to give **19**$[BF_4]$ as a red-orange solid (76.6 mg, 65%). ESIMS (positive ion) *m/z* 1720.99, 100%. $^{31}P\{^1H\}$-NMR (242.95 MHz, $CDCl_3$): δ 29.1 [m, $^1J_{(PtP)}$ *trans*-S 2820 Hz], 20.2 [m, $^1J_{(PtP)}$ *trans*-TeR 3080 Hz]. $^{195}Pt\{^1H\}$-NMR (129.02 MHz, $CDCl_3$): δ -4769 [dd, $^1J_{(PtP)}$ 2840, 3073, $^2J_{(PtPt)}$ 572 Hz]. *Anal.* Found: C, 53.19; H, 3.12%. $C_{80}H_{69}BF_4P_4Pt_2STe$ requires: C, 53.18; H, 3.85%. Suitable orange-red crystals for a single-crystal X-ray diffraction experiment were grown from layered propan-2-ol on a chloroform solution.

Reaction of **2** and hydrazine to give **21**[BPh_4]

To a freshly prepared clear red solution of **2**[BF_4]$_2$ (126 mg, 7.12×10^{-2} mmol) in methanol (15 mL) was added hydrazine solution (hydrazine dihydrochloride 10 mg, 9.5×10^{-2} mmol), resulting in a rapid change to a very pale-yellow color, still clear. After stirring for 30 minutes at ambient conditions, a slight molar excess of sodium tetraphenylborate was added resulting in the immediate formation of a yellow precipitate, the formation of which was aided by the addition of distilled H_2O (5 mL). A yellow solid was isolated by filtration on a sintered frit, and was successively with distilled H_2O (3 x 20 mL), ethanol (1 x 5 mL), and diethylether (2 x 10 mL) before drying under vacuum to give **21**[BPh_4] (106 mg, 82%). ESIMS (positive ion): *m/z* 1501.21, 100%. $^{31}P\{^1H\}$-NMR (242.95 MHz, $CDCl_3$) 21.7 [s, br, $^1J_{(PtP)}$ *trans*-S 2692 Hz], 16.2 [s, br, $^1J_{(PtP)}$ *trans*-N 3042 Hz]. $^{195}Pt\{^1H\}$-NMR (129.02 MHz, $CDCl_3$) -4140.2 [dd, $^1J_{(PtP)}$ 2707, 3052, $^2J_{(PtPt)}$ 900 Hz].

Chapter 6

Conclusion

The work reported herein provides many examples of ESIMS as an integral tool in pure inorganic chemistry. A significant caveat is of course that the system of interest is sufficiently soluble in organic solvent or H_2O and charged or easily ionisable. Throughout this thesis, ESIMS has been effectively used to screen large numbers of potential reactions quickly and in the micro-scale. This in turn, saved costly staring materials and allowed resources to be allocated to macroscopic reactions that often produced pure complexes. Additionally, ESIMS was typically found to give a reasonable picture of speciation in a reaction solution or isolated derivative, evidenced by a high consistency with acquired NMR spectra of the same sample. However care must always be taken with ESIMS when multiple ions are observed in a mass spectrum, as in the reaction between $[Pt_2(\mu\text{-}S)_2(PPh_3)_4]$ **1a** and *N*-methyl-2-chloropyridinium **14**. In this case, ESIMS detected two ions in the reaction solution ($[Pt_2(\mu\text{-}S)(\mu\text{-}Cl)(PPh_3)_4]^+$ **33** and $[Pt_2(\mu\text{-}S)(\mu\text{-}S{-}C_6H_7N)(PPh_3)_4]^{2+}$ **2**) with a roughly equal relative intensity. $^{31}P\{^1H\}$ NMR spectroscopy of the same reaction solution revealed only a trace amount of **33** to be present, the majority of the sample being **2**. Overall, ESIMS was found to be an excellent predictor when carrying out micro-scale reactions, and an excellent tool for following reaction progress over time.

6.1 Future work

Cyclohexene oxide has been shown to undergo nucleophilic ring-opening when exposed to $PhSe^-$,[178] and although this reaction was not examined with the selenide analogue of **1a** $[Pt_2(\mu\text{-}Se)_2(PPh_3)_4]$ **1b**, it is a strong candidate for further investigation. The rapid and predictable nature of substitution reactions of **2** with thiols are also a strong candidate for further examination with additional thiols, phosphines, and other suitable nucleophiles. Additionally, the selenium analogue of **2** is an attractive prospect for the expansion of the chemistry in the selenide system **1b**.

References

[1] (a) Wells, A. F., 1984; (b) Criddle, A. J.; Stanley, C. J. *Can. Mineral.* **1985**, *23*, 149–162.

[2] (a) Sellmann, D.; Geipel, F.; Heinemann, F. W. *Eur. J. Inorg. Chem.* **2000**, *2000*, 271–279; (b) Okuno, Y.; Uoto, K.; Yonemitsu, O.; Tomohiro, T. *J. Chem. Soc. Chem. Commun.* **1987**, 1018–1020; (c) Bottomley, F.; Grein, F. *Inorg. Chem.* **1982**, *21*, 4170–4178.

[3] Rauchfuss, T. B. *Inorg. Chem.* **2004**, *43*, 14–26.

[4] Wang, G.; Li, C.; Shan, H. *ACS Catal.* **2014**, *4*, 1139–1143.

[5] Dance, I.; Fisher, K. In 1994, pp 637–803.

[6] Seyferth, D.; Henderson, R. S.; Song, L. C. *Organometallics* **1982**, *1*, 125–133.

[7] (a) Chevrel, R.; Gougeon, P.; Potel, M.; Sergent, M. *J. Solid State Chem.* **1985**, *57*, 25–33; (b) Stiefel, E. I. In 1996; Vol. 653, pp 1–2.

[8] Hofmann, K. A.; Höchtlen, F. *Berichte der Dtsch. Chem. Gesellschaft* **1903**, *36*, 3090–3092.

[9] Gillard, R. D.; Wimmer, F. L. *J. Chem. Soc. Chem. Commun.* **1978**, 936–937.

[10] Chatt, J.; Hart, F. A. *J. Chem. Soc.* **1953**, 2363–2371.

[11] Chatt, J.; Hart, F. A. *Nature* **1952**, *169*, 673–674.

[12] Chatt, J.; Hart, F. A. *J. Chem. Soc.* **1960**, 2807–2814.

[13] Chatt, J.; Mann, F. G. *J. Chem. Soc.* **1938**, 1949–1954.

[14] Baird, M. C.; Wilkinson, G. *Chem. Commun.* **1966**, 514–515.

[15] Baird, M. C.; Wilkinson, G. *J. Chem. Soc. A: Inorg. Phys. Theor.* **1967**, 865–872.

[16] Skapski, A. C.; Troughton, P. G. H. *J. Chem. Soc. A: Inorg. Phys. Theor.* **1969**, 2772–2781.

[17] Chatt, J.; Mingos, D. M. P. *J. Chem. Soc. A: Inorg. Phys. Theor.* **1970**, 1243–1245.

[18] Ugo, R.; Segre, A.; Conti, F. *J. Chem. Soc. A: Inorg. Phys. Theor.* **1971**, 522–528.

[19] Briant, C. E.; Hor, T. S. A.; Howells, N. D.; Mingos, D. M. P. *J. Organomet. Chem.* **1983**, *256*, C15–C18.

[20] Bushnell, W. G.; Dixon, K. R.; Ono, R.; Pidcock, A. *Can. J. Chem.* **1984**, *62*, 696–702.

[21] Boag, N. M.; Browning, J.; Crocker, C.; Goggin, P. L.; Goodfellow, R. J.; Murray, M.; L, S. J. *J. Chem. Res., Syn.* **1978**, 228.

[22] (a) Moor, A.; Pregosin, P. S.; Venanzi, L. M. *Inorg. Chim. Acta* **1982**, *61*, 135–140; (b) Moor, A.; Pregosin, P. S.; Venanzi, L. M. *Inorg. Chim. Acta* **1981**, *48*, 153–157.

[23] Briant, C. E.; Hor, T. S. A.; Howells, N. D.; Mingos, D. M. P. *J. Chem. Soc. Chem. Commun.* **1983**, 1118–1120.

[24] Briant, C. E.; Calhorda, M. J.; Hor, T. S. A.; Howells, N. D.; Mingos, D. M. P. *J. Chem. Soc. Dalt. Trans.* **1983**, 1325–1330.

[25] Bos, W.; Bour, J. J.; Schlebos, P. P. J.; Hageman, P.; Bosman, W. P.; Smits, J. M. M.; van Wietmarschen, J. A. C.; Beurskens, P. T. *Inorg. Chim. Acta* **1986**, *119*, 141–148.

[26] (a) Zhou, M.; Xu, Y.; Tan, A.-M.; Leung, P.-H.; Mok, K. F.; Koh, L. L.; Hor, T. S. A. *Inorg. Chem.* **1995**, *34*, 6425–6429; (b) Zhou, M.; Xu, Y.; Lam, C. F.; Koh, L. L.; Mok, K. F.; Leung, P. H.; Hor, T. S. A. *Inorg. Chem.* **1993**, *32*, 4660–4662.

[27] Huang Liu; Tan, A. L.; Yan Xu; Mok, K. F.; Hor, T. *Polyhedron* **1997**, *16*, 377–382.

[28] Liu, H.; Tan, A. L.; Mok, K. F.; Hor, T. S. A. *J. Chem. Soc. Dalt. Trans.* **1996**, 4023–4026.

[29] (a) Devoy, S. M.; Henderson, W.; Nicholson, B. K.; Fawcett, J.; Hor, T. S. A. *Dalt. Trans.* **2005**, 2780–2787; (b) Gilmour, D. I.; Luke, M. A.; Mingos, D. M. P. *J. Chem. Soc. Dalt. Trans.* **1987**, 335–340; (c) Briant, C. E.; Gilmour, D. I.; Luke, M. A.; Mingos, D. M. P. *J. Chem. Soc. Dalt. Trans.* **1985**, 851–855; (d) Pilkington, M. J.; Slawin, A. M. Z.; Williams, D. J.; Woollins, J. D. *J. Chem. Soc. Dalt. Trans.* **1992**, 2425–2426.

[30] Zhou, M.; Xu, Y.; Koh, L. L.; Mok, K. F.; Leung, P. H.; Hor, T. S. A. *Inorg. Chem.* **1993**, *32*, 1875–1876.

[31] Yam, V. W.-W.; Yeung, P. K.-Y.; Cheung, K.-K. *Angew. Chemie Int. Ed. English* **1996**, *35*, 739–740.

[32] Li, Z.; Loh, Z.-H.; Fong, S. W. A.; Yan, Y.-K.; Henderson, W.; Mok, K. F.; Hor, T. S. A. *J. Chem. Soc. Dalt. Trans.* **2000**, 1027–1031.

[33] Henderson, W.; Robertson, S. H.; Nicholson, B. K. *J. Coord. Chem.* **2013**, *66*, 3412–3422.

[34] Clarke, H. M.; Henderson, W.; Nicholson, B. K. *Inorg. Chim. Acta* **2011**, *376*, 446–455.

[35] Fong, S. W. A.; Hor, T. S. A.; Henderson, W.; Nicholson, B. K.; Gardyne, S.; Devoy, S. M. *J. Organomet. Chem.* **2003**, *679*, 24–31.

[36] Henderson, W.; Oliver, A. G. *Inorg. Chim. Acta* **2011**, *378*, 121–126.

[37] Fong, S. W. A.; Yap, W. T.; Vittal, J. J.; Henderson, W.; Hor, T. S. A. *J. Chem. Soc. Dalt. Trans.* **2002**, 1826–1831.

[38] Fong, S. W. A.; Yap, W. T.; Vittal, J. J.; Hor, T. S. A.; Henderson, W.; Oliver, A. G.; Rickard, C. E. F. *J. Chem. Soc. Dalt. Trans.* **2001**, 1986–2002.

[39] Pham, K.; Henderson, W.; Nicholson, B. K.; Hor, T. S. A. *J. Organomet. Chem.* **2007**, *692*, 4933–4942.

[40] Henderson, W.; Chong, S. H.; Hor, T. S. A. *Inorg. Chim. Acta* **2006**, *359*, 3440–3450.

[41] Rose, S. L.; Henderson, W.; Nicholson, B. K.; Hor, T. S. A. *Inorg. Chim. Acta* **2009**, *362*, 5237–5244.

[42] (a) Hor, T. S. A. *J. Clust. Sci.* **1996**, *7*, 263–292; (b) Fong, S. W. A.; Hor, T. S. A. *J. Chem. Soc. Dalt. Trans.* **1999**, 639–651; (c) Henderson, W.; Oliver, A. G. *Inorg. Chim. Acta* **2014**, *416*, 49–56; (d) Henderson, W.; Nicholson, B. K.; Tiekink, E. R. T. *Inorg. Chim. Acta* **2006**, *359*, 204–214; (e) Li, Z.; Audi Fong, S. W.; Yeo, J. S. L.; Henderson, W.; Mok, K. F.; Hor, T. S. A. In Leigh, G. J., Winterton, N., Eds.; Royal Society of Chemistry, Cambridge: 2002; Chapter 8, pp 355–364; (f) González-Duarte, P.; Lledós, A.; Mas-Ballesté, R. *Eur. J. Inorg. Chem.* **2004**, *2004*, 3585–3599.

[43] Mas-Ballesté, R.; Aullón, G.; Champkin, P. A.; Clegg, W.; Mégret, C.; González-Duarte, P.; Lledós, A. *Chem. Eur. J.* **2003**, *9*, 5023–5035.

[44] Yeo, J. S. L.; Li, G.; Yip, W.-H.; Henderson, W.; Mak, T. C. W.; Hor, T. S. A. *J. Chem. Soc. Dalt. Trans.* **1999**, 435–442.

[45] Zhou, M.; Fui Lam, C.; Mok, K. F.; Leung, P. H.; Hor, T. S. A. *J. Organomet. Chem.* **1994**, *476*, c32–c34.

[46] Novio, F.; Mas-Balleste, R.; Gallardo, I.; Gonzalez-Duarte, P.; Lledos, A.; Vila, N. *Dalt. Trans.* **2005**, 2742–2753.

[47] Jeram, S.; Henderson, W.; Nicholson, B. K.; Hor, T. S. A. *J. Organomet. Chem.* **2006**, *691*, 2827–2838.

[48] Capdevila, M.; Clegg, W.; González-Duarte, P.; Jarid, A.; Lledós, A. *Inorg. Chem.* **1996**, *35*, 490–497.

[49] Møller, C.; Plesset, M. S. *Phys. Rev.* **1934**, *46*, 618–622.

[50] Duran, N.; González-Duarte, P.; Lledós, A.; Parella, T.; Sola, J.; Ujaque, G.; Clegg, W.; Fraser, K. A. *Inorg. Chim. Acta* **1997**, *265*, 89–102.

[51] Mason, R.; Law, D.; Mingos, D. M. P. unpublished work.

[52] Capdevila, M.; Carrasco, Y.; Gonzalez-Duarte, P.; Lledos, A.; Sola, J.; Ujaque, G.; Capdevila, M.; Clegg, W.; A. Coxall, R.; Gonzalez-Duarte, P. *Chem. Commun.* **1998**, 597–598.

[53] Liu, H.; Tan, A. L.; Mok, K. F.; Mak, T. C. W.; Batsanov, A. S.; Howard, J. A. K.; Hor, T. S. A. *J. Am. Chem. Soc.* **1997**, *119*, 11006–11011.

[54] Fong, S. W. A.; Vittal, J. J.; Henderson, W.; Hor, T. S. A.; Oliver, A. G.; Rickard, C. E. F. *Chem. Commun.* **2001**, 421–422.

[55] Aullón, G.; Capdevila, M.; Clegg, W.; González-Duarte, P.; Lledós, A.; Mas-Ballesté, R. *Angew. Chemie Int. Ed.* **2002**, *41*, 2776–2778.

[56] Henderson, W.; Thwaite, S.; Nicholson, B. K.; Hor, T. S. A. *Eur. J. Inorg. Chem.* **2008**, *2008*, 5119–5124.

[57] Gukathasan, R. R.; Morris, R. H.; Walker, A. *Can. J. Chem.* **1983**, *61*, 2490–2492.

[58] Briant, C. E.; Gardner, C. J.; Hor, T. S. A.; Howells, N. D.; Mingos, D. M. P. *J. Chem. Soc. Dalt. Trans.* **1984**, 2645–2651.

[59] Yam, V. W.-W.; Yeung, P. K.-Y.; Cheung, K.-K. *J. Chem. Soc. Chem. Commun.* **1995**, 267–269.

[60] Shaver, A.; Lai, R. D.; Bird, P. H.; Wickramasinghe, W. *Can. J. Chem.* **1985**, *63*, 2555–2558.

[61] Mas-Ballesté, R.; Capdevila, M.; Champkin, P. A.; Clegg, W.; Coxall, R. A.; Lledós, A.; Mégret, C.; González-Duarte, P. *Inorg. Chem.* **2002**, *41*, 3218–3229.

[62] (a) Chong, S. H.; Tjindrawan, A.; Hor, T. S. A. *J. Mol. Catal. A Chem.* **2003**, *204–205*, 267–277; (b) Henderson, W.; Nicholson, B. K.; Ujam, O. T. *J. Coord. Chem.* **2011**, *64*, 2771–2781; (c) Ujam, O. T.; Devoy, S. M.; Henderson, W.; Nicholson, B. K.; Hor, T. S. A. *Dalt. Trans.* **2012**, *41*, 12773.

[63] Deadman, B. J.; Henderson, W.; Nicholson, B. K.; Petchell, L. E.; Rose, S. L.; Hor, T. S. A. *Inorg. Chim. Acta* **2010**, *363*, 637–644.

[64] Chong, S. H.; Young, D. J.; Hor, T. S. A. *Chem.–Asian J.* **2007**, *2*, 1356–1362.

[65] Chong, S. H.; Koh, L. L.; Henderson, W.; Hor, T. S. A. *Chem.–Asian J.* **2006**, *1*, 264–272.

[66] Chong, S. H.; Henderson, W.; Hor, T. S. A. *Eur. J. Inorg. Chem.* **2007**, *2007*, 4958–4964.

[67] Henderson, W.; Oliver, A. G. *Inorg. Chim. Acta* **2011**, *375*, 248–255.

[68] Henderson, W.; Nicholson, B. K.; Devoy, S. M.; Hor, T. S. A. *Inorg. Chim. Acta* **2008**, *361*, 1908–1914.

[69] Li, J.; Li, F.; Koh, L. L.; Hor, T. S. A. *Dalt. Trans.* **2010**, *39*, 2441–2448.

[70] Liu, H.; Tan, A. L.; Cheng, C. R.; Mok, K. F.; Hor, T. S. A. *Inorg. Chem.* **1997**, *36*, 2916–2918.

[71] Fong, S. W. A.; Evans, K.; Henderson, W.; Nicholson, B. K.; Hor, T. S. A. *Inorg. Chim. Acta* **2010**, *363*, 301–307.

[72] Henderson, W.; Hor, T. S. A. *Inorg. Chim. Acta* **2014**, *411*, 199–211.

[73] (a) Yeo, J. S. L.; Vittal, J. J.; Henderson, W.; Hor, T. S. A. *Inorg. Chem.* **2002**, *41*, 1194–1198; (b) Yeo, J. S. L.; Vittal, J. J.; Henderson, W.; Hor, T. S. A. *J. Organomet. Chem.* **2002**, *659*, 92–94; (c) Yeo, J. S. L.; Vittal, J. J.; Henderson, W.; Hor, T. S. A. *J. Chem. Soc. Dalt. Trans.* **2002**, 328–336; (d) Yeo, J. S. L.; Vittal, J. J.; Henderson, W.; Hor, T. S. A. *Organometallics* **2002**, *21*, 2944–2949; (e) Yeo, J. S. L.; Vittal, J. J.; Henderson, W.; Hor, T. S. A. *J. Chem. Soc. Dalt. Trans.* **2001**, 315–321.

[74] (a) Ma, A. L.; Thoden, J. B.; Dahl, L. F. *J. Chem. Soc. Chem. Commun.* **1992**, 1516–1518; (b) Nishitani, C.; Shizuka, T.; Matsumoto, K.; Okeya, S.; Kimoto, H. *Inorg. Chem. Commun.* **1998**, *1*, 325–327; (c) Adams, R. D.; Wolfe, T. A.; Eichhorn, B. W.; Haushalter, R. C. *Polyhedron* **1989**, *8*, 701–703.

[75] Khanna, A.; Khandelwal, B. L.; Saxena, A. K.; Singh, T. P. *Polyhedron* **1995**, *14*, 2705–2710.

[76] Bencini, A.; Vaira, M. D.; Morassi, R.; Stoppioni, P. *Polyhedron* **1996**, *15*, 2079–2086.

[77] Fong, S. W. A.; Hor, T. S. A.; Devoy, S. M.; Waugh, B. A.; Nicholson, B. K.; Henderson, W. *Inorg. Chim. Acta* **2004**, *357*, 2081–2090.

[78] Fortney-Zirker, R. G.; Henderson, W.; Tiekink, E. R. T. *Inorg. Chim. Acta* **2017**, *462*.

[79] (a) Dole, M.; Mack, L. L.; Hines, R. L.; Mobley, R. C.; Ferguson, L. D.; Alice, M. B. *J. Chem. Phys.* **1968**, *49*, 2240–2249; (b) Fenn, J. B.; Mann, M.; Meng, C. K.; Wong, S. F.; Whitehouse, C. M. *Science (80-.).* **1989**, *246*, 64–71; (c) Fenn, J. B.; Mann, M.; Meng, C. K.; Wong, S. F.; Whitehouse, C. M. *Mass Spectrom. Rev.* **1990**, *9*, 37–70; (d) Fenn, J. B. *Angew Chem Int Ed Engl* **2003**, *42*, 3871–3894.

[80] Henderson, W.; McIndoe, J. S., *Mass Spectrometry of Inorganic and Organometallic Compounds: Tools - Techniques - Tips*; Inorg. Chem.: A Textbook Series; Wiley: 2005.

[81] Cech, N. B.; Enke, C. G. *Mass Spectrom. Rev.* **2001**, *20*, 362–387.

[82] White, B. C.; Harrison, D.; Henderson, W.; Nicholson, B. K.; Hor, T. S. A. *Inorg. Chim. Acta* **2010**, *363*, 2387–2393.

[83] Henderson, W.; Hor, T. S. A. *Inorg. Chim. Acta* **2010**, *363*, 1859–1863.

[84] Esselman, B. J.; Hill, N. J. *J. Chem. Educ.* **2016**.

[85] (a) Becke, A. D. *J. Chem. Phys.* **1993**, *98*, 5648–5652; (b) Parr, R. G.; Weitao, R. G. Y., 1995; (c) Koch, W., 2008.

[86] Kaduk, B.; Kowalczyk, T.; Van Voorhis, T. *Chem. Rev.* **2012**, *112*, 321–370.

[87] Roothaan, C. C. J. *Rev. Mod. Phys.* **1951**, *23*, 69–89.

[88] Bartlett, R. J. *J. Phys. Chem.* **1989**, *93*, 1697–1708.

[89] Cramer, C. J.; Truhlar, D. G. *Phys. Chem. Chem. Phys.* **2009**, *11*, 10757–10816.

[90] (a) Zhou, X.; Pan, Q.-J.; Xia, B.-H.; Li, M.-X.; Zhang, H.-X.; Tung, A.-C. *J. Phys. Chem. A* **2007**, *111*, 5465–72; (b) Akimov, A. V.; Prezhdo, O. V. *Chem. Rev.* **2015**, *115*, 5797–5890.

[91] Hohenberg, P.; Kohn, W. *Phys. Rev.* **1964**, *136*, B864–B871.

[92] Kohn, W.; Sham, L. J. *Phys. Rev.* **1965**, *140*, A1133–A1138.

[93] Kohn, W.; Becke, A. D.; Parr, R. G. *J. Phys. Chem.* **1996**, *100*, 12974–12980.

[94] (a) Becke, A. D. *J. Chem. Phys.* **1993**, *98*, 5648–5652; (b) Perdew, J. P.; Burke, K.; Ernzerhof, M. *Phys. Rev. Lett.* **1996**, *77*, 3865–3868; (c) Zhao, Y.; Schultz, N. E.; Truhlar, D. G. *J. Chem. Theory Comput.* **2006**, *2*, 364–382.

[95] Perdew, J. P.; Ruzsinszky, A.; Tao, J.; Staroverov, V. N.; Scuseria, G. E.; Csonka, G. I. *J. Chem. Phys.* **2005**, *123*, 62201.

[96] Perdew, J. P.; Ruzsinszky, A.; Constantin, L. A.; Sun, J.; Csonka, G. I. *J. Chem. Theory Comput.* **2009**, *5*, 902–908.

[97] Minenkov, Y.; Singstad, A.; Occhipinti, G.; Jensen, V. R. *Dalt. Trans.* **2012**, *41*, 5526–5541.

[98] Runge, E.; Gross, E. K. U. *Phys. Rev. Lett.* **1984**, *52*, 997–1000.

[99] Marques, M. A. L.; Gross, E. K. U. *Annu. Rev. Phys. Chem.* **2004**, *55*, 427–455.

[100] Geerlings, P.; De Proft, F.; Langenaeker, W. *Chem. Rev.* **2003**, *103*, 1793–1874.

[101] Tan, A. L.; Chiew, M. L.; Hor, T. S. A. *J. Mol. Struct. THEOCHEM* **1997**, *393*, 189–196.

[102] Aullón, G.; Ujaque, G.; Lledós, A.; Alvarez, S. *Chem. Eur. J.* **1999**, *5*, 1391–1410.

[103] Mas-Ballesté, R.; Champkin, P. A.; Clegg, W.; González-Duarte, P.; Lledós, A.; Ujaque, G. *Organometallics* **2004**, *23*, 2522–2532.

[104] Nova, A.; González-Duarte, P.; Lledós, A.; Mas-Ballesté, R.; Ujaque, G. *Inorg. Chim. Acta* **2006**, *359*, 3736–3744.

[105] Nova, A.; Mas-Balleste, R.; Ujaque, G.; Gonzalez-Duarte, P.; Lledos, A. *Dalt. Trans.* **2009**, 5980–5988.

[106] Henderson, W.; Nicholson, B. K.; Fortney-Zirker, R. G.; Patel, S.; Lane, J. R.; Wyllie, M. J.; Tiekink, E. R. T. *Inorg. Chim. Acta* **2015**, *425*, 154–163.

[107] Vivekananda, K. V.; Dey, S.; Maity, D. K.; Bhuvanesh, N.; Jain, V. K. *Inorg. Chem.* **2015**, *54*, 10153–10162.

[108] Fortney-Zirker, R. G. *https://github.com/redrumrussian/isopattern* **2020**, Isopattern.

[109] Ipsen, A. *Anal. Chem.* **2014**, *86*, 5316–5322.

[110] Schrödinger, LLC The PyMOL Molecular Graphics System, Version 1.8, 2015.

[111] Inkscape Developers Inkscape, 2022.

[112] Willcott, M. R. *Journal of the American Chemical Society* **2009**, *131*, 13180–13180.

[113] Chauhan, P.; Mahajan, S.; Enders, D. *Chem. Rev.* **2014**, *114*, 8807–8864.

[114] Hoyle, C. E.; Lowe, A. B.; Bowman, C. N. *Chem. Soc. Rev.* **2010**, *39*, 1355–1387.

[115] (a) Luly, J. R.; Yi, N.; Soderquist, J.; Stein, H.; Cohen, J.; Perun, T. J.; Plattner, J. J. *J. Med. Chem.* **1987**, *30*, 1609–1616; (b) Hammarström, S.; Samuelsson, B.; Clark, D. A.; Goto, G.; Marfat, A.; Mioskowski, C.; Corey, E. *Biochem. Biophys. Res. Comm.* **1980**, *92*, 946–953.

[116] (a) Gabbi, C.; Ghelfi, F.; Grandi, R. *Synth. Comm.* **1997**, *27*, 2857–2863; (b) Corey, E. J.; Clark, D. A.; Goto, G.; Marfat, A.; Mioskowski, C.; Samuelsson, B.; Hammarstroem, S. *J. Am. Chem. Soc.* **1980**, *102*, 1436–1439.

[117] Gao, P.; Xu, P.-F.; Zhai, H. *Tetrahedron Lett.* **2008**, *49*, 6536–6538.

[118] Fan, R.-H.; Hou, X.-L. *J. Org. Chem.* **2003**, *68*, 726–730.

[119] Fringuelli, F.; Pizzo, F.; Tortoioli, S.; Vaccaro, L. *Tetrahedron Lett.* **2003**, *44*, 6785–6787.

[120] Azizi, N.; Khajeh-Amiri, A.; Ghafuri, H.; Bolourtchian, M. *Phosphorus. Sulfur. Silicon. Relat. Elem.* **2010**, *185*, 1550–1557.

[121] Fringuelli, F.; Pizzo, F.; Tortoioli, S.; Vaccaro, L. *J. Org. Chem.* **2003**, *68*, 8248–8251.

[122] (a) Ranu, B. C.; Mandal, T.; Banerjee, S.; Dey, S. S. *Australian Can. J. Chem.* **2007**, *60*, 278–283; (b) Yang, M.-H.; Yan, G.-B.; Zheng, Y.-F. *Tetrahedron Lett.* **2008**, *49*, 6471–6474.

[123] Henderson, W.; Nicholson, B. K.; Bridson, J. H.; Kueh, J. T.; Hor, T. S. A. *Inorg. Chim. Acta* **2011**, *375*, 142–149.

[124] (a) Yeo, J. S. L.; Vittal, J. J.; Henderson, W.; Hor, T. S. A. *Inorg. Chem.* **2002**, *41*, 1194–1198; (b) Yeo, J. S. L.; Vittal, J. J.; Henderson, W.; Hor, T. S. A. *J. Organomet. Chem.* **2002**, *659*, 92–94; (c) Yeo, J. S. L.; Vittal, J. J.; Henderson, W.; Hor, T. S. A. *J. Chem. Soc. Dalt. Trans.* **2002**, 328–336; (d) Devoy, S. M.; Henderson, W.; Nicholson, B. K. *Inorg. Chim. Acta* **2013**, *406*, 81–86; (e) Devoy, S. M.; Henderson, W.; Nicholson, B. K.; Hor, T. S. A. *Inorg. Chim. Acta* **2009**, *362*, 1194–1198; (f) Fortney-Zirker, R. G.; Henderson, W.; Nicholson, B. K. *J. Struct. Chem.* **2015**, *56*, 730–736.

[125] (a) Colton, R.; D'Agostino, A.; Traeger, J. C. *Mass Spectrom. Rev.* **1995**, *14*, 79–106; (b) Henderson, W.; Nicholson, B. K.; McCaffrey, L. J. *Polyhedron* **1998**, *17*, 4291–4313; (c) Di Marco, V. B.; Bombi, G. G. *Mass Spectrom. Rev.* **2006**, *25*, 347–379.

[126] Henderson, W.; Nicholson, B. K.; Zhang, H.; Hor, T. S. A. *Inorg. Chim. Acta* **2006**, *359*, 221–227.

[127] Cawley, J. J.; Onat, E. *J. Phys. Org. Chem.* **1994**, *7*, 395–398.

[128] Benedetti, F.; Berti, F.; Fabrissin, S.; Gianferrara, T.; Risaliti, A. *J. Org. Chem.* **1991**, *56*, 3530–3537.

[129] Benedetti, F.; Berti, F.; Risaliti, A. *Tetrahedron Lett.* **1993**, *34*, 6443–6446.

[130] (a) Dennis, M.; Hall, L. M.; Murphy, P. J.; Thornhill, A. J.; Nash, R.; Winters, A. L.; Hursthouse, M. B.; Light, M. E.; Horton, P. *Tetrahedron Lett.* **2003**, *44*, 3075–3080; (b) Al Shuhaib, Z. et al. *Tetrahedron* **2017**, *73*, 845–852.

[131] (a) Merrill, G. N. *J. Phys. Org. Chem.* **2004**, *17*, 241–248; (b) Merrill, G. N. *J. Phys. Org. Chem.* **2007**, *20*, 19–29; (c) Shields, E. S.; Merrill, G. N. *J. Phys. Org. Chem.* **2007**, *20*, 1058–1071.

[132] Ujam, O. T.; Henderson, W.; Nicholson, B. K.; Fitchett, C. M. *Inorg. Chim. Acta* **2011**, *375*, 220–227.

[133] Ujam, O. T.; Henderson, W.; Nicholson, B. K.; Hor, T. S. A. *Inorg. Chim. Acta* **2011**, *376*, 255–263.

[134] Holmes, B. T.; Padgett, C. W.; Krawiec, M.; Pennington, W. T. *Cryst. Growth Des.* **2002**, *2*, 619–624.

[135] Etter, M. C.; Baures, P. W. *J. Am. Chem. Soc.* **1988**, *110*, 639–640.

[136] Etter, M. C.; Gillard, R. D.; Gleason, W. B.; Rasmussen, J. K.; Duerst, R. W.; Johnson, R. B. *J. Org. Chem.* **1986**, *51*, 5405–5408.

[137] McCaffrey, L. J.; Henderson, W.; Nicholson, B. K.; Mackay, J. E.; Dinger, M. B. *J. Chem. Soc. Dalt. Trans.* **1997**, 2577–2586.

[138] Albright, T. A.; Freeman, W. J.; Schweizer, E. E. *J. Org. Chem.* **1975**, *40*, 3437–3441.

[139] Maciel, G. E.; James, R. V. *Inorg. Chem.* **1964**, *3*, 1650–1651.

[140] Diemoz, K. M.; Franz, A. K. *J. Org. Chem.* **2019**, *84*, 1126–1138.

[141] (a) Yang, L.; Powell, D. R.; Houser, R. P. *Dalt. Trans.* **2007**, 955–964; (b) Okuniewski, A.; Rosiak, D.; Chojnacki, J.; Becker, B. *Polyhedron* **2015**, *90*, 47–57.

[142] Ahmad, S.; Zahoor, A. F.; Naqvi, S. A. R.; Akash, M. *Mol. Divers.* **2018**, *22*, 191–205.

[143] Evans, D. A.; Michael, F. E.; Tedrow, J. S.; Campos, K. R. *J. Am. Chem. Soc.* **2003**, *125*, 3534–3543.

[144] Saleh, N.; Bast, R.; Vanthuyne, N.; Roussel, C.; Saue, T.; Darquié, B.; Crassous, J. *Chirality* **2018**, *30*, 147–156.

[145] Fürst, A.; Plattner, P. A. *Helv. Chim. Acta* **1949**, *32*, 275–283.

[146] Zhou, Z.; Li, Z.; Li, K.; Yang, Z.; Zhao, G.; Wang, L.; Zhou, Q.; Tang, C. *Phosphorus. Sulfur. Silicon. Relat. Elem.* **2003**, *178*, 1771–1779.

[147] Li, Z.; Zhou, Z.; Li, K.; Wang, L.; Zhou, Q.; Tang, C. *Tetrahedron letters* **2002**, *43*, 7609–7611.

[148] Calvani, F.; Crotti, P.; Gardelli, C.; Pineschi, M. *Tetrahedron* **1994**, *50*, 12999–13022.

[149] Chini, M.; Crotti, P.; Flippin, L. A.; Macchia, F. *J. Org. Chem.* **1991**, *56*, 7043–7048.

[150] Hansen, T.; Vermeeren, P.; Yoshisada, R.; Filippov, D. V.; van der Marel, G. A.; Codée, J. D. C.; Hamlin, T. A. *J. Org. Chem.* **2021**, *86*, 3565–3573.

[151] Baracco, L.; Bombieri, G.; Degetto, S.; Forsellini, E.; Marangoni, G.; Paolucci, G.; Graziani, R. *J. Chem. Soc., Dalton Trans.* **1975**, 2161–2164.

[152] Borras, C.; Biosca, M.; Pamies, O.; Dieguez, M. *Organometallics* **2015**, *34*, 5321–5334.

[153] Ujam, O. T.; Devoy, S. M.; Henderson, W.; Wilkins, A. L.; Nicholson, B. K. *J. Coord. Chem.* **2011**, *64*, 2782–2790.

[154] Pregosin, P. In Webb, G., Ed.; Annual Reports on NMR Spectroscopy, Vol. 17; Academic Press: 1986, pp 285–349.

[155] Brammer, L. *Dalton Trans.* **2003**, 3145–3157.

[156] Baya, M.; Belío, Ú.; Martín, A. *Inorg. Chem.* **2014**, *53*, 189–200.

[157] Johnson, E. R.; Keinan, S.; Mori-Sánchez, P.; Contreras-García, J.; Cohen, A. J.; Yang, W. *J. Am. Chem. Soc.* **2010**, *132*, 6498–6506.

[158] Bader, R. F.; Nguyen-Dang, T. In *Advances in Quantum Chemistry*; Elsevier: 1981; Vol. 14, pp 63–124.

[159] Bader, R. F. In *Atoms in Molecules-A Quantum Theory*; Oxford University Press: London, England: 1990.

[160] Lane, J. R.; Contreras-García, J.; Piquemal, J.-P.; Miller, B. J.; Kjaergaard, H. G. *J. Chem. Theory Comput.* **2013**, *9*, 3263–3266.

[161] Arunan, E.; Desiraju, G. R.; Klein, R. A.; Sadlej, J.; Scheiner, S.; Alkorta, I.; Clary, D. C.; Crabtree, R. H.; Dannenberg, J. J.; Hobza, P.; Kjaergaard, H. G.; Legon, A. C.; Mennucci, B.; Nesbitt, D. J. *Pure Appl. Chem.* **2011**, *83*, 1619–1636.

[162] Emamian, S.; Lu, T.; Kruse, H.; Emamian, H. *J. Comp. Chem.* **2019**, *40*, 2868–2881.

[163] Azizi, N.; Saidi, M. R. *Catal. Comm.* **2006**, *7*, 224–227.

[164] Chini, M.; Crotti, P.; Giovani, E.; Macchia, F.; Pineschi, M. *Synlett* **1992**, 303–305.

[165] Gorenstein, D. G.; Luxon, B. A. In *Encyclopedia of Spectroscopy and Spectrometry (Second Edition)*, Lindon, J. C., Ed.; Academic Press: 1999, pp 2204–2212.

[166] Appleton, T. G.; Clark, H. C.; Manzer, L. E. *Coord. Chem. Rev.* **1973**, *10*, 335–422.

[167] Priqueler, J. R. L.; Butler, I. S.; Rochon, F. D. *Appl. Spectrosc. Rev.* **2006**, *41*, 185–226.

[168] Jaźwiński, J. In Webb, G., Ed.; Annual Reports on NMR Spectroscopy, Vol. 107; Elsevier Science: 2022; Chapter 5, pp 191–200.

[169] Gomez, M.; Muller, G.; Sainz, D.; Sales, J.; Solans, X. *Organometallics* **1991**, *10*, 4036–4045.

[170] Goggin, P. L.; Goodfellow, R. J.; Reed, F. J. S. *J. Chem. Soc. A: Inorg. Phys. Theor.* **1971**, 2031–2038.

[171] Koie, Y.; Shinoda, S.; Saito, Y. *Inorg. Nuc. Chem. Lett.* **1981**, *17*, 147–154.

[172] Kühl, O., *Phosphorus-31 NMR Spectroscopy: A Concise Introduction for the Synthetic Organic and Organometallic Chemist*; Springer Berlin Heidelberg: 2008.

[173] Pregosin, P. S.; Kunz, R. W. In Springer Science & Business Media: 1979.

[174] Henderson, W.; Nicholson, B. K. *Polyhedron* **1996**, *15*, 4015–4024.

[175] Ujam, O. T.; Devoy, S. M.; Henderson, W.; Nicholson, B. K.; Hor, T. S. A. *Inorg. Chim. Acta* **2010**, *363*, 3558–3568.

[176] Chong, S. H.; Henderson, W.; Hor, T. S. A. *Dalt. Trans.* **2007**, 4008–4016.

[177] Chong, S. H.; Young, D. J.; Hor, T. S. A. *J. Organomet. Chem.* **2006**, *691*, 349–355.

[178] Santi, C.; Santoro, S.; Testaferri, L.; Tiecco, M. *Synlett* **2008**, 1471–1474.

[179] Chopade, S. M.; Phadnis, P. P.; Wadawale, A.; Hodage, A. S.; Jain, V. K. *Inorg. Chim. Acta* **2012**, *385*, 185–189.

[180] Pasini*, A.; Rizzato*, S.; De Cillis, D. *Inorg. Chim. Acta* **2001**, *315*, 196–204.

[181] Battan, L.; Manassero, M.; Pasini, A. *Inorg. Chem. Comm.* **2001**, *4*, 606–609.

[182] Battan, L.; Fantasia, S.; Manassero, M.; Pasini, A.; Sansoni, M. *Inorg. Chim. Acta* **2005**, *358*, 555–564.

[183] Boeré, R. T.; Willis, C. J. *Can. J. Chem.* **1986**, *64*, 492–499.

[184] (a) Chatt, J.; Venanzi, L. M. *J. Chem. Soc.* **1955**, 2787–2793; (b) Bark, L.; Brandon, D. *Talanta* **1967**, *14*, 759–767; (c) Yeo, J. S. L.; Vittal, J. J.; Henderson, W.; Hor, T. S. A. *J. Organomet. Chem.* **2002**, *659*, 92–94.

[185] Davies, S. G.; Whitham, G. H. *J. Chem. Soc., Perkin Trans. 2: Phys. Org. Chem.* **1975**, 861–863.

[186] Bencini, A.; Lippolis, V. *Coord. Chem. Rev.* **2010**, *254*, 2096–2180.

[187] Juris, A.; Balzani, V.; Barigelletti, F.; Campagna, S.; Belser, P.; von Zelewsky, A. *Coord. Chem. Rev.* **1988**, *84*, 85–277.

[188] Juris, A.; Campagna, S.; Balzani, V.; Gremaud, G.; Von Zelewsky, A. *Inorg. Chem.* **1988**, *27*, 3652–3655.

[189] Sugihara, H.; Hiratani, K. *Coord. Chem. Rev.* **1996**, *148*, 285–299.

[190] Lavie-Cambot, A.; Cantuel, M.; Leydet, Y.; Jonusauskas, G.; Bassani, D. M.; McClenaghan, N. D. *Coord. Chem. Rev.* **2008**, *252*, 2572–2584.

[191] Mörtel, M.; Lindner, T.; Scheurer, A.; Heinemann, F. W.; Khusniyarov, M. M. *Inorg. Chem.* **2020**, *59*, 2659–2666.

[192] (a) Shen, Y.; Sullivan, B. P. *Inorg. Chem.* **1995**, *34*, 6235–6236; (b) Shen, Y.; Sullivan, B. P. *J. Chem. Ed.* **1997**, *74*, 685.

[193] Dwaraknath, S.; Tran, N.-H.; Dao, T.; Colbert, A.; Mullen, S.; Nguyen, A.; Cortez, A.; Cheruzel, L. *J. Org. Biochem.* **2014**, *136*, 154–160.

[194] Lezhnina, M. M.; Hofmann, D.; Santiago-Schübel, B.; Klauth, P.; Kynast, U. H. *New J. Chem.* **2012**, *36*, 2322–2327.

[195] Dotsenko, I. A.; Curtis, M.; Samoshina, N. M.; Samoshin, V. V. *Tetrahedron* **2011**, *67*, 7470–7478.

[196] Blades, A. T.; Ikonomou, M. G.; Kebarle, P. *Anal. Chem.* **1991**, *63*, 2109–2114.

[197] Kebarle, P.; Verkerk, U. H. *Mass Spectrom. Rev.* **2009**, *28*, 898–917.

[198] Shee, N. K.; Das, D.; Adekunle, O. F. A.; Drew, M. G. B.; Datta, D. *Inorg. Chim. Acta* **2011**, *366*, 198–202.

[199] Neese, F. *WIREs Comp. Mol. Sci.* **2022**, *12*, e1606.

[200] Perdew, J. P.; Ernzerhof, M.; Burke, K. *J. Chem. Phys.* **1996**, *105*, 9982–9985.

[201] Grimme, S.; Antony, J.; Ehrlich, S.; Krieg, H. *J. Chem. Phys.* **2010**, *132*, 154104.

[202] Grimme, S.; Ehrlich, S.; Goerigk, L. *J. Comput. Chem.* **2011**, *32*, 1456–1465.

[203] Andrae, D.; Häußermann, U.; Dolg, M.; Stoll, H.; Preuß, H. *Theor. Chim. Acta* **1990**, *77*, 123–141.

[204] Weigend, F.; Ahlrichs, R. *Phys. Chem. Chem. Phys.* **2005**, *7*, 3297.

[205] Lu, T.; Chen, F. *J. Comput. Chem.* **2012**, *33*, 580–592.

[206] Hunter, J. D. *Comput. Sci. Eng.* **2007**, *9*, 90–95.

[207] CrysAlis PRO, Rigaku Oxford Diffraction, Tokyo, Japan, 2015.

[208] Sheldrick, G. M. *Acta Crystallogr. Sect. A* **2015**, *71*, 3–8.

[209] Sheldrick, G. M. *Acta Crystallogr. Sect. C* **2015**, *71*, 3–8.

[210] Dolomanov, O. V.; Bourhis, L. J.; Gildea, R. J.; Howard, J. A. K.; Puschmann, H. *J. Appl. Cryst.* **2009**, *42*, 339–341.

[211] Bruker AXS, APEX-2, Bruker-Nonius AXS, Madison, Wisconsin, USA.

[212] Blessing, R. H. *Acta Crystallogr. Sect. A* **1995**, *51*, 33–38.

[213] Sheldrick, G. M. *Acta Crystallogr. Sect. A* **2008**, *64*, 112–122.

[214] Spek, A. *Acta Crystallogr. Sect. C* **2015**, *71*, 9–18.

[215] Spek, A. *J. Appl. Cryst.* **2003**, *36*, 7–13.

[216] De Meijere, A. *Angew. Chem., Int. Ed. in English* **1979**, *18*, 809–826.

[217] Schneider, T. F.; Kaschel, J.; Werz, D. B. *Angew. Chem., Int. Ed.* **2014**, *53*, 5504–5523.

[218] Dieter, R. K.; Pounds, S. *J. Org. Chem.* **1982**, *47*, 3174–3177.

[219] Illy, N.; Boileau, S.; Winnik, M. A.; Penelle, J.; Barbier, V. *Polymer* **2012**, *53*, 903–912.

[220] Reissig, H.-U.; Hirsch, E. *Angew. Chem., Int. Ed. in English* **1980**, *19*, 813–814.

[221] Reissig, H.-U. *Tetrahedron Lett.* **1981**, *22*, 2981–2984.

[222] Hu, X. *Tetrahedron* **2004**, *60*, 2701–2743.

[223] Bae, J. H.; Shin, S.-H.; Park, C. S.; Lee, W. K. *Tetrahedron* **1999**, *55*, 10041–10046.

[224] Kang, J.; Lee, J. W.; Kim, J. I. *J. Chem. Soc., Chem. Commun.* **1994**, 2009–2010.

[225] Marigo, M.; Wabnitz, T. C.; Fielenbach, D.; Jørgensen, K. A. *Angew. Chem., Int. Ed.* **2005**, *44*, 794–797.

[226] Smith, S. M.; Min, J.; Ganesh, T.; Diebold, B.; Kawahara, T.; Zhu, Y.; McCoy, J.; Sun, A.; Snyder, J. P.; Fu, H.; Du, Y.; Lewis, I.; Lambeth, J. D. *Chemistry & Biology* **2012**, *19*, 752–763.

[227] Tanini, D.; Capperucci, A.; Supuran, C. T.; Angeli, A. *Bioorganic Chem.* **2019**, *87*, 516–522.

[228] Chen, W.; Rosser, E. W.; Zhang, D.; Shi, W.; Li, Y.; Dong, W.-J.; Ma, H.; Hu, D.; Xian, M. *Organic Letters* **2015**, *17*, 2776–2779.

[229] Hof, R. P.; Poelert, M. A.; Peper, N. C.; Kellogg, R. M. *Tetrahedron Asymm.* **1994**, *5*, 31–34.

[230] Jin, M.-J.; Ahn, S.-J.; Lee, K.-S. *Tetrahedron Lett.* **1996**, *37*, 8767–8770.

[231] Cobb, A. J. A.; Shaw, D. M.; Longbottom, D. A.; Gold, J. B.; Ley, S. V. *Org. Biomol. Chem.* **2005**, *3*, 84–96.

[232] Movassagh, B.; Morovat, E. S. *J. Sulfur Chem.* **2011**, *32*, 117–122.

[233] Tanini, D.; Capperucci, A. *New J. Chem.* **2019**, *43*, 11451–11468.

[234] Stanković, S.; D'hooghe, M.; Catak, S.; Eum, H.; Waroquier, M.; Van Speybroeck, V.; De Kimpe, N.; Ha, H.-J. *Chem. Soc. Rev.* **2012**, *41*, 643–665.

[235] Crousse, B.; Narizuka, S.; Bonnet-Delpon, D.; Bégué, J.-P. *Synlett* **2001**, *2001*, 0679–0681.

[236] Llaveria, J.; Espinoza, A.; Negrón, G.; Isabel Matheu, M.; Castillón, S. *Tetrahedron Lett.* **2012**, *53*, 2525–2529.

[237] Wu, J.; Hou, X.-L.; Dai, L.-X. *J. Chem. Soc., Perkin Trans. 1* **2001**, 1314–1317.

[238] Albrecht, C.; Schwieger, S.; Bruhn, C.; Wagner, C.; Kluge, R.; Schmidt, H.; Steinborn, D. *J. Am. Chem. Soc.* **2007**, *129*, 4551–4566.

[239] Puddephatt, R. J. *Coord. Chem. Rev.* **1980**, *33*, 149–194.

[240] (a) Brown, D. B. *J. Organomet. Chem.* **1970**, *24*, 787–790; (b) Wiberg, K. B.; McClusky, J. V.; Schulte, G. K. *Tetrahedron Lett.* **1986**, *27*, 3083–3086; (c) Waddington, M. D.; Jennings, P. W. *Organometallics* **1982**, *1*, 1370–1373.

[241] Smith, A. B.; Scarborough, R. M. *Tetrahedron Lett.* **1978**, *19*, 4193–4196.

[242] Kobayashi, S.; Nagayama, S.; Busujima, T. *J. Am. Chem. Soc.* **1998**, *120*, 8287–8288.

[243] Bauzá, A.; Frontera, A.; Mooibroek, T. J. *Phys. Chem. Chem. Phys.* **2016**, *18*, 1693–1698.

[244] Kuznetsov, I. E.; Susarova, D. K.; Frolova, L. A.; Peregudov, A. S.; Shestakov, A. F.; Troyanov, S. I.; Stevenson, K. J.; Troshin, P. A. *Chem. Commun.* **2017**, *53*, 4830–4833.

[245] Scribner, R.; Sausen, G.; Prichard, W. *J. Org. Chem.* **1960**, *25*, 1440–1442.

[246] Goebbert, D. J.; Velarde, L.; Khuseynov, D.; Sanov, A. *J. Phys. Chem. Lett.* **2010**, *1*, 792–795.

[247] Hunt, C. T.; Matson, G. B.; Balch, A. L. *Inorg. Chem.* **1981**, *20*, 2270–2276.

[248] Choon Hong Chin; Hor, T. *J. Organomet. Chem.* **1996**, *509*, 101–104.

[249] Baratta, W.; Pregosin, P. S. *Inorg. Chim. Acta* **1993**, *209*, 85–87.

[250] Jain, V.; Rao, G. *Inorg. Chim. Acta* **1987**, *127*, 161–167.

[251] Puddephatt, R. J.; Thomson, M. A. *J. Organomet. Chem.* **1982**, *238*, 231–234.

[252] Trovo, G.; Bandoli, G.; Casellato, U.; Corain, B.; Nicolini, M.; Longato, B. *Inorg. Chem.* **1990**, *29*, 4616–4621.

[253] Jain, V. K.; Kannan, S.; Butcher, R. J.; Jasinski, J. P. *J. Chem. Soc. Dalt. Trans.* **1993**, 1509–1513.

[254] Sutton, R. B.; Henderson, W. *Inorg. Chim. Acta* **2020**, *506*, 119557.

[255] Lee, S.-K.; Jeannin, O.; Fourmigué, M.; Suh, W.; Noh, D.-Y. *J. Organomet. Chem.* **2012**, *716*, 237–244.

[256] Freeman, F. *Chem. Rev.* **1969**, *69*, 591–624.

[257] (a) Johnson, A. W.; LaCount, R. B. *J. Am. Chem. Soc.* **1961**, *83*, 417–423; (b) Corey, E. J.; Chaykovsky, M. *J. Am. Chem. Soc.* **1962**, *84*, 3782–3783; (c) Corey, E. J.; Chaykovsky, M. *J. Am. Chem. Soc.* **1965**, *87*, 1353–1364.

[258] (a) Linn, W. J.; Webster, O. W.; Benson, R. E. *J. Am. Chem. Soc.* **1963**, *85*, 2032–2033; (b) Linn, W. J.; Webster, O. W.; Benson, R. E. *J. Am. Chem. Soc.* **1965**, *87*, 3651–3656; (c) Middleton, W. J.; Buhle, E. L.; McNally, J. G.; Zanger, M. *J. Org. Chem.* **1965**, *30*, 2384–2386; (d) Achmatowicz, O.; Szymoniak, J. *Tetrahedron* **1982**, *38*, 1299–1302; (e) Li, S.; Li, P.; Xu, J. *Helv. Chim. Acta* **2019**, *102*, e1900164.

[259] Kayukov, Y. S.; Kayukova, O. V.; Kalyagina, E. S.; Bardasov, I. N.; Ershov, O. V.; Nasakin, O. E.; Tafeenko, V. A. *Russian Russ. J. Org. Chem.* **2011**, *47*, 392.

[260] Bieber, L. W.; De Araújo, M. C. F. *Molecules* **2002**, *7*, 902–906.

[261] Henderson, W.; Taylor, M. J. *Polyhedron* **1996**, *15*, 1957–1964.

[262] Menziani, M.; Cocchi, M.; De Benedetti, P. *J. Mol. Struct.: THEOCHEM* **1992**, *256*, 217–229.

[263] Beddoes, R. L.; Dalton, L.; Joule, J. A.; Mills, O. S.; Street, J. D.; Watt, C. I. F. *J. Chem. Soc., Perkin Trans. 2* **1986**, 787–797.

[264] Brameld, K. A.; Kuhn, B.; Reuter, D. C.; Stahl, M. *J. Chem. Inf. Model.* **2008**, *48*, 1–24.

[265] Petrov, V.; Petrova, V.; Girichev, G. V.; Oberhammer, H.; Giricheva, N. I.; Ivanov, S. *J. Org. Chem.* **2006**, *71*, 2952–2956.

[266] Kikkawa, S.; Okayasu, M.; Hikawa, H.; Azumaya, I. *Cryst. Growth Des.* **2021**, *21*, 1148–1158.

[267] Denehy, E.; White, J. M.; Williams, S. J. *Inorg. Chem.* **2007**, *46*, 8871–8886.

[268] Hansen, E.; Limé, E.; Norrby, P.-O.; Wiest, O. *J. Phys. Chem. A* **2016**, *120*, 3677–3682.

[269] Okbinoglu, T.; Kennepohl, P. *J. Phys. Chem. A* **2021**, *125*, 615–620.

[270] Blahun, O. P.; Rozhenko, A. B.; Rusanov, E.; Zhersh, S.; Tolmachev, A. A.; Volochnyuk, D. M.; Grygorenko, O. O. *J. Org. Chem.* **2020**, *85*, 5288–5299.

[271] Parkin, A.; Collins, A.; Gilmore, C. J.; Wilson, C. C. *Acta Crystallogr., Sect. B: Struct. Sci* **2008**, *64*, 66–71.

[272] Kato, M.; Okamura, T.-a.; Yamamoto, H.; Ueyama, N. *Inorg. Chem.* **2005**, *44*, 1966–1972.

[273] Kato, M.; Kojima, K.; Okamura, T.-a.; Yamamoto, H.; Yamamura, T.; Ueyama, N. *Inorg. Chem.* **2005**, *44*, 4037–4044.

[274] Suzuki, N.; Higuchi, T.; Urano, Y.; Kikuchi, K.; Uekusa, H.; Ohashi, Y.; Uchida, T.; Kitagawa, T.; Nagano, T. *J. Am. Chem. Soc.* **1999**, *121*, 11571–11572.

[275] Walters, M. A.; Roche, C. L.; Rheingold, A. L.; Kassel, S. W. *Inorg. Chem.* **2005**, *44*, 3777–3779.

[276] Blake, P. R.; Park, J. B.; Adams, M. W. W.; Summers, M. F. *J. Am. Chem. Soc.* **1992**, *114*, 4931–4933.

[277] Lane, J. R.; Schrøder, S. D.; Saunders, G. C.; Kjaergaard, H. G. *J. Phys. Chem. A* **2016**, *120*, 6371–6378.

[278] Andersen, C. L.; Jensen, C. S.; Mackeprang, K.; Du, L.; Jørgensen, S.; Kjaergaard, H. G. *J. Phys. Chem. A* **2014**, *118*, 11074–11082.

[279] Lehn, J. M. In 1970, pp 311–377.

[280] Rengaraju, S.; Berlin, K. D. *J. Org. Chem.* **1972**, *37*, 3304–3310.

[281] Lambert, J. B.; Packard, B. S.; Oliver, W. L. *J. Org. Chem.* **1971**, *36*, 1309–1310.

[282] Le Grel, P.; Salaün, A.; Potel, M.; Le Grel, B.; Lassagne, F. *J. Org. Chem.* **2006**, *71*, 5638–5645.

[283] Bock, H.; Nagel, N.; Näther, C. *Z. Naturforsch. B* **1998**, *53*, 1389–1400.

[284] Dittmer, D. In *Comprehensive Heterocyclic Chemistry*, Katritzky, A. R., Rees, C. W., Eds.; Pergamon: 1984, pp 131–184.

[285] Sander, M. *Chem. Rev.* **1966**, *66*, 297–339.

[286] Zoller, U. In John Wiley & Sons, Ltd: 1983; Chapter III, pp 333–629.

[287] Bryan, S. A.; Roundhill, D. M. *Acta Crystallogr. Sect. C* **1983**, *39*, 184–186.

[288] Mügge, C.; Rothenburger, C.; Beyer, A.; Görls, H.; Gabbiani, C.; Casini, A.; Michelucci, E.; Landini, I.; Nobili, S.; Mini, E.; Messori, L.; Weigand, W. *Dalton Trans.* **2011**, *40*, 2006–2016.

[289] Chen, Y.-D.; Zhang, L.-Y.; Shi, L.-X.; Chen, Z.-N. *Inorg. Chem.* **2004**, *43*, 7493–7501.

[290] Grant, G. J.; Galas, D. F.; Poullaos, I. M.; Carter, S. M.; VanDerveer, D. G. *J. Chem. Soc., Dalton Trans.* **2002**, 2973–2980.

[291] Latendresse, T. P.; Adams, S. J.; Grant, G. J.; Lee, J. P.; Oliver, A. G. *Polyhedron* **2016**, *114*, 80–87.

[292] Shao, Y. et al. *Mol. Phys.* **2015**, *113*, 184–215.

[293] Chai, J.-D.; Head-Gordon, M. *Phys. Chem. Chem. Phys.* **2008**, *10*, 6615–6620.

[294] Hay, P. J.; Wadt, W. R. *J. Chem. Phys.* **1985**, *82*, 299–310.

[295] Clark, T.; Chandrasekhar, J.; Spitznagel, G. W.; Schleyer, P. V. R. *J. Comput. Chem.* **1983**, *4*, 294–301.

[296] Ditchfield, R.; Hehre, W. J.; Pople, J. A. *J. Chem. Phys.* **1971**, *54*, 724–728.

[297] Hariharan, P. C.; Pople, J. A. *Theor. Chim. Acta* **1973**, *28*, 213–222.

[298] Hehre, W. J.; Ditchfield, R.; Pople, J. A. *J. Chem. Phys.* **1972**, *56*, 2257–2261.

[299] Francl, M. M.; Pietro, W. J.; Hehre, W. J.; Binkley, J. S.; Gordon, M. S.; DeFrees, D. J.; Pople, J. A. *J. Chem. Phys.* **1982**, *77*, 3654–3665.

[300] Gordon, M. S.; Binkley, J. S.; Pople, J. A.; Pietro, W. J.; Hehre, W. J. *J. Am. Chem. Soc.* **1982**, *104*, 2797–2803.

[301] Spitznagel, G. W.; Clark, T.; Schleyer, P. v. R.; Hehre, W. J. *J. Comput. Chem.* **1987**, *8*, 1109–1116.

[302] Humphrey, W.; Dalke, A.; Schulten, K. *J. Mol. Graph.* **1996**, *14*, 33–38.

[303] Eaborn, C.; Odell, K. J.; Pidcock, A. *J. Organomet. Chem.* **1979**, *170*, 105–115.

[304] Rigamonti, L.; Rusconi, M.; Manassero, C.; Manassero, M.; Pasini, A. *Inorg. Chim. Acta* **2010**, *363*, 3498–3505.

[305] Still, B. M.; Kumar, P. G. A.; Aldrich-Wright, J. R.; Price, W. S. *Chem. Soc. Rev.* **2007**, *36*, 665–686.

[306] Dalla Cort, A.; Mandolini, L.; Pasquini, C.; Schiaffino, L. *New J. Chem.* **2004**, *28*, 1198–1199.

[307] Szumna, A. *Chem. Soc. Rev.* **2010**, *39*, 4274–4285.

[308] Wu, Y.-T.; Hayama, T.; Baldridge, K. K.; Linden, A.; Siegel, J. S. *J. Am. Chem. Soc.* **2006**, *128*, 6870–6884.

[309] Główka, M.; Martynowski, D.; Kozłowska, K. *J. Mol. Struct.* **1999**, *474*, 81–89.

[310] Kumbhare, L. B.; Singh, U.; Singh, B. G.; Wadawale, A.; Kedarnath, G.; Zade, S. S.; Priyadarsini, K. I.; Jain, V. K. *Inorg. Chim. Acta* **2011**, *374*, 69–78.

[311] Yap, G. P.; Jensen, C. M. *Inorg. Chem.* **1992**, *31*, 4823–4828.

[312] Yamada, Y.; Matsumoto, R.; Kori, D.; Koikawa, M. *Inorg. Chim. Acta* **2021**, *515*, 120049.

[313] Tinnermann, H.; Wille, C.; Alcarazo, M. *Angew. Chem., Int. Ed.* **2014**, *53*, 8732–8736.

[314] Averesch, K. F.; Pesch, H.; Golz, C.; Alcarazo, M. *Chem. Eur. J.* **2019**, *25*, 10472–10477.

[315] Dey, S.; Jain, V. K.; Varghese, B. *J. Organomet. Chem.* **2001**, *623*, 48–55.

[316] Eisavi, R.; Zeynizadeh, B.; Baradarani, M. M. *Phosphorus. Sulfur. Silicon. Relat. Elem.* **2011**, *186*, 1902–1909.

[317] (a) Hoferkamp, L.; Rheinwald, G.; Stoeckli-Evans, H.; Suess-Fink, G. *Inorg. Chem.* **1995**, *34*, 5786–5790; (b) Hoferkamp, L. A.; Rheinwald, G.; Stoeckli-Evans, H.; Süss-Fink, G. *Organometallics* **1996**, *15*, 704–712; (c) Süss-Fink, G.; Bodensieck, U.; Hoferkamp, L.; Rheinwald, G.; Stoeckli-Evans, H. *J. Cluster Sci.* **1992**, *3*, 469–478.

[318] Okeya, S.; Kameda, H.; Kawashima, H.; Shimomura, H.; Nishioka, T.; Isobe, K. *Chem. Lett.* **1995**, *24*, 501–502.

[319] Koketsu, M.; Ishihara, H. *Curr. Org. Synth.* **2006**, *3*, 439–455.

[320] Koketsu, M. In *Handbook of Chalcogen Chemistry: New Perspectives in Sulfur, Selenium and Tellurium*, Devillanova, F. A., Du Mont, W.-W., Eds.; Royal Society of Chemistry: 2013, p 94.

[321] Rütherford, J.; Calvo, C. *Z. Kristallogr., Crystalline Mater.* **1969**, *128*, 229–258.

[322] Bibelayi, D.; Lundemba, A. S.; Allen, F. H.; Galek, P. T.; Pradon, J.; Reilly, A. M.; Groom, C. R.; Yav, Z. G. *Acta Crystallogr. Sect. B: Struct. Sci.* **2016**, *72*, 317–325.

[323] Walter, W.; Schaumann, E.; Rose, H. *Tetrahedron* **1972**, *28*, 3233–3239.

[324] (a) Krief; Derock, A.; Michel *Synlett* **2005**, *2005*, 1012–1014; (b) Krief; Derock, A.; Michel *Synlett* **2005**, *2005*, 1755–1757; (c) Jain, V. K.; Kannan, S. *J. Organomet. Chem.* **1991**, *418*, 349–357; (d) Jain, V. K.; Kannan, S. *J. Organomet. Chem.* **1991**, *405*, 265–271.

[325] Bhasin, K.; Singh, J. *J. Organomet. Chem.* **2002**, *658*, 71–76.

[326] Kubicki, M. M.; Glowiak, T. *Mater. Sci.* **1977**, *1*, 35–37.

[327] Altoum, A. O. S.; Vančo, J.; Křikavová, R.; Trávníček, Z.; Dvořák, Z.; Altaf, M.; Ahmad, S.; Sulaiman, A. A. A.; Isab, A. A. *Polyhedron* **2017**, *128*, 2–8.

[328] Henderson, W.; Nicholson, B. K.; Dinger, M. B. *Inorg. Chim. Acta* **2003**, *355*, 428–431.

[329] Fregona, D.; Graziani, R.; Faraglia, G.; Caselato, U.; Sitran, S. *Polyhedron* **1996**, *15*, 2523–2533.

[330] Braunstein, P.; Kervennal, J.; Richert, J.-L. *Angew. Chemie Int. Ed. English* **1985**, *24*, 768–770.

[331] Braunstein, P.; Richert, J.-L.; Dusausoy, Y. *J. Chem. Soc. Dalt. Trans.* **1990**, 3801–3814.

[332] Shams el din, A.; Arain, R. A. *Corros. Sci.* **1989**, *29*, 445–453.

[333] Jain, V. K.; Singhal, A.; Narayan, S. *Phosphorus. Sulfur. Silicon. Relat. Elem.* **1998**, *136*, 483–488.

[334] McFarlane, W. *Chem. Commun. (London)* **1968**, 755–756.

[335] Yeo, J. S. L.; Vittal, J. J.; Hor, T. S. A. *Eur. J. Inorg. Chem.* **2003**, 277–280.

[336] Chivers, T.; Laitinen, R. S. *Chem. Soc. Rev.* **2015**, *44*, 1725–1739.

[337] Köllemann, C.; Obendorf, D.; Sladky, F. *Phosphorus. Sulfur. Relat. Elem.* **1988**, *38*, 69–77.

[338] Beckmann, J.; Finke, P.; Hesse, M.; Wettig, B. *Angew. Chem., Int. Ed.* **2008**, *47*, 9982–9984.

[339] Watanabe, K.; Kataoka, T. In *Science of Synthesis: Houben-Weyl Methods of Molecular Transformations Vol. 31a*; Science of Synthesis, Vol. 31a; Georg Thieme Verlag KG: 2007, p 1159.

[340] Gondzik, S.; Schulz, S.; Bläser, D.; Wölper, C. *Chem. Commun.* **2014**, *50*, 1189–1191.

[341] Khandelwal, B. L.; Kundu, K.; Gupta, S. K. *Inorg. Chim. Acta* **1988**, *148*, 255–260.

[342] Robertson, S. D.; Ritch, J. S.; Chivers, T. *Dalton Trans.* **2009**, 8582–8592.

[343] Wolkers, H.; Dehnicke, K.; Fenske, D.; Khassanov, A.; Hafner, S. S. *Acta Crystallogr. Sect. C* **1991**, *47*, 1627–1632.

[344] Chauhan, R. S.; Kedarnath, G.; Wadawale, A.; Rheingold, A. L.; Muñoz-Castro, A.; Arratia-Perez, R.; Jain, V. K. *Organometallics* **2012**, *31*, 1743–1750.

[345] (a) Burley, S.; Petsko, G. A. *Science* **1985**, *229*, 23–28; (b) Hunter, C. A.; Sanders, J. K. M. *J. Am. Chem. Soc.* **1990**, *112*, 5525–5534.

[346] Nicholas, S. *Acta Crystallogr. Sect. C* **2015**, *71*, 211–215.

[347] (a) Zhang, Z.; Wu, Y.; Zhang, G. *CrystEngComm* **2011**, *13*, 4496–4499; (b) Zhang, Z.; Tong, H.; Wu, Y.; Zhang, G. *New J. Chem.* **2012**, *36*, 44–47; (c) Wang, L.; Zhang, Z.; Wang, Y.; Wu, Y.; Zhang, S. *CrystEngComm* **2012**, *14*, 7877–7881.

[348] Montet, Y.; Kozelka, J. *Inorg. Chim. Acta* **1999**, *284*, 103–106.

[349] Ly-Lan, N.; Kozelka, J.; Bois, C. *Inorg. Chim. Acta* **1991**, *190*, 217–221.

[350] Li, J. J.; Li, W.; James, A. J.; Holbert, T.; Sharp, T. P.; Sharp, P. R. *Inorg. Chem.* **1999**, *38*, 1563–1572.

[351] Xia, A.; Sharp, P. R. *Inorg. Chem.* **2001**, *40*, 4016–4021.

[352] Singhal, A.; Jain, V. K.; Varghese, B.; Tiekink, E. R. T. *Inorg. Chim. Acta* **1999**, *285*, 190–196.

[353] Jain, V. K.; Kannan, S. *Polyhedron* **1992**, *11*, 27–31.

[354] Krogsrud, S.; Toniolo, L.; Croatto, U.; Ibers, J. A. *J. Am. Chem. Soc.* **1977**, *99*, 5277–5284.

[355] (a) Dobinson, G.; Mason, R.; Robertson, G.; Ugo, R.; Conti, F.; Morelli, D.; Cenini, S.; Bonati, F. *Chem. Comm. (London)* **1967**, 739–741; (b) Keubler, M.; Ugo, R.; Cenini, S.; Conti, F. *J. Chem. Soc., Dalton Trans.* **1975**, 1081–1087.

[356] Henderson, W.; Sabat, M. *Polyhedron* **1997**, *16*, 1663–1677.

[357] Mastrorilli, P. *Eur. J. Inorg. Chem.* **2008**, *2008*, 4835–4850.

[358] O'Mahoney, C. A.; Parkin, I. P.; Williams, D. J.; Woollins, J. D. *J. Chem. Soc. Dalt. Trans.* **1989**, 1179–1185.

[359] Cunha, R. L. O. R.; Omori, Á. T.; Castelani, P.; Toledo, F. T.; Comasseto, J. V. *J. Organomet. Chem.* **2004**, *689*, 3631–3636.

[360] Chieffi, A.; Menezes, P. H.; Comasseto, J. V. *Organometallics* **1997**, *16*, 809–811.

[361] Le Page, Y. *J. Appl. Cryst.* **1987**, *20*, 264–269.